GEOLOGY OF ENDAKO MINE
BRITISH COLUMBIA

by

KENNETH MURRAY DAWSON
BSc., University of British Columbia, 1964

A THESIS SUBMITTED IN PARTIAL FULFILMENT OF

THE REQUIREMENTS FOR THE DEGREE OF

DOCTOR OF PHILOSOPHY

in the Department

of

Geology

We accept this thesis as conforming to the
required standard

THE UNIVERSITY OF BRITISH COLUMBIA

ABSTRACT

Endako molybdenite deposit and surrounding area were examined in detail, with particular attention to petrology and genesis of Topley Intrusions, regional structural setting and structural history of Endako orebody, sulphide and alteration mineralogy, fluid inclusion geothermometry of vein quartz, and minor element content of orebody pyrite. The host rock, Endako Quartz Monzonite, is a relatively early phase of Topley Intrusions that range in composition from diorite to granite, and in age from Middle Jurassic to Lower Cretaceous. Endako stockwork was localized by wrench faulting and doming generated by cooling of the batholith and intrusion of pre-mineral dykes. Hydrothermal fluids that altered and mineralized the stockwork were generated contemporaneously with the cooling of Endako pluton. Abundant early potassic alteration and relatively high fluid inclusion paleotemperatures attest to the paramagmatic affiliation of vein and alteration mineral assemblages. Cross-cutting relations indicate a relative age sequence among the potassic, sericitic and argillic alteration stages that is in agreement with a chemical control based primarily on the activity ratio of K^+/H^+. Alteration zonation suggests decreasing temperature from the ore zone towards the south, implying similar temperature variations for sulphide deposition. Fluid inclusion studies support this trend. Average minimum filling temperatures for fluid inclusions in quartz veins from potassic, sericitic and argillic assemblages are 500°C+, 480°C and 400°C, respectively. Minor element content of pyrite shows a similar temperature-dependent trend. In Q-mode factor analysis of 12-element spectrochemical data from 67 orebody pyrites, Mn, Ni and Sn define Factor I which coincides with the ore zone, whereas Factor II (Co and Cu) coincides with the pyrite

zone. Correlation of Factors I and II to ore and pyrite zone respectively implies that the factors are related to mineralizing processes that give rise to the two mineralogically distinct zones.

TABLE OF CONTENTS

TABLE OF CONTENTS   (Continued)

TABLE OF CONTENTS   (Continued)

TABLE OF CONTENTS   (Continued)

TABLE OF CONTENTS   (Continued)

LIST OF TABLES

LIST OF FIGURES

LIST OF FIGURES   (Continued)

LIST OF PLATES

LIST OF PLATES (Continued)

MAPS IN POCKET

Modal analysis specimens Endako Area, B.C. 1968

Geology of Endako Area, British Columbia, 1965-67

ACKNOWLEDGEMENTS

CHAPTER I

INTRODUCTION

A. SCOPE OF INVESTIGATION

Purpose of this study is to investigate factors governing origin and
localization of the large, low-grade molybdenite deposit of Endako Mines
Ltd. (N.P.L.) near Endako, British Columbia. Geochemistry of the deposit
was studied, with emphasis on metallic and alteration mineral assemblages,
minor-element content of pyrite, and geothermometry of vein quartz. The
petrology and structural relations of host rocks were examined in conjunc-
tion with a regional study of phases of the Topley Intrusions in Endako
area.

B. ENDAKO MAP-AREA

Endako map-area lies between latitudes 53°58' N and 54°05' N, and
longitudes 124°47' W and 125°09' W, an area of about 125 square miles in
central British Columbia (Fig. 1-1). The mapped area is centred roughly at
Endako mine, and is bounded on the north by Endako River and Fraser Lake
and on the south by Francois Lake and Nithi River. Nithi Mountain and
Savory Ridge bound the map-area to the east and west respectively. The
mine site of Endako Mines Ltd. (N.P.L.) is 6 miles by road southwest of the
town of Enkako. Townsite for the mine is the new community of Fraser Lake,
9 miles east of Endako on Highway 16, and 91 miles west of Prince George
(Fig. 1-2).

FIGURE I-I

LOCATION OF ENDAKO MAP-AREA
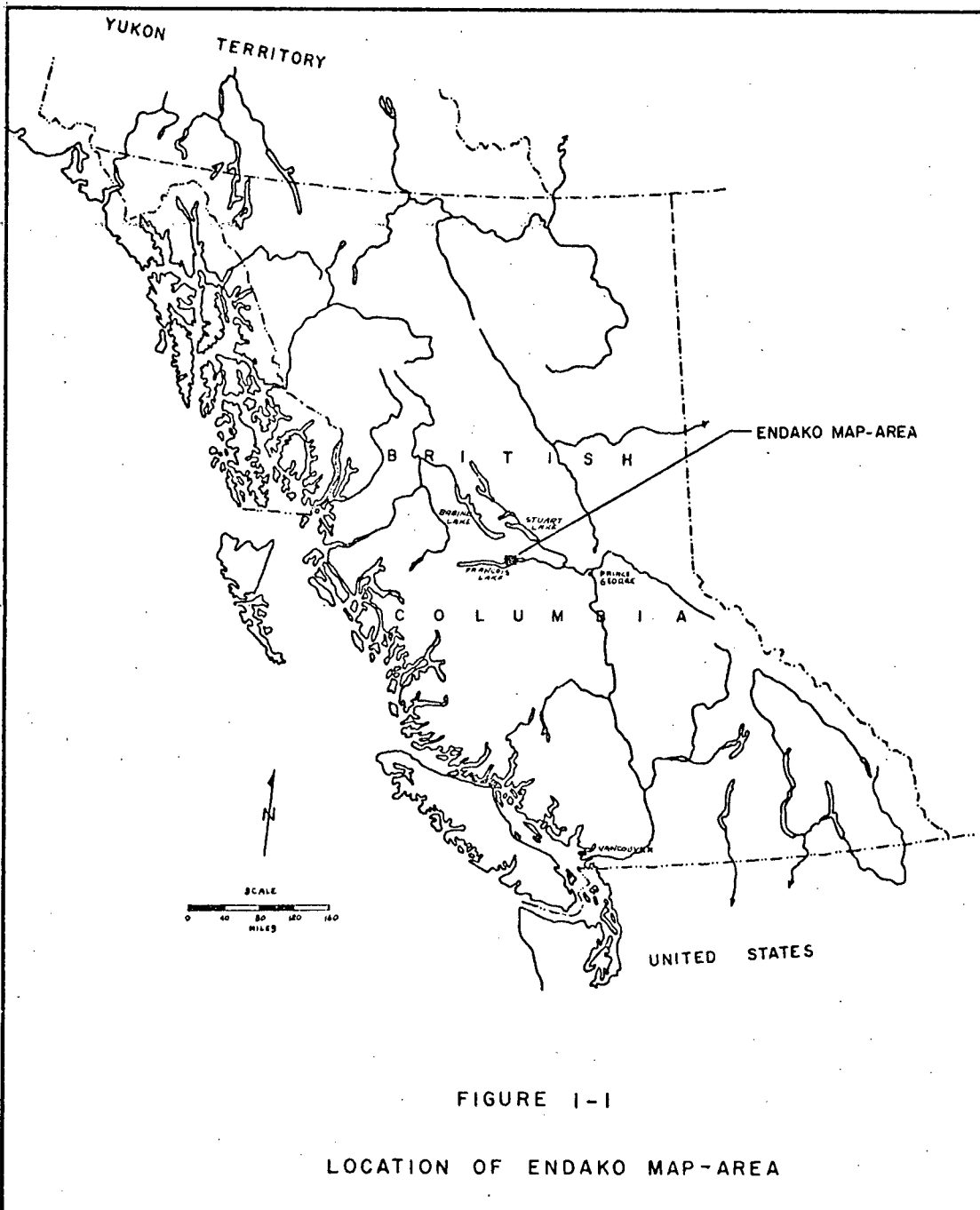
Canadian National Railways and Highway 16 (Northern Transprovincial Highway) cross the northern part of map-area and are the principal access routes. A paved route to Endako mine follows Glenannan Road three miles southward from the town of Endako and then Endako Mine Road three miles southwestward to the mine. Gravel automobile roads leading from Highway 16 to the mine, Francois Lake and Nithi River areas to the south, and north shore of Fraser Lake provide access to most of the map-area. Logging and diamond-drill site roads form a network of access routes for four-wheel drive vehicles. In general, access to the map-area is excellent. Very few parts of the mapped area are more than a one-mile hike from a traversable road.

The area is heavily forested with white spruce, lodgepole pine, aspen poplar and Douglas fir. Less abundant are black spruce, balsam, alpine fir, dwarf juniper, white birch and mountain alder. White spruce is abundant on slopes and black spruce and balsam are restricted to swampy areas. Lodgepole pine grows in well-drained sandy soils. Aspen poplar is widespread, and small groves of white birch grow locally in aspen forests. Douglas fir occurs along the north shore of Francois Lake, and alpine fir is found at higher elevations on Nithi Mountain and Savory Ridge, along with dwarf juniper. Willow, ground birch, alder, wild rose and Devil's club are abundant shrubs. Grasses, pea vine and vetch grow on open southern slopes providing feed for moose and deer and range land for cattle.

Wildlife is diverse and plentiful in the Endako area. Mammals encountered during field work were moose, mule deer, black bear, coyote, porcupine, beaver, rabbit, skunk, muskrat, lynx, mink, red squirrel, chipmunk and mouse. Game birds include Franklin's grouse (spruce hen),
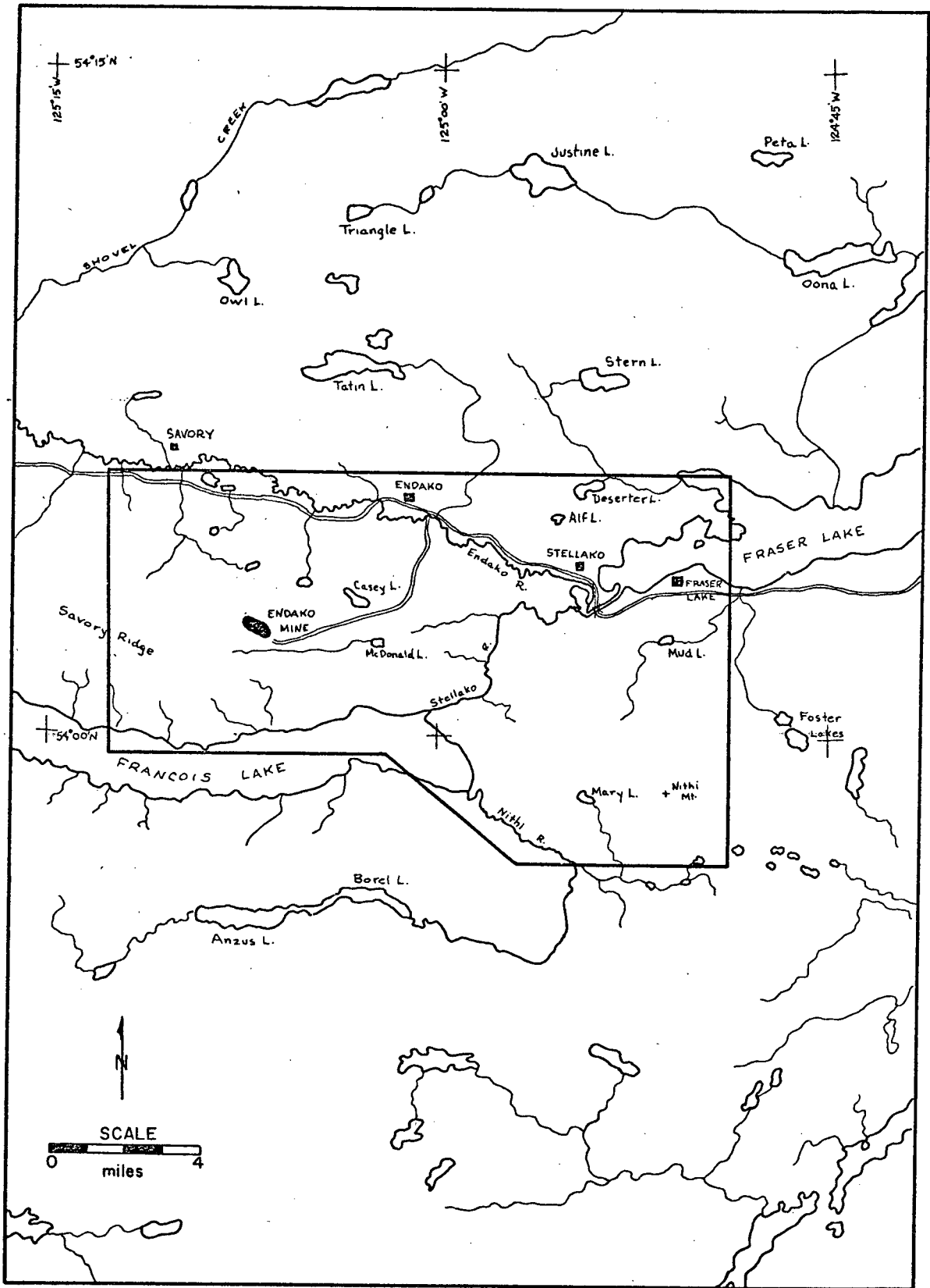
FIGURE 1-2
BOUNDARIES OF ENDAKO MAP - AREA

ruffed (willow) grouse, blue grouse and ptarmigan. Waterfowl are abundant on Fraser and Francois Lakes. Rainbow and lake trout in both lakes provide excellent sports fishing. Sockeye salmon ascend Stellako River from the Fraser system in August and September, and spawn in streams draining into Francois Lake.

The climate in Endake area and surrounding Nechako Plateau is typified by warm summers, long cold winters and light precipitation. Daily weather recording at Endako mine has provided the following statistics for a two-year period:

	1966	1967
Highest temperature	85°F (11 Jul.)	90°F (16 Aug.)
Lowest temperature	-32°F (5 Jan.)	-20°F (20 Dec.)
Annual mean temperature	35.2°F.	39°F.
Total annual rainfall	8.14 in.	11.06 in.
Total annual snowfall	136.13 in.	92.13 in.
Total precipitation	21.75 in.	20.27 in.

(E.T. Kimura and R. Thon, Pers.Comm., 1967; R. Thon, Pers.Comm., 1968)

Comparable low annual precipitations of 13.34 inches at Vanderhoof and 15.61 inches at Fort St. James (Armstrong, 1949, p. 5) reflect the dry summers and light winter snowfall common to the region. Snow is expected in the vicinity of Endako mine in October, and winter weather generally commences about the first week in November. Spring breakup comes about the end of April on the large lakes, but snow does not leave the higher areas until the end of May.

Endako-Fort Fraser area, with a population of about 2200, is one of the more densely-populated parts of north-central British Columbia. Recent influx of Endako Mines Ltd. (N.P.L.) personnel and their families to the expanded community of Fraser Lake has raised the population from a few

dozen families prior to 1964 to the present population of 1100. Other principal employers are Fraser Lake Sawmills, Fraser Lake Inn and a shopping centre. Older residents of the area are occupied in cattle ranching, farming, logging and big-game guiding. The community of Endako, a divisional point on the Canadian National Railway, has a population of about 400. Although the railway is the principal employer, other industries include a new Canadian Industries Ltd. explosives plant and service industries. The Indian population of the area is centred at Stellako Indian Reserve, a community of 100 persons at the west end of Fraser Lake. Tourism is an important source of income to the communities along Highway 16 and the six resorts at the east end of Francois Lake.

C. PREVIOUS GEOLOGICAL WORK

The first geological mapping in northern British Columbia was by Selwyn (1877, pp. 29-87) of the Geological Survey in 1875-1876. He examined the country along a route between Quesnel and Peace River, and although he passed to the east of Endako area, he noted diorite near Stuart Lake which was later recognized as part of the Topley batholith. In 1876 Dawson (1878, pp. 17-94) made a geological reconnaissance in the basins of Blackwater, Salmon (Dean) and Nechako Rivers, and on Fraser and Francois Lakes. From his brief examination of the three principal rock units in Fraser Lake - Francois Lake area, i.e. Takla and Hazelton Groups, Topley Intrusions and Endako Group volcanics, Dawson (Ibid., pp. 83-93) came to remarkably astute conclusions on the regional correlation and relative ages of the rocks.

In 1915 Camsell (1916, pp. 70-75) made a rapid reconnaissance from Fort St. James to Germansen Landing and Manson Creek, skirting the Topley Intrusions but examining some southern members of the Omineca Intrusions.

In 1928 Hanson and Phemister examined the area between Topley and Babine Lake (1929, pp. 50-77). They were the first to recognize the Topley Intrusions, and assigned a "pre-Jurassic" age to the granitic rocks (Ibid., pp. 56-59).

The Geological Survey of Canada commenced mapping of the Fort St. James area in 1936 on a scale of 1 inch to 4 miles. Between 1936 and 1944, and excepting 1938 and 1939, one or more field parties operated each year. In 1936 and 1937 Gray (1938) and Armstrong (1937, 1938, 1941) mapped the east and west halves of the Fort Fraser map-area respectively. These preliminary reports were combined with results of later mapping in the northern part of the Fort St. James area in Memoir 252 (Armstrong, 1949). Among the many problems considered in this Memoir is the probable pre-Jurassic age of Topley Intrusions.

Between 1949 and 1952 the Nechako River area south of Francois Lake was mapped by Tipper (1959, 1963). Significant aspects of Tipper's work were revision of the Takla and Hazelton Groups (1959) and an examination of their contact relations with Topley Intrusions in the Nechako area (1959, p. 32; 1963, p. 41).

In the summer of 1965 Carr of the British Columbia Department of Mines and Petroleum Resources mapped an area of 250 square miles centred on Endako and extending north of Highway 16, on a scale of 1 inch to one-half mile (1966, pp. 114-135). Carr, in defining thirteen principal intrusive phases

of the Topley Intrusions, was the first to examine in detail the lithologic complexity of the batholith. E.G. Bright assisted Carr in the field in 1965, and wrote a Master's thesis at the University of British Columbia (1967) on petrology and genesis of Topley rocks in Endako area.

Reports on molybdenite occurrences in Endako area have appeared in the literature since 1927. Examinations of the Stella Molybdenite property, now the western part of Endako orebody, and other mineral deposits in the area have been made by Lay (1927, 1928, 1929, 1934) for the British Columbia Department of Mines. In 1934 Kerr (1936, pp. 163-165) examined important mineral deposits, including Stella property, along the Canadian National Railway between Prince Rupert and Prince George. Armstrong (1949, pp. 192-193) visited the Stella Molybdenite property in 1936. Stevenson (1940, pp. 11-17) examined the Stella property in July 1938 and published a complete description of workings and molybdenite occurrences. Vokes (1963, pp. 242-245) also visited the property in July 1938, and was the first to recognize the potential for a large-tonnage mine.

Renewed interest in Endako area in 1961 and the incorporation of Endako Mines Ltd. (N.P.L.) in 1962 was reflected in reports by Holland and Bapty (1962, pp. 17-19; 1963, pp. 30-38). Carr (1964, pp. 58-64) made a comprehensive examination of Endako mine prior to commencement of production, and, with Bapty, examined other molybdenite occurrences in the area.

Since the 1962 option agreement between Endako Mines Ltd. (N.P.L.) and Canadian Exploration Ltd., several unpublished reports on geology of Endako mine and Endako area have been prepared by staff geologists. Reports relevant to the present study are those by Ball (1963a, 1963b), Dawson (1965a, 1965b, 1967), Drummond (1966a, 1966b, 1966c, 1966d, 1966e, 1967),

Dummett (1967), and Kimura and Drummond (1966, 1967, 1969).

While employed as a summer student at Endako mine in 1967, P. Beaudoin made petrographic studies and a 1" = 200' geological map of Takla Group and related rocks on the north shore of Francois Lake as a Bachelor öf Applied Science thesis at the University of British Columbia (1968).

D. MOLYBDENITE OCCURRENCES

The successful development of Endako mine has encouraged other mining companies to explore molybdenite deposits in the area. Notable among several occurrences are deposits at Nithi Mountain, Owl Lake and adjacent to the western part of Endako orebody (Fig. 1-3).

At Nithi Mountain, five miles south of the town of Fraser Lake, widespread low-grade molybdenite mineralization occurs on various claim groups held by R and P Metals Corp. Ltd., New Indian Mines Ltd., Jodee Mines Ltd., Dundee Mines Ltd., and Fort Reliance Minerals Ltd. The Molly Claims of R and P Metals were examined by C.W. Ball (1963b) for Canex Aerial Exploration Ltd., and the Nithi Mountain area in general was examined by Drummond and Dawson (1966e). Rock types, mineralization, alteration and structural setting are similar to that at Endako but degree of fracturing and mineralization are significantly lower. Mineral potential, based on assays of 7910 feet of diamond-drill core, and results of induced polarization and soil geochemistry surveys, appears too low to be of economic value at present.

Outside of Endako map-area, United Buffadison Mines Ltd. holds 70 claims in the K and S groups near Owl Lake, 3 miles north of Savory Station.
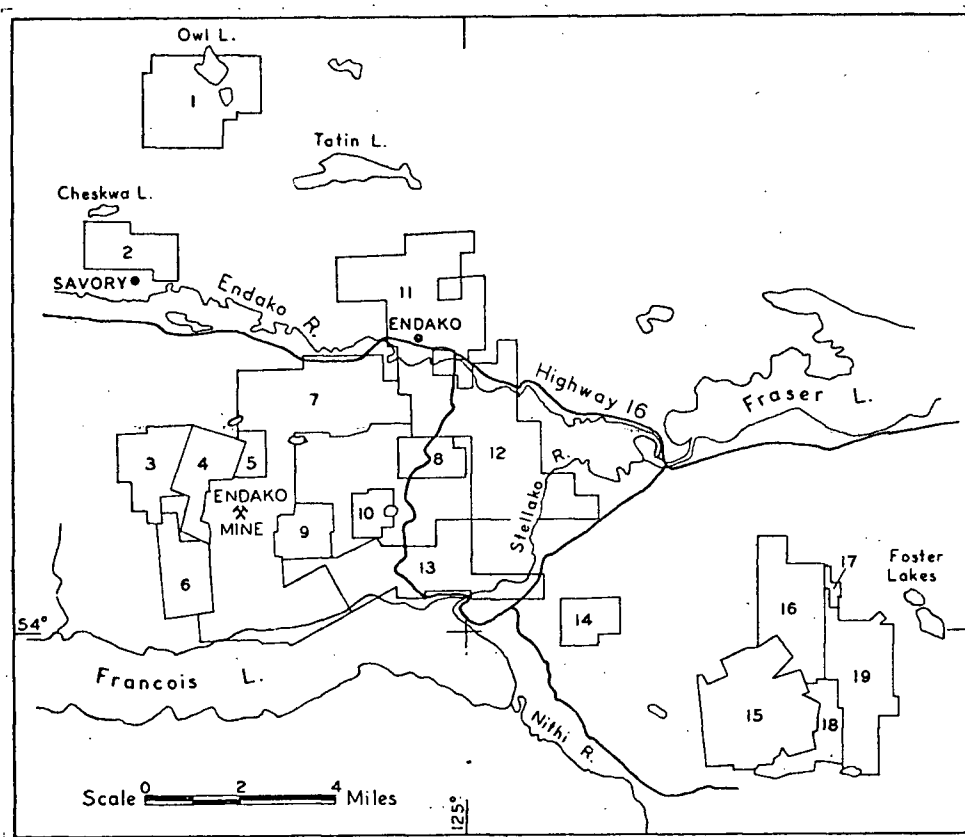
FIGURE 1-3

INDEX MAP OF PROPERTY BOUNDARIES, ENDAKO AREA

(After Carr, 1966, Fig. 26)

1. K, S groups (United Buffadison Mines Ltd.)
2. Aly group (National Explorations Ltd.)
3. Dis, Dat groups (Julian Mining Co. Ltd.)
4. Nu, Elk groups (Julian Mining Co. Ltd.)
5. Deer group (Julian Mining Co. Ltd.)
6. Rob group (Utica Mines Ltd.)
7. Endako Mines Ltd.
8. Endako Mines Ltd.
9. Bell group
10. C.M. group (Torwest Resources (1962) Ltd.)
11. Joe, DI, Ex groups (Copper Ridge Mines Ltd.)
12. Nurd, Dave, Vera groups (Copper Ridge Mines Ltd.)
13. Rac, Bingo, Pal, Ol, Tab groups (Copper Ridge)
14. KO group (Julian Mining Co. Ltd.
15. Andy, Scott, Enco, Molly groups (R & P Metals Corp. Ltd. and New Indian Mines Ltd.)
16. Tip, Tan groups (Fort Reliance Minerals Ltd.)
17. MJM group (Scope Development Ltd.)
18. Jen, Beaver groups (Jodee Explorations Ltd.)
19. Nithi group (Dundee Mines Ltd.)

Scattered molybdenite mineralization occurs in Casey alaskite near the intersection of two regional structures; i.e. the northern extension of Casey Lake fault and a zone of fractures and dykes with northeast trend. Over 6000 feet of diamond-drilling revealed some high-grade intersections, but most mineralization, in the form of small quartz-molybdenite-pyrite veins, is well below ore grade.

In 1967 Denak Mines, a private company controlled by Wenner Gren in partnership with Anaconda, completed diamond-drilling of the Nu and Elk groups held by Julian Mining Co. Ltd. (Anaconda) adjacent to the western boundary of Endako Mines Ltd. (N.P.L.). Development work indicated a molybdenite deposit of economic proportions having continuity with mineralization in the adjoining Endako orebody. Endako Mines Ltd. (N.P.L.) negotiated a purchase agreement with the owners in June 1968 and has incorporated the deposit in a western extension of the present open pit.

The CM group consists of 32 mineral claims located east of Endako mine in the vicinity of Casey and MacDonald Lakes, and is registered under Torwest Resources Ltd. and Vimy Explorations Ltd. Under an option agreement with the two companies, Endako Mines completed over 4100 feet of diamond-drilling on the ground in 1967. A few small quartz-molybdenite veins were intersected in four drill holes. Drill core provided structural and petrological information on the Casey Lake fault and a parallel dyke zone in this area of negligible rock exposure (Kimura and Drummond, 1967).

Utica Mines Ltd. encountered minor veinlets containing molybdenite and pyrite in diamond-drilling on the Rob group southwest of Endako orebody in 1965. National Explorations Ltd. has diamond-drilled and trenched the Ron group of mineral claims west of Oval Lake where a two-foot-wide quartz vein

containing minor molybdenite crops out. Molybdenite rosettes occur on fractures in Casey alaskite in Tailings Creek canyon north of Tailings Pond.

E. HISTORY OF ENDAKO MINE

In 1927, C.H. Foote and Alf Langley of Fraser Lake staked the four original Stella Mining Claims which covered the western part of the present Endako orebody. In the period 1927-1934 the owners sank a 27-foot inclined shaft on a 3-foot wide quartz-molybdenite vein, drove a short adit below the shaft, and opened several surface cuts. The main vein had an indicated length of 250 feet, an attitude of 075/60 S, and assayed 1.6% MoS_2 across a 32-inch width. Several smaller veins were exposed, and molybdenite float was abundant in the area (Armstrong, 1937, pp. 27-28; Kerr, 1936, pp. 163-165; Lay, Ann. Repts. Minister Mines, B.C., 1927, pp. C152-153; 1928, pp. C179-180; 1929, p. 182; 1934, p. C13).

In the following years Stella Molybdenite property was examined by various individuals and companies. After the original claims lapsed in 1959, they were restaked by Dr. C. Riley and Dr. H.T. James of Vancouver. Andrew Robertson signed an examining option with the owners in July, 1961. Although stripping, trenching and drilling work which followed were not conclusive, evidence of a major ore body prompted Robertson to stake more claims and negotiate a purchase agreement on behalf of his own company, R and P Metals Corporation Ltd., in January 1962. Encouraging results from the diamond-drilling program led to the incorporation of Endako Mines Ltd. (N.P.L.) as a private company on June 21, 1962, and with additional financing, as a public company on August 10, 1962.

Following examination of the property on August 22, 1962, Canadian

Exploration Ltd. entered into an option agreement with Endako Mines and a

vigorous program of exploration was started. Diamond-drilling continued

until the end of February, 1964, at which time 190 drill holes had been cut

for a total of 82,902 feet, and 2,755 feet of underground work related to

bulk sampling had been completed. Confirmation of tonnage and grade by

underground work led to the announcement on March 15, 1964 of a decision to

equip the mine for production. Clearing of plant site and open pit started

immediately. Mill and ancillary building construction and machinery instal-

lation continued all winter, and by mid-May 1965 the project was completed.

Official opening was June 8, 1965, slightly more than three years after the

first drill hole was driven (Stephens, 1965, pp. 38-40).

Production is currently being maintained at 25,000 tons per day at an

average ore grade of 0.16% MoS_2. Molybdenum is produced as both oxide

roaster product and sulfide. Reserves are estimated at 209 million tons of

ore averaging 0.15% MoS_2, calculated at a cut-off grade of 0.08% MoS_2 (1971

figures).

F. FIELD WORK

A total of 11 months field work was done in the three periods May to

September, 1965; May to September, 1966; and June to August, 1967. The

1965 field season was spent mapping the area south of Endako mine on a

scale of 1 inch to 200 feet, preliminary regional mapping on a scale of 1

inch to 1000 feet, and detail mapping in Endako open pit on a scale of 1

inch to 40 feet. The majority of Endako area was mapped on a scale of 1

inch to 1000 feet during the 1966 field season. Nithi Mountain and the

eastern part of the map-area were mapped on a scale of 1 inch to one-quarter mile. The 1967 field season was spent in completion of regional mapping and collection of pyrite specimens for minor element study.

The following base maps were used in regional geological mapping:

1. A reconnaissance topographic map of Endako mine area, scale 1 inch to 200 feet, contour interval 10 feet, was prepared by Hunting Surveys Ltd., Vancouver, for Endako Mines Ltd. (N.P.L.).

2. A reconnaissance topographic map of Endako area, east and west halves, scale 1 inch to 1000 feet, contour interval 25 feet, was prepared by Hunting Surveys Ltd., Vancouver for Endako Mines Ltd. (N.P.L.).

3. British Columbia Department of Mines and Petroleum Resources Manuscript Map No. 1 - Geology of Endako Area, 1966, scale 1 inch to one-half mile, was adapted from British Columbia Department of Lands and Forests Interim Map 93 K/3a, 1961, and served as a base map for area north of Highway 16.

4. British Columbia Department of Mines and Petroleum Resources Manuscript Map No. 3 - Detailed Geology of Endako Area (Eastern Part), 1966, scale 1 inch to one-quarter mile, was adapted from British Columbia Department of Lands and Forests Interim Map 93 K/3a, 1961, and served as base map for eastern part of area, including Nithi Mountain.

Outcrops were surveyed by pace and compass, and plotted directly on base maps in the field. Aerial photographs were used for locating areas of potential rock outcrop, and ascertaining precise positions of outcrops on working and final copies of outcrop maps.

Four quadrant sheets, each covering 30,000 feet by 40,000 feet, comprise the final outcrop map. Scale is 1 inch to 1000 feet. The surveyed grid at Endako mine has been extended to include the area within the outcrop map, with grid lines on 5000-foot centres. A geological map was traced from the four outcrop maps in two halves, and draughted in final form. The two sheets were then photographically reduced by Riley's Ltd., Vancouver to one-half size, producing a single sheet measuring 42" by 27" plus margins. Scale of the finished map of Endako area geology is 1" = 2000'. (In jacket.)

CHAPTER II

PHYSIOGRAPHY AND GLACIATION

A. PHYSICAL FEATURES

The Endako area lies south and west of the Fraser River – Skeena River
divide, and is drained by streams flowing eastward in the Fraser drainage
system. Streams in the southern half of the area flow into Francois Lake
which drains northeastward into Fraser Lake by the Stellako River. Streams
in the northern part of the area drain eastward to Fraser Lake via Endako
River. Fraser Lake empties into the Nechako River at the village of Nautley
on the east end of the lake.

Endako area is in the southern part of the Nechako Plateau (Bostock,
1948, p. 42) and its topography typifies the dissected upland ridges and
broad major valleys common to this physiographic unit (Armstrong, 1949, p.
8). Rounded hills and broad ridges are grouped into no particular arrange-
ment of distinct ranges. The area is bounded on the west by east-trending
hills of Savory Ridge which reach an elevation of 4500 feet, the highest in
the area. Endako mine, at elevation 3500 feet, occupies the western crest
of a broad east-trending ridge which separates Francois Lake to the south
from Endako River valley to the north. At the southeastern end of the
ridge, twelve miles east of Endako mine, the average ground elevation of
2600 feet rises through a series of small hills to 4435 feet at the crest
of Nithi Mountain, then drops off eastward to the Nechako Plain south of
Fort Fraser (Armstrong and Tipper, 1948, p. 285). Elevations range from
2197 feet at Fraser Lake to 4500 feet at Savory Ridge, but local relief is
considerably less. The Endako River meanders at low gradient through its

one- to two-mile-wide glaciated valley. At the southern edge of the map-
area, the lower portion of the Nithi River occupies the headward end of a
two-mile-wide meltwater channel which drained Francois Lake in early post-
glacial times (Tipper, 1963, p. 12). Francois Lake is presently drained by
the Stellako River which occupies a steep, V-shaped valley incised in
bedrock.

Endako area topography shows a marked relation to the underlying rocks.
'The terrain consists of broken upland ridges and wide major valleys, and
exhibits a predominant easterly grain. Although greatly accentuated by the
prevailing easterly movement of Pleistocene ice, this grain appears to have
originated prior to glaciation, and the topography of the area is broadly
expressive of bedrock structure, notably joint and fault systems.' (Carr,
1966, p. 115). Minor drainage and topographic trends discordant to dominant
easterly glacial grain commonly reflect underlying major faults and intru-
sive contacts where depth of till is not excessive. Joint patterns, where
extensively studied in Endako mine area, show only minor relation to topo-
graphy. Rock type also influences topography. Low, rounded hills and
ridges are underlain by Topley Intrusions which have undergone subaerial
erosion since final withdrawal of the sea that occupied a Middle Jurassic
marine basin in central British Columbia, and emergence in Late Jurassic
to Early Cretaceous times (Tipper, 1963, p. 49). Contrasting topography is
developed over flat-lying Eocene volcanics of the Endako Group which over-
lie Topley rocks at Savory Ridge and Fraser Lake. Typical volcanic
topography is steep-sided, often flat-topped ridges deeply dissected along
vertical joints by recent streams.

B. PHYSIOGRAPHY

The Nechako Plateau, a northern subdivision of the interior Plateau of the Canadian Cordillera (Bostock, 1948, p. 42), is underlain mainly by pre-Tertiary volcanic, sedimentary and granitic rocks. Moderate local relief of 1500 to 2500 feet has been developed upon the Plateau surface which lies between 4000 and 5000 feet elevation (Armstrong, 1949, p. 8; Holland, 1964, p. 68). This physiographic unit, which includes Endako map-area, is bounded immediately to the east by Vanderhoof basin, one of three glacial lake basins constituting the Nechako Plain (Armstrong, 1949, p. 15). Although underlain mainly by flat-lying volcanic rocks, Nechako Plain probably derives its relatively even surface of 2200 to 2500 feet elevation from extensive erosion which truncated rocks of several ages, and from a deep covering of glacial till or silt, and glacial lake clay (Ibid., p. 8; Tipper, 1963, p. 7). Tipper (Ibid.) has assigned to the group of randomly distributed hills south of Francois Lake and underlain mainly by Hazelton-Takla rocks, the name Francois Lake Highlands. Geographical proximity and similarity of topography, if not bedrock lithology, should warrant the inclusion of the Endako area hills north of Francois Lake in this physiographic subdivision (Fig. 2-1).

C. GLACIATION

Endako map-area was completely covered by glacier ice at least 2500 feet thick in order to cover all the hills, and probably of maximum thickness in the order of 5000 feet according to evidence in the Nechako River area to the south (Tipper, 1963, p. 9) and Fort St. James area to the north (Armstrong, 1949, pp. 11-14). Pre-glacial topography expressive of bedrock

structure may have influenced easterly ice movement in Endako area. Glacial features are common, and prominent features observed in the field and on air photos have been plotted on Fig. 2-2.

(1) Drumlins and Striae

Drumlins are developed in thick glacial deposits in Endako mine area, occurring either singly or in pairs. Seventeen drumlins were studied, ranging in length from 250 to 4500 feet and in height from 25 to 150 feet. Average length and height are 1850 feet and 60 feet respectively. Drumlins are an elongated oval shape in plan with the width about one-quarter the length and the stoss generally steeper and higher than the lee. Drumlins are composed essentially of unstratified till, although a bedrock core may be present. Three rock drumlins are included in the seventeen mentioned above. Two rock drumlins along the Francois granite-Endako quartz monzonite contact southeast of Endako mine (Fig. 2-2) are small, narrow features about 500 feet long and 100 feet wide with leeward ends mantled by till. A third "rock" drumlin near the Glenannan granite-Casey alaskite contact west of Stellako River has a rock ridge exposed at its higher leeward end, probably due to recent erosion. Most drumlins exhibit stoss and lee profiles indicative of easterly sense of ice movement. Long axes range in attitude from N 45 E to S 80 E, and a calculated average attitude for the seventeen drumlins is N 80 E.

Glacial striae occur on most exposed rock surfaces near crests of hills. Average striae trend is east-west, although divergence of ice around exposed rock crags has given rise to striae trending from northeast to southeast within a single outcrop. Few striae were of use in detecting sense of ice movement, with two notable exceptions. Stripping in the

FIGURE 2-1· Physiographic subdivisions of central B.C.

After Holland, 1964
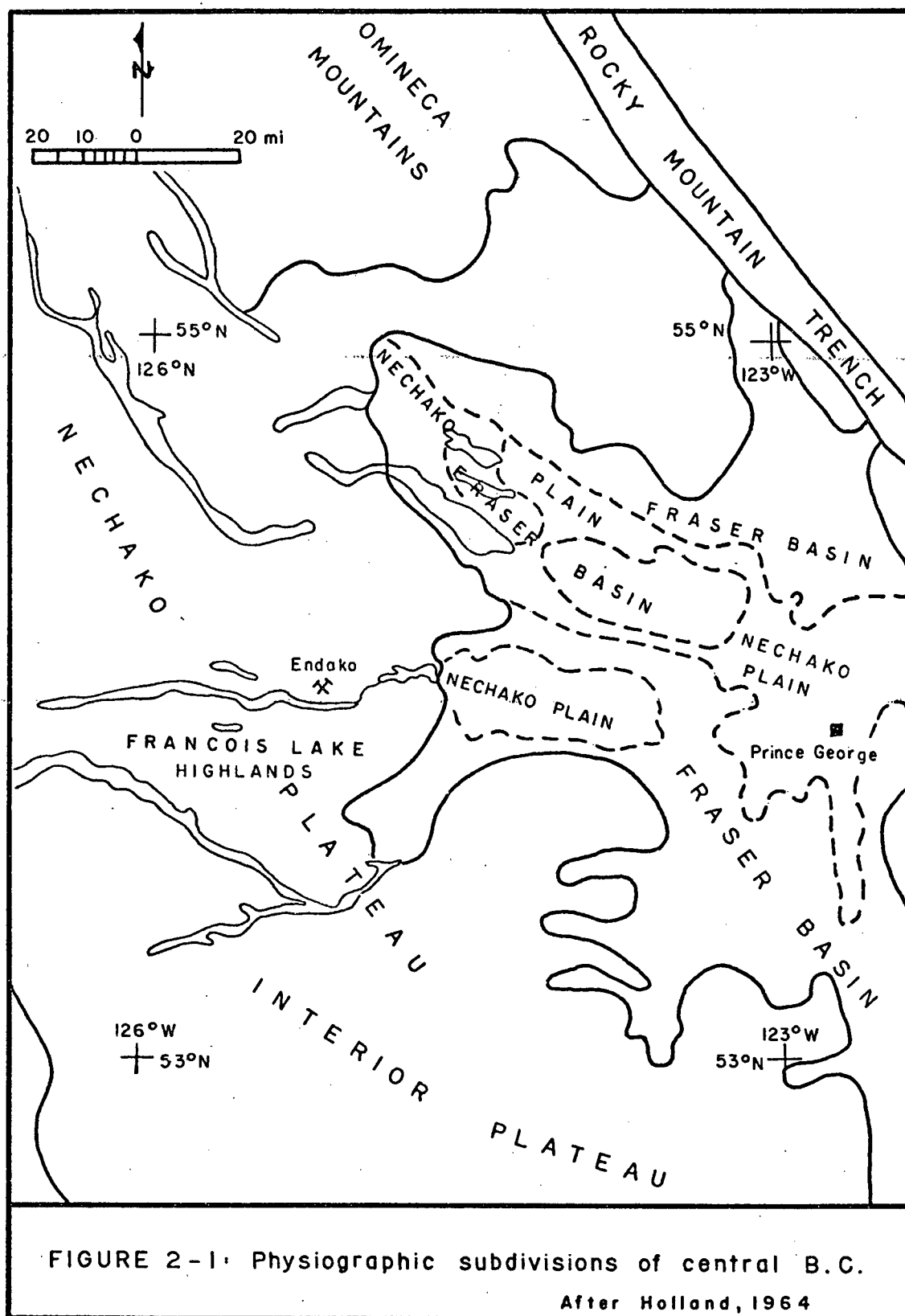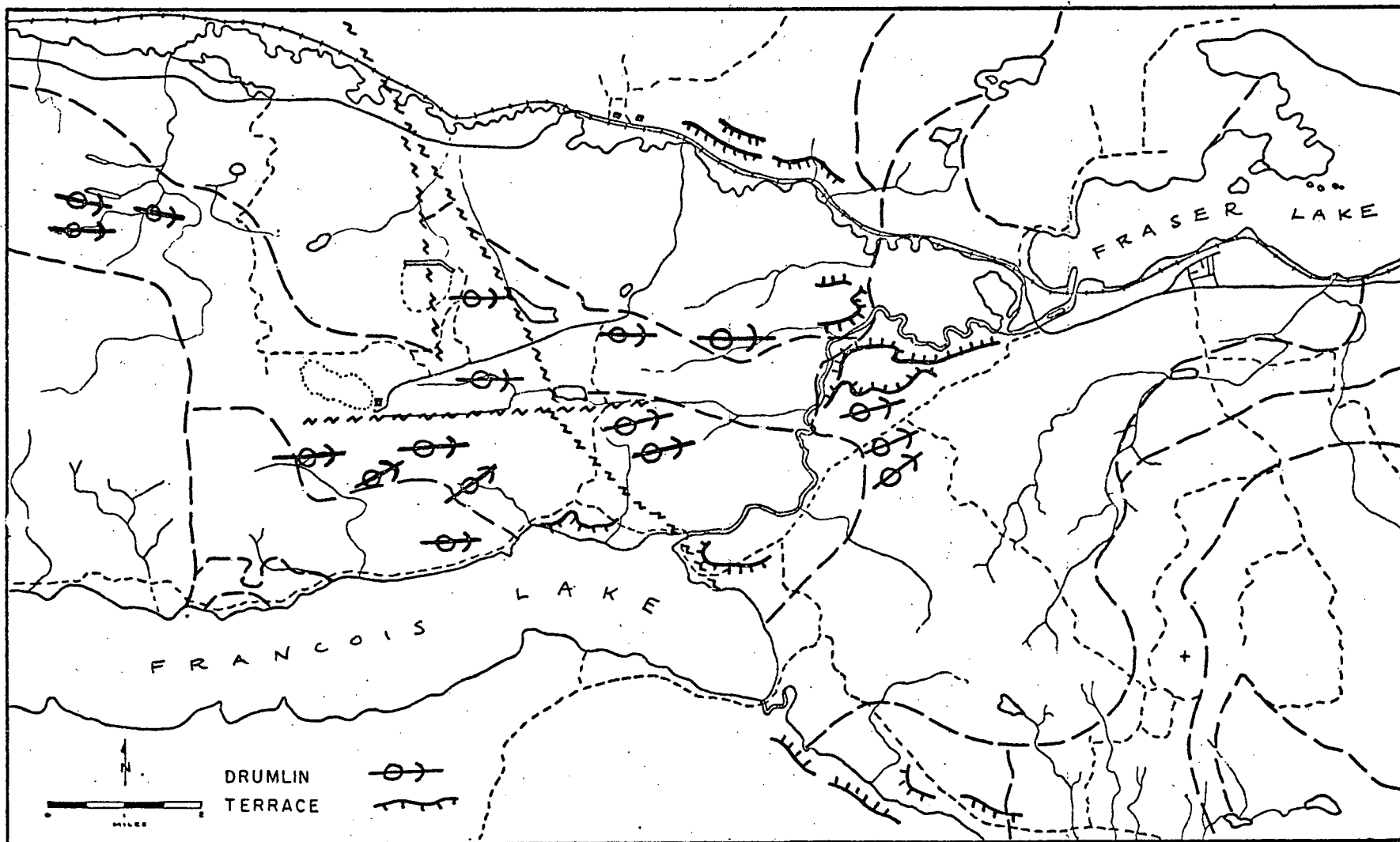
FIGURE 2-2

GLACIAL FEATURES IN ENDAKO AREA

southwest part of Endako mine pit revealed a group of "nailhead" striae which indicated east and east-southeast ice movement. An outcrop at the crest of a small drumlinoid hill east of Glenannan Road-Endako mine road intersection showed striae striking 090 with a well-developed crescentic crack indicating eastward ice movement.

(2) Till and Erratics

A thick blanket of glacial deposits mantles much of the bedrock in the Endako area. Glacial deposits attain greatest thickness in major valleys and upland areas of low relief. Maximum thickness of till recorded in diamond-drilling in Endako mine area is 167 feet on the Vimy property mid-way between Casey and MacDonald Lakes. Alluvium and till thicknesses in the order of 300 feet have been encountered in diamond-drill holes in the Endako valley. Original topography of Endako mine pit area included two east-trending ridges of 3500 feet elevation mantled with till up to 50 feet thick in depressions and 20 feet thick on the average. At the mine and elsewhere in the Endako area rocks crop out mainly on high ground, particularly at or near the crests of south-facing slopes. Some outcrops were discovered in the steep canyons of post-glacial streams. Bedrock exposure constitutes about 3% of the map-area.

Economic factors have instigated studies of till composition in Endako mine area. The majority of bedrock exposed by stripping at the mine is immediately overlain by 5 to 15 feet of very compact lodgement till composed of rounded granitic and volcanic pebbles and cobbles embedded in dense brown clay. Overlying lodgement till, and comprising the bulk of glacial deposits is a thick, unstratified layer of sand, gravel and pale brown silt interspersed with boulder erratics. The fabric and composition of this

deposit indicate origin as an ablation till or moraine, lowered on to sub-glacial deposits by ice melting during glacial recession. Stratified deposits of sand, gravel and silt near Pump Lake, one mile east of Endako mine, have provided material for road construction. Coarsely-stratified, 3 to 10 feet thick beds of sand and sandy gravel are interbedded with 6 inch to 1 foot thick beds of sand and silt. Coarse cross-bedding and pebble lenses occur in the sand. These stratified deposits overlie unstratified till, and represent fluvatile reworking of ablation deposits during inter-glacial times.

Erratics are generally found east of their place of origin. In the Fort St. James area to the north, Armstrong (1949, p. 11) observed: "On the east side of this (Topley) batholith the till boulders and erratics consist predominantly of granite, whereas on the west side the till is devoid of granite boulders and no granite erratics were observed." On a local scale abundant erratics and boulders in till serve as a useful guide to rock type and mineralized areas to the west. Molybdenite-bearing float occurs in a 7000-foot-long zone east of Endako mine, creating anomalous molybdenum values in the soil geochemistry.

(3)   Glacio-lacustrine Deposits, Terraces and Meltwater Channels

Remnant patches of thin-bedded glacio-lacustrine silt, clay and sand overlying bedrock along the north shore of Francois Lake represent at least three ages of glacial terraces. The youngest and most prominent terrace stands 50 feet above present lake level and several remnant terrace deposits 150 to 250 feet above lake level occur east and west of the head of Stellako River (Fig. 2-2). Terraces at similar elevations (2500 to 3000 feet) border a large meltwater channel which follows lower Nithi River valley and runs

eastward to join the Vanderhoof basin in the vicinity of Lily Lake (Tipper, 1963, Fig. 1). Meltwater from receding glaciers and early post-glacial Francois Lake drainage flowed eastward through the Nithi River meltwater channel. At maximum lake level this drainage was inadequate and Francois Lake overflowed southward to Cheslatta Lake through Uncha and Binta Lakes (Ibid., p. 12 and Fig. 1). In later glacial times, Nithi River was dammed with stagnant ice near the south foot of Nithi Mountain and Francois Lake drainage turned northward through its present rock-cut spillway, the Stellako River (Carr, 1966, p. 115).

The Stellako River, at its point of entrance to the Endako River valley 2 miles west of Fraser Lake, has cut down through glacio-lacustrine deposits and formed terraces at 2300 and 2400 feet elevation (Fig. 2-2). Varved, one-half inch to 3 inch-thick beds of grey to light brown silt and clay similar to deposits in Vanderhoof basin to the east (Tipper, 1963, p. 13) are mantled by fluvatile sand and gravel. Lacustrine deposits of similar lithology and elevation were observed in Highway 16 road-cuts along the north side of Endako River valley between the villages of Stellako and Endako. These deposits indicate Fraser Lake and the lower Endako valley were a westward extension of Vanderhoof basin in early post-glacial times. The relative youth of Stellako River is indicated by its erosion of these lacustrine deposits.

D. GLACIAL HISTORY

The Nechako Plateau is an area into which ice moved rather than one in which it accumulated. Mountain ice-sheets flowed out from their places of accumulation in the Coast, Omineca, Cariboo and Rocky Mountains as piedmont

glaciers which coalesced to form an ice-cap up to 6000 feet thick on the Interior Plateau (Tipper, 1963, p. 14). At maximum thickness the Cordilleran ice-sheet flowed in a general outward direction from the centre of the province, while in the Nechako Plateau movement was dominantly eastward and northeastward from the Coast Mountains to the Rocky Mountain Trench (Armstrong, 1949, p. 17). In detail the ice movement was more variable, the topography being the governing factor as ice thinned. Ice moving southeast along Takla and Babine valleys coalesced with ice moving northeastward and eastward in the Nechako River area to the south (Ibid.), creating a dominantly eastward flow of ice in the intervening Endako area. While eastward movement in general is substantiated by orientation of glacial features and distribution of till and erratics, the elongation of drumlins and intervening groovings in the Nechako Plain may be related to a late re-advance of ice after recession of the major ice-sheet (Ibid.). The last ice advance was followed by stagnation in the low-lying parts of the Nechako Plateau, the formation of ephemeral glacial lakes and large meltwater channels, and widespread lacustrine deposition in basins within the Nechako Plain (Tipper, 1963, pp. 14-15).

CHAPTER III

GENERAL GEOLOGY

A. REGIONAL SETTING

The Topley Intrusions occur within an area of geological complexity in
the central interior of British Columbia (Fig. 3-1). Intrusive, volcanic
and sedimentary rocks of Permian to Late Tertiary age represent several
major periods of orogeny, repetitive volcanic activity and sedimentation.

(1) Cache Creek Group

Oldest rocks in the area are a very thick assemblage of interbedded
sediments and volcanics of the Cache Creek Group of mainly Permian age
(Armstrong, 1949, p. 32). Two elongate, fault-bounded belts of Cache
Creek rocks, the Manson Creek and Stuart Lake Highs (Souther and Armstrong,
1966, p. 171) are parallel to the northwesterly Cordilleran trend. Stuart
Lake High is flanked to the west and locally intruded by the Topley batho-
lith. Volcanic and sedimentary rocks and their metamorphosed equivalents
(of similar lithology to rocks of Cache Creek Group) occur marginally to,
and as roof pendants within, Coast Intrusions near Terrace (Duffell and
Souther, 1964, p. 14).

(2) Takla-Hazelton Assemblage

Rocks of the predominantly volcanic Takla-Hazelton Assemblage underlie
most of central British Columbia. A northwesterly trending belt of marine
volcanic and sedimentary rocks of the Upper Triassic to Lower Jurassic
Takla Group unconformably overlies Cache Creek rocks in the Fort St. James

LEGEND

Tv	Tertiary volcanics
KTg	Cret-Tert granite
Kg	Cassiar x'lne belt
Ks	Bowser Group
Jg	Topley Intrusions
Mg	Coast x'lne belt
TrJ	Takla-Hazelton As.
Pub	Trembleur Int's
Ps	Cache Ck. Gp

FIGURE 3-1   GEOLOGICAL   SETTING
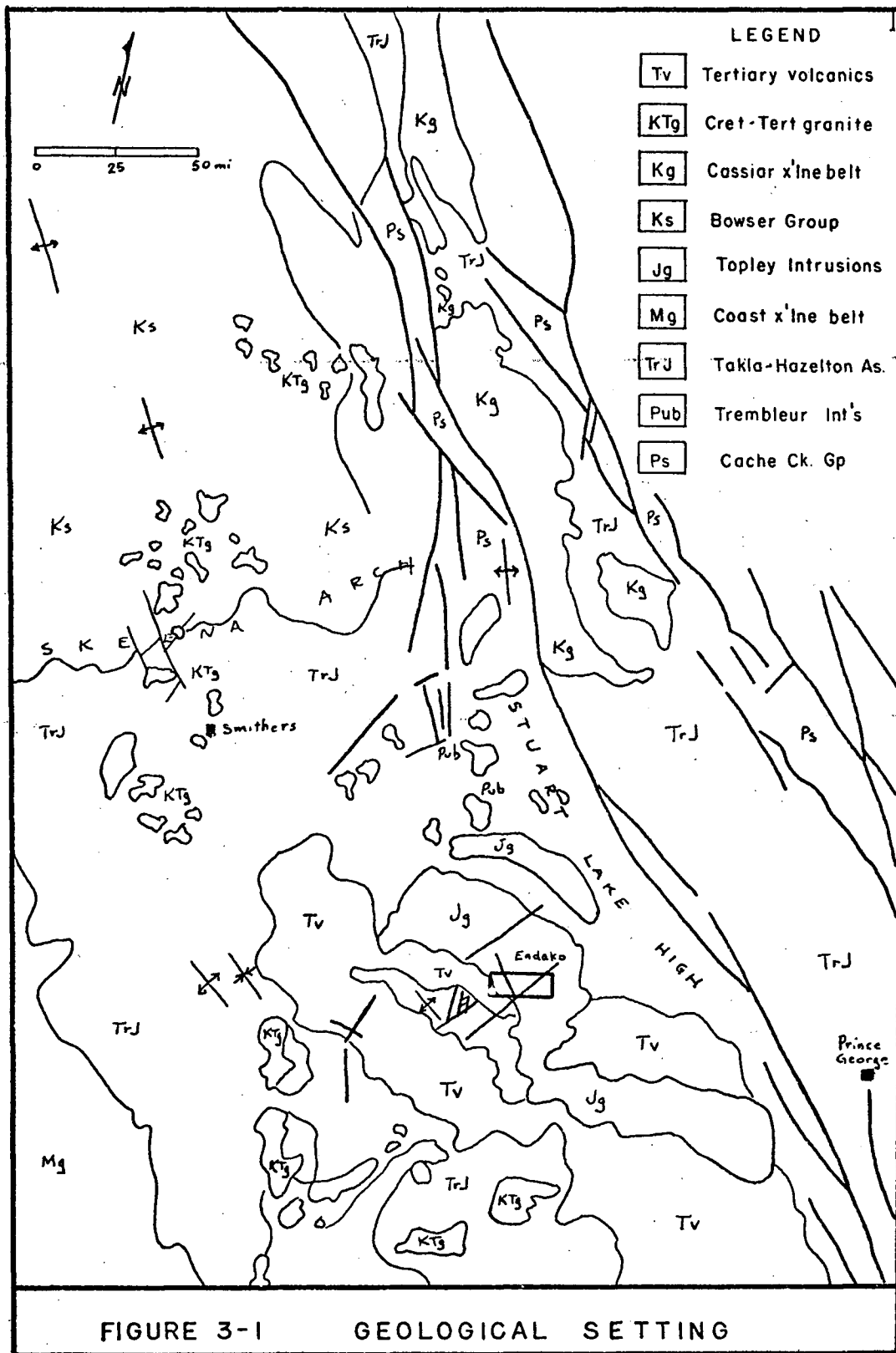
area (Armstrong, 1949, p. 56). In the Nechako River area, disconnected belts of Takla rocks that form the southwestern margin of the Topley Intrusions (Tipper, 1963, p. 18) extend westward into Whitesail Lake area (Duffell, 1959), and southward into Anahim Lake area (Tipper, 1957) where Takla and older rocks flank the Coast Intrusions. The Hazelton Group of central British Columbia is a conformable succession, possibly 10,000 feet thick, of interbedded marine and non-marine pyroclastic sedimentary rocks and porphyritic flows of Middle Jurassic age (Tipper, 1963, p. 23). Hazelton rocks underlie most of the area west of Babine Lake and south of Skeena River, and form a discontinuous belt flanking the east side of Coast Intrusions to the south and peripheral to Bowser Basin in the north. The Takla and Hazelton Groups may represent essentially continuous deposition with change in lithology due to a change in depositional environment from marine to non-marine (Tipper, 1959, pp. 28-29). In discussing structural relations between the two units, Tipper (1963, p. 28) states "The Hazelton Group rests with angular discordancy on the Takla Group in Fawnie Range (Nechako River area) but elsewhere may be conformable."

Topley granites cut Takla Group volcanics on the north shore and to the southeast of Francois Lake (Tipper, 1959, pp. 31-32). Basal sections of Hazelton Group containing pebbles derived from Topley granites have been observed in Nechako River area (Tipper, 1963, p. 25) and in Topley area (Hanson and Phemister, 1929, pp. 55-59). In view of Tipper's revised ages of Takla and Hazelton Groups (1959), an Early Jurassic age of the Topley Intrusions as indicated.

This age, however, is not consistent with age obtained from recent isotopic dating of some younger phases of the Topley in Endako area. The

bulk of Topley rocks and alteration minerals associated with Endako

molybdenum deposit have potassium-argon ages of about 138 m.y. (White, et

al, 1970). The Late Jurassic ages obtained from these rocks indicate that

the entire batholith may be considerably younger than previously shown by

limited stratigraphic evidence. The oldest recognized Topley unit, the

Simon Bay Diorite Complex, yields a Middle Jurassic age of 155+6 m.y.

(Ibid.) that may be a maximum age of the batholith.

(3) Bowser Group

Sedimentary rocks of the Upper Jurassic to Lower Cretaceous Bowser

Group underlie an extensive area in north central British Columbia (Roots,

1954) and rest unconformably on Hazelton rocks in Terrace area (Duffell and

Souther, 1956). Tipper (1963, p.30) describes two small areas of Upper

Jurassic argillite in Nechako River area which show no direct connection to

the Bowser Basin and may be related to rocks of similar age in Ashcroft

area (Duffell and McTaggart, 1952, pp. 31-33).

(4) Tachek Group

In the Fort St. James area Armstrong (1949, p. 64) has mapped a small

group of strata lithologically similar to Hazelton rocks but of presumably

Jurassic and Cretaceous age to which he has assigned the name Tachek Group.

Sedimentary strata at the base of the predominantly andesitic unit uncon-

formably overlie Topley granite at Tachek Mountain.

(5) Ootsa Lake Group

Acidic volcanic rocks of Ootsa Lake Group are widespread but not

continuous or locally extensive throughout central British Columbia.

Armstrong has mapped three units in Francois Lake-Tchesinkut Lake area

(1949, pp. 68-74) composed of interbedded andesitic and rhyolitic volcanic

rocks, chert conglomerate and sandstone ranging in age from Late Cretaceous

to Eocene or Oligocene which together are equivalent to Ootsa Lake Group in

Nechako River area to the south (Tipper, 1963, p. 35) and the Whitesail

Lake type area to the southwest (Duffell, 1959, p. 67). Ootsa Lake Group

volcanic rocks also occur in Anahim Lake area (Tipper, 1957), in Carp Lake

area (Armstrong, Tipper and Hoadley, 1947), and in Quesnel area (Tipper,

1959).

(6)   Endako Group

The youngest major rock unit in central British Columbia is the Endako

Group. Flat-lying andesitic and basaltic massive, vesicular and amygdaloidal

lava flows rest unconformably on Ootsa Lake Group and older rocks (Tipper,

1963, p. 38). Endako Group volcanics unconformably overlie members of

Topley Intrusions in western and northeastern parts of Endako map-area.

Named by Armstrong (1949, pp. 74-76) for its abundant occurrence in the

area drained by Endako River, the Endako Group extends without apparent

break into Nechako River area and southern parts of Interior Plateau.

Features common to Tertiary plateau basalts; columnar jointing, flat-topped

horizontally-bedded hills and lack of pillow structure are exhibited by

these widespread lava flows. Plant fossils from sedimentary rocks at the

base of the group have been assigned an Oligocene age by Armstrong (1949,

pp. 72-73) and Tipper (1963, p. 38) in separate localities, indicating an

Oligocene or younger age for the Endako Group. A potassium-argon age

determination of Endako lava from Hick's Hill, 2 miles south of Priestly,

gave an age of 48$\pm$ 2 million years or Middle Eocene (Mathews, 1964,

pp. 465-468). Biotite from a probably related andesite dike that intruded the Casey Lake fault zone near Stellako River yields a potassium-argon age of 50 ± 2 m.y. (White, et al, 1970).

Intrusive Rocks

Intrusive rocks are widespread in central British Columbia. They range in age from post-Middle Permian to Tertiary and in composition, from ultramafic to granitic with rocks of quartz monzonitic and quartz dioritic composition predominating.

(7) Trembleur Intrusions

Sills, stocks and batholiths of peridotite, dunite, pyroxenite, gabbro and altered equivalents occur in the Trembleur Lake-Stuart Lake region of central British Columbia. These bodies occur within Permian Cache Creek rocks adjacent to Pinchi Fault, and are cut by plutonic rocks of Topley and Omineca Intrusions, indicating a post-Middle Permian, pre-Late Triassic age (Armstrong, 1949, p. 91). Several small bodies of peridotite in Telegraph Range southwest of Prince George occupy the same stratigraphic position.

(8) Topley Intrusions

The name Topley Intrusions has been given to a group of acidic intrusive rocks first recognized in Topley area (Hanson and Phemister, 1929). Topley rocks underlie much of the southern part of Fort St. James area and the northeast part of Nechako River area, and extend northwestward into Houston area and southeastward to Quesnel (Fig. 3-2). Discontinuous patches of volcanic strata of Hazelton, Tachek, Ootsa Lake and Endako Groups overlie

Topley intrusive rocks in many places, and Cache Creek rocks locally inter-

rupt continuity of exposures of plutonic rock. It is possible most of the

exposed areas of Topley Intrusions form parts of one large batholith

extending from Topley Landing on Babine Lake 180 miles southeast to Quesnel,

with a maximum area of about 5500 square miles (Fig. 3-2). Lithology,

structural relations and age of Topley Intrusions will be dealt with in

following sections.

(9) Omineca Intrusions

Armstrong (1949, p. 97) applied the name Omineca Intrusions to numerous

bodies of intrusive rocks exposed in the Omineca Mountains of north central

British Columbia. Omineca Intrusions occur as elongate bodies concordant

with the Cordilleran trend. The composition of Omineca rocks is mainly

granodiorite and granite, with minor basic and syenitic phases. An age

similar to that of Coast Intrusions, i.e. Late Jurassic to Early Creteceous

is proposed by Armstrong (1949, p. 113). Some southern members of Omineca

Intrusions, notably Mitchell batholith, bear considerable lithologic resem-

blance to Topley rocks immediately to the south (Armstrong, p. 113). Biotite

from Duckling Creek syenite, a phase of Hogem batholith, yields a radiometric

age of 178 M. yr. (Koo, 1968), identical to age of Topley diorite at Grizzly

Mountain southwest of Stuart Lake (Tipper, 1962, p. 134-136). A belt of

Omineca plutons intruding Cache Creek rocks between Stuart and Takla Lakes

may be a northern extension of the Topley batholith.

(10) Post-Middle Jurassic Intrusions

Relatively young plutonic rocks of granitic to dioritic composition

occur as stocks and batholiths in Nechako River and Whitesail Lake areas
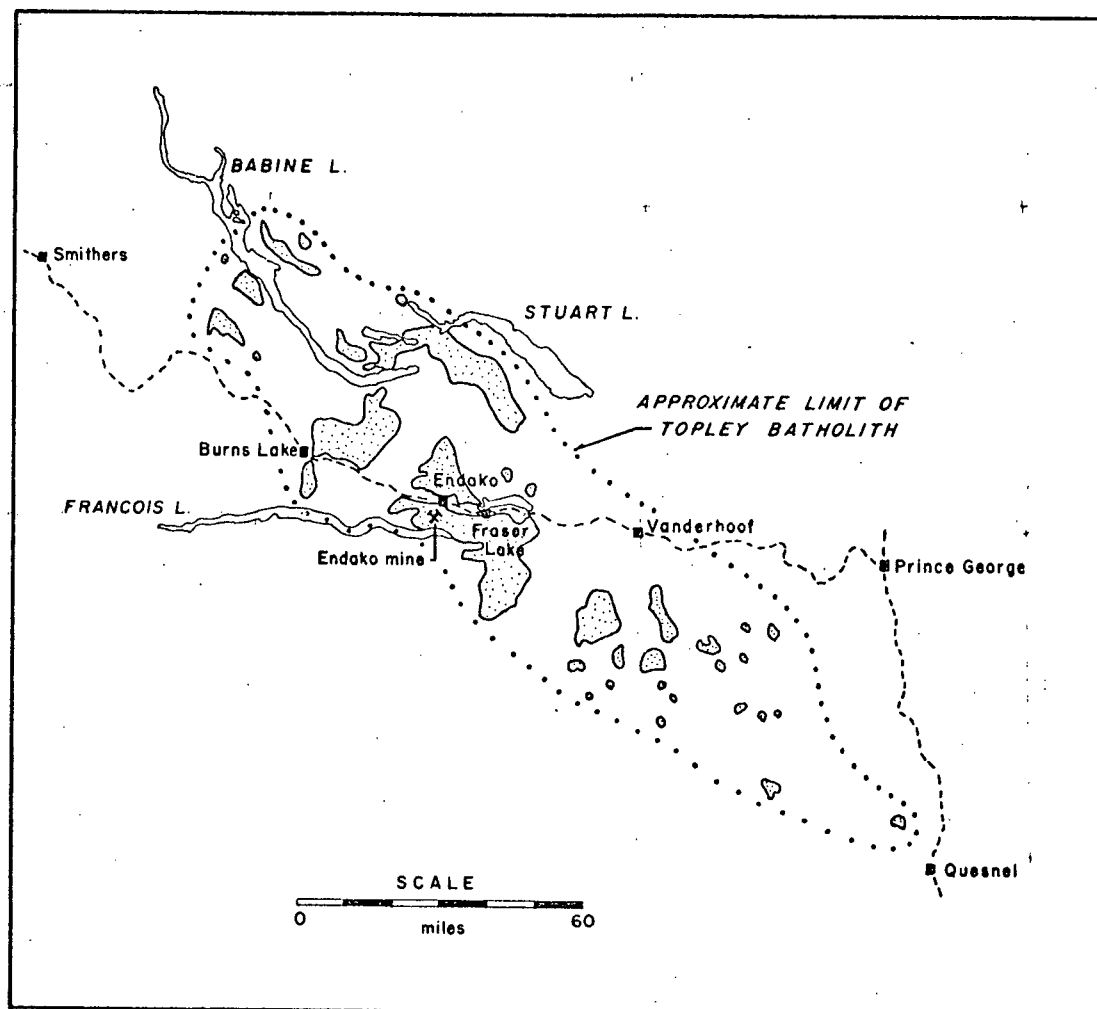
FIGURE   3-2

REGIONAL   DISTRIBUTION   OF   TOPLEY   INTRUSIONS

After G.S.C. Map 932A

(Tipper, 1963; Duffell, 1959) and define the northeast-trending Skeena

Arch in Bulkley and Babine Ranges (Souther and Armstrong, 1966, p. 171).

These intrusions differ from most granitic batholiths of British Columbia

in that they are discordant to regional structural trends. Many bodies are

irregular in shape but most are roughly equidimensional. Granites intrude

Lower Jurassic Takla Group and Middle Jurassic Hazelton Group rocks in

Nechako River and Whitesail Lake areas (Tipper, 1963, p. 42; Duffell, 1959),

and cut Hazelton volcanics and Upper Jurassic to Lower Cretaceous Bowser

Group sediments in Terrace area (Duffell and Souther, 1964, p. 33). Grano-

diorites of the Bulkley and Babine Ranges are considered by Armstrong

(1944a, 1944b) to be satellites of the Coast Intrusions.

B. ENDAKO AREA

(1) General Statement

Intrusive rocks of the Topley batholith, including seven plutons and

one small stock, form approximately 80% of the bedrock in Endako map-area.

A small area of Takla Group volcanic rocks in the southwest is intruded by

Topley granite. Endako Group volcanic rocks overlie older units in the

western and northeastern parts of the map-area.

Topley rocks range from dioritic to granitic in composition, with

quartz monzonite predominant. Average modal compositions of the eight units

are plotted together in Fig.3-20. The units are subdivided lithologically

after the Peterson classification (1960) using the criteria K-feldspar/total

feldspar ratio, anorthite content of plagioclase, and mafic mineral content,

as derived from modal analyses. Most plutons are lithologically homogeneous

but show textural variations, although minor compositional changes in border

phases exist. Exceptions are the Simon Bay diorite complex which is pre-
dominantly diorite and granodiorite with minor gneiss, gabbro and amphibo-
lite; the zoned Glenannan complex which exhibits gradational compositional
changes from granite to granodiorite; and the Stellako intrusions composed
of quartz monzonite and granodiorite. The rock units are readily distin-
guishable in the field and in hand specimen. Although correlations based
on field mapping have been somewhat restricted by scarcity of outcrop, good
contacts and cross-cutting relationships have been observed for most units.

Three stages of Topley plutonism are distinguished on the basis of
field and petrographic studies. These stages are tabulated below (Table
3-1).

Table 3-1

Stages of the Topley Intrusions

STAGE	AGE (PERIOD)	PHASE
Stage 3 (youngest)	Lower Cretaceous	Fraser quartz monzonite Stellako quartz monzonite and granodiorite
Stage 2	Upper Jurassic	Francois granite Casey alaskite Glenannan granite and quartz monzonite Nithi quartz monzonite Endako quartz monzonite
Stage 1 (oldest)	Middle Jurassic	Simon Bay diorite complex

J.M. Armstrong, in the first petrographic descriptions of Topley
Intrusions in the Endako area (1949, pp. 92-96) distinguished "Topley Pink
Granite" from a "border phase" of gray granite and granodiorite, and
"Topley Diorite". From specimen locations cited, these general subdivisions
may be correlated with more recent petrographic studies (Table 3-2). J.M.
Carr has assigned names to thirteen intrusive members of the Topley

batholith in the Endako area (1966, p. 114). E.G. Bright (1967), with additional petrographic study, modified Carr's nomenclature slightly and proposed a new geographical term, the "Simon Bay Complex" corresponding to Carr's "Quartz Diorite Complex". The Topley nomenclature of Carr and Bright has been retained in this study, with minor modifications to petrographic terms as described in following sections and illustrated in Table 3-2. Notable changes to the existing schemes are the deletion of "Pond quartz diorite" or "Pond quartz monzonite" of Carr and Bright respectively, and the retention of the Nithi Quartz Monzonite as a distinct Topley unit rather than a phase of the Glenannan Complex. Four Topley phases designated the Tatin, Titan, Triangle and Rex Quartz Monzonites by Carr (1966), and included within the Glenannan Complex of Bright (1967), all occur to the north of the area covered in this study and were not examined. A correlation of petrographic nomenclature is given in Table 3-2, and geology of the Endako area is summarized in Table of Formations (Table 3-3).

(a) <u>Modal Analysis</u>

Specimens representative of each unit were selected from field collections for modal analysis. The number of specimens studied for each unit was governed mainly by abundance and distribution of outcrop. Map (in Jacket) gives locations of all modal analysis specimens in this study, plus the approximate locations of some modal analysis specimens of Carr and Bright.

Table 3-2

Correlation of Topley Nomenclature

Armstrong (1949)	Carr (1965)	Bright (1967)	Dawson (1972)
-	Fraser granodiorite	Fraser quartz monzonite	Fraser quartz monzonite
-	Pond quartz diorite	Pond quartz monzonite	Deleted
Topley gray granite and granodiorite	Younger quartz monzonites and quartz diorites	Stellako quartz monzonite	Stellako quartz monzonite and granodiorite
	Francois quartz monzonite	Francois granite	Francois granite
	Casey quartz monzonite	Casey quartz monzonite-alaskite	Casey alaskite
Topley Pink Granite	Glenannan quartz monzonite	Glenannan Complex	Glenannan granite and quartz monzonite
	Nithi quartz monzonite	(Included in Glenannan Complex)	Nithi quartz monzonite
	Endako quartz monzonite	Endako quartz monzonite	Endako quartz monzonite
Topley Diorite	Quartz Diorite Complex	Simon Bay Complex	Simon Bay diorite complex

Initially, point-counting of standard size thin-sections was employed to determine modes. This method was discarded when it became apparent that the relatively coarse grain size of most specimens would probably render invalid modal analyses based on small areas. Large thin-sections are more suitable, but cost and difficulty of preparation of an adequate number of sections rendered this technique infeasible. Standard size thin-sections were prepared from each specimen and minerals were identified under the petrographic microscope. A visual estimation of mode was made under the microscope for comparison with modes determined by the following stained-slab method. A sawn slab of the same specimen, measuring at least 5 cm by 4 cm, was stained with sodium cobaltinitrate (cf. Sinclair and Libby, 1969). A grain count was made by laying a clear plastic sheet with inscribed grid on the stained surface. Grid spacings of either 3 mm or 5 mm were used, depending upon the average grain size of the specimen. Approximately 100 and 240 points were obtained from the 5 mm and 3 mm grids, respectively. Where size of stained surface permitted, multiple counts were made.

Modal analysis results are tabulated for each rock unit, along with available data from Bright (1967), Carr (1966), Drummond (1966a, 1966e, 1967), Kimura and Drummond (1966), and Armstrong (1949). Individual quartz-K-feldspar-plagioclase modes are recalculated to 100% and plotted on a quartz-K-feldspar-plagioclase ternary diagram for each unit, along with the calculated average mode.

Table 3-3

Table of Formations - Endako Area

ERA	PERIOD OR EPOCH		NAME	LITHOLOGY
CENOZOIC	RECENT			Stream deposits, talus, soil
	PLEISTOCENE			Silt, clay, sand, gravel, till, boulder clay, erratics
	UNCONFORMITY			
	EOCENE		Endako Group	Vesicular and amygdaloidal andesite and basalt flows and related dykes; flow breccia, tuff and conglomerate
	UNCONFORMITY, INTRUSIVE			
MESOZOIC	LOWER CRETACEOUS	TOPLEY INTRUSIONS	Fraser quartz monzonite	Medium-grained sub-porphyritic pink biotite-hornblende quartz monzonite
	UNCONFORMITY, INTRUSIVE			
	LOWER CRETACEOUS		Stellako quartz monzonite and granodiorite	Medium-grained pink hornblende-biotite quartz monzonite; medium-grained gray hornblende granodiorite
	UNCONFORMITY, INTRUSIVE			
	UPPER JURASSIC		Francois granite	Medium-grained red biotite granite
	UNCONFORMITY, INTRUSIVE			
	UPPER JURASSIC		Casey alaskite	Coarse-to fine-grained leucocratic pink granite and quartz monzonite
	UNCONFORMITY, INTRUSIVE			
	UPPER JURASSIC		Glenannan granite and quartz monzonite	Coarse-grained porphyritic pink biotite granite; coarse-grained pink biotite-hornblende quartz monzonite

ERA	PERIOD OR EPOCH		NAME	LITHOLOGY
MESOZOIC	UPPER JURASSIC	TOPLEY INTRUSIONS	Nithi quartz monzonite	Medium- to coarse-grained subporphyritic pink to gray biotite quartz monzonite
			UNCONFORMITY, INTRUSIVE	
	UPPER JURASSIC		Endako quartz monzonite	Coarse- to medium-grained subporphyritic pink biotite-hornblende quartz monzonite
			UNCONFORMITY, INTRUSIVE	
	MIDDLE JURASSIC		Simon Bay diorite complex	Foliated diorite, quartz diorite and granodiorite; hybrid gneiss, amphibolite and gabbro
	UNCONFORMITY, INTRUSIVE			
	UPPER TRIASSIC AND LOWER JURASSIC	TAKLA GROUP	Menard rhyodacite stock	Red to purple feldspar-biotite porphyry stock and dykes
			INTRUSIVE	
			Rhyodacite pyroclastics	Dark green rhyodacite crystal tuff and breccia

(2) Petrology

(a) Takla Group

In Endako area, rocks assigned to the Upper Triassic and Lower Jurassic Takla Group by Tipper (1959, 1963) and Carr (1966) occupy an area of less than 1 square mile on the north shore of Francois Lake at the southwestern edge of the Topley batholith (Fig. 3-3). Takla rocks include rhyodacite tuffs and breccias, a small rhyodacite porphyry stock, and related rhyodacite porphyry dykes. Takla volcanic rocks are intruded by a northwest-trending group of large quartz monzonite dykes possible related to a body of Topley granite to the north which also intrudes Takla rocks. Takla Group pyroclastic rocks are uncon-formably overlain on the west by Eocene Endako Group andesite flows. Minor andesitic dykes probably related to Endako lavas cut all rocks in the area.

RHYODACITE CRYSTAL TUFFS AND BRECCIAS:

Massive dark-coloured pyroclastic rocks in which bedding is not discernible comprise the majority of Takla Group in the area. White crystal fragments of plagioclase, K-feldspar and quartz in a greenish-black matrix give the rock a pseudoporphyritic texture. Crystal fragments range in size from microscopic to 3 mm diameter and are interspersed with rounded to angular blocks and lapilli of rhyodacite porphyry. Matrix is composed of crystalline and rock fragments, ash and minor glass. Visual estimation of six thin-sections gives the following approximate mode: oligoclase-andesine (An_{25}-An_{31}) 48%; orthoclase 17%; quartz 21%; hornblende

FRASER LAKE

54°N
125°W

FRANCOIS   LAKE

N

MILES

KMD, 1968
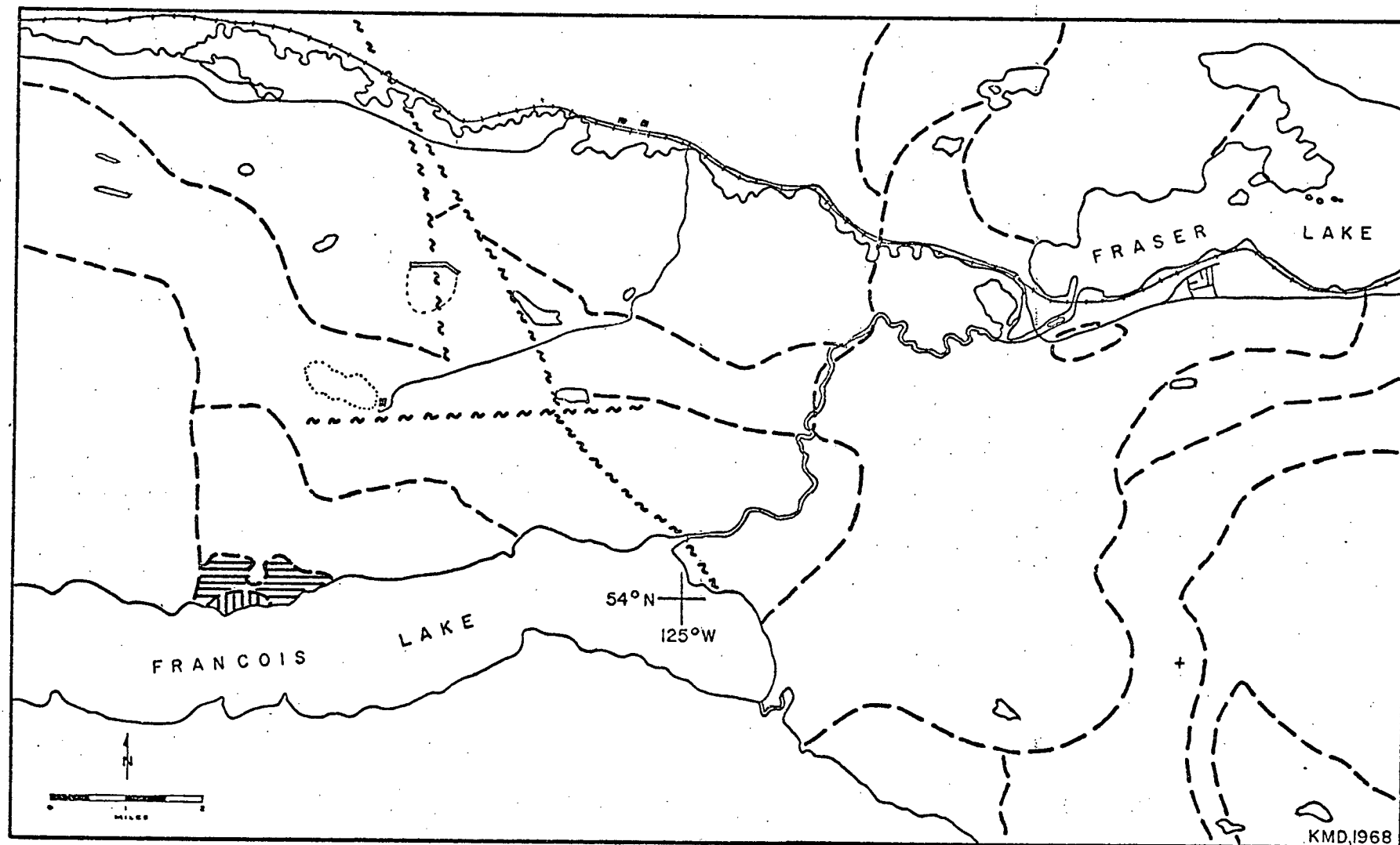
FIGURE 3-3

REGIONAL DISTRIBUTION OF TAKLA GROUP ROCKS

plus biotite 8%; opaque minerals 6%. Rocks are fractured and
mafic minerals are altered to epidote, chlorite, specularite and
pyrite; whereas feldspars are relatively fresh.

RHYODACITE PORPHYRY STOCK:

A small stock of about one-quarter square mile area which intrudes
Takla pyroclastics was named "Menard quartz latite porphyry" by
Carr (1966, p. 126) for its occurrence near Menard's Resort on
Francois Lake. The porphyry, rhyodacite according to the Peterson
classification (1960), contains abundant phenocrysts of feldspar,
biotite and quartz in a purple to red-brown groundmass. Euhedral,
white or flesh-coloured, 1-5 mm diameter phenocrysts of andesine
predominate over thick books of chloritized biotite and subhedral
corroded quartz phenocrysts. Less abundant are small phenocrysts
of orthoclase and slender prisms of hornblende. About one-half
the groundmass is tiny plagioclase laths and the remainder a
mosaic intergrowth of quartz-orthoclase interspersed with grains
of magnetite and pyrite. Xenoliths of rhydacite tuff probably
derived from adjacent pyroclastics are abundant locally.

The composition of rhydacite porphyry as deduced from visual esti-
mation of thin-sections is similar to that of rhyodacite tuff:
andesine (An_{34}) 45%; biotite plus hornblende 20%; quartz 18%;
orthoclase 13%; opaque minerals 4%.

Fine-grained sericite-epidote-hematite alteration of feldspars
imparts a reddish colour to the rock. Mafics minerals are
altered to chlorite and epidote, and quartz-epidote-carbonate

veinlets are common. Hematite and pyrite alteration products are abundant locally.

MINOR INTRUSIONS:

Takla Group rocks are cut by a northwest-trending group of coarse-grained quartz monzonite dykes ranging from a few feet to over 200 feet wide. Although dykes could not be traced northward across the Takla-Topley contact, similarities in texture and composition indicate relationship to Francois granite. Large rhyodacite porphyry dykes petrographically identical to rocks of Menard stock intrude Takla Group pyroclastic rocks and have a northwest trend. Minor aplite and quartz-orthoclase porphyry dykes resemble similar minor intrusions in adjacent Toply Intrusions. Small porphyritic andesite and dacite dykes that cut Takla volcanic rocks, Francois Granite and acidic dykes probably are related to Endako Group andesitic flows to the west.

STRUCTURAL RELATIONS AND AGE:

Near Menard's Resort, pyroclastic rocks resembling the Upper Triassic Main Takla Unit (Tipper, 1963, pp. 19-20) are intruded by Topley Intrusions and overlain unconformably by Endako Group volcanic rocks to the west. Contacts between rhyodacite pyroclastic rocks and the rhyodacite porphyry stock are not exposed but intrusive relations are indicated by the presence of rhyodacite tuff xenoliths within the porphyry, and by dykes similar to Menard porphyry cutting the pyroclastic unit. Compositional and textural similarities of the two rhyodacite units suggest a common

origin. The porphyry stock was probably emplaced into tuffs as a later sub-volcanic phase of rhydacitic volcanism.

A north-trending intrusive contact between Francois Granite and Takla rhyodacite tuff is exposed 3000 feet north of Scott's Resort (Beaudoin, 1968). One-half mile to the east an apophysis of Francois Granite extends 2000 feet southward into rhyodacite tuff. Older volcanics are also intruded by a group of quartz monzonite dykes apparently related to adjacent Topley Intrusions. A pre-Topley, and more precisely, pre-Francois Granite age of rhyodacite tuff and porphyry is indicated.

Some ambiguity exists in Tipper's (1963) description of contacts between Takla Group and Topley Intrusions. Tipper notes that Topley Granite on the north shore of Francois Lake intrudes the marine parts of the Takla Group "Red Bed Unit" but is not in contact with the upper part of the red bed sequence. This indicates that Topley granites were emplaced while part of the Red Bed Unit was being deposited and "would then be of latest Triassic age or more probably Lower Jurassic." (Ibid., p. 41). Along the south shore of Francois Lake and elsewhere the Red Bed Unit is an assemblage of sedimentary rocks including shale, conglomerate, quartzite greywacke and limestone (Ibid., pp. 21-22) bearing little apparent resemblance to pyroclastic rocks and porphyry near Menard's Resort. A small outcrop of Takla Group Red Bed Unit is shown on Tipper's map (1963, Map 1131A) 15 miles west of Menard's on the north shore of Francois Lake, but no adjacent granite is shown. Since rocks at Menard's correspond closely to the andesitic

and basaltic pyroclastic rocks and lavas typical of the Upper Triassic "Main Takla Unit" (Ibid., pp. 19-20), the intrusive contact in this area is not likely to be that described by Tipper.

(b)   Topley Intrusions

(i)   Simon Bay Diorite Complex:

A broad belt of Topley dioritic rocks extends southeastward from Stuart Lake (Armstrong, 1949, p. 94), through the eastern part of Endako area, and southward to the Nulki Hills in Nechako River area (Tipper, 1963, p. 40). Dioritic rocks form the northeastern and eastern margins of the Topley Batholith. Isolated masses of dioritic rocks form an irregular chain which trends northward across the eastern part of the map-area (Fig. 304). The regional northwest trend of these older rocks is not apparent in the map-area as younger Topley plutons have broken the continuity of the unit, and primary foliation in southern outcrops does not parallel the northwest foliation trend at Simon Bay and Deserter Lake.

Rocks of the Simon Bay Complex are predominantly foliated, dark gray, medium- to coarse-grained diorite and granodiorite. Foliation grades from aligned mafic mineral grains and clots to alternating broad bands, 10 to 100 feet thick, differing in both composition and grain size. Mafic layers and lenses, which impart a gneissic texture locally, may be variously quartz diorite, gabbro or amphibolite containing labradorite plagioclase, augite and diopside. Within the predominant diorite and granodiorite

phases of the complex, plagioclase is andesine (An_{28} - An_{38}) and shows limited normal zoning. Minor amounts of quartz and pink orthoclase are interstitial to plagioclase, poikilitic brown biotite and green hornblende. Accessory minerals include magnetite, sphene and pyrite. Rocks of the Simon Bay complex are commonly fresh but may be strongly sheared and altered locally, with the development of chlorite, epidote and iron oxides. Actinolite and scapolite have been reported by Carr (1965, p. 118). Modal analyses are given in Table 3-4 and Fig. 3-5.

STRUCTURAL RELATIONS AND AGE:

Foliation, as defined by alignment of mafic minerals, textural and compositional layering, and trains of inclusions, is apparently of primary origin in all exposures of Simon Bay dioritic rocks. In the northern part of the area foliation is parallel to the trend of the Topley Batholith, in general: northwest at Alf and Deserter Lakes, and westnorthwest to east-west at Simon Bay. The divergence of foliation directions from the regional trend in southern exposures, i.e. north-northeast at Mudhole Lake and westnorthwest to east-west near Nithi Mountain, may be due to rotating or shifting of large blocks during emplacement of younger intrusions as suggested by Bright (1967, p. 22), or may simply represent local fabric variations within the pluton. Large lenses of gabbro and amphibolite at Simon Bay may represent partial assimilation or granitization of screens of older volcanic and sedimentary rocks in a mesozonal environment of emplacement.
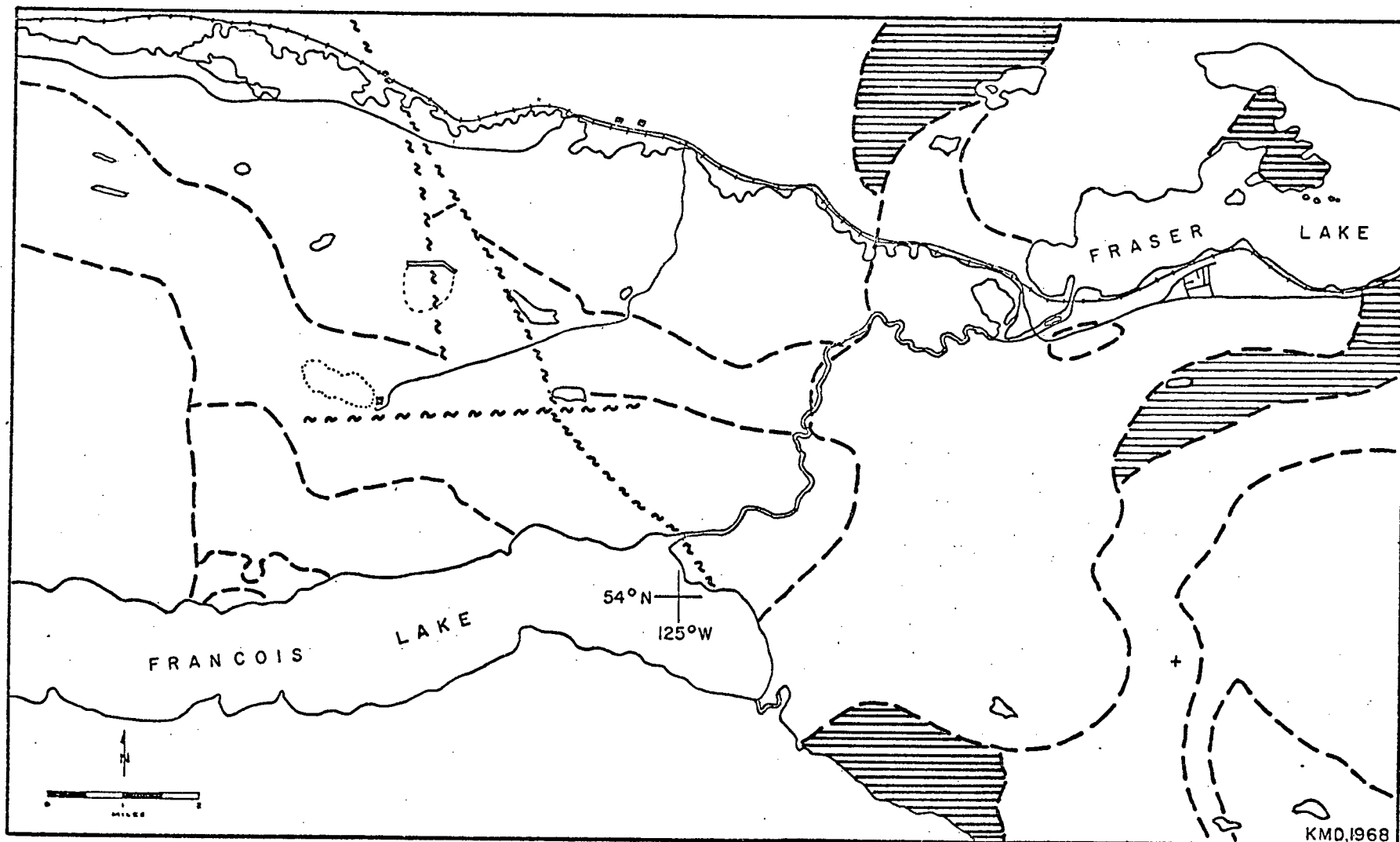
FIGURE 3-4

REGIONAL DISTRIBUTION OF SIMON BAY DIORITE COMPLEX

FRASER LAKE

FRANCOIS LAKE

54°N
125°W

KMD,1968

48.

Simon Bay diorite contacts with Stellako Intrusions were
observed on the north shore of Fraser Lake and near Mudhole
Lake. Adjacent to contacts in both localities, small aplite,
feldspar porphyry and basalt dykes cut both units and minor
K-feldspar alteration follows fractures in diorite. Diorite
contacts with other Topley units were not observed in the
field. Contacts with Glenannan and Nithi quartz monzonites
are inferred east of Endako and on the northern and southern
flanks of Nithi Mountain. Andesitic flows of the Endako
Group overlie foliated diorite at Simon Bay.

The Simon Bay diorite complex is apparently the oldest Topley
unit in the area, and possibly the earliest phase of the
batholith. A potassium-argon radiometric date obtained from
"diorite" at Shass (Grizzly) Mountain south of Stuart Lake
gives an age of 178 million years, or Lower Jurassic (Leech
et al, 1963, pp. 134-136). Another radiometric date obtained
from "granite" near Fort Fraser (54°04' N, 124°41' W) gives
an age of 163 million years, or Middle Jurassic (Baadsgaard,
et al, 1961, pp. 689-702). Field evidence cited in follow-
ing sections indicates Simon Bay diorite is older than the
Upper Jurassic Topley units in Endako area. If Simon Bay
diorite is the earliest phase of the batholith, it would then
be of similar age or younger than the Lower Jurassic members
of the Takla Group which it intrudes (Tipper, 1963, p. 41).

The Lower Jurassic radiometric ages do not agree with more
recent ages obtained from five Simon Bay diorite specimens

in the Endako area by White, et al (1970). Three diorites
yield identical 155 m.y. ages, and where diorite is intruded
by pegmatite, discordant ages of 145 and 138 m.y. are
obtained. The recorded position of Baadsgaard's (1961) 163
m.y. sample is within the limits of the Simon Bay Diorite
Complex. A Middle rather than Lower Jurassic maximum age of
the Topley Intrusions is favoured by White's age determina-
tions.

(ii) <u>Endako Quartz Monzonite</u>:

Endako Quartz Monzonite forms a regular, two-mile-wide belt
containing Endako mine and extending from Stellako River west-
northwestward for 12 miles across the map-area (Fig. 3-6).
Boundaries of the belt are formed by younger intrusions, namely
Francois Granite on the south, Casey Alaskite on the north and
Stellako Quartz Monzonite and granodiorite on the east. Three
miles northwest of Savory Lake, near Sheskwa Lake, Carr (1966,
p. 118) reports a small isolated body of sheared and altered
Endako Quartz Monzonite within Casey Alaskite. Endako Group vol-
canic rocks overlie the southwestern part of the belt at Savory
Ridge.

Typical Endako Quartz Monzonite is a pink or pinkish-gray,
medium-grained hypidiomorphic granular to subporphyritic rock.
Subhedral pale pink to orange phenocrysts of perthitic orthoclase
locally attain 1 cm in length but are more commonly 5 to 7 mm
long. With decreasing size and abundance of phenocrysts the
quartz monzonite becomes an essentially equigranular rock with

Table 3-4

Modal Analyses of Simon Bay Diorite Complex

| | Gabbro | Diorite | | | | | Granodiorite | | |
	1	1	1	2	500	585	579	582	3
Plagioclase[4]	69.1	62.5	40.8	59.5	59	62	61	52	46
Hornblende	-	2.2	49.7	31.1	16	16	9	18	6
Orthoclase	-	-	-	-	12	9	10	14	20
Biotite	-	33.3	6.1	2.1	5	5	5	-	6
Quartz	-	tr.	1.0	4.0	6	5	12	13	20
Magnetite	-	1.5	2.5	2.2	2	3	3	3	2
Augite	29.1	-	-	-	-	-	-	-	-

1. Armstrong, 1949.

2. Bright, 1967, p. 19 (point counter and stained-slab)

3. Carr, 1966, p. 124 (visual estimation)

4. Plagioclase composition ranges from An_{28} to An_{38} (excluding gabbro)

500, 579, 582, 585. Dawson (point counter and stained-slab)

FIGURE 3-5

Simon Bay Diorite Complex Modes

Armstrong specimen   °   Dawson specimen   +
Bright specimen   O   Average mode   □
Carr specimen   X
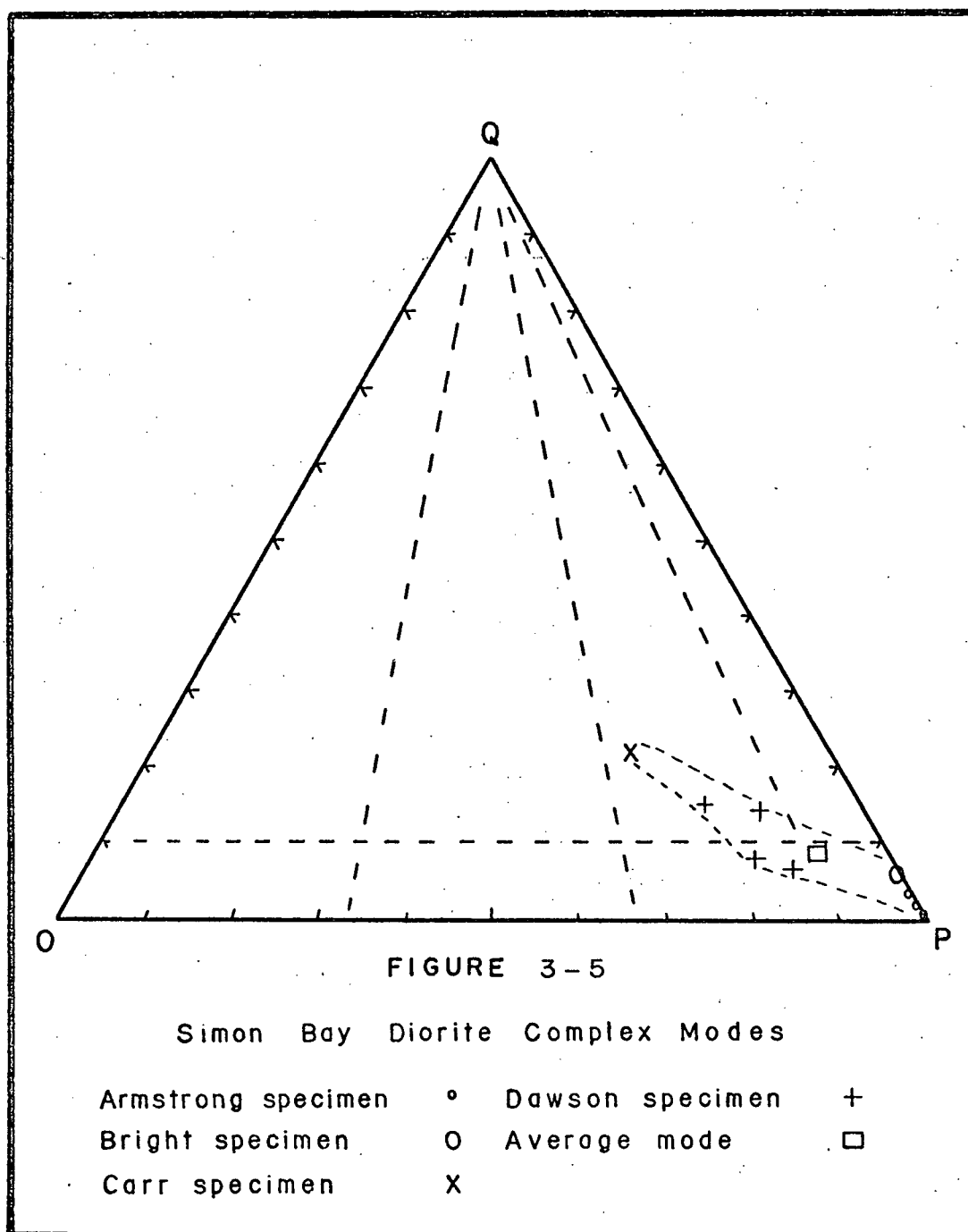
crystals of orthoclase, quartz, biotite and minor hornblende interstitial to oligoclase. Exposures near the Francois Granite contact south and southeast of the mine are finer-grained than average, and approach granite in composition.

Irregular grain boundaries of orthoclase are commonly myrmekitic adjacent to corroded plagioclase grains, and may be graphically intergrown with quartz in finer-grained rocks. Euhedral to subhedral white plagioclase grains generally show weak normal zoning, emphasized by preferential argillic alteration of calcic cores. Hexagonal plates and irregular clusters of partially chloritized brown biotite enclose grains of sphene, apatite, magnetite and brown hornblende. Fine-grained pale brown to green secondary biotite forms veins and rims associated with primary mafic minerals, along with carbonate and minor epidote. Quartz occurs as anhedral grains enclosing plagioclase, mafic and accessory minerals, or as granular phenocrystic aggregates. Minor accessory minerals include pyrite, rutile and zircon.

Modal analyses of Endako Quartz Monzonite are given in Table 3-5 and Fig. 3-7. Details of alteration, mineralization and structure of Endako Quartz Monzonite at Endako mine are dealt with in subsequent sections.

STRUCTURAL RELATIONS AND AGE:

Contacts of Endako Quartz Monzonite with younger intrusions to the north, south and east are described under "Casey
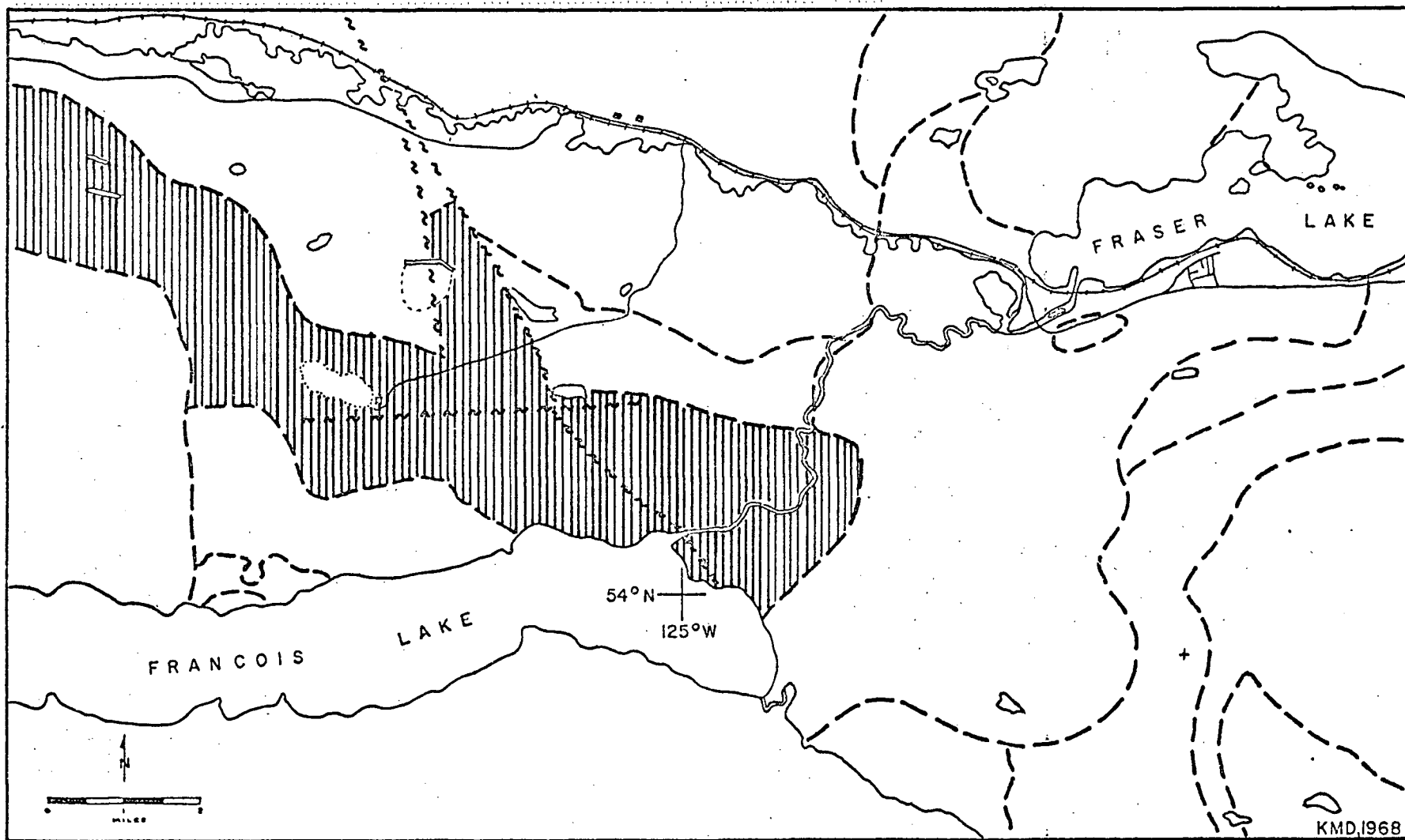
FIGURE 3-6

REGIONAL DISTRIBUTION OF ENDAKO QUARTZ MONZONITE

Alaskite", "Francois Granite" and "Stellako Quartz Monzonite

and Granodiorite" respectively. The Casey-Endako contact is

well defined over most of its length in outcrops, trenches

and diamond-drill core. Sheared Endako Quartz Monzonite is

intruded by a large, northeast-trending diorite dyke imme-

diately south of a chilled Casey Alaskite contact in a small

canyon west of Savory Lake. A similar relationship was noted

in Tailings Creek canyon where a Casey-Endako contact has

been intruded by a large northeast-trending diorite dyke

prior to displacement as a unit 8500 feet northward along

Tailings Creek fault. West of Oval Lake a quartz vein two

feet wide containing minor molybdenite occupies a N 15° E

fracture zone south of a contact between Endako Quartz Mon-

zonite and chilled porphyritic Casey Alaskite which trends

east-west.

North of Endako orebody, Casey Alaskite is fine-grained,

intruded by pegmatite dykes and veined with barren quartz.

Endako Quartz Monzonite contact with porphyritic alaskite is

observed in diamond-drill hole J-1. A large Casey porphyry

dyke trends southwestward from alaskite into Endako Quartz

Monzonite.

The Casey-Endako contact is inferred from MacDonald Lake

2-1/2 miles eastward to Stellako River. In Stellako River

canyon the Endako Quartz Monzonite contact with porphyritic

Casey Alaskite is intruded by orthoclase-plagioclase porphyry

dykes on the west bank, and by Stellako Quartz Monzonite on

the east bank.

A wedge of Endako Quartz Monzonite approximately one mile wide and 2-1/2 miles long has been displaced northward on two major faults, the Casey Lake fault and the Tailings Creek fault, dividing the elongate body of Casey Alaskite in half. A discussion of this structure is given under "Regional Structure".

Contacts of Endako Quartz Monzonite with older Simon Bay Diorite Complex were not observed. Foliation in diorite south of Mary Lake oriented N 70° W and N 85° W is parallel to a hypothetical extension of southern contact of Endako Quartz Monzonite. Emplacement of Endako Quartz Monzonite may have been concordant with a pre-existing west-northwest grain in older diorite complex.

Evidence of foliation in Endako Quartz Monzonite is almost non-existant. Minor northerly planar orientation of relatively abundant xenoliths was observed along west bank of Stellako River by Bright (1967, p. 24). Fine-grained quartz diorite xenoliths rich in biotite are common throughout the unit but in no other location exhibit foliation or local concentration. Xenoliths are rounded, one-to two-inch diameter bodies with resorbed outlines, and are of unknown origin.

Endako Quartz Monzonite has petrological, compositional and structural similarities with Nithi quartz monzonite indicative of either a similar origin or original continuity of the two units (see pp. 63-65).

A new phase of Topley plutonism, the compositionally-zoned Glenannan complex probably was confined during emplacement by the belt of older Endako Quartz Monzonite on the south. Casey Alaskite apparently has intruded the contact between Endako and Glenannan rocks. A unit similar in age and origin, the Francois Granite, intruded the contact between Endako Quartz Monzonite and Takla Group rocks at the southern edge of the batholith. Casey Alaskite and older units have been cut by a discordant, northward-trending belt of Stellako Quartz Monzonite and Granodiorite.

Structural relations indicate Endako Quartz Monzonite is one of the oldest members of Topley Intrusions in Endako area, preceded only by Simon Bay Diorite Complex of Middle Jurassic age.

White, et al (1968) have obtained the following potassium-argon ages from widely-spaced specimens of Endako Quartz Monzonite: 140 $\pm$ 6, 141 $\pm$ 5, 143 $\pm$ 6 m.y.

Table 3-5

Modal Analyses of Endako Quartz Monzonite

	ETK,ADD°	ADD+	EGB-4*	EGB-5*	EGB-14*	EN-174*	EGB-11*	EN-175*	EN-Stella*	EN-5*	EN-173*	S9-607	S11-109	S1-279	S25-459	S32-47.5	89	294	378	252	530	U1-215	S104-230B	S261-318	S99-184
Orthoclase	40	35	54.9	51.1	50.1	40.8	43.3	45.9	46.9	43.0	34.7	43	43	30	48	48	52	38	51	48	50	46	43	44	44
Plagioclase	20	30	25.9	31.1	28.4	36.4	28.6	26.6	4.6	18.0	41.9	19	31	34	24	26	23	31	22	23	25	27	29	27	26
Quartz	30	30	14.5	14.3	14.7	16.6	21.6	17.7	40.3	32.0	15.4	33	19	28	24	21	19	26	20	23	17	22	21	21	24
Biotite	10	5	2.2	1.0	3.0	4.0	2.5	3.5	7.1	4.0	4.5	4	6	6	3	4	5	4	5	4	6	4	6	6	4
Hornblende	0	0	1.3	0.4	2.0	1.0	0.8	2.0	0.5	1.0	2.0	.2	0	.1	0	0	.1	0	0	0	0	0	0	0	0
Magnetite	0	0	0.5	1.0	1.2	1.8	0.6	1.5	1.0	1.0	1.0	.5	1	1	1	1	1	1	1	2	1	1	.3	1	1
Sphene	0	0	0.8	0	0	1.3	0.5	1.2	0	0	0.5	.2	.1	.1	.1	.2	0	0	1	.1	1	.1	.4	.5	.6

1. Calculated average mode: orthoclase 44.5%; plagioclase 26.3%; quartz 22.6%; biotite 4.6%; hornblende 0.5%; accessories 2.0%.

2. Average composition of plagioclase is An_{19}. Composition ranges from An_{11} to An_{26}.

3. Modal analyses by other authors: [o]Kimura and Drummond, 1966 (visual estimation)
    +Drummond, 1967 (visual estimation)
    *Bright, 1967 (point counter and stained slab)

FIGURE 3 — 7

Endako Quartz Monzonite Modes

Bright specimen   O   Drummond specimen   △
Dawson specimen   +   Average mode   □
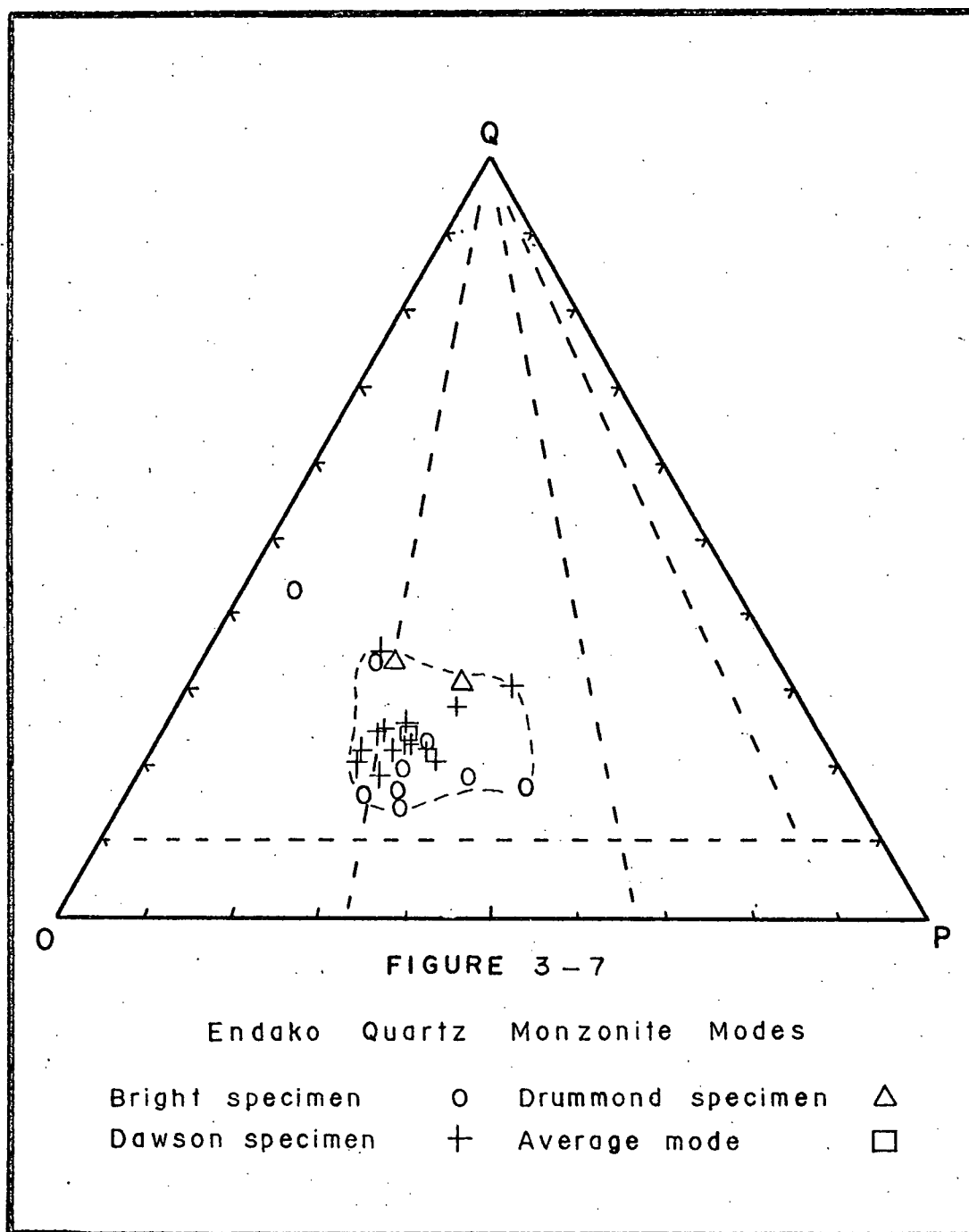
(iii)   <u>Nithi Quartz Monzonite</u>:

Exposures of Nithi Quartz Monzonite on the summit and slopes of Nithi Mountain probably comprised a continuous body extending more than two miles east of the map-area prior to being separated into several outcrop areas by emplacement of a younger intrusive phase, Casey Alaskite. Nithi Quartz Monzonite is truncated by Stellako Quartz Monzonite and Granodiorite on the west, and unconformably overlain by Endako Group volcanic rocks east of Foster Lakes, 2-1/2 miles east of the map-area (Fig. 3-8).

The quartz monzonite unit consists of a medium-grained subporphyritic variety and a coarser-grained porphyritic variety which appear intergradational and occur alternately without an obvious pattern. No concentration of porphyritic quartz monzonite along an inferred western margin was seen.

The more abundant medium-grained variety of Nithi Quartz Monzonite is a pink to gray, inconspicuously porphyritic rock with subhedral to anhedral enterlocking feldspar crystals and aggregates of rounded quartz grains. Perthitic microcline commonly is intergrown with quartz along grain boundaries in a subgraphic texture similar to Endako Quartz Monzonite. White oligoclase shows strong oscillatory normal zoning and kaolinized cores. Relatively abundant small plates of biotite predominate over prismatic green hornblende. Modal analyses of Nithi Quartz Monzonite are given in Table 3-6 and Fig. 3-9.
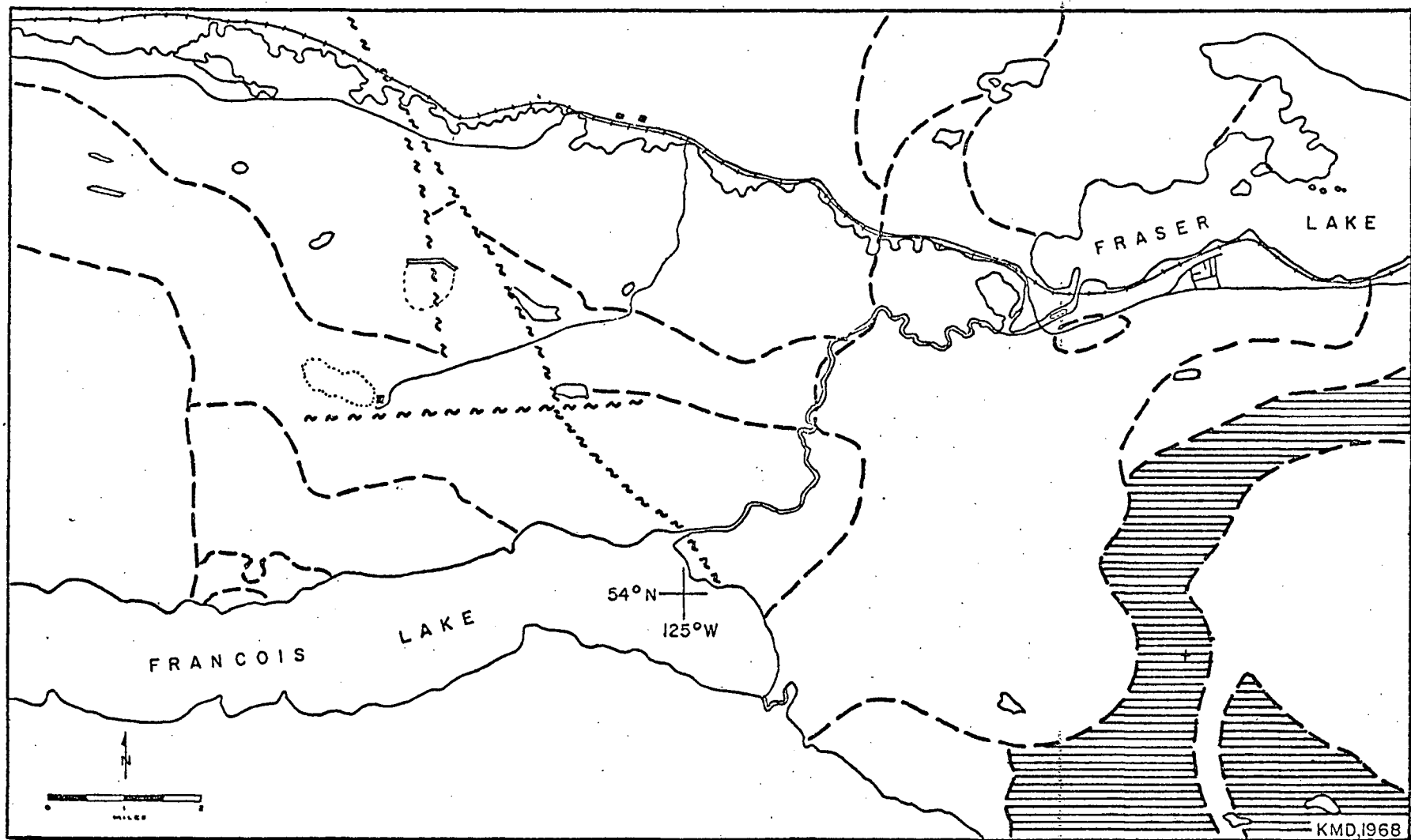
FIGURE 3-8

REGIONAL DISTRIBUTION OF NITHI QUARTZ MONZONITE

Porphyritic variety of Nithi quartz monzonite is distinguished by pink microcline phenocrysts up to 2 cm long, intergrown at margins and enclosing smaller crystals of other minerals. Subhedral plagioclase and rounded quartz grains are 5 to 7 mm in size. Aligned phenocrysts define a weak northwest-striking foliation north of Nithi Mountain summit. Small, dark inclusions, similar to those found in Endako Quartz Monzonite are found throughout the unit.

ALTERATION:

In general, Nithi Quartz Monzonite underlying the entire summit area of Nithi Mountain shows some degree of alteration and mineralization. Drummond, in a study of geology and mineral potential of Nithi Mountain area (1966e, p. 4) classifies alteration features into three groups:

1. K-feldspar envelopes are developed locally on some quartz-molybdenite and/or quartz-molybdenite-pyrite veins.

2. Quartz-sericite-pyrite envelopes up to 2 feet thick surround quartz-pyrite veins, and appear to be more abundant than K-feldspar envelopes.

3. Pervasive kaolinization of feldspars varies from weak (plagioclase cores altered) to intense (plagioclase destroyed and primary K-feldspar attacked).

Drummond (Ibid.) notes a similarity of host rock and correlation of alteration types between Nithi Quartz Monzonite

and Endako Quartz Monzonite at Endako mine.

MINERALIZATION:

Sulphides at Nithi Mountain appear identical to those at Endako mine but degrees of alteration and mineralization differ. Large molybdenite-bearing quartz veins are rare at Nithi. Quartz-molybdenite, quartz-molybdenite-pyrite, quartz-pyrite and quartz-hematite veins occur in Nithi Quartz Monzonite, aplite and porphyry dykes, and to a lesser extent in adjacent Casey Alaskite. The most prominent orientation of quartz veining in the area is 070/90. Joints and minor shears strike between northeast and east. Mineral deposition appears to have been controlled by the intersection of the above structures with faults and fractures that strike northwest.

STRUCTURAL RELATIONS AND AGE:

Systematic textural variations indicative of marginal facies of a pluton are absent in exposures of Nithi Quartz Monzonite. Rare phenocrysts are distributed in an apparently random manner; foliation, where present, is vague; and no chilled phases were detected. Absence of these structures in exposures on flanks of Nithi Mountain suggests the original pluton extended a considerable distance westward of its presently-defined contact.

Nithi Quartz Monzonite is truncated on the west by younger Stellako intrusions. The elongate Endako Quartz Monzonite

body, separated from Nithi Mountain by 4 miles of heavily
drift-covered ground with sparse Stellako exposures, is
similarly truncated at its eastern extremity by Stellako
rocks. External structural relations of Endako and Nithi
quartz monzonites support the view that the units formed a
continuous west-northwest trending body prior to emplacement
of Stellako intrusions.

Although apparent relationships between Endako and Nithi
quartz monzonites are evident, subtle differences in minero-
logy and texture necessitate mapping as distinct units. An
Ab-Or-SiO$_2$ ternary plot of Endako and Nithi modes (Fig. 3-21)
shows the units to be of similar feldspathic composition,
and Nithi Quartz Monzonite to have the higher average quartz
content. Relationship between the two bodies may be one of
the following:

1. A gradational change along the strike of a proposed,
   originally continuous west-northwest trending body; or

2. Two generations of magma from the same source, emplaced
   within the same structural zone as separate units, and
   their hypothetical contact later intruded by a northward-
   trending belt of quartz monzonite and granodiorite.

A minimum Late Upper Jurassic or pre-Casey Alaskite age of
Nithi Quartz Monzonite is indicated by abundant contacts with
the younger unit in exposures and diamond-drill core at Nithi
Mountain. Intrusive contacts with Simon Bay diorite at Mary

and Mudhole Lakes are inferred. An age of emplacement
similar to that of Endako Quartz Monzonite is implicit in
the foregoing discussion of relations between the units,
i.e. Late Jurassic. Radiometric dating of two Nithi Quartz
Monzonite specimens from the northern and southern flanks of
Nithi Mountain by White (et al, 1970) yields ages of 141 and
138 million years, respectively. These radiometric dates
confirm that the Nithi and Endako Quartz Monzonites are
essentially the same age. Nithi Quartz Monzonite, on the
basis of a higher quartz content, is considered the younger
of the two units.

(iv) Glenannan Granite and Quartz Monzonite:

Glenannan Granite and Quartz Monzonite, which underlies a
17-square-mile area centred on the town of Endako, may represent
the southern extremity of a large composite body extending more
than 8 miles northwest of the map-area (Fig. 3-10). Bright (1967,
p. 46) has defined the "Glenannan Complex" to include northern
units mapped by Carr as Tatin, Titan, Triangle and Rex quartz
monzonites (1966, pp. 120-122), as well as Glenannan Granite and
Quartz Monzonite and Nithi Quartz Monzonite in the south. Bright
notes that units within Glennanan Complex have certain common
mineralogical and textural features, notably ubiquitous perthite
megacrysts, and apparently exhibit gradational compositional
change from marginal glomeroporphyritic granite through quartz
monzonite to granodiorite. An hypothesis involving successive
intrusions from a differentiating parental granodiorite magma,

Table 3-6

Modal Analyses of Nithi Quartz Monzonite

	Microcline	Plagioclase[1]	Quartz	Biotite	Hornblende	Magnetite
J.M.C.[2]	21	35	35	7	1	1
J.M.C.[2]	30	23	40	6	1	tr
A.D.D.[3]	30	30	35	5	–	–
468[4]	35	39	20	5	1	tr
473[4]	35	37	22	5	1	tr
N5-79[4]	38	32	26	3	1	–
N7-314[4]	42	32	23	3	tr	tr
N14-700[4]	39	30	26	4	1	–
N13-15[4]	36	28	29	6	1	tr

1. Plagioclase composition An_{22} to An_{28}

2. J.M. Carr, 1966, pp. 119-120 (visual estimation)

3. A.D. Drummond, 1966e, p. 2 (visual estimation)

4. K.M. Dawson (point counter and stained slab)

FIGURE 3-9

Nithi Quartz Monzonite Modes

Carr specimen   X   Drummond specimen   △

Dawson specimen   +   Average mode   □
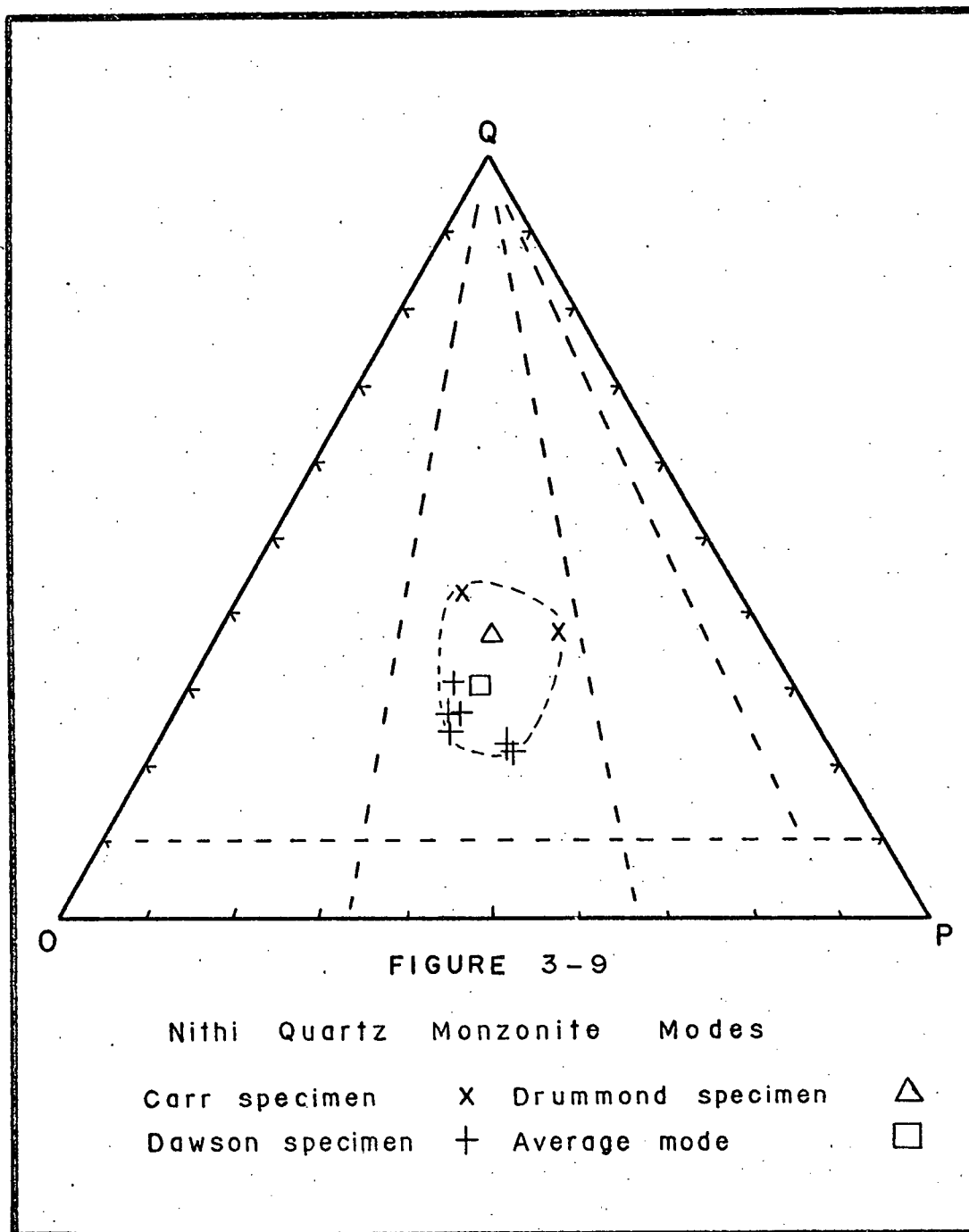
with some wall rock assimilation, resulting in a zoned complex is put forth (Bright, 1967, pp. 77-84).

In Endako area Glenannan Granite and Quartz Monzonite are fresh, pink and white, coarse-grained and commonly conspicuously porphyritic. A gradational change from granite bordering Casey Alaskite northward to quartz monzonite along Highway 16 is marked by a slight increase in plagioclase and hornblende and a decrease in perthitic microcline phenocrysts. In granite, pink microcline phenocrysts may attain a length of 4 cm whereas rounded quartz and white subhedral plagioclase grains are commonly 5 to 7 mm in size. Grain boundaries are well-defined in general, with minor myrmekitic intergrowths along microcline-oligoclase boundaries visible in thin-section. Thick books of brown biotite enclose minor amounts of green hornblende prisms and accessory magnetite, apetite and sphene. Traces of allanite (cerian epidote) are reported by Bright (1967, p. 56). Glenannan quartz monzonite shows a minor textural variation from associated granite in less well-defined boundaries of microcline phenocrysts and tendency of microcline to poikilitically enclose plagioclase and quartz crystals. Glenannan modal analyses are given in Table 3-7 and Fig. 3-11.

Similarities between Glenannan rocks and Nithi Quartz Monzonite were noted by Carr (1966, p. 120). Bright redefined Nithi Quartz Monzonite as a phase of the "Glenannan Complex" (1967, p. 47). The similarity of the two units appears to lie mainly in a superficial resemblance of coarse-grained pink and white feldspars
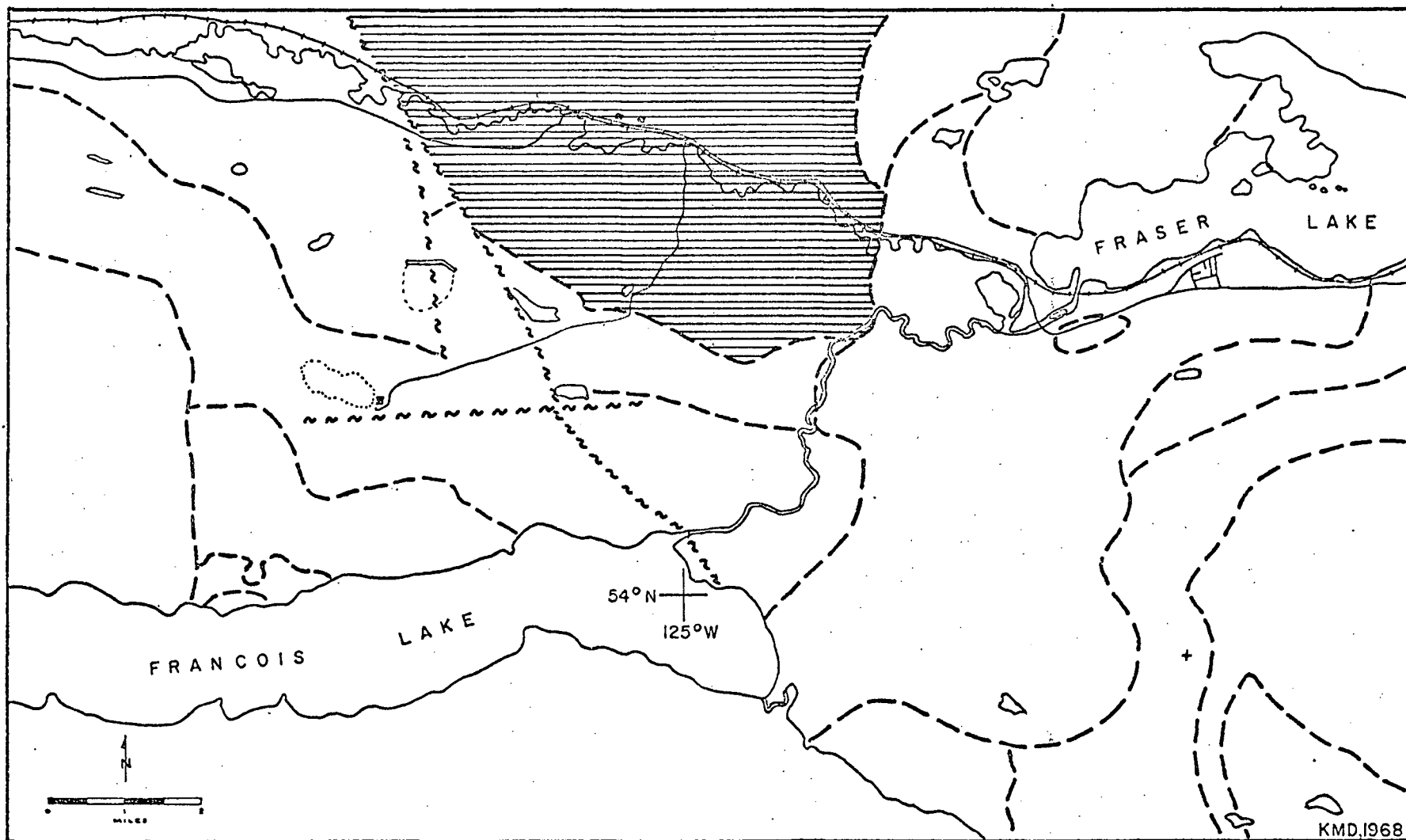
FIGURE 3-10

REGIONAL DISTRIBUTION OF GLENANNAN GRANITE

AND QUARTZ MONZONITE

and is offset by the following dissimilarities:

1. Microcline phenocrysts in Nithi Quartz Monzonite are smaller, less abundant even in strongly porphyritic phases, and have less well-defined margins than those in Glenannan intrusives.

2. In all textural variations of Nithi Quartz Monzonite plagioclase and microcline occur as irregular, subhedral to anhedral interlocking grains compared to the dominant inequigranular texture of Glenannan rocks.

3. Nithi quartz monzonite is predominantly a medium-grained, subporphyritic, relatively biotite-rich rock bearing stronger resemblance to Endako quartz monzonite than to any phase of Glenannan intrusions.

STRUCTURAL RELATIONS AND AGE:

Glenannan Granite is intruded by Casey Alaskite along a well-defined contact which trends northwest from Stellako River to Casey Lake fault. Glenannan Granite is truncated on the west by a wedge of Endako Quartz Monzonite and Casey Alaskite that has been displaced northward along the Casey Lake fault. To the east contacts with Simon Bay diorite and Stellako Quartz Monzonite are inferred. No chilling of Glenannan Granite was evident adjacent to observed or inferred contacts. Casey Alaskite is chilled against Glenannan granite in diamond-drill holes northeast of Tailings Pond and east of Glenannan Road, and has partially assimilated Glenannan Granite in a 20-foot-wide hybrid zone east of Casey Lake.

Limited foliation within Glenannan intrusions, as defined by crude alignment of microcline phenocrysts, tends to follow the regional northwest to west-northwest Topley trend rather than the sinuosities of adjacent Casey Alaskite contacts, hence may be primary in origin. The southern extremity of Glenannan pluton was probably controlled during emplacement by an older belt of Endako Quartz Monzonite. A zone of weakness along their mutual contact was later intruded by Casey Alaskite. The general southeast trend of Glenannan pluton was apparently terminated against an older Simon Bay Diorite body to the east. Contact between these units was later intruded by a north-northeast trending belt of Stellako quartz monzonite and granodiorite.

Structural relations indicate a post-Endako Quartz Monzonite, pre-Casey Alaskite age of Glenannan emplacement. Endako and Casey units yield similar Late Jurassic radiometric ages (White, et al, 1968), therefore closely bracket Glenannan emplacement in Late Jurassic time. White, et al (1970) obtained the following potassium-argon ages for Glenannan "Quartz Monzonites": 134 $\pm$ 5, 135 $\pm$ 5, 140 $\pm$ 6 m.y. A spread in ages between the younger pegmatitic samples and the older quartz monzonite may represent a period of differentiation of the Glenannan magma.

Table 3-7

Modal Analyses of Glenannan Granite and Quartz Monzonite

Granite

Speci-men	Micro-cline[1]	Plagio-clase[2]	Quartz	Bio-tite	Horn-blende	Magne-tite	Sphene	Apatite
ADD[3]	55	15	25	5	-	-	-	-
EGB-1[4]	70.1	11.2	17.1	1.0	0.3	0.4	0.5	tr
EGB-2[4]	55.0	25.0	20.0	2.0	1.0	0.5	tr	tr
EGB-169[4]	55.5	14.3	27.7	2.3	0.5	0.6	tr	tr
EN-171[4]	55.8	25.3	17.2	1.6	0.7	1.5	0.4	tr
EN-168[4]	51.9	25.0	17.7	2.8	1.3	1.0	0.8	0.3
P4-100[5]	41	14	43	1	-	0.5	0.2	0.3
534[5]	50	23	21	4	0.2	1.0	0.6	0.2
416[5]	54	20	23	2	-	0.7	0.2	0.1
376[5]	45	30	22	2	-	0.3	0.6	0.1
427[5]	48	22	25	3	-	1.5	0.1	0.4

Quartz Monzonite

EGB-8[4]	41.4	35.5	14.7	3.5	1.8	1.2	1.4	0.3
EN-170[4]	46.5	32.6	16.3	3.0	1.2	1.0	0.5	tr
EGB-12[4]	42.0	30.0	26.0	2.0	1.0	tr	tr	tr
531[5]	39	31	23	5	0.2	1	0.5	0.3

1. Alkali feldspar composition Or_{90}-Or_{95} in granite and Or_{85}-Or_{88} in quartz monzonite and granodiorite (Bright, 1967, p. 12).

2. Plagioclase composition ranges An_{22} to An_{29}.

3. A.D. Drummond, 1966a, p. 3 (visual estimation)

4. E.G. Bright, 1967, p. 49 (point counter and stained slab)

5. K.M. Dawson (point counter and stained slab)

FIGURE 3-11

Glenannan Quartz Monzonite and Granite Modes

Bright specimen   O   Drummond specimen   △
Dawson specimen   +   Average mode   □
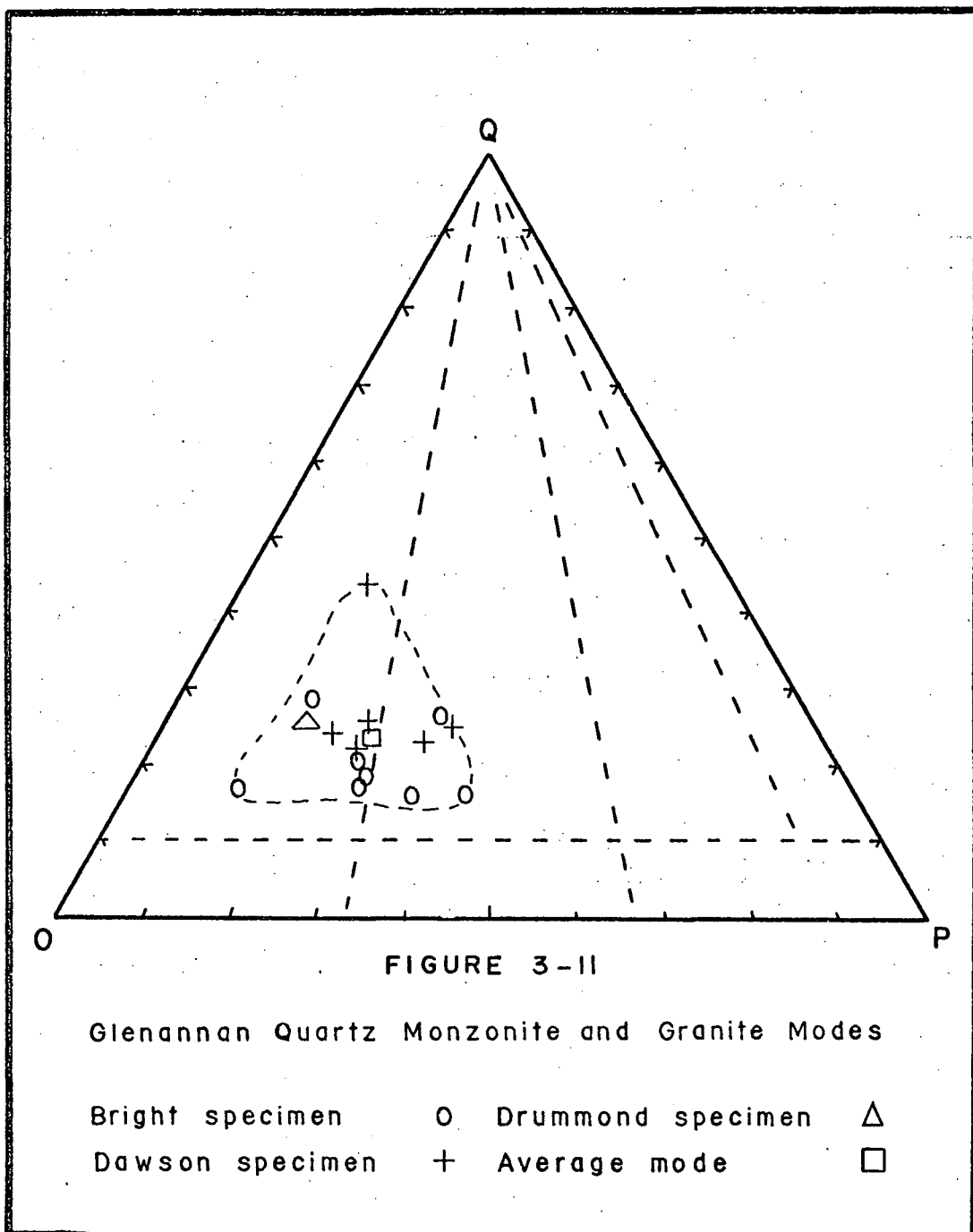
(v) <u>Casey Alaskite</u>:

Casey Alaskite is dominantly a fine- to medium-grained pink
or buff leucocratic granite with minor amounts of medium- to
coarse-grained porphyritic phases that grade to quartz monzonite.
The main body of Casey Alaskite lies outside the map-area to the
north of Savory Lake, from which large dyke-like bodies extend
eastward around Tatin Lake and east-southeast across Endako area
to Stellako River. A second large arcuate body of Casey Alaskite
underlies the eastern flanks of Nithi Mountain from which a 1500-
foot-wide dyke extends southward to Nithi River (Fig. 3-12).

Although the Casey Alaskite unit as a whole is non-uniform
in appearance due to varying grain size and degree of development
of phenocrysts, all varieties are characterized by inequigranular
texture, low biotite content, traces of muscovite and absence of
hornblende. The fine-grained phase of alaskite generally is
localized along margins of the bodies with a gradational change
inwards to coarse-grained variety. Fine-grained alaskite resembles
aplite with low biotite content (1-2%) and granophyric intergrowth
of quartz-microcline-oligoclase crystals. A chilled phase with
2 to 3 mm euhedral quartz phenocrysts in a granophyric groundmass
and associated pegmatite dykes occurs adjacent to contacts in
several localities. Medium-grained alaskite exhibits a more
granular, sugary texture with abundant aggregated rounded quartz
grains of characteristic greasy gray appearance. Coarse-grained
alaskite is a hypidiomorphic inequigranular rock with 5 to 8 mm
anhedral grains of perthitic microcline and quartz poikilitically

FRASER LAKE

54°N
125°W

FRANCOIS LAKE

KMD,1968
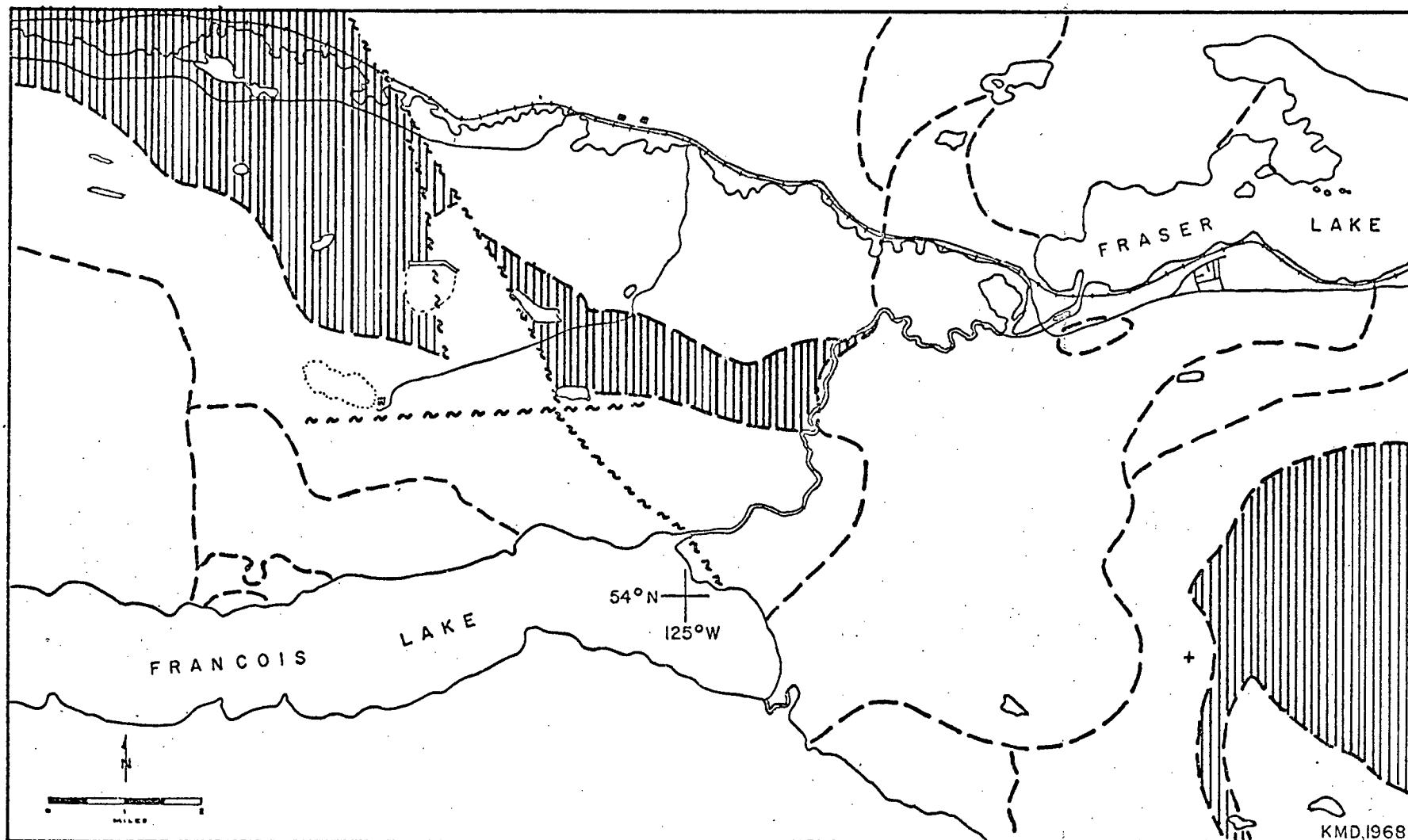
FIGURE 3-12

REGIONAL DISTRIBUTION OF CASEY ALASKITE

enclosing subhedral plagioclase and minor minerals. Phenocrysts

of microcline up to 1.5 cm long are abundant locally, and a bio-

tite content of 2 to 4% is slightly higher than in finer-grained

phases. Casey alaskite modal analyses are given in Table 3-8 and

Fig. 3-13.

Microcline in fine-grained alaskite is microperthitic, with

plagioclase comprising about 1% of the individual grains. In

coarse-grained phases plagioclase forms larger lamellae within

microcline and also occurs as marginal aggregates. Plagioclase

constitutes about 5 percent of coarse-grained perthite. Subhedral

oligoclase (An_{22}-An_{24}) grains have narrow unaltered rims, broad

sericitic and argillic cores, and show weak oscillatory zoning in

coarse-grained phases. Accessory minerals include apatite, mag-

netite and sphene. Allanite was reported by Bright (1967, p. 90).

STRUCTURAL RELATIONS AND AGE:

The main body of Casey Alaskite in Endako area is a large

satellite dyke 11 miles long and 1 to 2 miles wide extending

east-southeast from a stock north of Savory Lake. The

alaskite body has sharp intrusive contacts with Glenannan

Granite to the north and Endako Quartz Monzonite to the

south. Chilled contacts with Endako Quartz Monzonite occur

west of Savory Lake, west of Oval Lake and north of Endako

mine. In specimens from these localities, effects of shear-

ing are shown by deformed plagioclase and biotite grains,

and quartz with strong undulose extinction. A 20-foot-wide

zone of hybrid rock occurs at Glenannan-Casey contact east

of Casey Lake where large microcline, plagioclase and biotite
phenocrysts derived from Glenannan Granite wall rocks are
incorporated in a granophyric matrix. Small aplite and peg-
matite dykes are abundant adjacent to most alaskite contacts,
and Carr (1966, p. 123) noted miarolitic cavities near Tatin
Lake.

Casey porphyry dykes, in two cases exceeding 100 feet in
width, intrude host rocks adjacent to alaskite contacts.
The strongly porphyritic dykes contain phenocrysts of micro-
cline, quartz and plagioclase in an aplitic matrix, and are
compositionally similar to alaskite.

A stock of Casey Alaskite about 15 square miles in area
underlies the eastern flank of Nithi Mountain. Alaskite
shows well-defined contacts with Nithi Quartz Monzonite on
surface and in diamond-drill core, with a textural gradation
from fine-grained to medium- or coarse-grained inward from
contacts, and narrow chill zones. Outside the map-area, the
eastern boundary of Casey Alaskite stock is defined by a
contact with Nithi Quartz Monzonite south of Foster Lakes,
and both units are overlain by Endako Group volcanic rocks
east of Foster Lakes.

Emplacement of the Casey Alaskite satellite dyke apparently
has been controlled by a weakened zone along a pre-existing
west-northwest-trending Endako Quartz Monzonite-Glenannan
Granite contact. Continuity of the satellite dyke is dis-
rupted by a northward-displaced fault block of Endako Quartz

Table 3-8

Modal Analyses of Casey Alaskite

Granite

Speci-men	Micro-cline	Plagio-clase[1]	Quartz	Bio-tite	Muscovite	Magnetite	Accessories
ADD[2]	45	18	35	2	–	tr	tr
JMC[3]	40	25	33	2	–	–	–
EN-184[4]	52.0	11.0	37.0	tr	tr	tr	tr
EN-202[4]	45.3	20.1	33.1	1.5	–	tr	tr
EN-185[4]	40.0	25.0	33.0	1.0	tr	tr	tr
546[5]	46	23	29	2	–	–	tr
286[5]	51	17	31	1	tr	–	tr
311[5]	41	21	36	2	tr	–	tr
406[5]	45	18	35	2	tr	–	tr
480[5]	41	21	37	1	–	–	tr

Quartz Monzonite

Speci-men	Micro-cline	Plagio-clase[1]	Quartz	Bio-tite	Muscovite	Magnetite	Accessories
EN-186[4]	30	30	36	3	tr	1	–
495[5]	41	25	31	3	tr	tr	tr
299[5]	40	24	34	2	–	tr	tr

1. Plagioclase composition ranges An_{22} to An_{24}

2. A.D. Drummond, 1967, p. 6 (visual estimation)

3. J.M. Carr, 1966, p. 123 (visual estimation)

4. E.G. Bright, 1967, p. 87 (point counter and stained-slab)

5. K.M. Dawson, (point counter and stained slab)

FIGURE 3-13

Casey Alaskite Modes

Bright specimen   O   Drummond specimen   △

Carr specimen   X   Average mode   □

Dawson specimen   +
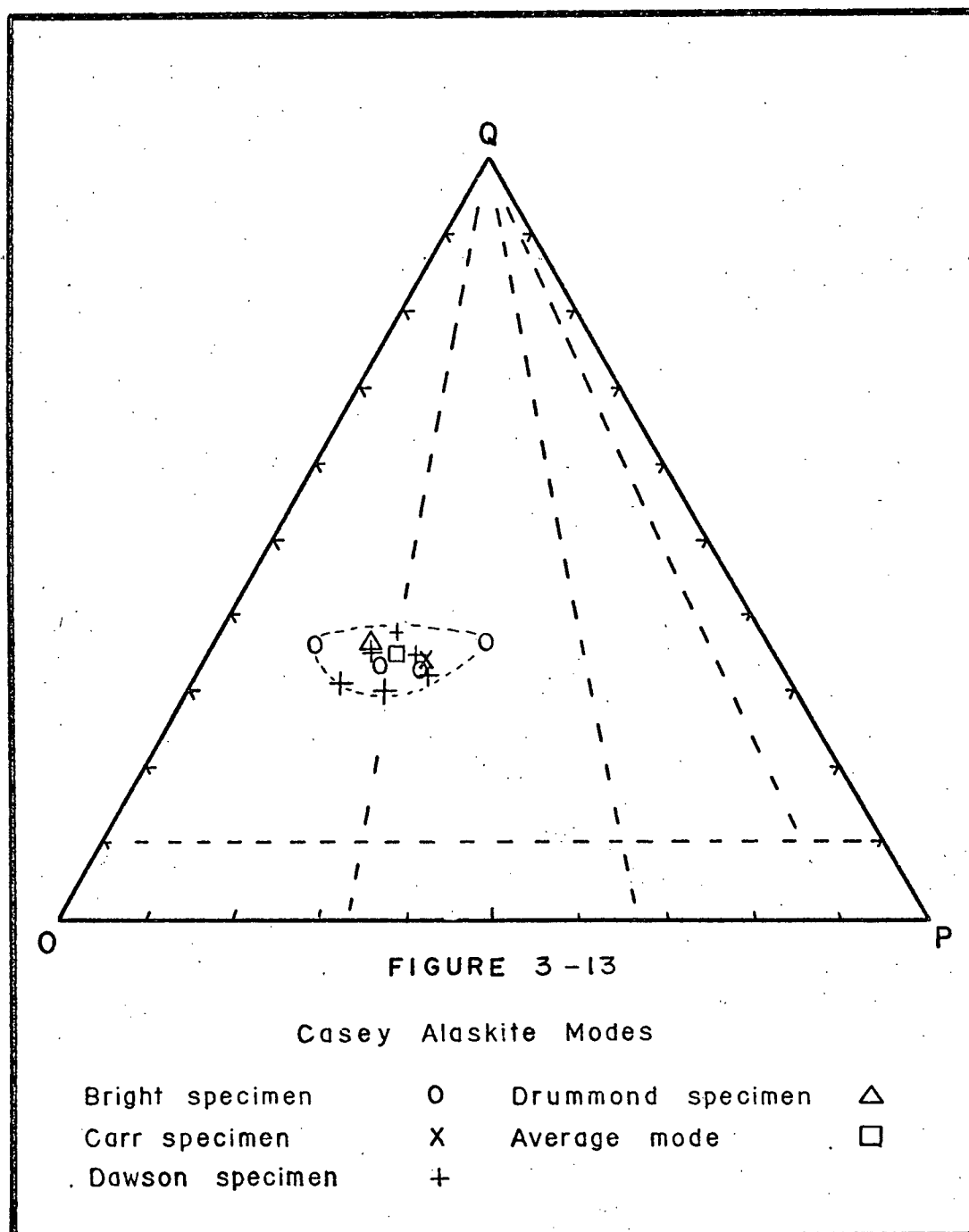
Monzonite and a north-northeast-trending belt of younger

Stellako intrusions. The central part of Nithi Quartz Mon-

zonite stock has been intruded by a smaller stock of Casey

Alaskite probably originally connected with the satellite

dyke at depth. Although Casey Alaskite exhibits some

assimilation of wall rocks; a general lack of xenoliths and

foliation and presence of chilled contacts and miarolitic

cavities indicate a high level of emplacement.

Structural relations show Casey Alaskite to be younger than

Endako, Nithi and Glenannan phases of Topley Intrusions, and

older than Stellako intrusions and Endako Group volcanic

rocks. The Late Jurassic age indicated by field relations is

verified by radiometric dating. Casey Alaskite from the

eastern shore of Casey Lake yields a potassium-argon age of

139 ± 5 million years (White, et al, 1968), and a specimen

located 3 miles northeast of the village of Endako yields an

age of 137 ± 6 million years (White, et al, 1970).

(vi) Francois Granite:

This unit forms the southwestern margin of the batholith,

where it underlies an irregular wedge-shaped area 4 miles long and

averaging 1-1/2 miles wide (Fig. 3-14). The granite body trends

west-northwestward from Francois Lake and is overlain partially by

Tertiary volcanic rocks to the west. Intrusive contacts with

Takla Group pyroclastic rocks on the south and Endako Quartz Mon-

zonite on the north are well defined.

The rock is typically a red, medium-grained, hypidiomorphic granular biotite granite. It is readily distinguished by its colour, lack of phenocrysts larger than 5 mm, "mottled" texture of poikilitic red microcline and greenish-white subhedral plagioclase, small quartz grains often graphically intergrown with microcline, low hornblende content and lack of foliation. Grain size is mainly 3 to 4 mm, with fine-grained weakly porphyritic chilled phases adjacent to Takla Group and Endako Quartz Monzonite contacts, and a slightly coarser-grained variety which grades locally to quartz monzonite along Francois Lake to the east.

Microperthitic microcline is either graphically intergrown with quartz in a granophyric texture in fine-grained phases óf˙the rock, or with quartz is interstitial to plagioclase in medium-grained rocks. Oligoclase is normally zoned with calcic cores altered to a light green argillic mixture of kaolinite, sericite and carbonate. Biotite is chloritized commonly and is associated with minor prismatic green hornblende and secondary yellow biotite. Also associated with biotite are the accessory minerals magnetite, sphene, apatite, pyrite and zircon with pleochroic halos. Modal analyses of Francois Granite are given in Table 3-9 and Fig. 3-15.

All minerals of Francois Granite show various stages of deuteric or hydrothermal alteration. Rocks near margins of the unit are most intensely altered and show a distinctive brick red colour due, in part, to fine-grained argillic alteration of feldspars and oxidation of iron ores.
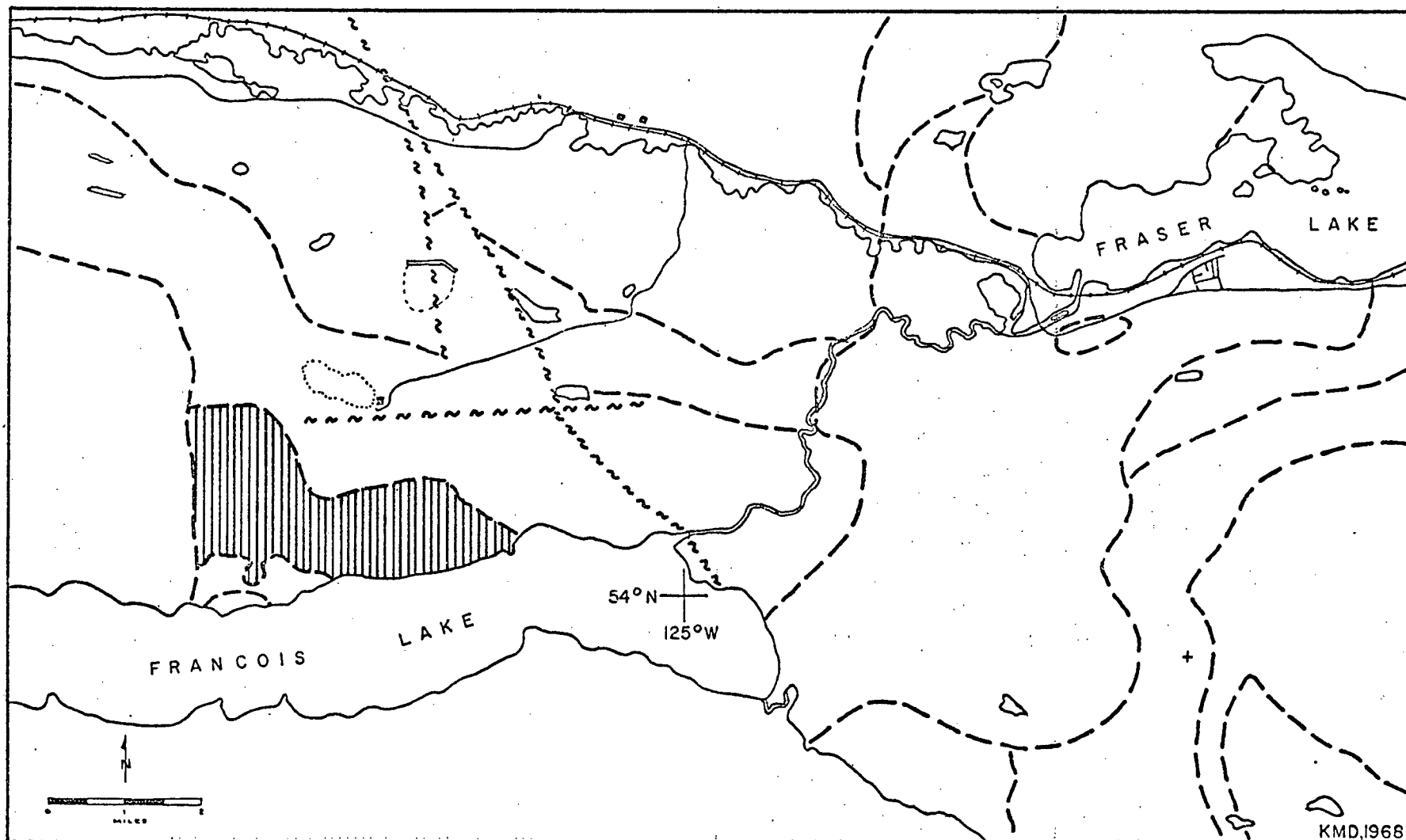
FIGURE 3-14

REGIONAL DISTRIBUTION OF FRANCOIS GRANITE

MINOR INTRUSIONS:

Two dyke rocks, porphyritic quartz monzonite and "rapakivi"
porphyry cut Francois Granite. The three units are similar
in composition and may be related genetically.

Porphyritic Quartz Monzonite:

Large quartz monzonite dykes that intrude Takla Group rocks
to the south strike northwestward towards adjacent Francois
Granite contact. Dykes are medium- to coarse-grained rocks
containing pink microperthitic microcline phenocrysts up to
2 cm long. Texture of the phaneritic matrix, with microcline
and quartz interstitial to oligoclase is not unlike that of
Francois Granite, although coarser-grained. These dykes
probably were emplaced into fractured wall rocks as a late
porphyritic phase of Francois magma, being similar in this
respect to Casey porphyry dykes to the north. Two small
equigranular quartz monzonite dykes which cut Endako quartz
monzonite adjacent to Francois granite contact southeast of
Endako mine are probably of similar origin.

"Rapakivi" Porphyry:

West of Endako mine, on Nu-Elk claims, dykes whose pheno-
crysts include pink orthoclase mantled by white plagioclase
have been called variously "QOP dykes" by Carr (1966, p. 128)
and "rapakivi porphyry" by Drummond (1966a, p. 4). The rock
contains quartz, orthoclase and plagioclase phenocrysts in
a reddish, aphanitic matrix, and resembles chilled Francois

Granite. A similar dyke in Francois Granite was noted two miles southwest of Endako mine on Utica Mines claims. Mantled K-feldspar grains have been reported in Francois Granite by Drummond, leading him to conclude that rapakivi porphyry is probably a dyke phase of Francois Granite (Ibid., pp. 2-4). Occurrence of this unique dyke cutting Endako Quartz Monzonite in diamond-drill holes U-1 and J-3 west of Endako mine has led to the interpretation of an inferred Francois Granite contact a short distance to the south.

STRUCTURAL RELATIONS AND AGE:

Weakly porphyritic Francois Granite is chilled, altered and occasionally sheared adjacent to its well-defined intrusive contact with Takla Group pyroclastic rocks. No thermal metamorphism of Takla rocks was detected.

Francois Granite-Endako Quartz Monzonite contact is sharply defined for 4000 feet in an area of good rock exposure southeast of Endako mine. Narrow chilled zones along the contact show small phenocrysts of plagioclase and quartz in a granophyric matrix. Aplite and pegmatite dykes are common in both units near the contact. Miarolitic cavities one inch in diameter lined with euhedral quartz crystals occur in fine-grained Francois Granite near a small lake south of the contact. Contacts to the east and west of this zone are largely inferred.

Francois Granite lacks foliation and contains small rounded inclusions similar to those in Endako Quartz Monzonite. Dominant attitudes of shearing, joints and dykes within the unit are west-northwest, north and northeast with steep dips to southwest, west and northwest.

Intrusive relations of Francois Granite with both Takla Group volcanic rocks and Endako Quartz Monzonite indicate a Late Jurassic or younger age. An inferred, unconformable contact with Endako Group flows sets a minimum age for the unit as Eocene. Radiometric dating of two specimens of Francois Granite by White, et al (1970) yielded identical ages of 137 million years. Francois Granite, by this evidence, is the same age as Casey Alaskite or slightly younger.

Francois Granite and Casey Alaskite are similar in some respects other than radiometric age. Both units are predominantly granitic in composition, differing in this respect from the predominantly quartz monzonitic composition of most other Topley units. The two plutons have in common several of Buddington's (1959, p. 674) epizonal criteria including discordant form, non-foliated texture, chilled granophyric margins and miarolytic cavities. Distinctive porphyry dykes that probably are related to each unit intrude host rocks near contact zones. Casey Alaskite and Francois Granite are elongate plutons that follow parallel west-northwest trends flanking Endako Quartz Monzonite on the north and south, respectively.

Similarities between the units in composition, structure and radiometric age support the view that Francois Granite is more closely related to Casey Alaskite in origin, mode of emplacement and age than to other members of the Topley Intrusions. A ternary quartz-K-feldspar-plagioclase plot of modal compositions of the units (Fig.3-20) shows all but one of the Casey Alaskite modes plot within the Francois Granite field. An Ab-Or-SiO$_2$ ternary plot of average modal compositions of the Topley units (Fig.3-21) shows Francois Granite to be the highest in orthoclase content and Casey Alaskite the highest in quartz. Since structural and radiometric evidence attest to the youth of these units relative to other Stage 2 Topley plutons, a differentiation trend with enrichment in silica and alkalies is evident. As the last rock unit in a series that ranges from diorite through to granite, Francois Granite marks the terminus of the second stage of Topley plutonism.

(vii)   <u>Stellako Quartz Monzonite and Granodiorite</u>:

Relatively young quartz monzonites and granodiorites form a discordant belt trending north-northeastward across the eastern half of the map-area. Isolated exposures separated by wide areas of overburden occupy a zone 8-1/2 miles long and 3-1/2 miles wide that trends north from the mouth of Nithi River to Deserter Lake and Parker Bay on Fraser Lake (Fig. 3-16).

Table 3-9

Modal Analyses of Francois Granite

Speci-men	Micro-cline	Plagio-clase	Quartz	Biotite	Horn-blende	Magne-tite	Sphene	Pyrite
D°	45	15	34	5	0	.5	.5	0
EN-190*	48.0	9.8	29.8	8.7	2.4	1.2	tr	0
EM-193*	39.4	18.8	32.0	2.5	1.0	0.5	tr	0
EN-191*	46.0	16.0	32.0	5.0	tr	1.0	tr	0
EN-194*	35.7	31.0	25.3	6.2	1.5	1.0	tr	0
EN-192*	33.7	28.8	29.9	5.4	0.7	1.2	tr	0
C+	35	29	30	5	0	.5	.5	0
137	54	21	23	1	0	1	0	0
148	43	22	31	3	0	1	0	0
149	60	16	21	2	0	.5	.5	0
169	53	10	35	1	0	.2	.5	.3
171	60	12	25	.5	.5	1	.5	.5
173	65	10	21	2	0	0	0	2
PB-21	49	15	35	1	0	0	0	0
FG	43	18	35	3	0	1	0	0
243	55	18	23	1	0	2	1	0
253	44	15	38	2	0	1	0	0
260	55	16	25	3	0	1	0	0
282	49	21	27	2	0	.5	0	0
290	51	23	22	4	0	.5	0	0
291	41	28	25	5	0	1	0	0
343	48	18	34	0	0	0	0	0
360	41	18	37	3	0	1	.1	0
365	52	19	27	1	0	1	0	0

Table 3-9   (Continued)

1.   Calculated average mode: microcline 48%; plagioclase 18%, quartz 29%; biotite 3%; accessories 2%.

2.   Average composition of plagioclase is An_{24}. Composition ranges from An_{13} to An_{28}.

3.   Modal analyses by other authors:

    °Drummond, 1967 (visual estimation)
    *Bright, 1967 (point counter and stained slab)
    +Carr, 1966 (visual estimation)

4.   Alkali feldspar from fine-grained granite has composition Or_{100} (Bright, 1967, p. 12).

FIGURE 3-15

Francois Granite Modes

Carr specimen   X   Drummond specimen   △
Bright specimen   O   Average   mode   □
Dawson specimen   +
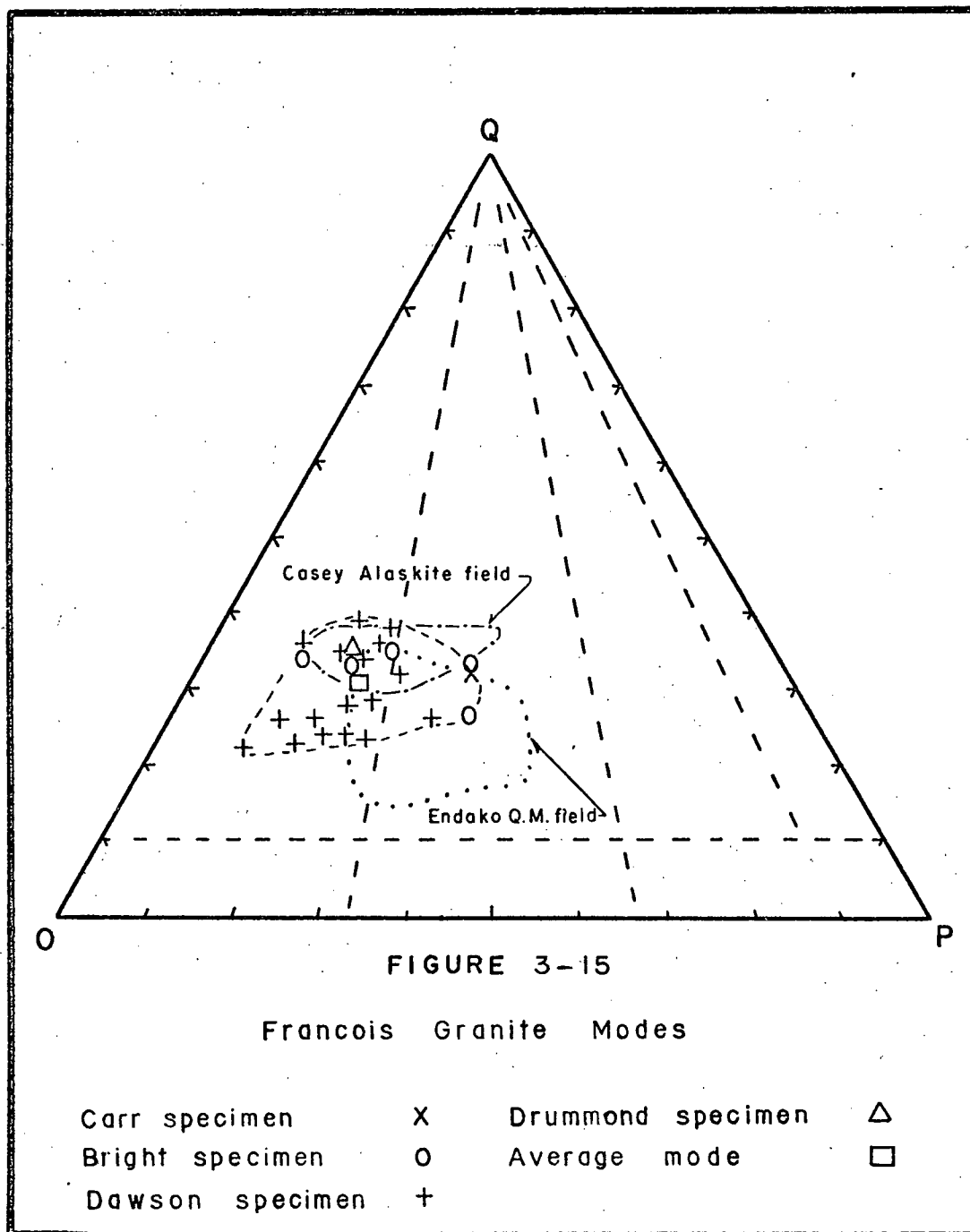
Stellako quartz monzonites vary somewhat in appearance but are generally fine- to medium-grained grayish-pink hypidiomorphic granular rocks distinguishable from other Topley quartz monzonites by their finer grain size and higher mafic mineral content. Typical fine- to medium-grained inconspicuously porphyritic quartz monzonites occur along Stellako River and near Mary Lake. In both localities, minor foliation of hornblende and biotite is accentuated parallel to contacts with older units. Porphyritic phases of Stellako Quartz monzonite with microcline phenocrysts up to 1 cm long occur near Alf and Mudhole Lakes and on the western flank of Nithi Mountain.

Stellako Granodiorite is distinguished from associated Quartz Monzonite by gray colour, non-porphyritic texture and higher mafic mineral content, with hornblende commonly in excess of biotite. Granodiorite is generally a hypidiomorphic inequigranular rock, locally foliated, and containing rare 3 to 5 mm phenocrysts of plagioclase and hornblende. Fine-grained, non-foliated granodiorite on Doe mineral claims at east end of Francois Lake contrasts with medium-grained, foliated and weakly porphyritic granodiorite to the north along Stellako Road. Exposures of granodiorite on Fraser Lake contain sub-rounded xenoliths of diorite and amphibolite which are particularly abundant adjacent to the contact with Simon Bay diorite. Although Stellako granodiorite contains minor dioritic phases and shows some foliation, the unit may be distinguished from Simon Bay diorite and granodiorite by finer grain size, lower mafic mineral content and lack of strong foliation characteristic of the older rock. Modal analyses are given in Table 3-10 and Fig. 3-17.
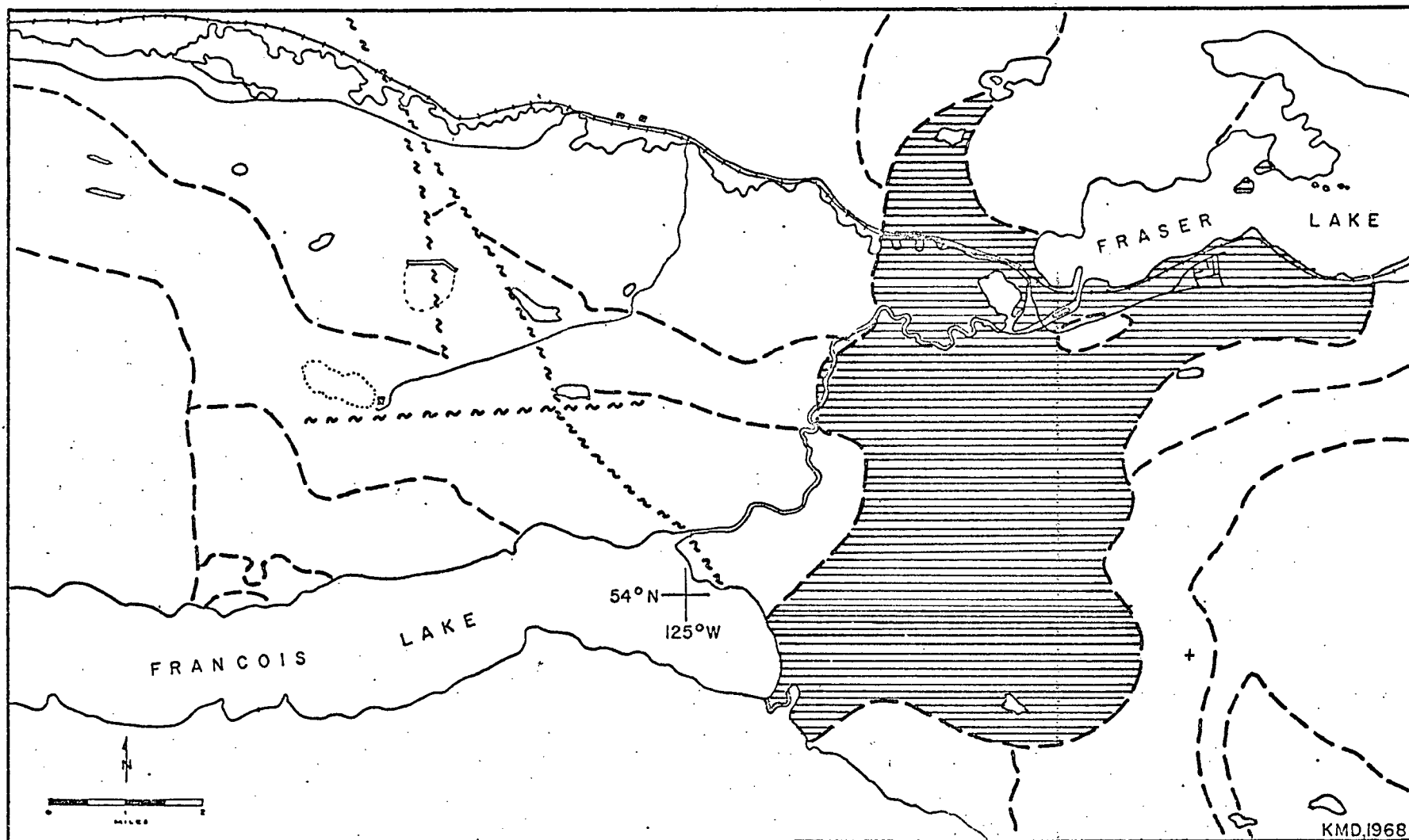
FIGURE 3-16

REGIONAL DISTRIBUTION OF STELLAKO QUARTZ MONZONITE

AND GRANODIORITE.

MINOR INTRUSIONS:

Fine-grained hornblende diorite and quartz diorite dykes,
commonly more than 25 feet wide, cut Stellako intrusions at
Stellako River and Mouse Point on Fraser Lake. Similar
dykes occur at or near contacts between other Topley members,
particularly Casey Alaskite - Glenannan Granite contact east
of Casey Lake, Casey Alaskite-Endako Quartz Monzonite contact
at Tailings Creek and west of Savory Lake, and in Simon Bay
diorite adjacent to its contact with Stellako quartz monzon-
ite near Alf Lake. The quartz diorite exposure in the canyon
of Tailings Creek was mapped as "Pond quartz diorite stock"
by Carr (1966, p. 125), whereas detailed mapping has shown
it to be a 60-foot-wide dyke trending N 15 E. Spatial
relationships, relative age and composition of these minor
intrusions suggest a genetic relation to Stellako Quartz
Monzonite and Granodiorite.

STRUCTURAL RELATIONS AND AGE:

Stellako Quartz Monzonite and Granodiorite has been emplaced
as a broad discordant, north-northeast-trending belt at
right angles to the regional west-northwest trend of older
Topley rocks. Stellako intrusions exhibit degrees of foli-
ation, shearing and chilling at all observed contacts with
members of the Topley Intrusions bordering the belt of
younger rocks. Stellako Quartz Monzonite sharply truncates
Casey Alaskite along Stellako River where shearing and
gneissic banding of mafix occurs parallel to a well-defined

contact along the west bank of the river. An adjacent con-
tact with Endako Quartz Monzonite is obscured by talus, and
contact with the Glenannan granite downstream is inferred.
Quartz monzonite is foliated parallel to foliation in Simon
Bay diorite at Mary and Mudhole Lakes, and potash metasoma-
tism of the diorite adjacent to its contacts was noted
(Bright, 1967, p. 97). At Mudhole Lake porphyritic quartz
monzonite decreases in grain size towards a contact with
Simon Bay diorite and the resulting chilled rock contains
local segregations of granite pegmatite (Carr, 1966, p. 124).
A small exposure of Stellako granodiorite on Nithi Mountain,
lying 100 feet west of the main body of Nithi quartz monzon-
ite, exhibits strong foliation parallel to the inferred
contact.

Discordant trend and contact relations of Stellako intrusions
indicate the rocks were emplaced by forceful intrusion with
stoping, assimilation and metasomatism of host rocks, as a
late phase of Topley plutonism. A Late Jurassic or younger
age is indicated by sharp truncation of the elongate Casey
Alaskite body at Stellako River. Stellako Quartz Monzonite
is overlain by Endako Group andesitic and basaltic lavas of
Eocene age east of Alf Lake and along the northwest shore of
Fraser Lake.

Field relations are in accord with radiometric ages straddling
the Upper Jurassic-Lower Cretaceous boundary as defined by
Howarth (1964). Stellako Quartz Monzonite from the Lower

Table 3-10

Modal Analyses of Stellako Quartz Monzonite and Granodiorite

Quartz Monzonite

Speci-men	Plagio-clase[1]	Micro-cline	Quartz	Biotite	Horn-blende	Magne-tite	Accessories
St-1[2]	20	38	32	5	3	–	–
St-2[2]	37	20	35	6	2	–	–
St-3[3]	29	35	30	3	2	–	1
QM[3]	37	20	35	6	–	–	2
QM[3]	20	40	35	3	2	–	–
584	38	23	21	2	15	tr	1
478	38	29	24	7	2	tr	–
567	41	31	21	6	1	tr	–
569	37	34	24	5	–	tr	–
433	36	35	22	6	1	tr	–

Granodiorite

GD[2]	55	14	23	4	2	–	–
QD[3]	46	15	30	6	2	–	1
QD[3]	45	25	20	8	–	–	2
518	59	19	13	2	7	tr	–
576	58	11	10	4	14	3	–
479	55	15	13	4	12	1	–

1. Plagioclase composition ranges An_{24} to An_{34}.

2. E.G. Bright, 1967, p. 94 (point counter and stained slab)

3. J.M. Carr, 1966, p. 124-125 (visual estimation)

FIGURE 3-17

Stellako Quartz Monzonite and Granodiorite Modes

| Bright specimen | O | Dawson specimen | + |
| Carr specimen | X | Average mode | □ |

Stellako River yields a radiometric age of 136 ± 5 million

years (White, et al, 1970). Stellako Granodiorite from a

road-cut on Stellako Road yields an age of 137 million years

(Ibid.). The radiometric dates confirm that Stellako Quartz

Monzonite and Granodiorite are indeed related temporally as

well as spatially. Stellako intrusions probably were

emplaced shortly after Francois Granite, possibly with the

quartz monzonitic phase succeeding the earlier granodioritic

phase.

(viii)   Fraser Quartz Monzonite:

Two adjacent exposures of a distinctive pink quartz monzonite

occur along Highway 16 at the west end of Fraser Lake (Fig. 3-18).

The exposures occur within a restricted area of contrasting low

magnetic susceptibility indicating the unit probably forms a

small stock which transects adjacent Stellako Quartz Monzonite

and Granodiorite (Carr, 1966, p. 125).

The rock is a fresh, medium-grained, subporphyritic pink

biotite-hornblende quartz monzonite. Perthitic microcline is

sub-graphically intergrown with quartz and poikilitically encloses

smaller subhedral plagioclase, prismatic green hornblende and red-

brown biotite. The finer-grained groundmass is partly granophyric.

Accessory minerals include magnetite, sphene and apatite. Rounded

dioritic inclusions similar to those in adjacent Stellako intru-

sives occur in both outcrops. Three modal analyses are given in

Table 3-11 and Fig. 3-19.

FRASER LAKE

FRANCOIS LAKE

54° N
125° W

N

MILES

KMD, 1968
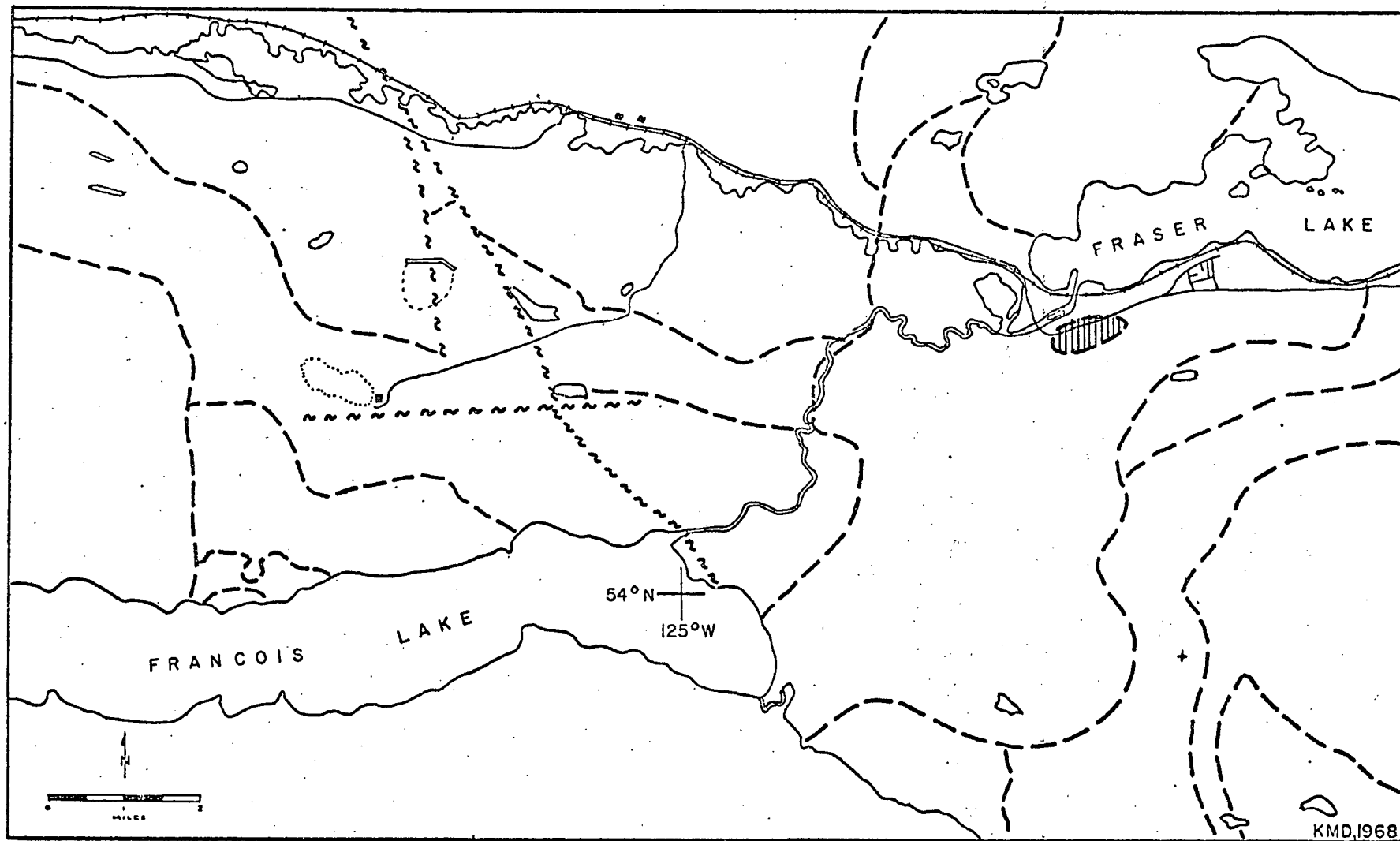
FIGURE 3-18

REGIONAL DISTRIBUTION OF FRASER QUARTZ MONZONITE

STRUCTURAL RELATIONS AND AGE:

The westernmost of the two Fraser Quartz Monzonite outcrops is the finer-grained and probably is closer to the edge of a stock of about one square mile area. Granophyric texture and absence of foliation indicate a high level of emplacement within the belt of Stellako intrusions. Early Cretaceous radiometric ages of 112 and 114 m.y. obtained from Fraser quartz monzonite (W.H. White, et al, 1970) show the stock to be the youngest phase of Topley Intrusions recognized in the Endako area.

Table 3-11

Modal Analyses of Fraser Quartz Monzonite

	Microcline	Plagioclase[1]	Quartz	Hornblende	Biotite	Accessories
JMC[2]	30	50	15	2	3	1
EGB[3]	32	43	18	5	2	1
536	34	41	19	4	2	1

1. Plagioclase composition is An_{18}.

2. J.M. Carr, 1966, p. 126 (visual estimation)

3. E.G. Bright, 1967, p. 100 (point counter and stained slab)

FIGURE 3-19

Fraser Quartz Monzonite Modes

Carr specimen	X	Dawson specimen	+
Bright specimen	O	Average mode	□
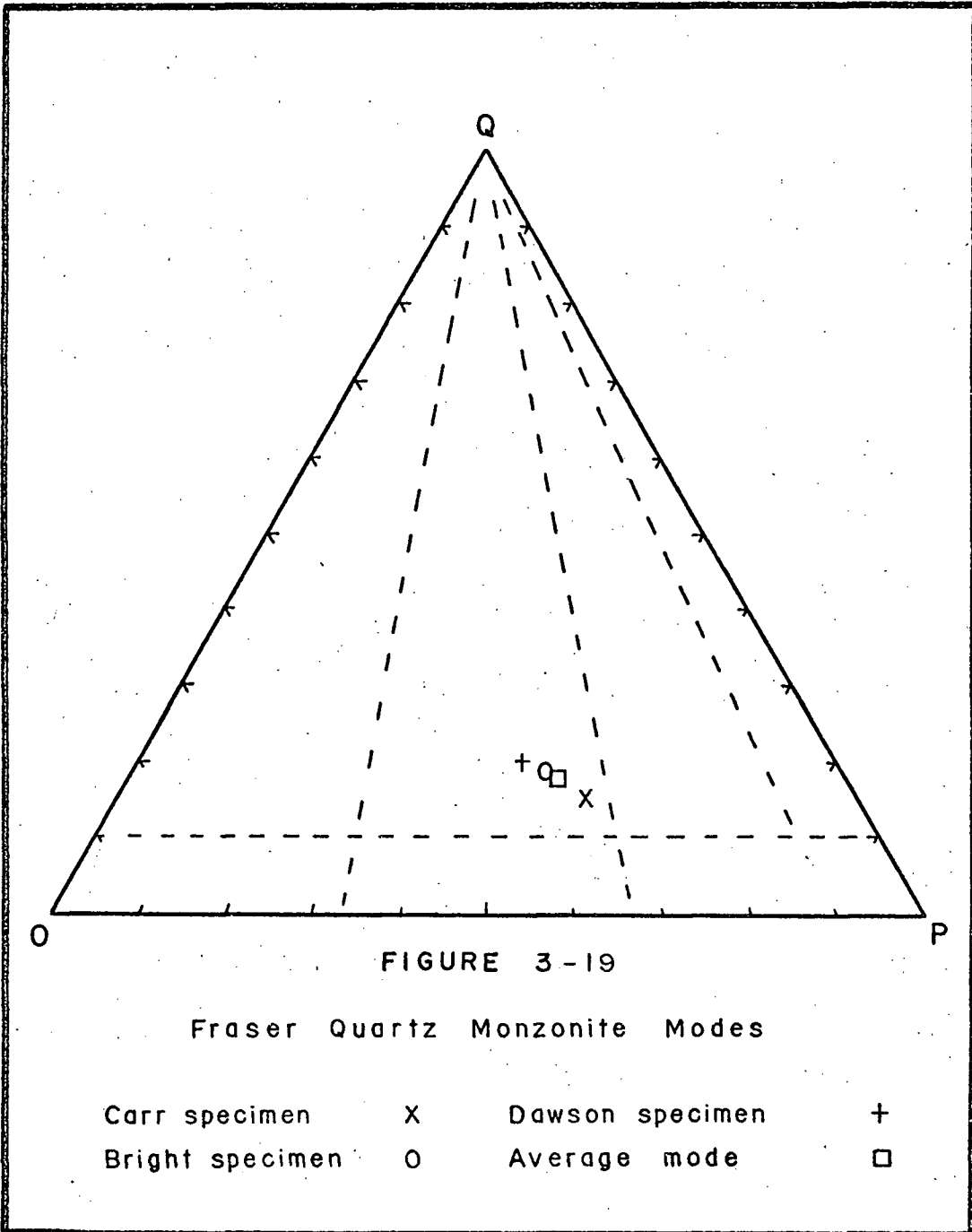
(c) Evolution of the Batholith

Stage 1:

Foliated rocks of the Simon Bay Diorite Complex are the oldest
members of Topley Intrusions recognized in Endako area. Similar dio-
ritic phases of the batholith northeast of the map-area form partly
concordant plutons flanking and intruding Cache Creek Group rocks
along the western margin of the Stuart Lake High. Foliation in Simon
Bay rocks is mainly of primary origin and generally conforms to the
regional northwest trend of the batholith. Foliation in unsheared
dioritic rocks, as defined by aligned mafic minerals and inclusions
associated with interlocking feldspars and quartz, probably was
generated during emplacement of a magma. Lenses and bands of gabbro,
amphibolite and gneiss aligned parallel to foliation probably represent
screens of wallrock which have undergone various stages of metamorphism
and metasomatism in a mesozonal environment. The presence of abundant
angular xenoliths of dioritic composition supports a mechanism of mag-
matic stoping and assimilation rather than granitization. The Simon
Bay Diorite Complex is the southwestern extension of a large mesozonal
pluton which was intruded along regional northwest zones of weakness
flanking Stuart Lake High, in Middle Jurassic time.

Stage 2:

Topley units of Stage 2 represent a short, almost continuous
period of relatively shallow level igneous activity in Late Jurassic
time. Limited radiometric data indicate a time span of about 18
million years between emplacement of Stage 1 dioritic phases and the

predominantly quartz monzonitic rocks of Stage 2. Stage 2 units, including Endako, Nithi, Glenannan, Casey and Francois plutons, were emplaced in a northwest to west-northwest trend which follows a pre-existing grain in older diorites and also represents repeated fracturing and intrusion under northeasterly-directed compression.

Endako and Nithi Quartz Monzonites are medium- to coarse-grained sub-porphyritic, non-foliated rocks. Structural and petrological evidence cited previously indicates the units may be one, originally continuous body or two generations of magma from the same source. An Ab-Or-SiO$_2$ plot of their average modal compositions (Fig. 3-21) shows Nithi Quartz Monzonite to be slightly more siliceous than Endako, hence possibly the younger. Absence of foliation in Endako and Nithi Quartz Monzonites suggests a mainly liquid mode of transfer from depth to an epizonal environment of emplacement. Average Ab-Or-SiO$_2$ compositions in Fig. 3-21 show that Endako Quartz Monzonite has the most basic composition of the Stage 2 Topley plutons. Composition of successive intrusions show enrichment in silica and/or potash, culminating in Francois Granite. The sequence of Stage 2 plutons may represent differentiation of a parental granodioritic magma. It is of interest to note that mineral deposits are preferentially associated with earlier phases of the batholith in this case, i.e. Endako and Nithi Quartz Monzonites, rather than later, granitic differentiates.

Following the consolidation of Endako and Nithi plutons was the emplacement of a new generation of magma, represented by Glenannan Granite and Quartz Monzonite in Endako area, and related bodies to the north. The large zoned pluton, which grades from porphyritic granite

in the south to granodiorite north of the map-area, was emplaced along a regional, northwest zone of weakness between Endako and Simon Bay plutons. An epizonal environment of emplacement (Buddington, 1959) similar to that of earlier intrusions is indicated by the presence of granophyre and conspicuously porphyritic granite border phases. A weak northwest foliation, defined by aligned microcline phenocrysts in the granite zone, is evidently a primary flow structure developed in a fluid magma. Bright (1967, pp. 77-84) has developed an hypothesis explaining zonation in the Glenannan pluton by differentiation of a parent granodiorite magma. Bright postulates original differentiation within the magma chamber to an upper granitic fraction, enriched in alkalies and perthite megacrysts, an intervening quartz monzonitic fraction, and a granodiorite magma at depth. Successive intrusion of these phases, with granite preceding quartz monzonite and granodiorite, and younger phases mixing completely with older intrusions along their contacts, resulted in a gradationally-zoned pluton.

Intrusion of discordant stocks and satellite dykes of Casey Alaskite closely followed the cooling and consolidation of Glenannan intrusives. These bodies of distinctive leucocratic granite and quartz monzonite intruded regional northwest and west-northwest fracture systems, zones of intersection of northwest and northeast regional fractures, and a zone of weakness along the Endako-Glenannan contact. Form and trend of alaskite bodies indicates origin by forceful injection of a mobile granitic magma. Epizonal characteristics, including chilled, granophyric border zones, lack of foliation and xenoliths, and presence of miarolitic cavities, indicate a shallow depth of emplacement. Radiometric dating shows Casey Alaskite to be closely

related in time to Glenannan plutonism, yet no petrological similarities indicative of genetic relationship between the two units were noted. While the Glenannan pluton was still cooling, a new magma high in silica and alkalies (Fig. 3-13) and low in mafic constituents was probably forming at depth. A period of strong regional fracturing related to stresses generated by cooling of the Glenannan pluton and upward pressure of alaskite magma controlled the emplacement of discordant stocks and dykes of alaskite.

Contemporaneously with or slightly later than emplacement of Casey Alaskite, the parent magma of red Francois Granite intruded Endako Quartz Monzonite along the south-western margin of Topley batholith. Francois Granite and Casey Alaskite have strong epizonal characteristics in common, as well as petrological and structural similarities. The units probably were emplaced almost simultaneously as elongate dyke-like bodies following zones of weakness along contact zones flanking Endako Quartz Monzonite on the north and south. Granite and alaskite probably were derived from a common residual magma enriched in silica and alkalies relative to earlier Endako, Nithi and Glenannan quartz monzonitic phases. Francois Granite is richer in K-feldspar and possibly is slightly younger in radiometric age than Casey Alaskite, therefore probably is the final differentiate of the second stage of Topley plutonism. Fig. 3-21 illustrates a proposed differentiation trend that involves enrichment in both silica and potash and proceeds from earliest Simon Bay Diorite through the Stage 2 plutons and terminates in Francois Granite.

Stage 3:

The last major period of plutonism recognized in Endako area is represented by Stellako Quartz Monzonite and Granodiorite of Early Cretaceous age. This family of young intrusions, which range from porphyritic quartz monzonite to granodiorite, has been emplaced as a broad discordant belt trending north-northeast at right angles to the regional trend of older Topley rocks. Fractures which controlled emplacement of Stellako intrusions may have been opened by release of regional north-northeast compressional stress in late stages of Topley plutonism (see "Structural Analysis of Orebody"). Minor foliation in Stellako units is accentuated parallel to sharply-defined chilled contacts with wall rocks. Shearing, brecciation and alteration of wall rocks indicate that the Stellako pluton was emplaced by forceful magmatic intrusion. Primary foliation is weakly developed relative to that of adjacent Simon Bay Diorite, and probably represents local magmatic flow in an epizonal environment. Stellako rocks bear no evident genetic relation to older quartz monzonites and granites of Stage 2, although the time lapse between emplacement of the stages, as shown by radiometric dating, was only a million years. The rocks are more basic than earlier Topley units, with an average modal composition between quartz monzonite and granodiorite (Table 3-10 and Fig. 3-17). Contacts between Stellako phases are not exposed, but radiometric ages indicate quartz monzonite is the younger. The phases may represent several periods of intrusion from a differentiating granodioritic magma, possibly of deeper origin than preceding acidic plutons.

The Fraser quartz monzonite stock, the youngest phase of Topley Intrusions recognized in the map-area, is a small body which intrudes the Stellako pluton. Epizonal characteristics include granophyric texture and lack of foliation. A considerable time lapse of approximately 20 million years (W.H. White, personal communication, 1967) occurred between emplacement of Stellako and Fraser quartz monzonites. Modal analyses (Table 3-11 and Fig. 3-19) show Fraser Quartz Monzonite to be lower in quartz and K-feldspar than adjacent Stellako Quartz Monzonite. Origin of Fraser Quartz Monzonite as a late differentiate of Stellako magma appears unlikely. Late stresses within the Stellako belt may have effected deep fracturing which, in turn, generated a local pocket of quartz monzonitic magma.

(d) Minor Intrusions

Regional Topley Dykes:

Minor intrusions of aplite, pegmatite and various compositions ranging from granitic to dioritic are related to the cooling stages of the Topley Batholith. Of the eight dyke rocks in this group, aplite and pegmatite are common to most Topley units, whereas other dykes may be related genetically to specific plutons, as described.

1. Rhyodacite porphyry:

Large porphyry dykes which cut Takla Group pyroclastic rocks in a northwest trend are a phase of the Menard rhyodacite stock (see "Takla Group").
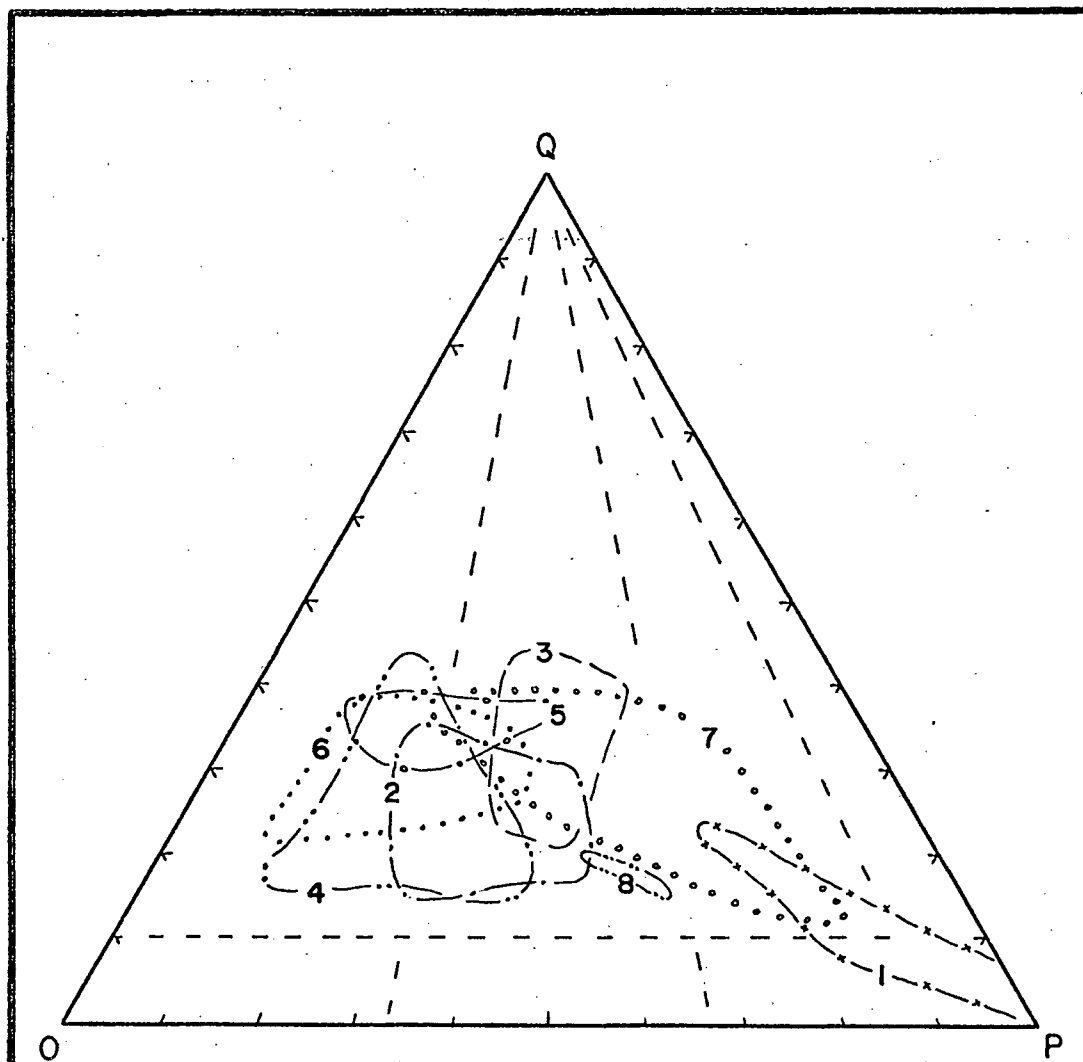
FIGURE 3-20

Modal Analyses Fields of Topley Plutons in Endako Area.

8. Fraser   4. Glenannan
7. Stellako   3. Nithi
6. Francois   2. Endako
5. Casey   1. Simon Bay

FIGURE   3-21

Average   Ab - Or - SiO$_2$ Compositions of Topley Plutons

8. Fraser	4. Glenannan	4a. granite
7. Stellako 7a. granodiorite	(unit)	4b. qtz. monzonite
(unit) 7b. qtz. monzonite	3. Nithi	
6. Francois	2. Endako	
5. Casey	1. Simon Bay	
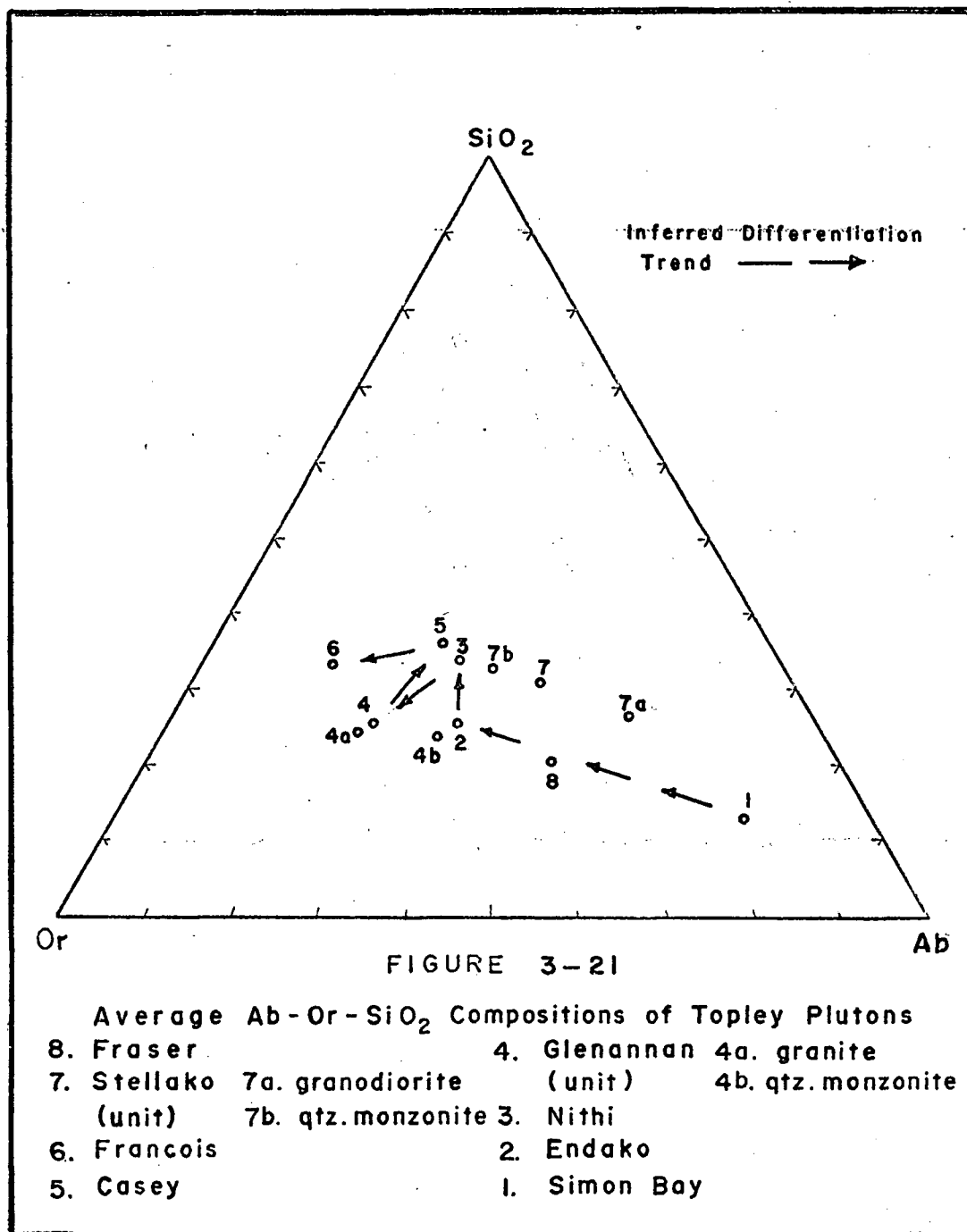
2.   <u>Aplite</u>:

Abundant aplite dykes ranging from 1 inch to over 30 feet wide
intrude all members of the batholith. Pink aplites have a typi-
cal granophyric or micrographic texture, and locally contain
small, rounded quartz phenocrysts. In composition, the dykes
contain 40 to 45% each of quartz and microcline, 10 to 20% plagio-
clase (An_{20}), and less than 1% biotite and accessory minerals.
Aplite is the earliest pre-mineralization dyke at Endako mine.
Aplite dykes, which may border or grade to pegmatite, are late
phases of various plutons hence not necessarily all of the same
age.

3.   <u>Pegmatite</u>:

Pegmatite dykes are not common in the map-area. They generally
occur, in association with aplite, near the margins of plutons.
Several pegmatites enclose lenticular barren quartz veins.
Crystals of quartz and pink orthoclase, one to three inches long,
predominate over white plagioclase and traces of biotite and
muscovite.

4.   <u>Quartz Monzonite</u>:

Porphyritic and equigranular quartz monzonite dykes of similar
composition and possibly similar origin to Francois Granite intrude
rocks adjacent to Francois contacts in two localities (see
"Francois Granite").

5. Porphyritic Granite:

Reddish-brown porphyritic granite dykes apparently related to

Endako Quartz Monzonite occur mainly in the mine area. Two

porphyritic granite dykes occur west of the mine, one of which

is cut by quartz-molybdenite-pyrite veinlets. Two porphyritic

granite dykes intrude Francois Granite adjacent to an Endako

Quartz Monzonite contact southwest of the mine. Dykes outside

the orebody are parallel to the northeast trend of a porphyritic

granite dyke swarm exposed in the open pit (see "Mine Area Dykes").

6. Rapakivi Porphyry:

Reddish porphyritic dykes which contain unique phenocrysts of

microcline mantled by plagioclase are probably a dyke phase of

Francois Granite (see "Francois Granite").

7. Casey Porphyry:

Strongly porphyritic dykes similar in composition to Casey Alas-

kite intrude host rocks adjacent to alaskite contacts, and probably

represent a late phase of the Casey pluton. Dykes with a northeast

trend and exceeding 100 feet in width cut Endako Quartz Monzonite

north of the mine, and Glenannan Granite west of Casey Lake.

Smaller dykes occur within Glenannan Granite to the north. The

dyke rock is composed of about 35% phenocrysts in a pink to gray

aplitic matrix. Phenocrysts are composed of pink microcline

(50%), quartz (25%), plagioclase (20%), and biotite (5%).

8. <u>Diorite</u>:

Fine-grained diorite and quartz diorite dykes that intrude contact
zones of several Topley units are probably related to the Stellako
intrusions (see "Stellako Quartz Monzonite and Granodiorite").

<u>Porphyry Dykes</u>:

Abundant porphyry dykes of various types cut batholithic and older
rocks in Endako area. Dykes range in age from pre-Endako mineralization
to Tertiary, and in composition from rhyolite to andesite. Porphyry
dykes have been mapped and classified according to the nomenclature
proposed by Carr (1966, p. 127), i.e. dykes are grouped according to
presence of light-coloured phenocrysts which are variously quartz (Q),
orthoclase or microcline (O), and plagioclase (P).

1. <u>QOP Porphyry</u>:

Dykes in which quartz, orthoclase and plagioclase form phenocrysts
are common. Included in this category, but distinguished because
of genetic relations to various Topley plutons are Casey porphyry,
Rapakivi porphyry and porphyritic quartz monzonite. A pinkish-
brown dyke containing phenocrysts of quartz, feldspars and biotite
("Quartz-Feldspar Porphyry" or "QFP") is a common pre-ore dyke at
Endako mine, and also occurs at Tailings Creek and MacDonald Lake.
Similar dykes at Nithi Mountain trend north to northwest and, like
QFP dykes at Endako, are sheared, altered, and mineralized. Small
QOP dykes cut Francois Granite southwest of Endako mine and also
intrude Stellako-Simon Bay contact at Mudhole Lake. The dykes
which may be pink, gray or brown, are mainly quartz latites and
rhyodacites.

2. <u>QO Porphyry</u>:

Pinkish-gray dykes containing quartz and orthoclase phenocrysts
are fairly abundant in Francois and Takla rocks south of Endako
mine, and in Stellako and Endako plutons along Stellako River.
The dykes are mainly rhyolite and, with minor plagioclase in the
groundmass, quartz latite. A unique QO dyke containing oval
phenocrysts of purple amethystine quartz cuts Francois Granite
south of the No. 2 tailings dam.

3. <u>QP Porphyry</u>:

Dykes with quartz and plagioclase phenocrysts occur in the east-
ern part of the map-area. The dykes vary from pink to gray and
may be quartz latites or rhyodacites depending on abundance of
quartz and plagioclase. Most dykes of this type contain minor
amounts biotite or hornblende.

4. <u>OP Porphyry</u>:

Dykes with orthoclase and plagioclase phenocrysts occur mainly
west and south of Endako mine. An OP porphyry dyke intrudes the
contact between Endako and Casey plutons at Stellako River. The
dykes vary from pink to brown, and resemble adjacent QO and O
porphyry dykes except in their phenocryst assemblage. Depending
on abundance of quartz in groundmass, the dykes are variously
quartz latites, rhyodacites or latites. Dykes of this type
intersected in trenches and diamond-drill holes west of the mine
are frequently veined with pyrite, and less commonly,
molybdenite.

5. <u>O Porphyry:</u>

Pinkish-gray dykes containing orthoclase phenocrysts alone are
uncommon in the area. A group of O porphyry dykes is exposed in
trenches near diamond-drill hole U-1 west of Endako mine, and
several dykes occur near the Francois-Takla contact to the south.
O porphyry dykes in both localities follow a northwest trend.
The dykes, which contain minor biotite in a quartzo-feldspathic
groundmass, are predominantly quartz latites.

6. <u>P Porphyry:</u>

Plagioclase porphyry dykes are of two distinct types. Small
brown or gray dykes resembling the O and OP porphyry dykes with
which they are associated are distributed throughout the western
part of the area, and are probably pre-molybdenite mineralization
in age.

Large gray or grayish-green dykes containing phenocrysts of
plagioclase (10-15%), biotite and augite (2-5%) are widely dis-
tributed, and are all post-ore in age. A plagioclase porphyry
dyke at the head of Stellako River yields a radiometric age of
50 million years (White, et al, 1970), essentially the same age
as Eocene Endako Group flows (Mathews, 1964). A zone of these
andesite dykes follows Casey Lake fault in a N 30 W trend for
6-1/2 miles across the map-area. The dyke zone, in places 2000
feet wide, is exposed at the head of Stellako River, in a canyon
of Sweetnam Creek, north of Nithi Lodge, in trenches north of
the Tailings Pond, and is intersected in diamond-drill holes

between MacDonald and Casey Lakes. Small basalt dykes intrude

plagioclase porphry dykes and wall rocks within the dyke zone.

Andesite and basalt dykes exhibit both sheared and unsheared,

chilled contacts with wall rocks, indicating late movement along

the fault zone.

North of Highway 16, Carr (1966, Fig. 22) has mapped large P and

OP porphyry dykes following a topographic lineament which may be a

northwesterly extension of Casey Lake fault.

At Endako mine, porphyritic andesite dykes of unknown attitude

are intersected in diamond-drill holes. At the mine and MacDonald

Lake the dykes cut molybdenite-bearing Endako Quartz Monzonite but

are not mineralized.

West of Deserter Lake, a large porphyritic andesite dyke intrudes

Simon Bay diorite in a northwest trend. Biotite andesite flows of

the Endako Group overly diorite immediately to the east. P.porphyry

dykes bear strong resemblance to porphyritic andesite flows exposed

on Savory Ridge. The andesite bodies parallel to Casey Lake fault

probably served as feeder dykes for Eocene flows which subsequently

have been removed by erosion and glaciation.

Basalt Dykes:

Fine-grained, dark green dykes of basaltic composition are the

youngest intrusions recognized in the area. Large basalt dykes,

ranging from 10 to 30 feet wide at Endako mine and 100 feet wide south

of new tailings dam, follow an east-west trend. Smaller dykes occur

throughout the area, and are particularly abundant in the Casey Lake
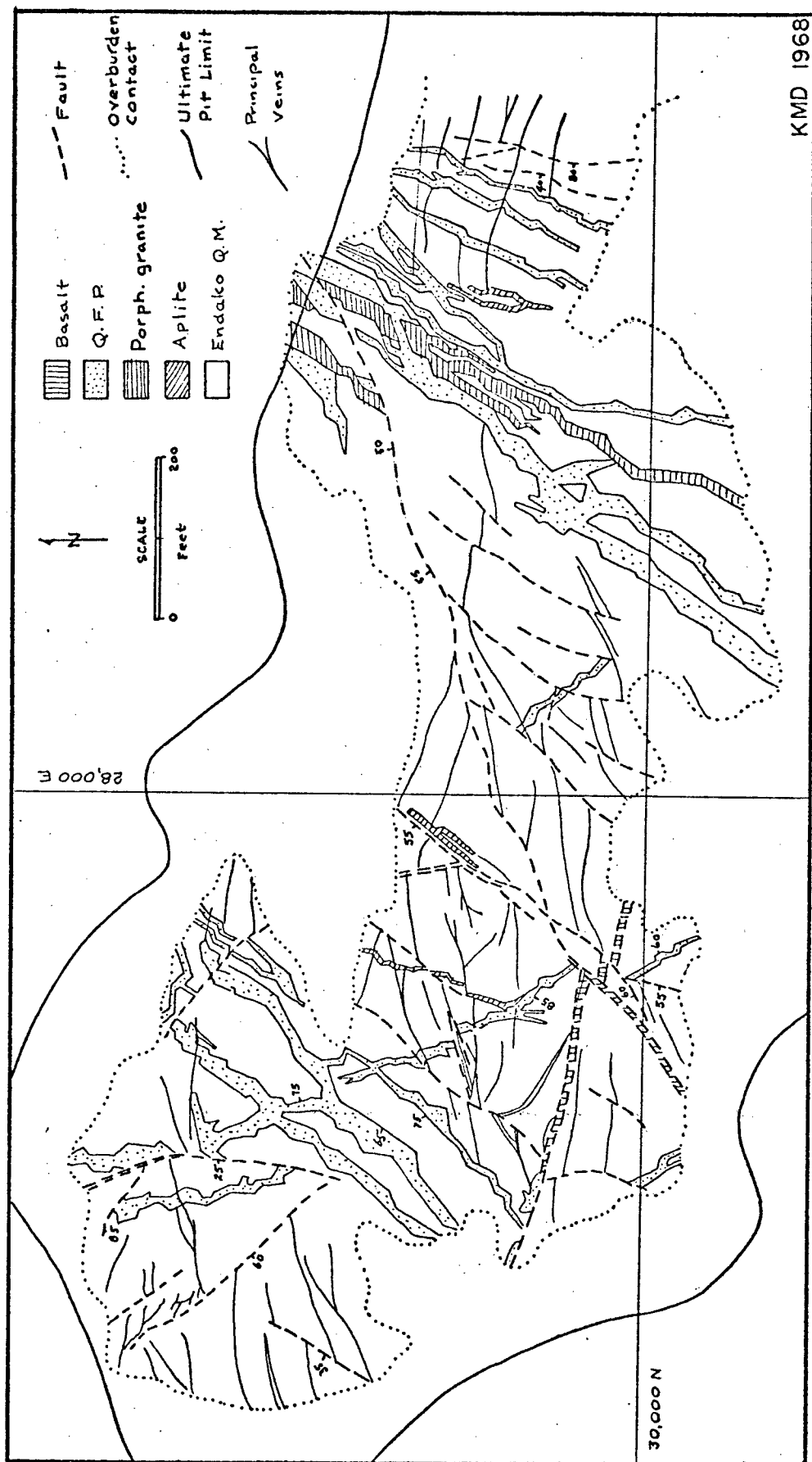
FIGURE 3-22

Surface Map of Dykes, Endako Mine Pit Area

fault zone, and south of Simon Bay. The dykes, which have been called lamprophyres by other authors, are composed almost entirely of fine-grained plagioclase-hornblende intergrowths, with minor magnetite. Small phenocrysts of plagioclase and hornblende are rare. Basalt dykes may be sheared and altered to chlorite and calcite, but are devoid of mineralization. Basalt dykes, like porphyritic andesite dykes, probably are related to Eocene volcanism.

Mine Area Dykes:

Dykes mapped within the open pit at Endako mine are illustrated in Fig. 3-22. Approximately two-thirds of the optimum open pit area has been covered by detailed mapping at present. All acidic dykes are pre-ore, and follow either a northwesterly or northeasterly trend, with steep westward dips. Attitudes of pre-ore dykes reflect the stress orientation in Endako quartz monzonite prior to mineralization (see "Structural Analysis of Orebody").

1. Aplite:

Aplite dykes are the earliest pre-ore dykes at the mine, and the least abundant. Small dykes, generally less than 15 feet wide, comprise three groups which strike N 10° E, N 20° E and N 40° E and dip steeply westward. The dykes are of similar composition and texture as aplites elsewhere in the area. They are truncated by QFP dykes and cut by both mineralized and unmineralized faults and fractures.

2. <u>Porphyritic Granite</u>:

Reddish-brown porphyritic granite dykes up to 100 feet wide are
intruded by QFP dykes in a northeast-trending swarm in the central
pit area. Average attitude of the porphyritic granite dykes is
N 25° E with steep westward to vertical dips. Phenocrysts of
pink, Carlsbad-twinned orthoclase 2 to 7 mm long in a seriate-
textured matrix comprise 3 to 5% of the rock. The modal composi-
tion, as determined by visual estimation of thin-sections, is
orthoclase (45%), quartz (30%), plagioclase (An_{17}) (20%), biotite
(5%), plus accessory zircon, apatite and sphene. Although con-
tacts with aplite are not exposed, porphyritic granite is assumed
to be younger due to its intimate association with QFP dykes.
Like aplite, porphyritic granite is cut by mineralized and
unmineralized faults and fractures.

3. <u>Quartz-Feldspar Porphyry (QFP)</u>:

Quartz-feldspar porphyry dykes, the most abundant dykes in the
mine vicinity, are 20 to 50 feet wide and extend across the width
of the pit. An intersecting set of QFP dykes with northeast and
northwest strikes and steep dips occurs in the western part of
the pit, and a northeast-trending swarm of porphyritic granite
and QFP dykes occupies the central pit. Two phases of the dyke
have been observed: (1) a pinkish-brown rock containing pheno-
crysts of orthoclase 2 to 4 mm in size which comprise up to 5% of
the rock, and small, rounded phenocrysts of quartz; (2) a brown
rock with predominantly quartz phenocrysts (5-10%), scattered
large orthoclase phenocrysts up to 1 cm long, and small biotite

flakes (1 to 3%). The latter is termed "QFP-biotite phase".
The dense aphanitic matrix of both phases is composed predomin-
antly of quartz and orthoclase in equal amounts with minor
plagioclase (10%), biotite (1 - 5%) and accessory apatite, zircon
and sphene. QFP dykes cut both aplite and porphyritic granite,
and are faulted, fractured and mineralized.

Aplite, porphyritic granite and quartz-feldspar porphyry dykes
are apparently all late phases of Endako Quartz Monzonite. Dykes
were emplaced after cooling and crystallization of the pluton and
prior to hydrothermal alteration and mineralization. Radiometric
dating by White, et al (1968), shows these three events to be of
essentially the same age, indicating that both dyke emplacement
and hydrothermal activity are late phases of the Endako Quartz
Monzonite.

4. Plagioclase Porphyry:

Grayish-green porphyritic andesite dykes containing phenocrysts
of euhedral white plagioclase 4 to 6 mm long (10%) and biotite
(2 to 3%) are intersected in several diamond-drill holes at the
mine. The dykes are not exposed in the pit hence their attitudes
are not known. The dykes intrude Endako Quartz Monzonite,
commonly exhibit sheared contacts, and are not mineralized.

5. Basalt:

Basalt dykes are late intrusions at Endako mine. A single dyke,
1000 feet long and ranging from 10 to 30 feet wide has average
attitude N 82° W/64°S. The dyke is bounded by faults over most

of its length, and is offset on northeast faults with right-lateral displacement. Basalt dykes are commonly sheared, particularly along their contacts, and are extensively altered to chlorite and carbonate. Basalt dykes are not mineralized and, like porphyritic andesite, are probably related to Endako Group volcanic rocks.

(e)   Endako Group

The regional distribution of Endako Group volcanic rocks was briefly described under "Regional Setting". In the map-area Endako Group rocks underlie an area of about 8 square miles at Savory Ridge in the southwest, and about 6 square miles along the north shore of Fraser Lake (Fig. 3-23). Unconformable contacts with underlying rocks of the Topley Intrusions and Takla Group are approximately defined at both localities.

At Savory Ridge, Endako Group rocks are predominantly dark green andesite and basalt flows containing phenocrysts of plagioclase, hornblende and/or pyroxene. Flows are commonly vesicular and may contain amygdules of agate, calcite, chlorite and zeolites. Individual flows are 25 to 50 feet thick on the average, and are interbedded with breccia, agglomerate, tuff and conglomerate. A distinctive porphyritic green andesite flow observed in northern exposures at Savory Ridge bears strong resemblance to a dyke rock ("plagioclase porphyry") that occupies a wide zone parallel to Casey Lake fault, and also occurs as post-ore dykes at Endako mine.
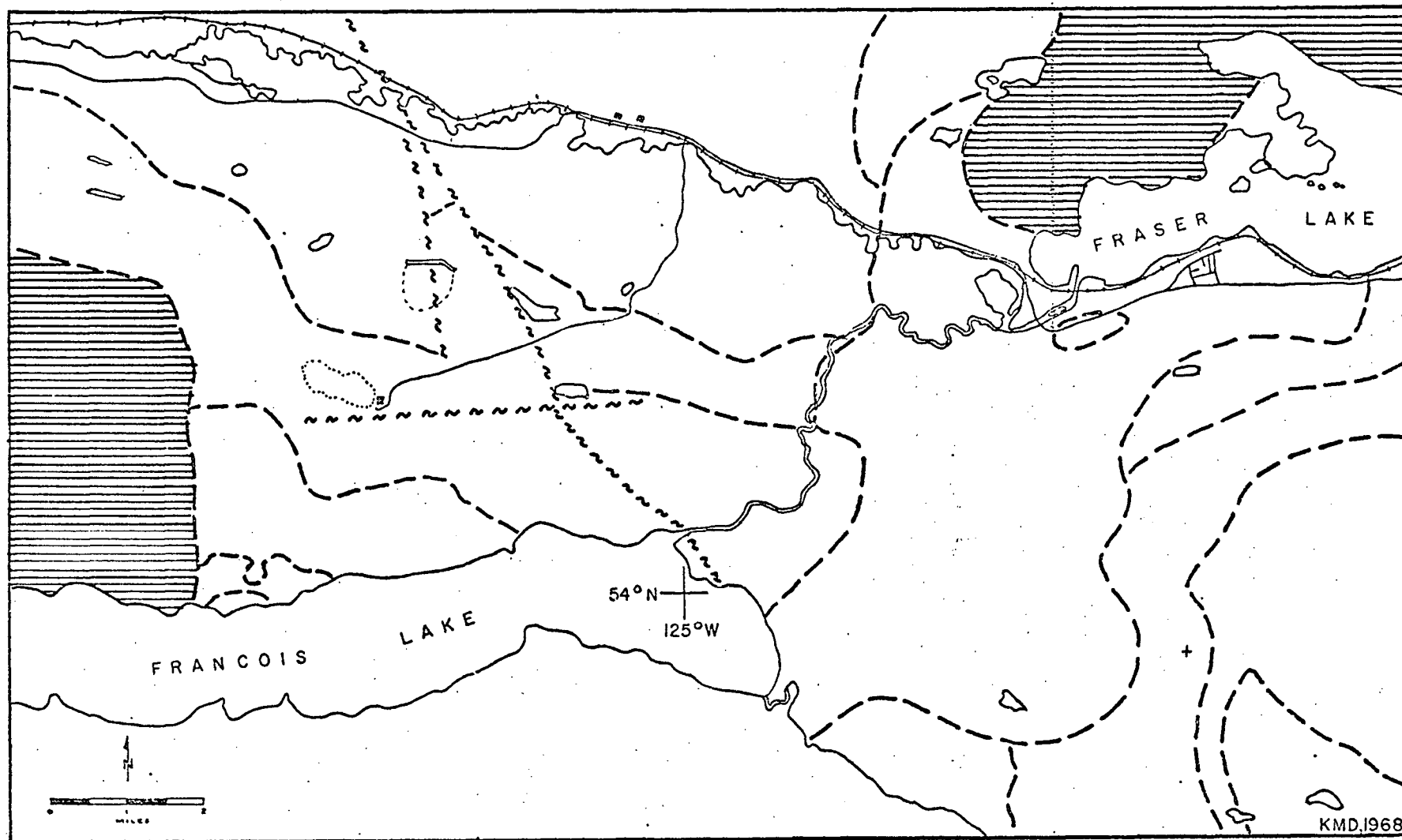
FIGURE 3 – 23

REGIONAL DISTRIBUTION OF ENDAKO GROUP ROCKS

At Fraser Lake, Endako Group rocks are similar to those at
Savory Ridge although less conspicuously porphyritic. Near Simon Bay,
brown trachytic andesite flows that dip gently to the northeast are
apparently similar to light-coloured biotite andesites described by
Carr (1966, p. 117) in the vicinity of Owl Lake 12 miles northwest of
Simon Bay. North of Stellako Indian Reserve, flat-lying flows of dark
green, fine-grained andesite are veined by calcite and stained red by
iron oxide weathering products.

STRUCTURAL RELATIONS AND AGE:

A scarp and dip-slope topography with flat-topped hills and
ridges is developed on the essentially flat-lying Endako Group
flows at Savory Ridge and Stellako Reserve. No exposures of the
contact between Endako Group flows and underlying rocks were
observed in the map-area. At Dry William Lake, 5 miles east of
map-area, Bright (1967, p. 6) observed an unconformity between
deeply-weathered Topley granite and overlying lava of the Endako
Group. In Nechako River area to the south, Endako Group flows
rest unconformably on Ootsa Lake Group volcanic and sedimentary
rocks ranging in age from Late Cretaceous to Eocene (Tipper, 1963,
p. 38). Green porphyritic Endako lava from Hick's Hill, about
four miles west of Savory Ridge, yielded a radiometric age of
48 $\pm$ 2 million years, or Middle Eocene (Mathews, 1964, pp. 465-
468).

CHAPTER IV

STRUCTURE

A. REGIONAL STRUCTURAL TRENDS

The dominant structural controls on emplacement of Topley Batholith are
related to the Stuart Lake High, an elongate fault-bounded belt of Cache
Creek Group rocks in central British Columbia. This belt of folded and
metamorphosed sedimentary and volcanic rocks was uplifted along steeply-
dipping faults parallel to the Cordilleran trend in Late Triassic time
(Souther and Armstrong, 1966, pp. 172-174). Contemporaneous Takla volcanism
mantled lower-lying Cache Creek rocks to the east and west with thick marine
volcanic and sedimentary deposits. A major southwest flexure in the trend
of the Stuart Lake High is defined by (a) a westerly divergence in strike
of major fold axes in Cache Creek rocks at Trembleur Lake (Armstrong, 1949,
Map 907A); (b) occurrence of Cache Creek outliers west and south of Babine
Lake and northwest of Quesnel; (c) faults that bound Cache Creek rocks and
diverge from Pinchi Fault trend to N 30° E at Babine Lake (N.C. Carter,
personal communication, 1968), and N 60° W at Quesnel (G.S.C. Map 932A, 2nd
ed., 1962). Topley plutons, the oldest of which were emplaced in Middle
Jurassic time, flank and intrude the southwestern margin of the flexure in
Stuart Lake High in a N 50° W trend from Quesnel to Babine Lake. A zone of
faults peripheral to the emergent area may have provided conduits for rising
Topley magma.

South and west of Endako area, a belt of igneous rocks of varying ages
defines an axis that intersects Stuart Lake High at the centre of Topley
Batholith. The northeast-trending zone of repetitive igneous activity

extends from Tertiary granite and syenite bodies near Bella Coola (Roddick, et al, 1965), to Jurassic and Cretaceous granitic plutons in Whitesail Lake and Nechako River areas (Duffell, 1959; Tipper, 1963), and Triassic volcanic islands in Nechako River area (Ibid.). Deep faulting accompanying early stages of igneous activity in this belt may have intersected faults peripheral to Stuart Lake High, providing a localized zone of weakness subject to intrusion by phases of the Topley Batholith. Generally speaking, emplacement of the Topley Batholith within a flexure in Cache Creek rocks is analagous to emplacement of the Nelson Batholith and other plutons within the Kootenay Arc, a major regional flexure in Purcell, Windermere and Lardeau rocks in southeastern British Columbia (Wheeler, 1966, p. 38).

Most volcanic and sedimentary rocks south of Francois Lake are folded to some degree, and practically all fold axes trend northwestward. Adjacent plutons of the Topley Intrusions also trend northwestward, but younger granites south of Francois Lake and Cretaceous members of Topley Intrusions east of Stellako River have a divergent trend. Broad folds in older volcanic rocks of the Takla-Hazelton Assemblage (Upper Triassic to Middle Jurassic) distinctly and consistently trend northwest, whereas overlying Ootsa Lake Group volcanics of Late Cretaceous to Eocene age show no consistent fold pattern. The youngest rocks in the area, Endako Group flows of Eocene age, are the least-deformed (Tipper, 1963, p. 45).

South of Francois Lake and six to ten miles south of Endako mine sets of intersecting, steeply-dipping faults strike north and N 45° E (Ibid., p. 46). These appear in plan to be a conjugate set of shears generated by compression along a line trending N 22° E (Fig. 4-1). Displacement of Takla and Hazelton units indicates movement into the acute angle of the conjugate fault sets.
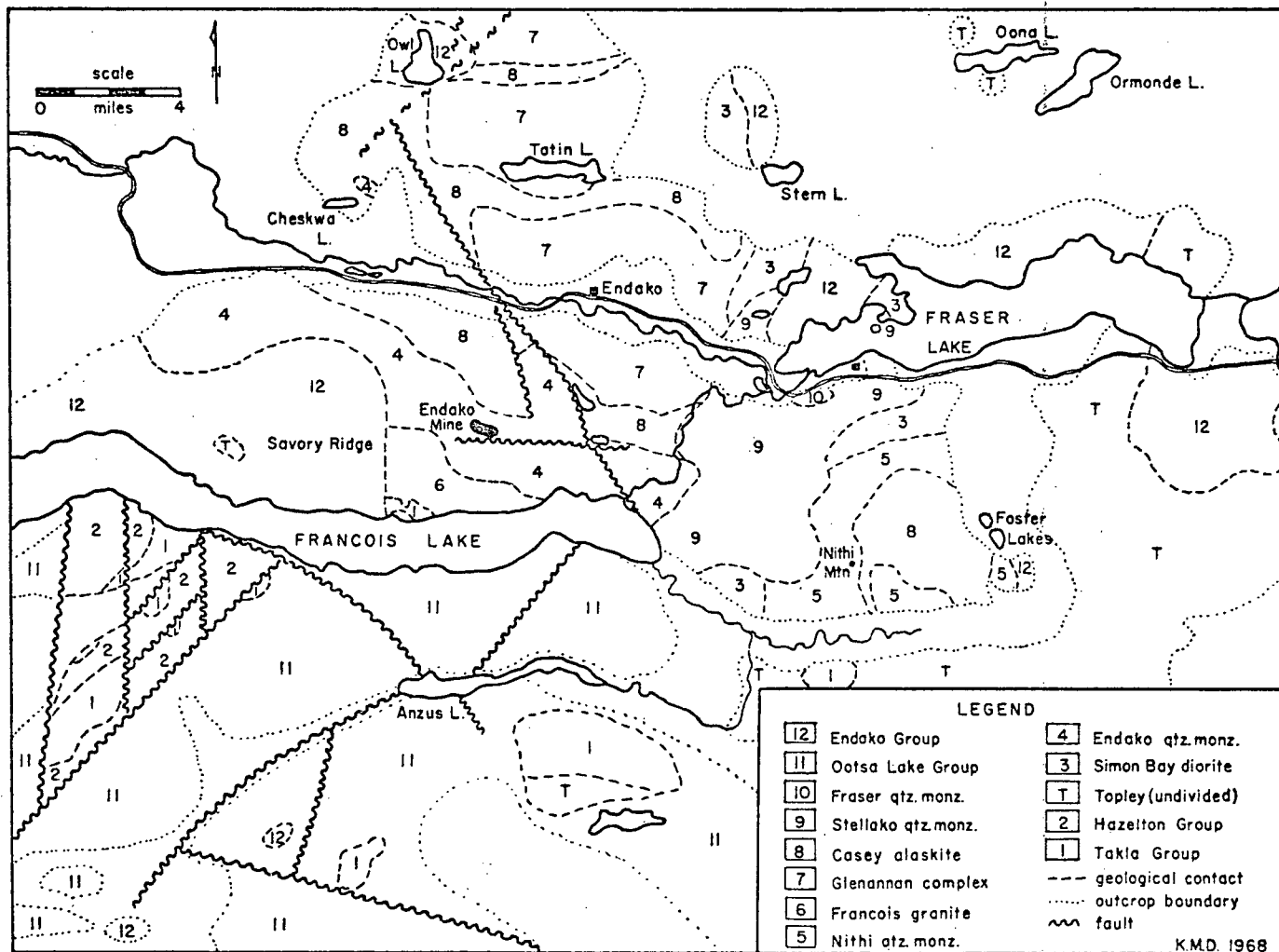
FIGURE 4-1

REGIONAL   STRUCTURAL   TRENDS.

The oldest Topley unit in Endako area, the Simon Bay Diorite Complex, is a concordant mesozonal pluton foliated parallel to its regional northwest trend. Stage Two epizonal phases of Topley Batholith (Endako, Nithi, Glenannan, Casey and Francois units) all show west-northwest elongation in Endako area. Radiometric dating by White, et al (1970) has shown these younger plutons to be of Late Jurassic, hence post-Hazelton age. The concordance of northwest structural trends within the Topley batholith, the parallelism of this trend with fold axes in the older Takla-Hazelton Assemblage to the south, and conjugate fault evidence of a post-Hazelton compressional axis trending N 22° E, support the view that Topley Intrusions in the Endako area were emplaced as elongate, possibly domal bodies essentially normal to a regional N 22° E compression.

The age of conjugate faults that cut Takla and Hazelton rocks south of Francois Lake is not known precisely. Tipper (1963, Map 1131A) has indicated fault contacts between older rocks and Ootsa Lake Group volcanic rocks; hence the faulting may be, in part, as young as Eocene. However, the parallelism of structures in both Hazelton-Takla and the Topley units, normal to the implied compressional axis, and the lack of similar structures in Ootsa Lake Group rocks support the view that these conjugate shears were developed contemporaneously with emplacement of the Topley batholith. Renewed faulting along the same directions in Eocene time could account for displacement of Ootsa Lake rocks.

B.   ENDAKO AREA - FAULTS AND JOINTS

Casey Lake Fault

A major fracture, the Casey Lake fault has been mapped for 6-1/2 miles

in a N 30° W trend across the map-area. Intersections in drill holes

between Casey and MacDonald Lakes and good exposures in a creek canyon

north of Nithi Lodge show dips of 70°W to 90° on the fault. Fault contacts

between Endako Quartz Monzonite on the west and Casey Alaskite on the east

are intersected in three drill holes south of Casey Lake. Trenches north

of No. 1 Tailings Pond expose an intrusive contact between Casey Alaskite

and Endako Quartz Monzonite which trends northeast and lies between Casey

Lake and Tailings Creek faults. Projection of this contact eastward to

Casey Lake fault, and measurement along the fault southeastward to the

inferred origin of the contact results in a horizontal component of right-

lateral movement along the fault of 13,000 feet. A large wedge of Endako

Quartz Monzonite and Casey Alaskite, approximately 3 miles long and averag-

ing 1 mile wide has been displaced over 2 miles northward along Casey Lake

fault and the subparallel Tailings Creek fault to the west.

The Casey Lake fault zone is intruded by andesite porphyry and basalt

dykes throughout its length (see "Minor Intrusions"). Both andesite and

younger basalt dykes exhibit chilled contacts with wall rocks, but more

commonly contacts are sheared. The dykes, apparently related to Eocene

volcanism, intruded the pre-existing fault zone and were sheared by late

movements along the fault. Similar dykes occur within a N 30° W topographic

lineament north of Highway 16 (Carr, 1966, Fig. 22) that may be a northwest-

ern extension of the fault. Casey Lake fault may be a major regional

structure approximately 15 miles long, extending from Shovel Creek on the

north to Nithi River on the south.

Age of Casey Lake fault is defined as post-Late Jurassic (Casey

Alaskite) and pre-Eocene (Endako Group). Fault intersection with Stellako

intrusions is not exposed. The South Boundary fault extends from Endako

mine to MacDonald Lake in an east-west trend and intersects Casey Lake

fault. A small discordancy of trend in Casey Lake fault north and south

of MacDonald Lake indicates some displacement along South Boundary fault

at that locality. Movements on Casey Lake, Tailings Creek and smaller

post-ore faults (N 15°W/90°) at Endako mine may have been in response to

north or north-northeast-directed stress prior to emplacement of Stellako

pluton. A zone of NNE fractures (XY tension fractures) may have opened

upon release of this stress, permitting intrusion of Stellako pluton.

Lateral movement on South Boundary fault and smaller parallel and subparal-

lel faults at the mine probably is related to later east-west stresses

generated during emplacement and consolidation of Stellako intrusions.

Tailings Creek Fault

This fault strikes northward subparallel to Casey Lake fault and forms

the western side of the fault block. The fault is exposed in Tailings Creek

canyon where it shows steep eastward to vertical dips. The block bounded

by these two faults apparently tapers inward with depth. Some rotation of

the block accompanying northward translation is required to account for the

room problem evident in its wedge-shaped geometry. Left-hand rotation

relative to Tailings Creek fault plane, i.e. elevation of the leading edge

of the "wedge" during northward displacement, must have occurred.

A southern extension of Tailings Creek fault is inferred from exposures

of Casey Alaskite and Endako Quartz Monzonite to the west and east, respec-

tively. Scarcity or outcrop and drill core data east of Endako mine

precludes southward projection of the fault through this area. A zone of

north-south shearing and minor faults in Francois granite along Francois

Lake may mark the southern extension of Tailings Creek fault.

South Boundary Fault

This major east-west structure is intersected in drill holes south of

Endako mine and west of MacDonald Lake, and is marked by a topographic

lineament over most of its five-mile length. Dip of the fault is approxi-

mately 45° to 60° north. Movement on the South Boundary fault is considered

to be primarily normal, although minor lateral movement has occurred under

the influence of late east-west stress. The fault is a pre-ore structure

which has influenced development of major veins and stockwork at Endako

mine. Early compressional stresses, active during emplacement of Endako

pluton, apparently created localized doming and fracturing in the vicinity

of the mine, which occupies the intersection of regional east-west, north-

east and northwest fracture systems. Intrusion of pre-ore dykes preceded

the principal structural adjustment of the pluton; wrench faulting along

principal orebody faults, doming of the orebody, and antithetic faulting

along the South Boundary fault and southward and northwestward-dipping frac-

tures. Many large veins and smaller stockwork veinlets follow the predomi-

nant east-west and northeast fracture directions.

Orebody Faults

Two major fault trends are recorded within the Endako pit but are not

observed in regional mapping outside the orebody area. A family of non-

mineralized faults with average attitude N17W/85SW occurs throughout the

orebody but no faults of similar attitude were mapped beyond the limits of

the pit. Another family of faults and joints having average attitude

N50E/70NW are the largest and most abundant post-ore fractures mapped in
the pit. No similar northeast structures have been observed in the mine
vicinity.

In observing apparent offsets in Endako Quartz Monzonite-Casey Alaskite
and Endako Quartz Monzonite-Francois Granite contacts west of the mine,
Drummond (1967) infers that the three Topley units have been offset in a
right-lateral manner along a major fault striking about N 20 W. Because
the western extension of the orebody, that crosses the trace of the inferred
fault, is not displaced, whereas the Endako, Francois and Casey plutons
apparently are offset, mineral deposition would have had to occur after the
relatively young Francois and Casey plutons had been emplaced. Radiometric
ages of the rocks and the orebody are not in agreement with this structural
hypothesis. The configuration of these contacts may have been influenced
by a fault of northwest trend that pre-dated intrusion of Endako quartz
monzonite. Intersection of this old fault with a major east-west fault of
similar age may have weakened the host diorite locally and channeled quartz
monzonitic magma along the two dominant fault directions. Movement along
the old northwest fault may have resumed under northerly stress generated
by cooling and crystallization of the pluton, and influenced stockwork
development by localizing shearing and doming stresses. Post-ore northwest
fault movements apparently have been distributed across the numerous faults
throughout the orebody rather than along the older fault zone.

Although regional northeasterly-trending faults corresponding to
abundant N 50 E mine faults were not detected in mapping, evidence for such
structures exists. An aeromagnetic survey of Endako mine and vicinity
flown by Amax Explorations Inc. in 1966 revealed a deflection of magnetic

isopleths in a northeast linear trend between the eastern end of the ore-
body and No. 1 Tailings Pond (W. Lodder, personal communication, 1970).
The projected intersection of this interpreted fault with the South Boundary
fault is close to a zone of intense stockwork development and abundant post-
ore northeast faulting in the southeastern part of the orebody. A family
of N 40 E/5-30 NW fractures that developed antithetically to south-dipping
fractures during doming are concentrated in the general vicinity of the
projected northeast fault.

Movements on northeast faults in the orebody are all post-ore. No
displacement of the Casey-Endako contact or the South Boundary fault along
the inferred northeast fault is detected in mapping. The northeast fault
apparently has undergone pre-ore movement like its northwest-striking
counterpart at the west end of the orebody.

Regional Joints

Predominant joint attutides were recorded in field mapping, but a
thorough and systematic mapping of joints in all units of the batholith was
not attempted. Low outcrop density over most of the map-area is a limiting
factor in application of stress analysis to the various plutons. Conse-
quently, only general conclusions could be reached from the available data.

Joints in Takla Group rocks southwest of Endako mine consistently
strike N 30°W to N 60° W with steep dips to the southwest. Early rhyodacite
dykes satellitic to Menard stock, later Topley porphyritic quartz monzonite
dykes, and youngest andesite and basalt dykes all follow the same northwest
trend. Early fractures in Takla rocks pre-date Topley batholith and may
reflect the trend of old northwest faults peripheral to Stuart Lake High.

Joints in widely-separated outcrops of Simon Bay Diorite trend variously northwest, northeast and north, and commonly are intruded by small basalt and porphyry dykes. Fractures in this old pluton generally show evidence of movement, and minor shears with the above trends are more abundant than joints. Stresses related to younger orogenic activity in the area have evidently superimposed fractures and faults upon the earlier structural framework.

The four Stage Two plutons in the western part of the map-area show a similar distribution of joint attitudes. Joints in Endako, Francois, Glenannan and Casey plutons strike predominantly northeast and north with steep to vertical dips. East-west and northwest fractures are less common. Periodic increase and release of regional north-northeast compression during emplacement and consolidation of these elongate, subparallel bodies apparently has generated tension fractures of essentially parallel north to northeast trend. Similar joints, interpreted as XY fractures, are intruded by pre-ore dykes at Endako mine.

Stellako intrusions are cut by steeply-dipping north and northwest fractures near Fraser Lake, many of which are intruded by dykes. Predominant northwest and northeast fracture trends in the pluton to the south are also marked by intrusion of small basalt and porphyry dykes. Joints, dykes and minor shears tend to be either parallel or perpendicular to margins of the Stellako pluton, where local stresses generated during emplacement and cooling of the body apparently influenced their development.

Relatively intense jointing, accompanied by quartz-molybdenite-pyrite mineralization occurs in several areas of intersection of regional faults and fractures. Generally, the intersection of northwest and east-west

structures in Endako area produces one or more mineralized fracture directions. At Nithi Mountain, quartz-molybdenite veins with dominant N 70° E/90 attitude occur at the intersection of joints of similar attitude and small faults trending N 60° W/90. On the United Buffaddison property at Owl Lake sparse quartz-molybdenite-pyrite mineralization occurs as a widespread stockwork at the intersection of the northwest extension of Casey Lake fault and a zone of fractures and dykes with northeast trend. Minor jointing with rare molybdenite mineralization occurs west of Mac-Donald Lake, at the intersection of Casey Lake and South Boundary faults. At Endako mine, stress conditions localized by intersection of regional east-west, northwest, and possibly northeast faults, have produced at least five major fracture directions.

C. STRUCTURAL ANALYSIS OF ENDAKO OREBODY

A body of structural data on the attitudes of veins, faults, joints and dykes at Endako mine has been assembled by geological mapping of the 3399, 3135, 3102 and 3069 benches, surface mapping in the same area and underground mapping of adits driven for bulk sampling. Structural data used in this study has been gathered by the following staff geologists in the period 1965 to 1970: E.T. Kimura, S. Wise, A.D. Drummond, D.W. Petersen, M. Waldner and the author. Data from bench mapping is compared with data from underground and surface mapping, and dominant trends are compared with air-photo lineaments. Structural features of Endako mine are correlated with the regional structural trends previously described in this chapter. Geology of 3399 Bench is depicted in Fig. 4-2.

Structural data were originally plotted on an 8-inch Schmidt equal-area

FIGURE 4-2

GEOLOGY OF 3399 BENCH

LEGEND

Quartz monzonite (<0.08% MoS₂)

Quartz feldspar porphyry

Basalt

High grade ore (+0.12% MoS₂)

Low grade ore (0.08-0.12% MoS₂)

Overburden

Faults: major, minor

Quartz-molybdenite veins

scale   0   200   400
              feet
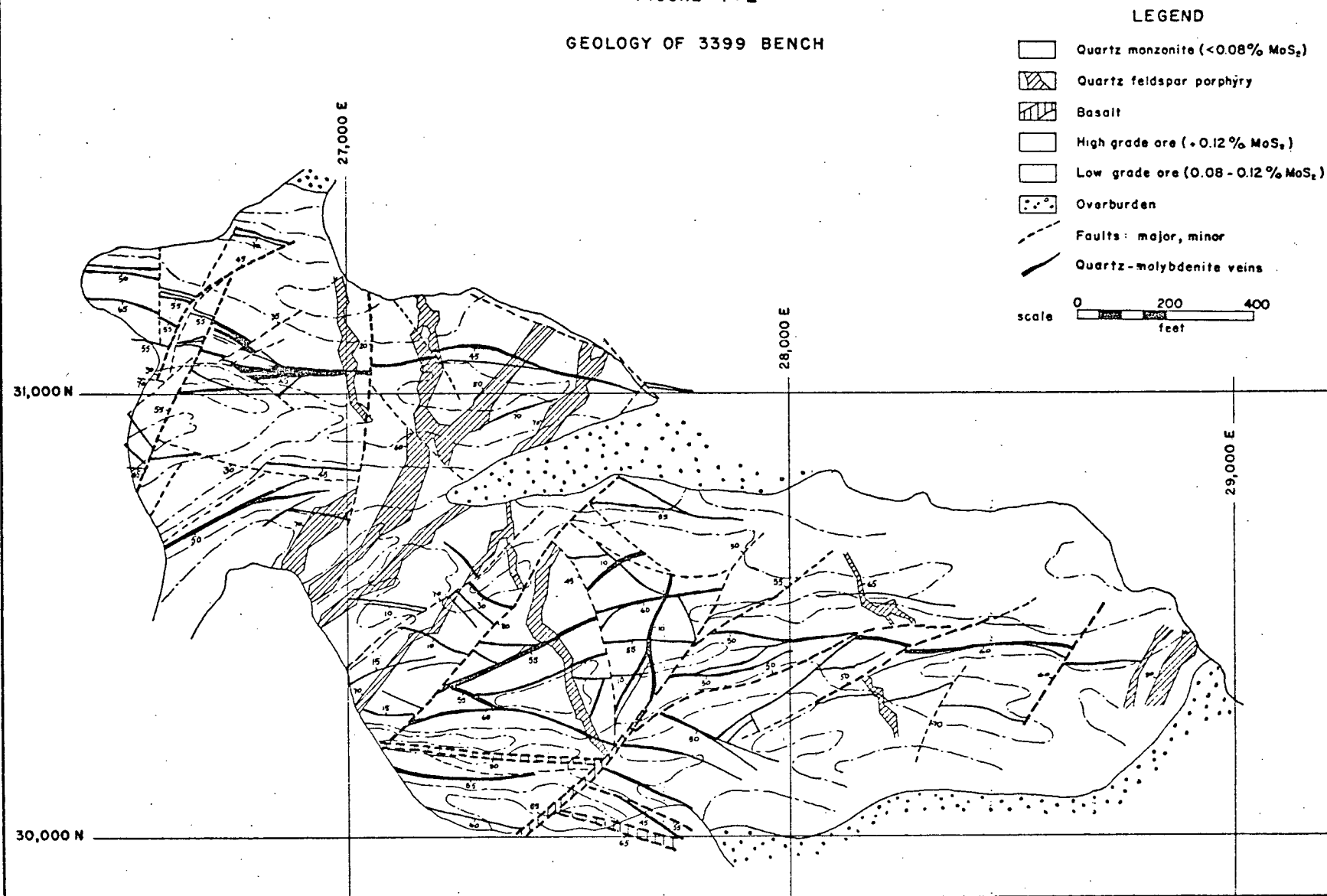
stereo-net and then reduced, as depicted in Fig. 4-3 and 4-6. Dominant

attitudes were obtained by contouring point densities with a moveable 1%

area circle.

(1) Structural Features of the Western Pit Area

   (a) 3399 Bench - Veins and Faults

   Quartz-molybdenite veins on 3399 bench were subdivided into two

groups: those 6 inches wide or greater, and veins less than 6 inches

wide. Only veins wider than 1/2 inch are mapped due to the difficulty

of distinguishing hairline fractures and veins less than 1/4 inch wide

on a freshly-blasted surface in the pit.

   Fig. 4-3A is a stereogram plot of poles to 312 quartz-molybdenite

veins less than 6 inches wide. Major vein directions, in decreasing

order of importance, are as follows:

$$N\ 86°\ E/54°\ S$$
$$N\ 73°\ E/56°\ SE$$
$$N\ 59°\ W/47°\ SW$$
$$N\ 12°\ W/27°\ W$$
$$N\ 47°\ E/10°\ NW$$

   Fig. 4-3B is a plot of poles to 96 quartz-molybdenite veins 6

inches or more wide. Dominant attitudes are:

$$N\ 71°\ E/56°\ SE$$
$$N\ 89°\ W/48°\ S$$
$$N\ 48°\ W/45°\ SW$$

These attitudes correspond closely with the three most predominant

vein trends in Fig. 4-3A, but show a higher degree of preferred

orientation than do the smaller veins.

FIG. 4-3A

3399 bench - poles to 312 quartz - molybdenite veins less than 6 inches wide.

FIG. 4-3B

3399 bench - poles to 96 quartz - molybdenite veins greater than 6 inches wide.

FIG. 4-3C

3399 bench - poles to 163 non-mineralized faults.

FIG. 4-3D

3399 bench - poles to 66 non-mineralized joints.

FIG. 4-3E

3399 bench - poles to 30 quartz - feldspar porphyry and 4 basalt dykes.

FIG. 4-3F

Adit - poles to 125 molybdenite - bearing veins and fractures.

FIG. 4-3G

Adit - poles to 56 non-mineralized faults and fractures.

FIG. 4-3H

Surface-West Pit - poles to 179 veins and non-mineralized fractures.

FIGURE 4-3

Stereogram plots of Western Pit structural features.

Fig. 4-3C is a plot of poles to 163 non-mineralized faults on 3399 bench, indicating the following dominant attitudes:

N 49° E/55° NW
N 04° E/48° N
N 14° W/90°
E-W°   /75°S
N 11° W/60° W
N 18° E/80° W

Faults along veins, or mineralized faults were both mapped as veins. The marked lack of correspondance between principal vein attitudes in Figs. 4-3A and 4-3B, and fault directions in Fig. 4-3C may be slightly misleading since close inspection of the adit area showed that some veins lie along the northeast fault directions, and that some faults lie along the east-west and northwest vein directions (Drummond, 1966c). However, the overall lack of correspondance in vein and non-mineralized fault trends is valid.

(b)   3399 Bench - Joints

Jointing in the pit is accentuated by blasting, hence joints must be carefully examined before mapping. Consequently, only 66 joint attitudes are recorded for 3399 bench in Fig. 4-3D. Dominant attitudes are:

N 49° E/65° NW
N 19° W/77° SW
N 31° E/75° NW
N 24° E/68° NW
N 72° W/50° S

These attitudes are correlated with other non-mineralized structures in Table 4-2

(c) 3399 Bench - Dykes

Fig. 4-3E is a plot of poles to 30 quartz-feldspar porphyry dykes
exposed on 3399 bench. Dyke contacts are very irregular locally, but
the two dominant attitudes in Fig. 4-3E; N 15° E/65° W to N 34° E/
50° NW, and N 36° W/90°, accurately reflect predominant attitudes of
dykes as seen on a geological plan of 3399 bench (Fig. 4-2). These
acidic dykes are cut by all mineralized and non-mineralized structures
in the mine; their attitudes reflect the stress orientation in Endako
Quartz Monzonite prior to mineralization.

Fig. 4-3E also includes a plot of 4 poles to a large basalt dyke
in the west pit. The basalt dyke has average attitude N 82° W/64° S.
It is a late, non-mineralized dyke and follows the dominant east-west
structure. The dyke is displaced by younger northeast-trending faults.

(d) Adit Area - Sections 10,000 and 10,150

The adit area mapped by E.T. Kimura is relatively small compared
to the size of the west pit, but underground mapping allows closer
examination of details of relations between veins and fractures. Fig.
4-3F is a plot of poles to 125 quartz-molybdenite veins and mineralized
fractures in the adit. Principal attitudes are:

> N 68° W/50° SE
> N 69° E/30° NW
> N 86° W/37° S
> N 34° E/84° SE

Fig. 4-3G is a plot of poles to 56 non-mineralized faults and
fractures in the adit area. The dominant attitudes of these structures
are:

> N 49° E/67° NW
> N 23° W/90°
> N 89° E/53° S

These attitudes correspond well to similar structures on 3399 bench
(Tables 4-1 and 4-2). A comparison of Figs. 4-3F and 4-3G reveals a
rough correlation between northeast and east-west faults and veins,
indicating that some fault movements do parallel vein directions.

(e) Surface Mapping

Drummond (1966c) plotted poles to 179 molybdenite-bearing and
non-molybdenite-bearing veins and faults from surface mapping in the
west pit area, and noted the major directions N 80° E/47° SE and
N 63° E/68° NW; with a minor direction N 24° W/90° to 85° SW. These
attitudes correspond with principal trends tabulated in Table 4-1.

(f) Air-Photograph Lineations

V. Zay Smith and Associates Ltd. of Calgary, Alberta produced a
lineament map based on air-photo interpretation for Endako Mines Ltd.
(N.P.L.). From the region between Highway 16 and Francois Lake cover-
ing the mine area, a total of 254 lineaments were compiled by Drummond
(1966c). Trends of these lineaments are diagrammatically represented
in Fig. 4-4. The following strikes are prominent:

> E-W to N 80° E
> N 50° W
> N 30° W
> N-S
> N 52° E

Structures mapped at the mine coincide closely with these lineament
directions (Table 4-1), indicating that regional lineations bear a

FIGURE 4-4

Diagrammatic plot of 254 lineations, from V. Zay Smith Associates

airphoto interpretation for the Endako mine area, showing most

prevalent directions. Area from Highway 16 south to Francois Lake.

After A. D. Drummond, 1966.
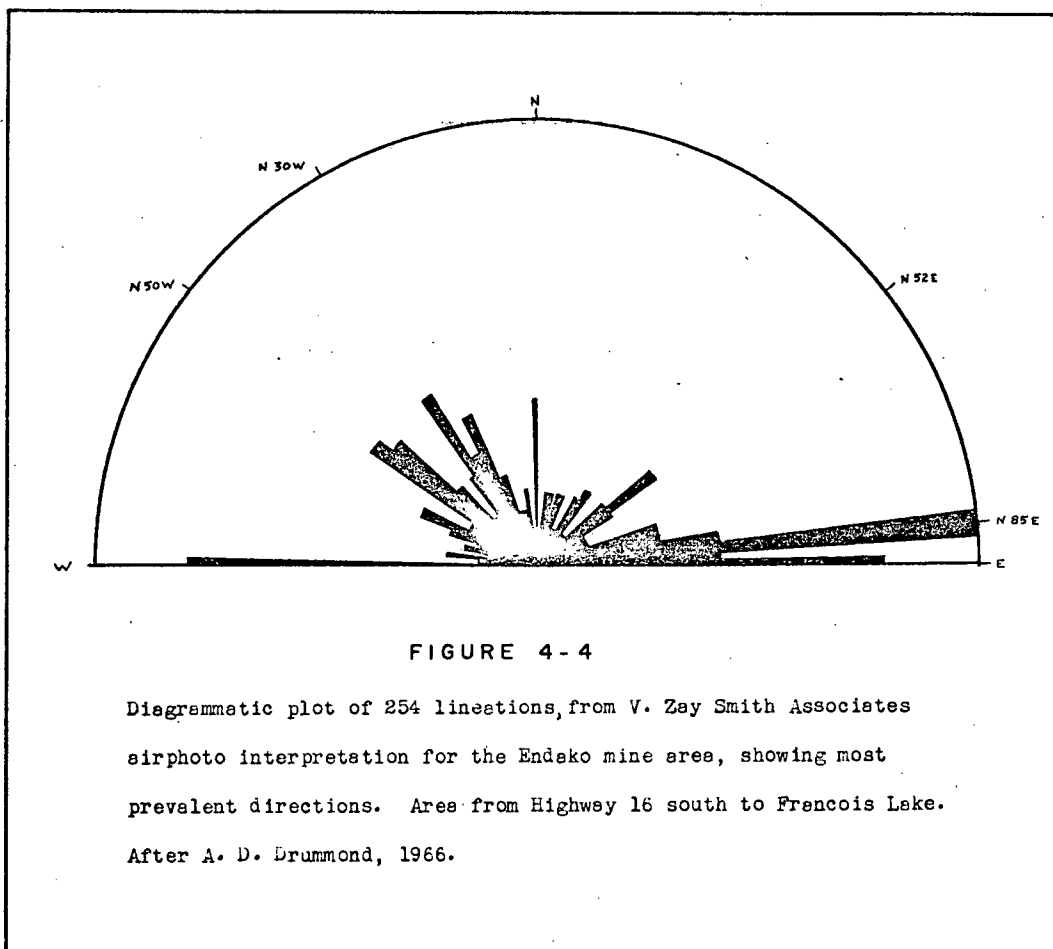
direct relationship to the structural features of the mine.

J.M. Carr (1966, Fig. 25) prepared a sketch map of lineaments near the Endako orebody from Department of Transport air photographs (Fig. 4-5). These lineament trends correspond with those of the V. Zay Smith map in Fig. 4-4 and with the major structural trends outlined in mine mapping.

The location of the orebody at the intersection of three major regional fracture systems is evident in Fig. 4-5. Mineralized east-west, northwest and northeast fractures may reflect the trends of earlier fractures which controlled emplacement of the pluton. Configuration of Endako Quartz Monzonite contacts with Casey Alaskite and Francois Granite shows a marked change in trend of the elongate pluton in the vicinity of the mine, indicative of intersection of east-west and northwest fracture zones. Northeast lineaments correspond to both post-ore faults and joints as well as flat-dipping veins in the mine. Predominance of N 50° W lineaments in Fig. 4-5 evidently is due to accentuation of topography over underlying structures by local ice movements in this direction.

(2) Structural Features of the Central-Eastern Pit Area

Structural data from benches 3267 and 3333 in the central-eastern pit area were compiled by Kimura and Drummond (1969). The data are presented in two groups: quartz-molybdenite veins, and non-mineralized faults and joints. The area includes a large central swarm of porphyritic granite and quartz-feldspar porphyry dykes, and the eastern pit north of grid line 30,000 N.
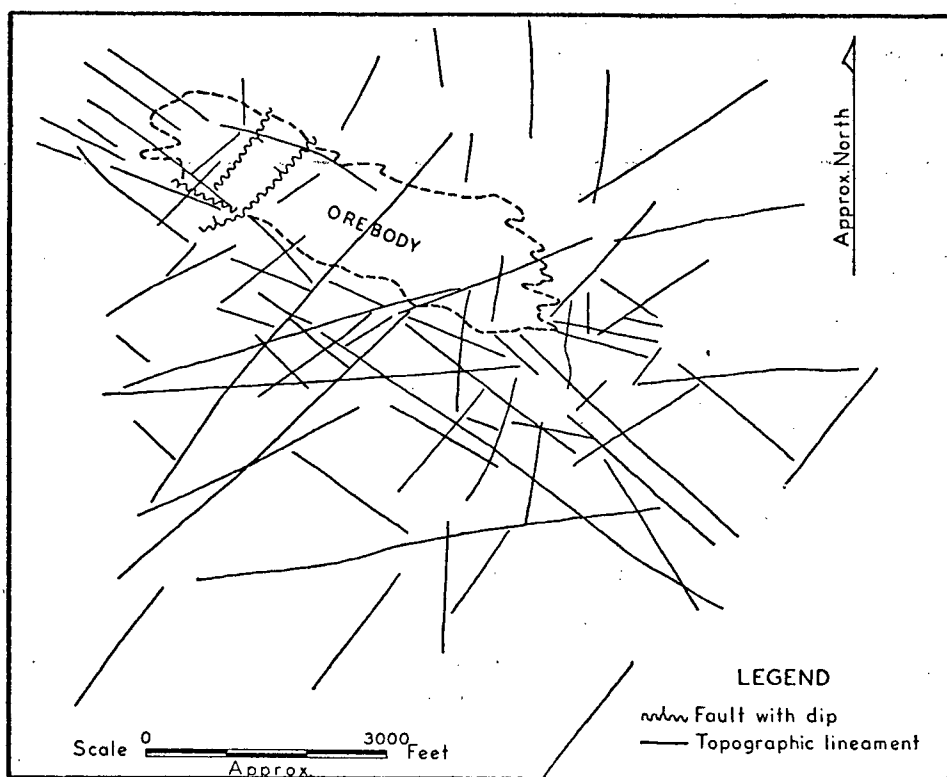
FIGURE 4-5

AIR - PHOTO LINEAMENT TRENDS.

From J.M. Carr, 1966, FIG. 25.

Table 4-1

Correlation of Structures in Western Pit,

Adit and Surface at Endako Mine

Structure	Location			
	3399 Bench	Adit	Lineations	Surface
Quartz-molybdenite veins	N86E/54S to		N85E	N80E/47SE
	N73E/56SE	N68E/50SE		
	N59W/47SW	----	N50W	
	----	N69E/30NW	N70E	
Non-mineralized faults	N49E/55NW	N49E/67NW	N52E	N62E/68NW
	N14W/90	N23W/90	N30W	N24W/90
	N04E/48W	----	N-S	
	E-W/75S	N89E/53S	E-W	

Table 4-2

Correlation of Non-mineralized Structures at Endako Mine

Faults-3399 Bench	Faults-Adit	Joints-3399 Bench	Basalt Dykes
N49E/55NW	N49E/67NW	N49E/65NW	----
N14W/90	N23W/90	N19W/77SW	----
E-W/75S	N89E/53S	N72W/50S	N82W/64S
N18E/80W	----	N24E/68NW	----

(a) Quartz-molybdenite Veins

The stockwork of small quartz-molybdenite veins is more extensively developed in the central-eastern pit area than in the west. Large veins dip moderately southward, and large flat-lying veins are more abundant than to the west but less abundant than in the southeastern pit. Veins show preferred orientation of strikes in the range northeast to east-west, but dips are distinctly more variable.

A stereogram of poles to 147 quartz-molybdenite veins is given in Fig. 4-6A. Principal vein attitudes are:

<div align="center">

N 88° E/ 5° N
N 80° E/40° N
N 85° E/45° S
N 35° E/60° SE
N 58° E/60° NW

</div>

(b) Non-mineralized Faults and Joints

The dominant trend of faults and joints in the central-eastern pit is northeast, with minor trends northwestward and due northward. East-west faults generally follow major veins and are not plotted as faults. Non-mineralized fractures show a consistent preferred northeast trend throughout the orebody. No significant differences in fault and joint attitudes were detected between the three sub-areas studied.

Poles to 50 non-mineralized faults and joints in the central-eastern pit are plotted in Fig. 4-6B. Predominant attitudes are:

<div align="center">

N 42° E/85° NW
N 30° W/85° SE
    N/30° E
N 12° E/80° SE
N 38° E/60° SE

</div>

(3) Structural Features of the Southeastern Pit Area

Benches 3069, 3102 and 3135 in the southeastern pit area were mapped
in 1969 and 1970. Data from this area south of grid line 30,000 N and east
of the central dyke swarm are considered in four groups below:

(a) Quartz-molybdenite Veins

Poles to 511 veins 6 inches wide or greater are given in Fig. 4-6C.
The largest concentration is centred at N 39° E/13° NW. The only other
significant attitude is N 84° E/51° S. Fig. 4-6D is a stereogram of
poles to 977 veins less than 6 inches wide. The strongest concentra-
tion of small veins, N 37° E/30° NW, corresponds with a concentration
of large veins in the same area, except for the steeper average dip of
the small veins. A secondary concentration of small veins at N 86° E/
54° S corresponds with the secondary concentration of large veins in
Fig. 4-6C. Veins in the southeastern pit are strongly concentrated in
two sets: veins with flat to 30° northwestward dips and northeast
strikes, and veins with moderate southward dips and east-west strikes.

The stockwork of large and small molybdenite-bearing veins is
more intensely and uniformly developed in the eastern and southeastern
parts of the pit than elsewhere. A progressive increase in stockwork
development is evident from the western towards the eastern and south-
eastern areas. In the western pit largest veins dip 50°-60° southward,
whereas largest veins in the southeastern pit are flat or dip shallowly
northwestward.

FIG. 4-6A EAST PIT
Benches 3267, 3333: Poles to 147 quartz-molybdenite veins.

FIG. 4-6B EAST PIT
Benches 3267, 3333: Poles to 50 non-mineralized faults and joints.

FIG. 4-6C SOUTHEAST PIT
Benches 3069, 3102, 3135: Poles to 511 quartz-molybdenite veins > 6" wide.

FIG. 4-6D SOUTHEAST PIT
Benches 3069, 3135, 3102: Poles to 977 quartz-molybdenite veins <6" wide.

FIG. 4-6E SOUTHEAST PIT
Benches 3069, 3102, 3135: Poles to 229 non-mineralized faults.

FIG. 4-6F SOUTHEAST PIT
Benches 3069, 3102, 3135: Poles to 352 non-mineralized joints.

FIG. 4-6G
Orientation of early stress.

FIG. 4-6H
Orientation of doming and fracturing stress.

FIG. 4-6I
Orientation of late stress.

FIGURE 4-6

Eastern and southeastern pit structures and stress orientation.

(b) Faults and Joints

Non-mineralized faults in the southeastern pit show the same tendency of northeast strikes and moderate to steep northwest dips as do faults elsewhere at the mine. Poles to 229 faults are plotted in Fig. 4-6E. Dominant attitudes, in diminishing order of importance, are as follows:

N 55° E/65° NW
N 48° E/89° NW
N 61° E/32° NW
N 06° W/90°
N 70° E/90°
N 30° E/73° NW

East-west faults often follow major veins, therefore these "mineralized" structures are not plotted with other faults.

Non-mineralized joints show a strong tendency to strike north-eastward and dip steeply to vertically. Poles to 352 joints are plotted in Fig. 4-6F. Dominant attitudes are:

N 43° E/88° NW
N 12° W/90°
N 30° E/90°
N 71° E/85° NW
N 38° E/73° SW

Similar concentrations of joint attitudes were mapped in the central-eastern and western pit areas.

(c) Dykes

Dips of dyke contacts were seldom recorded in mapping of the eastern pit. Where measured, dyke contacts dip steeply to vertically, and the average dip is taken as vertical. Acidic dykes are small and

sparsely distributed in the southeastern pit in comparison to the two

dyke swarms in the central and western areas.

Dyke attitudes occur in two distinct groups. The average atti-

tude of 25 northeast-trending dykes is N 26° E/90°, and the average

attitude of 11 northwest-trending dykes is N 20° W/90°. Dyke swarms

in the western pit show the same predominant north-northeast strikes

and minor north-northwest strikes.

Summary

Mineralized and non-mineralized structures are correlated among the

three sub-areas of the orebody studied (Table 4-3). Two dominant vein atti-

tudes are noted throughout the pit: E-W/50° S and NE/5-30° NW. Three

principal attitudes of non-mineralized faults and joints are noted, with a

N 50° E/70° NW set predominant. Other principal attitudes are N 30° E/

70° NW and N 15° W/90°. Structures located by surface and underground map-

ping, and airphoto lineations also correlate with the dominant attitudes

listed in Table 4-3.

(4)   Interpretation of Mine Structures

(a)   The Stress Indicatrix

The stress indicatrix technique, as proposed by J.W. Ambrose

(pers. comm., 1967), has been used in analysis of mine structures. A

theory of relations between stress and failure directions in rocks was

first proposed by Coulomb (1773), later restated by Mohr (1882), and

recently proven mathematically by Hubbert (1951). Several authors

have applied Mohr's hypothesis to studies of geometry and kinematics

<u>Table 4-3</u>

Correlation of Structures at Endako Mine

Quartz-molybdenite Veins		
Western Pit	Central-Eastern Pit	Southeastern Pit
N 86° E/54° S (sm) N 89° W/49° S (lg) N 47° E/10° NW (sm)	N 85° E/45° S N 88° E/ 5° N	N 86° E/54° S (sm) N 84° E/48° S (lg) N 39° E/13° NW (lg) N 37° E/30° NW (sm)
Non-Mineralized Faults and Joints		
N 49° E/55° NW (ft) N 49° E/65° NW (jt) N 31° E/75° NW (jt) N 14° W/90° (ft) N 19° W/77° SW (jt) E-W /75° S	N 42° E/85° NW N 22° E/60° NW N 38° E/60° SE N 30° W/85° SE ---	N 48° E/89° NW (ft) N 55° W/65° NW (ft) N 30° E/73° NW (ft) N 30° E/90° (jt) N 06° W/90° (ft) N 12° W/90° (jt) N 71° E/90°

Abbreviations: sm = small veins, up to 6" wide

lg = large veins, over 6" wide

ft = faults

jt = joints

of brittle failure in rocks. Anderson (1942) suggested that the three
orthogonal stress directions, P, Q and R, in any fault system may be
determined by measuring the angle 2θ between the faults. De Cizancourt
(1947) defined several types of fractures and developed a statistical
method for their analysis. Sander (1930), in a comprehensive study of
mesoscopic and microscopic structures, translated from the German by
Knopf and Ingerson (1938), emphasizes oriented fabric due to movement,
and symmetry of elements and movements in structural analysis. In a
synthesis of the ideas of Anderson, de Cizancourt and Sander, the stress
indicatrix of Ambrose employs arrangement of structural elements
(geometry) and movements of the elements (kinematics) to predict forces
causing movement (dynamics).

The stress indicatrix is a three-dimensional model of intersect-
ing planes of tension fracture and shear (Fig. 4-7). Three mutually
perpendicular planes in an X-Y-Z orthogonal system (XY, XZ and YZ planes)
are tension fracture planes, i.e. planes of zero shear. Their inter-
sections define the X, Y and Z axes which correspond dynamically to
principal, intermediate and minimum stress (σ_1, σ_2, σ_3 or P, Q, R)
respectively. The two shear planes of Mohr intersect in the Y axis
and define the angle 2θ which is measured in the XZ plane and bisected
by the XY plane. Direction of motion on shear planes is given by
lineations (slickensides) parallel to their intersection with the XZ
plane. Sense of movement is determined from field observations and
the nature of the slickenside surface. In the kinematic nomenclature
of the Sander school, the direction of forward motion on the shear
plan "S" is designated "a"; "b" is perpendicular to "a" lineations in
the S plane and corresponds to the Y axis or intermediate stress; and
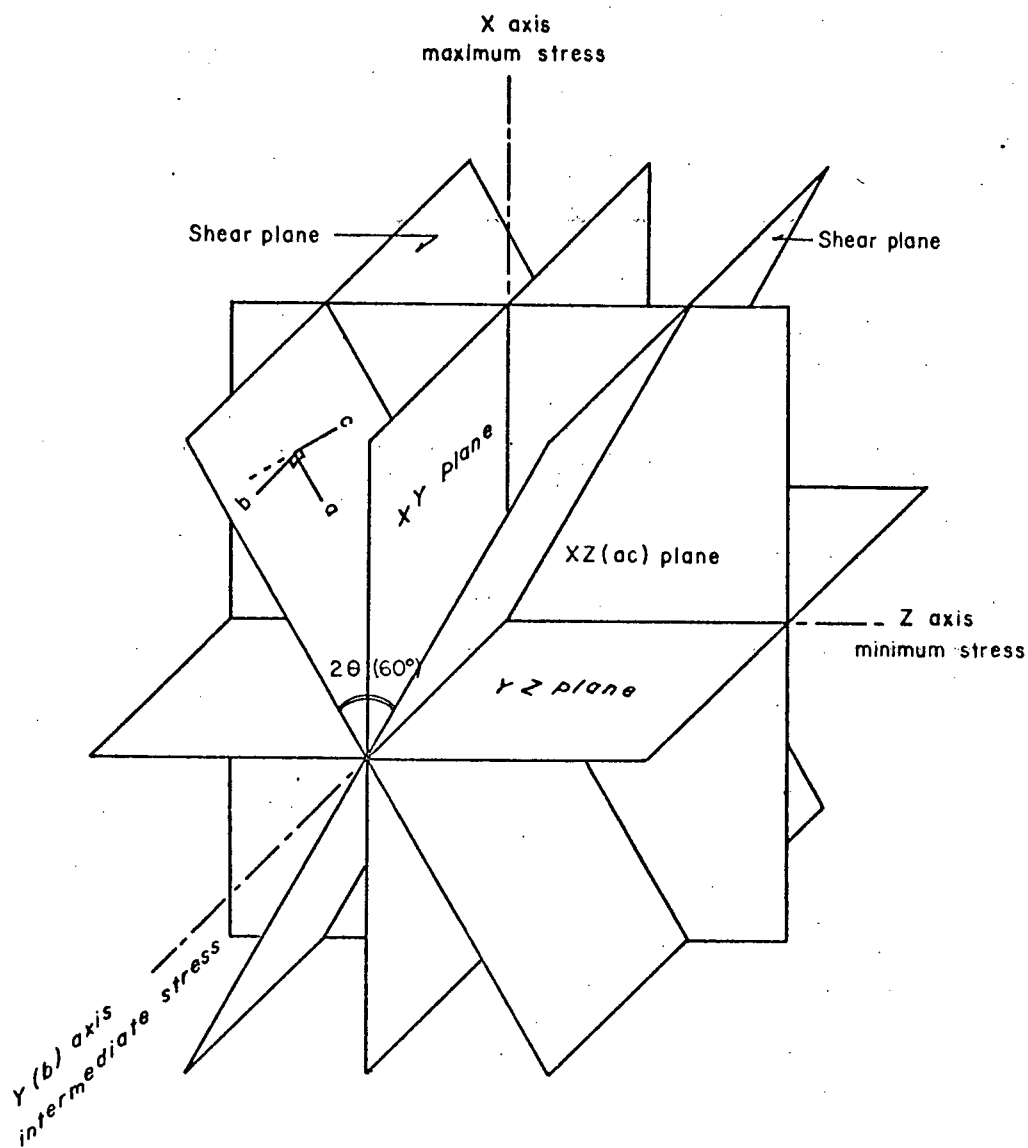
FIGURE 4-7

The Stress Indicatrix

"c" is perpendicular to the S plane containing a and b, therefore lies in the XZ or ac plane.

The orientation of structural elements and movements of a system according to the stress indicatrix will:

1. relate elements to one another;

2. relate movements to one another, and to elements;

3. establish the symmetry of the system;

4. indicate the directions of principal stresses;

5. distinguish those elements not related to the system.

(b) Structural Interpretation

The development of Endako orebody was influenced by three related igneous events: emplacement and crystallization of Endako Quartz Monzonite; intrusion of residual granitic magma as pre-ore dykes; and ascent of hydrothermal fluids through the localized zone of intense fracturing.

Pre-existing faults probably influenced both the trend of Endako Quartz Monzonite pluton and the localization of stresses in the mine area. The pluton follows a regional west-northwest foliation trend in Simon Bay Diorite, and may have either flanked the older unit on the south or intruded it. Deep-seated northwest and east-west faults following this old Topley trend could have served as conduits for the quartz monzonitic magma. Intersection of these faults plus a northeast fault in the vicinity of the mine localized early compressional and shear stresses with resultant doming and fracturing in a restricted area.

(i) Orientation of Early Stress

The Endako Quartz Monzonite pluton was emplaced as an elongate body, probably under stress normal to its long axis. As the body cooled and crystallized, stresses were released by movement along major wrench faults, and by fracturing parallel to the north-northeast principal stress in the orebody area (Fig. 4-8A). Early movements along major orebody faults generated secondary shears, one set of which coincided with the early tension fractures. Swarms of acidic pre-ore dykes with dominant attitudes N 22° E/60° NW intruded the fracture zones (Fig. 4-8B). Fig. 4-6G is a stereogram of the stress indicatrix representing early stress orientation at the mine. Acidic dykes define the XY plane, parallel to the principal stress.

Continued movements along orebody faults subsequent to intrusion of the north-northeast fracture zone by pre-ore dykes developed the other member of the conjugate set of secondary shears, parallel to the South Boundary fault. East-west secondary shears developed in an en echelon array between the bounding N 20°W and N 43°E wrench faults, creating a restricted zone of intersection with north-northeast fractures and dykes, elongated in a west-northwest direction (Fig. 4-8C). Sporadic relaxation of north-northeast stress opened release joints essentially normal to the principal stress, augmenting the zone of early E-W shears of the same attitude, and causing pre-existing shear fractures to gape as tension fractures.

In the stress indicatrix model of early stress orientation (Fig. 4-6G) the large family of E-W/50° S fractures corresponds to the YZ plane, normal to the XY plane defined by pre-ore dykes. Intersection of these two planes defines the Y or b axis. The XZ (or ac) plane is constructed normal to the b axis. Intersection of the XY and ac planes defines the X axis, the direction of principal stress. In this model, the principal stress plunges N 04° W at 37°.

North and northeast-trending zones of incipient shearing probably were generated by early compressive stress. Little or no pre-ore movements occurred along these two directions due to the development of previously described secondary shears by movements along major orebody faults. Conjugate shears that developed under north-northeast stress ideally would intersect the ac plane about 30° either side of the XY plane, defining a 2θ angle of 60°, and intersecting in the Y axis, as depicted in Fig. 4-6G. Major non-mineralized fault attitudes correspond to the two predicted shear directions, indicating a resumption of northerly-trending stress occurred subsequent to mineral deposition.

(ii) Orientation of Doming and Fracturing Stress:

Doming was initiated throughout the west-northwest-trending weakened zone of intersecting fractures and dykes (Fig. 4-8C). A combination of lateral compression and vertical uplift caused doming and resultant fracturing throughout the weakened zone. Regional north-northeast compression was waning as the terminal stage of cooling of the pluton approached. Rise of residual

FIGURE 4-8A

Pre-doming stress and early fractures.

FIGURE 4-8B

Shear stress orientation in the fault-bounded orebody block. Shear S_1 augments existing N22E fractures. Shear S_2 develops after S_1 is intruded by pre-ore dykes.

FIGURE 4-8C

Doming occurs over the weakened zone of intersecting S_2 shears and NNE dykes and fractures. S_2 shears first become YZ tension fractures under release of lateral NNE stress then become normal faults during domal uplift and subsidence.

FIGURE 4-8D

Schematic plan of orebody showing en echelon array of E-W veins, with antithetic NE veins.

FIGURE 4-8: Localization and development of Endako stockwork.

granitic magma that crystallized, successively, as pre-ore aplite, porphyritic granite and quartz-feldspar-porphyry dykes provided continuing vertical stress after orebody dykes were emplaced. With the onset of doming, the principal stress changed from the early sub-horizontal attitude to an essentially vertical orientation.

Fig. 4-6H is a stereogram of the stress indicatrix model of stress orientation during the main stage of fracturing and sulphide deposition. The two principal vein attitudes define a conjugate set of antithetic fractures along which normal displacement occurred during expansion and collapse of the domal structure. A hypothetical ac plane, constructed through the two concentrations of poles to veins, corresponds to a large group of faults and joints with average attitude N 15° W/83° E. The essentially horizontal b axis in this model is defined by both the pole to the ac plane and the intersection of the two average shear planes. The XY plane, constructed through the b axis and bisecting the angle 2θ of 64° measured in the ac plane, corresponds to a family of non-mineralized faults and joints with a similar attitude of N 73° E/72° N. The intersection of XY and ac planes defines the X axis, or direction of maximum stress, that plunges N 08° E at 70°.

The main set of east-west veins formed first as secondary shears, then became YZ release fractures normal to the early compressive stress. With uplift of the dome these fractures became planes of vertical displacement. Vertical adjustments of the

orebody to doming were taken up by the east-west set of south-dipping fractures, by a newly-formed set of antithetic fractures with northeast strikes and shallow northwest dips, and also by the South Boundary fault. Lack of appreciable normal displacement of pre-ore dykes along mineralized southward and northwestward-dipping fractures indicates that doming effects occurred over a relatively small vertical range.

An intensely-developed stockwork of fractures in the eastern and southeastern pit areas was developed during uplift and subsidence of the domal structure. Shallow northwestward-dipping fractures formed a conjugate set with the south-dipping fractures and sustained antithetic normal displacement. Networks of veins with these two predominant attitudes are common in eastern pit stockworks. A related set of horizontal fractures, oriented essentially normal to the vertical stress, opened during uplift and/or subsidence of the dome. In the eastern pit, large Stage 3 quartz-molybdenite veins fill these flat fractures, indicating that the fractures gaped during the last stage of molybdenite deposition. Apparently the flat fractures are YZ release joints that formed as a late structural adjustment of the domed orebody to cessation of vertical stress.

(iii) Orientation of Late Stress:

The Endako orebody has undergone several stages of post-mineralization faulting. A resumption of northerly-trending compressive stresses presumably accompanied the intrusion of younger plutons flanking Endako Quartz Monzonite, with resultant

shearing along pre-existing north and northeast zones of weakness and displacement of earlier dykes and veins. Limited movement along east-west veins may have occurred at this stage, along with opening of northeast-trending non-mineralized joints. Minor quartz-specularite, calcite and chalcedony veins which follow post-ore fractures in the orebody may have attended this period of late fracturing.

The nature of displacement of Topley units along Casey Lake and Tailings Creek faults indicates these are major wrench faults generated by north-trending compression. Movement on these faults and smaller post-ore N 15° W/90° and N 50° E/65° NW faults at the mine probably pre-dates intrusion of the Stellako pluton, and may be in response to renewed northerly compression accompanying emplacement of young Topley units north of the map-area.

Fractures controlling emplacement of the discordant, north-northeast trending Stellako pluton may have opened upon release of the aforementioned stress or a later stress of similar orientation. The central axis of Stellako pluton trends N 22° E (Figs. 4-1 and 4-6I), in precise alignment with earlier tension fractures at Endako mine and the implied regional compressional axis. East-west stresses generated in this Early Cretaceous period of orogenic activity could have renewed movements on old northeast faults at the mine, and caused new shearing movements parallel and subparallel to the main vein attitude of E-W/55° S (Fig. 4-6I). Small lateral movement along South Boundary fault, effecting displacement of Casey Lake fault, is probably related to this stress.

A minor group of non-mineralized N 15° W/90° fractures at the mine, and joints of similar trend in plutons flanking Endako quartz-monzonite may have resulted from release of this late east-west stress.

Insufficient data on sense of movements on post-mineralization faults prevents a more thorough analysis of stress orientation and shear directions. The general sense of movements on principal faults is shown in Fig. 4-6I as deduced from displacements of major structures depicted in 3399 bench plan (Fig. 4-2), the surface map of the west pit area (Fig. 3-22), and the regional geological map (Jacket). Displacements observed in pit mapping are generally small, and represent only the final period of faulting.

(iv) Localization, Development and Zonation of Stockwork

The principal cause of localization of fracturing in the mine area is the intersection of three major faults or fault zones. Secondary shears generated by early movements on these faults, and tension joints that opened under increase and cessation of north-northeast stress intersect to form an elongate weakened zone. Continuation of north-northeast compression plus commencement of vertical stresses accompanying the rise of late granitic magma and emplacement of pre-ore dykes caused doming of the west-northwest-trending weakened zone.

Doming of the weakened area created an elongated, ellipti-cally-shaped zone of intense fracturing and veining. More than

one period of uplift is involved in the development of domal
fracturing. The three types of acidic pre-ore dykes were
emplaced by at least the same number of pulses of rising granitic
magma. Extent and intensity of stockwork indicate that repeated
conditions of uplift and collapse prevailed. However, uniformity
of principal vein attitudes indicates that doming occurred within
a single stress environment. Minor offset of pre-ore dykes by
mineralized fractures shows that the range of vertical movement
during doming was small. Doming of the orebody apparently occurred
in response to numerous sporadic pulsations rather than one or a
few major periods of uplift.

Most veins in the stockwork originated as one member or the
other of a conjugate pair of antithetic faults. Release of verti-
cal stress was distributed mainly over the predominant E-W/50° S
and NE/5-30° NW families of fractures. Intersection of large
east-west and northeast conjugate veins and associated stockwork
veinlets in the eastern orebody created a shallow southwest-
plunging zone of high-grade ore. Large flat veins in the eastern
pit formed as release joints to the vertical stress. Antithetic
faulting dies out vertically and horizontally southward toward the
South Boundary fault. The pyrite zone could be considered as
defining the southern limit of stockwork, although weak fracturing,
alteration and sulphide mineralization occur south of the pyrite
zone. Stockwork fracturing terminates more abruptly to the north
of the orebody, where limits of economic molybdenite deposition
essentially define the northern limits of fracturing.

The South Boundary fault apparently served as a preliminary

fracture flanking the incipient dome, as described in numerous

localities by Wisser (1960). The lack of fracturing adjacent to

this major fault indicates it did not sustain significant move-

ment during doming and subsidence. Schematic cross-sections of

the orebody (Fig. 4-9) show that only the southeastern corner of

the orebody was close enough to the fault for stockwork fracturing

to be influenced.

In the eastern and southeastern parts of the orebody intense

stockwork development apparently is influenced primarily by a

major N 43° E fault zone that crosses the eastern end of the ore-

body. Intersection of this fault with the zone of E-W secondary

shears probably created a zone of intense fracturing in the

eastern orebody. Abundant, small northeast faults associated with

northeast stockwork veins attest to the importance of this fault

zone in generating intense local fracturing. Vertical movements

may have been of relatively greater magnitude and/or frequency in

the eastern orebody, as witnessed by the local abundance of large

flat veins that probably originated as release fractures. Domal

movements in this eastern area probably were enhanced by pre-

fractured ground adjacent to the N 43° E fault, resulting in

relatively intense domal fracturing.

Neither the N 43° E nor the N 20° W regional faults have

generated significant fracturing at their intersections with the

South Boundary fault. A possible explanation for this structural

anomaly is that east-west secondary shears accommodated most of

SECTION AA' : West Pit
The orebody is a narrow zone of large, mainly south-dipping veins. A few flat and shallow northerly-dipping veins occur. The stockwork is very limited in extent. Post-ore NE fractures are abundant. Orebody is at the maximum distance from S. Boundary fault.

SECTION BB' : Central Pit
A combination of vein trends occur. Large EW/45S veins are predominant. Flat to moderate northerly-dipping veins occur. Stockwork is well-developed. A large NNE zone of dykes occupies the central orebody.

SECTION CC' : Southeast Pit
Strongest vein trend is NE/O-30°NW. Flat veins are the largest. EW/50S veins are of secondary importance. Stockwork is most intensely developed here. Apparent shallow south dip of orebody is due to flat veins. South Boundary fault passes close by.

FIGURE 4-9: Schematic sections showing veins and stockwork.

the pre-doming fault movements, and little lateral movement occurred along the South Boundary fault (Fig. 4-8C). This hypothesis also offers explanations for two other structural anomalies: the lack of stockwork at the western end of the orebody and the continuity of east-west veins across the N 20° W fault with no apparent offset. Left-hand movement would have occurred along the N 43° E fault and the zone of en echelon east-west shears, but not along the South Boundary fault and the northern part of the N 20° W fault (Fig. 4-8C). East-west shearing, once established, would cut the N 20° W fault, creating the elongate vein zone in the western extension (Denak Zone) of the orebody. If the N 20° W fault was not active during east-west shearing, as was the N 43° E fault in the eastern pit, then intense localized fracturing would not be generated at the intersection of the two zones. Stockwork in the western pit is restricted to narrow zones of small fractures adjacent to large veins.

(v) The Structural Level Model:

A structural model of Endako orebody involving the concept of differing structural levels has been proposed by Kimura and Drummond (1969). The model explains the two significant trends of (1) apparent decrease eastward in the dip of east-west veins, and (2) concomitant increase in fracturing intensity by depicting the orebody as an antithetic, south-dipping structure that has rotated as a unit in the plane of the South Boundary fault. Tilting of the block by 10 to 20 degrees westward and subsequent erosion would reveal a steeply-dipping, relatively unfractured

and structurally "high" western orebody as compared to a gently-dipping, intensely fractured and structurally "low" eastern end.

The structural level model, although ingenious, evidently is based upon erroneous premises. Southward dips of large and small east-west veins do not show any systematic decrease from west to east. At the western end, large and small veins have average dips of 48°S and 54°S, respectively. In the central-eastern pit veins dip 45°S and in the south-eastern pit large veins dip 48°S and small veins dip 54°S. A minimum depth of economic mineralization occurs at the eastern end of the orebody, due to a relative abundance of shallow-dipping and flat veins. Large east-west veins persist to depth throughout the orebody, at dips ranging between 40°S and 60°S.

The structural level concept is based mainly upon the premise that antithetic fracturing diminishes upward from the intersection of principal antithetic faults at depth. However, the geometry of a domed structure necessitates that the structurally highest rocks undergo the greatest tensile stress, analagous to the stress in the uppermost beds of a concentric fold. In any environment, tension fractures will proliferate with decreasing confining pressure at shallower structural levels. The distribution of antithetic fracturing relative to depth at Endako is similar to that displayed by a clay cake model of a structural dome prepared by the writer at Queen's University (Dawson, 1967). In the model, antithetic fracturing increased in intensity upward from a minimum adjacent to major antithetic fractures to a maximum at surface.

163.

The structural level model somewhat simplistically depicts
the whole orebody as an integral antithetic structure that dips
southward to meet the South Boundary fault. Continuity of this
proposed structural unit is disrupted in the eastern orebody
where flat and northwestward-dipping veins are of equal or greater
importance. The model fails to account for these antithetic,
northwestward-dipping veins that have accommodated much of the
domal movement, but instead assumes that most normal displacement
northward occurred along the South Boundary fault. A structural
dome of the type proposed would be unrealistically assymetrical in
cross section, considering the numerous south-dipping antithetic
fractures. The proposed domal structure is also assymetrical in
plan, as witnessed by the divergence of the western end of the
orebody from the South Boundary fault, leaving the intervening
ground relatively unfractured (Fig. 4-9). Rotation of the proposed
integral structure as a unit is unlikely. A 15 degree rotation
over the 6400-foot length of the orebody would incur a minimum
vertical displacement of 800 feet at the ends of the structure,
if pivoted at the centre. The structurally weak orebody could not
sustain displacement of this magnitude without exhibiting substan-
tial normal and reverse faulting at the western and eastern
extremities, respectively. Displacement of this sense and magni-
tude is not observed on the post-ore northeast faults.

(vi) Summary:

The west-to-east zonation in stockwork intensity at Endako
is best related to variation in magnitude and/or frequency of

domal movements, rather than to a concept of structural level. Abundance of northwest-dipping antithetic fractures and flat-dipping release fractures in the eastern orebody is contrasted to weakly developed stockwork in the western pit, grading westward to a zone of large, south-dipping veins in the Denak Zone. The pre-fractured eastern orebody was amendable to greater domal movements that progressively diminished westward. Tension fracturing and normal faulting also diminished westward with the vertical movements, until only local fracturing was generated adjacent to large veins.

The Endako orebody is considered to be a stockwork of dykes, veins and fractures localized essentially by one period of increase and relaxation of compression normal to the west-northwest trend of the Topley Intrusions. Late fracturing and faulting may be related to stresses generated during the emplacement of younger Topley plutons. The overall structure of the Endako orebody is an intensely-fractured stockwork similar to that of typical porphyry copper deposits of the American southwest where several periods of orogenic activity have developed a restricted zone of repeated fracturing and faulting.

CHAPTER V

ENDAKO OREBODY

A. GENERAL STATEMENT

Endako orebody occurs entirely within Endako Quartz Monzonite. In plan it has an elliptical shape, measuring 6400 feet by 1200 feet, and is elongated in a N 65° W direction. Major veins and mineralized stockwork follow a general east-west trend with shallow to steep southward dips. Six stages of fractures and veins are recognized in the development of the stockwork. Relatively uniform stockwork in the eastern orebody grades westward to a less homogeneous distribution of ore values in large veins and minor stockwork in the western pit and western extension (Denak Zone).

Vein mineralogy is simple, consisting mainly of combinations of the following minerals: (1) quartz, (2) molybdenite, (3) magnetite, (4) pyrite, and (5) chalcopyrite. Bornite, sphalerite, beryl and bismuthinite are rare. Post-ore veins contain calcite, chalcedony and quartz-specularite. Secondary minerals include limonite, hematite, ferrimolybdite, powellite, pyrolusite and malachite.

Several stages of hydrothermal alteration attend metallic mineralization in the mine, but are more widespread than ore-grade material. Predominant phases exhibit crude zonation parallel to the long axis of the orebody. Characteristic alteration features of mine rocks are: (1) K-feldspar-bearing envelopes, (2) quartz-sericite-pyrite envelopes, and (3) pervasive kaolinization. K-feldspar envelopes enclosing quartz-molybdenite veins are larger and more abundant within the orebody than are sericitic envelopes.

Plagioclase in country rock throughout the orebody exhibits various degrees of breakdown to a greenish mixture of kaolinite and sericite. Cross-cutting relations indicate a relative age sequence among alteration assemblages that is in agreement with a chemical control based on the decreasing activity ratio of K+/H+.

The systematic distribution of ore values, alteration zones and minor element abundances in pyrite indicate temperature as well as chemical controls acted during the mineralization period. Fluid inclusion geothermometry of vein quartz from each alteration environment has established approximate temperatures for the assemblages in accord with published experimental data. Inferred temperature gradients apparently dropped off sharply to the north of a high-temperature axis coincident with the K-feldspar zone, and decreased more gradually southward across the orebody. Assymetric distribution of temperature gradients was influenced primarily by fracture density distribution with resultant preferential southward migration of hydrothermal fluids.

B. SEQUENCE OF ALTERATION AND MINERALIZATION

Relative ages of veins and associated alteration features have been established from observations of cross-cutting relationships in diamond-drill core and the open pit. With the progressive development of the Endako stockwork, several stages of fracture and vein development have been superimposed one upon the other. Stages 1 to 5 are defined by characteristic vein and alteration minerals, with molybdenite occurring in veins of the first three stages. Stage 6 is defined by post-ore unmineralized fractures. The chronology of mineralization and alteration is based upon vein and

fracture relationships similar to those depicted in an "ideal" hand specimen in Fig. 5-1.

Stage 1 veins may contain quartz, quartz-molybdenite, and quartz-magnetite-molybdenite, with or without pyrite. Small amounts of beryl and bismuthinite occur in veins of this type. Stage 1 veins are enclosed by K-feldspar envelopes that locally contain biotite, quartz and/or altered plagioclase.

Stage 2 veins contain quartz-magnetite, quartz-molybdenite, quartz-magnetite-molybdenite (with or without pyrite and/or chalcopyrite), and quartz-pyrite with or without molybdenite and/or magnetite. All Stage 2 veins are enclosed by quartz-sericite-pyrite envelopes. Introduced K-feldspar of Stage 1 envelopes is replaced by Stage 2 sericite at intersections of the two vein types.

There is no apparent correlation between a specific type of envelope and any one combination of vein minerals. However, in general, within the orebody K-feldspar envelopes are developed more commonly around quartz-molybdenite veins, and sericitic envelopes are developed more commonly around quartz-magnetite veins. In the pyrite zone that flanks the orebody on the south, quartz-sericite-pyrite envelopes generally are developed around quartz-pyrite veins. Envelopes range in width from a fraction of an inch to 8 inches. Width of an envelope is not related to vein width or mineralogy. Some large veins have narrow envelopes, and vice versa. Envelope width appears to be a function of the time interval the fracture was open to altering fluids.
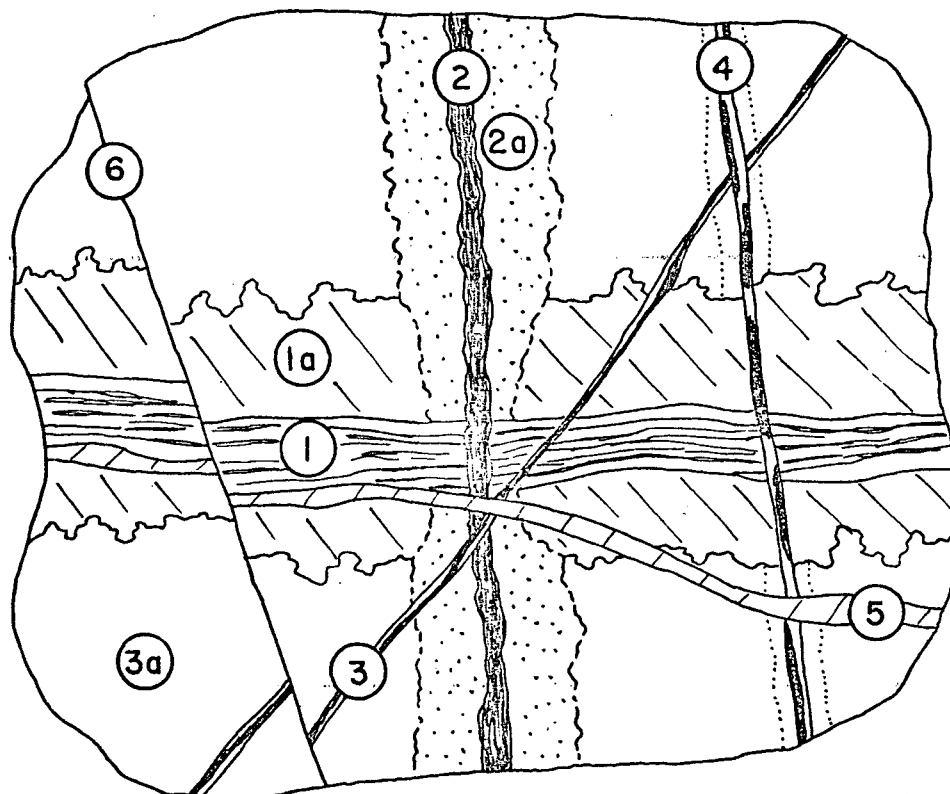
STAGE ① Quartz-molybdenite vein with ⓐ K-feldspar envelope.

STAGE ② Quartz-magnetite-molybdenite vein with ㉒ quartz-sericite-pyrite envelope.

STAGE ③ Quartz-molybdenite-pyrite vein in ③ₐ pervasively kaolinized quartz monzonite.

STAGE ④ Quartz-pyrite vein with bleached halo.

STAGE ⑤ Calcite vein.

STAGE ⑥ Late unmineralized fault.

SCALE : FULL SIZE

KMD, 1968

FIGURE 5-1

Sequence of alteration and mineralization.

Stage 3 veins are composed of quartz, quartz-molybdenite, quartz-magnetite, and quartz-molybdenite-magnetite, all of which may or may not contain pyrite and/or chalcopyrite. Pervasive kaolinization of quartz monzonite host rock extends outward from the stockwork of Stage 3 veins and, to a lesser extent, outward from K-feldspar and sericite envelopes. Degree of kaolinization varies from weak to intense, and within the orebody the commonest alteration type lies between weak and moderate kaolinization. Intensity of kaolinization bears no apparent correlation with vein mineralogy.

Quartz-pyrite veins that lack alteration envelopes are in places enclosed by narrow bleached halos up to 1/2 inch wide, in which iron and magnesium have been leached from the wallrocks. Although of minor abundance, these veins are unique in the sequence of mineralization hence constitute Stage 4. The veins occur within pervasively kaolinized quartz monzonite; hence, they may have served as conduits for fluids effecting kaolinization.

Small calcite, chalcedony and quartz-specularite veins occupy post-ore fractures in the orebody, and constitute Stage 5 of vein and fracture development. Post-ore veins may be either a terminal stage of deposition from ore-bearing fluids, or younger epithermal deposits related to Tertiary volcanism. No wallrock alteration accompanies these veins.

Post-ore faults and fractures represent Stage 6 of stockwork development. These late, unmineralized structures have a dominant north and northeast trend, and a minor east-west trend. Northeast-trending post-ore faults offset major east-west veins with a right-lateral sense of movement. Post-ore movements also occurred along major vein directions. Stage 6 fractures probably were generated by several sources of stress over a protracted

period (see "Structural Analysis of Orebody").

The foregoing sequence of veins, fractures and alteration features is summarized in Table 5-1 (after Drummond, 1967, p. 26).

<u>Table 5-1</u>

Relative Ages of Vein and Alteration Minerals

STAGE	VEIN MINERALOGY	ALTERATION MINERALOGY
1 (old- est)	Quartz, quartz-molybdenite, quartz-magnetite ($\pm$ pyrite, beryl, bismuth-inite.)	K-feldspar, K-feldspar-biotite, quartz-K-feldspar-biotite-plagioclase envelopes
2 ·	Quartz-magnetite, quartz-molybdenite, quartz-magnetite-molybdenite ($\pm$ pyrite, chalcopyrite). Quartz-pyrite ($\pm$ molybdenite, magnetite)	Quartz-sericite-pyrite envelopes
3	Quartz, quartz-molybdenite, quartz-magnetite, quartz-magnetite-molybdenite ($\pm$ pyrite, chalcopyrite)	Weak to intense pervasive kaolinization. No envelopes.
4	Quartz, quartz-pyrite	Bleached halos. Possible kaolinization. No envelopes.
5	Calcite, chalcedony, quartz-specularite.	No alteration.
6 (Youngest)	Post-mineralization faults and fractures	

C.   VEIN MINERALOGY

(1)   Minerals Associated with Molybdenite-bearing Veins

(a)   Molybdenite

Molybdenite, the commonest metallic vein mineral, occurs with
magnetite, pyrite and chalcopyrite in quartz veins of two types: (1)
large veins ranging from 6 inches to 5 feet wide containing laminae of
fine- and coarse-grained molybdenite; and (2) abundant small veins,
ranging from hairline fractures to several inches wide and constituting
stockwork mineralization.

Large veins generally are continuous structures, traceable for
several hundreds of feet along strike with numerous minor offsets by
post-ore faults.   The majority of large quartz-molybdenite veins are
of Stage 3 type, i.e. the veins lack K-feldspar and sericitic envel-
opes, and wallrock exhibits weak to intense kaolinization.   Large
veins have undergone several periods of refracturing and movement
parallel to their trends, with accompanying mineralization.   Vein
structures illustrating periodic reopening, mineral deposition and
movement are listed below:

1.   Molybdenite shows strong laminar distribution within veins.
   Assuming ribbons of molybdenite were deposited along two vein
   walls during each fracture period, then large veins with up to
   30 distinct laminae represent at least 15 periods of reopening
   and mineralization.   Coarser-grained molybdenite laminae generally
   are younger than finer-grained material, indicating a decrease in
   frequency of refracturing movements late in the mineralization
   period.

2. Several ages of quartz within a single vein are discernible in thin-section. Cross-cutting relations are evident. Younger quartz veinlets are a mosaic of fine, unstrained crystals whereas quartz grains in older veinlets become progressively more strained, fractured and granulated with increasing relative age (Plate 5-1).

3. Anastomosing zones of brecciated vein material trend parallel and subparallel to vein walls. Black mylonite composed essentially of quartz, molybdenite and pyrite is developed locally. Matrix of vein breccia is composed of younger vein minerals including quartz, coarse-grained molybdenite, calcite and chalcedony (Plate 5-2).

4. Massive molybdenite stringers commonly serve as planes of shearing within veins, as shown by polished and slickensided molybdenite surfaces.

5. Post-molybdenite minerals occupy late fractures within major veins. Abundant crystalline calcite fills gaping fractures and vugs. Banded or massive chalcedony and quartz-specularite veins are less common.

Although high-grade ore zones are delimited mainly by large veins, the majority of economic mineralization consists of stockworks of small quartz-molybdenite veins in sufficient density to constitute ore. Stockwork veins form zones several tens of feet wide surrounding major veins in the western part of the orebody, but are more widespread in the eastern orebody, yielding more homogeneous ore values. Continuity of small veins is disrupted by numerous offsets along closely-spaced

interlocking fractures, both mineralized and non-mineralized. A single hand specimen might contain six or seven ages of veins and fractures. Veins of Stage 1 through Stage 3 are molybdenite-bearing, may contain any of magnetite, pyrite and chalcopyrite, and may be associated with K-feldspar, sericite or kaolinite alteration. Presence of molybdenite in stockwork veins does not correlate preferentially with any one stage of fracture and vein development, any distinct combination of vein mineralogy, nor any phase of alteration.

Laminated textures in quartz-molybdenite veins less than one inch wide are less common than in larger veins. Molybdenite occurs as finely-divided flakes within small quartz veins, as parallel or sub-parallel ribbons marginally or medially distributed in the veins, or as massive veinlets. Where one or more of the minerals magnetite, pyrite and chalcopyrite coexist with molybdenite, mutual boundaries are irregular or ragged indicating penetration without replacement. Molybdenite exhibits no textural relationships with these minor minerals indicative of contemporaneous deposition, solid solution or replacement. Euhedral to anhedral inclusions of magnetite and pyrite in molybdenite are common, but exsolution relations are absent.

In Stage 1 veins (K-feldspar envelopes) minor amounts of magnetite generally precede molybdenite, and both minerals are veined locally by pyrite. Magnetite is predominant over molybdenite in Stage 2 veins (quartz-sericite-pyrite envelopes) within the orebody, whereas pyrite is more abundant than both magnetite and molybdenite in the "pyrite zone" of Stage 2 veins which flanks the orebody on the south. Abundant molybdenite associated with Stage 3 veins (pervasive kaolinization)
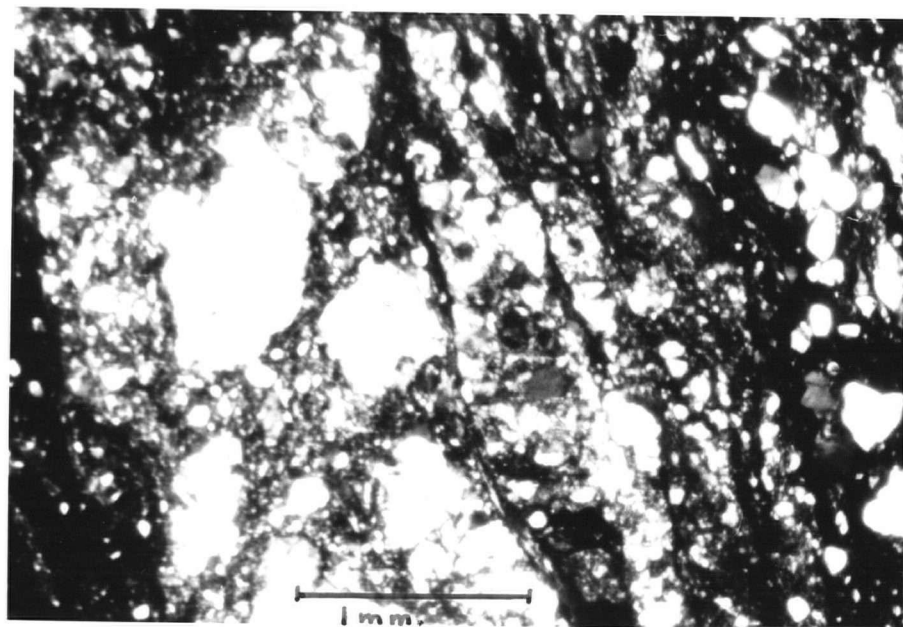
Plate 5-1

Several ages of vein quartz within a single quartz-molybdenite vein (Stella Vein - Centre Ridge). Magnification 40X. Crossed nicols.
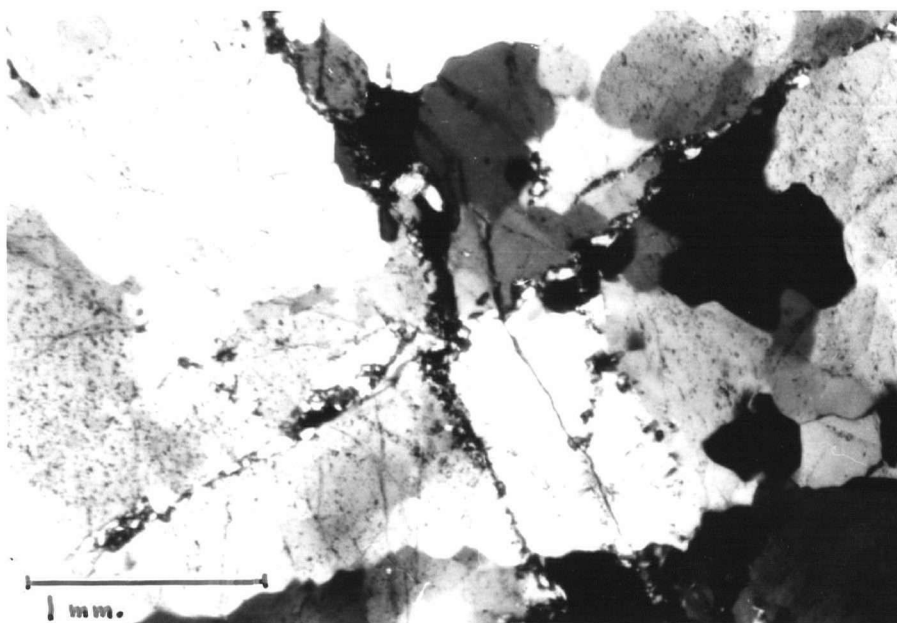
Plate 5-2

Vein breccia; quartz-molybdenite fragments in a matrix of quartz, calcite and mylonite. From the Stella Vein. Magnification 40X. Crossed nicols.

occurs as successive pulses comprising a period that overlaps the depositional periods of magnetite, pyrite and chalcopyrite. Molybdenite both cuts and is cut by all three minor minerals in Stage 3 veins, but pyrite and minor quantities of chalcopyrite tend to be late in the depositional sequence. Plate 5-3 depicts a 7" laminated quartz-molybdenite vein typical of Stage 3. Coarse-grained molybdenite laminae fill the central part of the vein, and laminae of pyrite and chalcopyrite occur near one edge.

(b) <u>Magnetite</u>

Magnetite occurs either alone or with molybdenite, pyrite and minor amounts of chalcopyrite in quartz veins of Stage 1 through Stage 3. Limited cross-cutting relations between Stage 1 quartz, quartz-magnetite and quartz-molybdenite veins indicate magnetite may be the earliest metallic vein mineral (Plate 5-4). However, the depositional periods of magnetite and molybdenite overlap throughout Stage 1 to Stage 3 of vein development, and either mineral may be the earlier in any one vein. Magnetite is most abundant in quartz veins less than one inch wide with quartz-sericite-pyrite envelopes (Plage 5-5), and least abundant in major veins and stockwork veinlets that lack alteration envelopes (Stage 3). Numerous examples of quartz-magnetite or quartz-magnetite-molybdenite veins enclosed by quartz-sericite-pyrite envelopes and cutting K-feldspar-enveloped quartz-molybdenite veins have been observed within the orebody (Plate 5-6). The veins occur within pervasively kaolinized quartz monzonite and commonly are cut by small Stage 3 quartz-molybdenite veins. Cross-cutting relations of sericite-enveloped quartz-magnetite veins have provided important

Plate 5-3

A 7-inch laminated quartz-molybdenite vein typical of Stage 3. Coarse-grained molybdenite laminae occur in the central vein, and pyrite-chalco-pyrite laminae at the top edge. Six-inch ruler gives scale.

Plate 5-4

A Stage 1 quartz-magnetite-molybdenite vein showing magnetite (grey, low relief) cut by a quartz-molybdenite veinlet. Magnification 17.5X.

Plate 5-5

A one-eighth-inch wide quartz-magnetite vein enclosed by a one-inch wide
quartz-sericite-pyrite envelope. The Stage 2 vein is cut by a Stage 5
calcite veinlet. Six-inch ruler gives scale.

Plate 5-6

A Stage 1, K-feldspar-enveloped quartz-molybdenite vein is cut by a Stage
2, quartz-sericite-pyrite-enveloped quartz-magnetite vein and a Stage 5
calcite veinlet. Ruler gives scale.

information on chronology of alteration and mineralization at the mine.

The presence of magnetite with molybdenite and/or pyrite in all three stages of molybdenite-bearing veins proves it to be an integral member of the mineral assemblage. Textural relations between oxide (magnetite) and sulphides (molybdenite, pyrite) indicative of equilibrium conditions, reaction or replacement are absent. Magnetite, like molybdenite, exhibits simple penetration textures with adjoining minerals. Since magnetite may precede or follow deposition of sulphides in all stages of molybdenite-bearing veins, temperature does not appear to have been a principal controlling factor in magnetite deposition. Changes in partial pressures of sulphur and oxygen, possibly attending related changes in alteration chemistry, could control the alternate deposition of oxide and sulphide minerals.

Physical properties of "magnetite" in quartz veins vary with depth. At or near surface, so-called "magnetite" is mainly earthy hematite with a red streak and weak to negative magnetic susceptibility. Specimens give only hematite peaks on X-Ray diffraction patterns. With depth, "magnetite" becomes harder, the streak changes to brown or brownish-black, and the mineral is weakly to strongly magnetic. X-Ray diffraction patterns show both magnetic and hematite peaks from these specimens. Freshest magnetite at depth is hard, strongly magnetic and shows a black streak. Polished sections taken from the freshest specimens which show only magnetite peaks on an X-Ray pattern reveal minor amounts of hematite developed along grain boundaries and irregular fractures (Plate 5-7). Edwards (1954, pp. 78-79) notes this texture originates from replacement of magnetite by hematite (martitization)
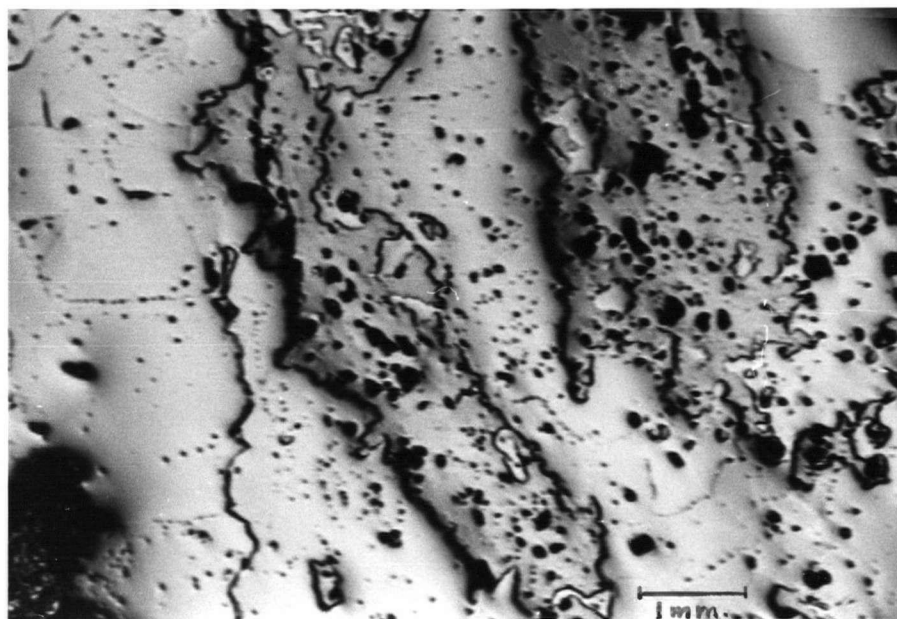
Plate 5-7

Hematite lamellae (light grey) penetrate and replace magnetite (medium grey).
Specimen is taken from drill core 150 feet below surface. Magnification 17X.
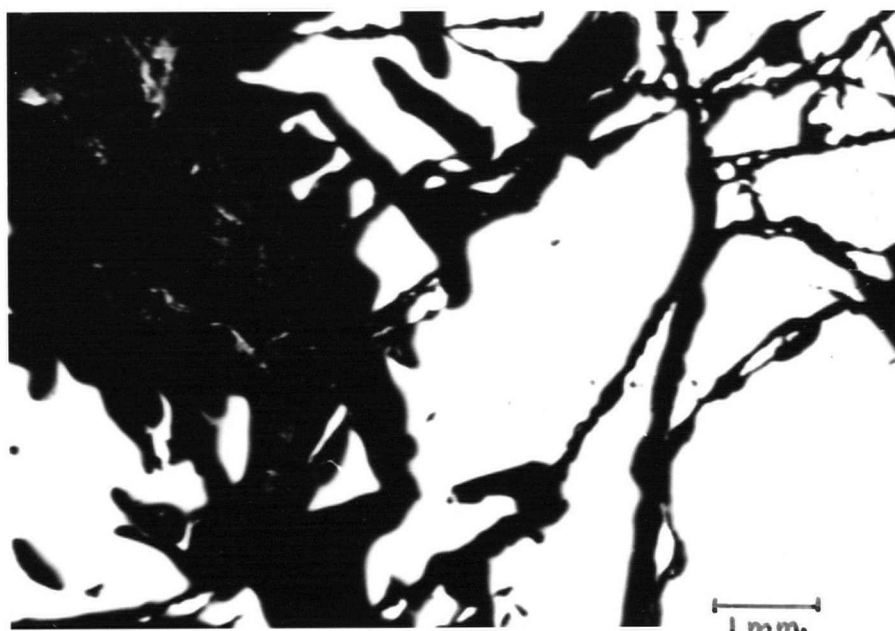
Plate 5-8

Fractures in pyrite (white) filled by molybdenite (black). Matching veinlet
walls show that molybdenite has not replaced pyrite. Magnification 17X.

rather than from unmixing of a magnetite-hematite solid solution. The progressive decrease in hematite relative to magnetite with increasing depth and the texture of magnetite-hematite intergrowth indicate the development of hematite is a secondary feature related to the present erosional level. Circulating groundwater has oxidized ferrous iron in magnetite to the ferric state, producing hematite. The development of secondary hematite is observed at depths in excess of 100 feet below the limit of limonite and ferrimolybdite development on near-surface fractures.

(c) Pyrite

Pyrite occurs in minor amounts in all stages of molybdenite-bearing veins. Early quartz-molybdenite and quartz-magnetite veins contain pyrite as cross-cutting veinlets or isolated grains and lenses enclosed by the principal vein minerals. Pyrite is most abundant in sericite-enveloped veins up to one inch wide within the "pyrite zone" flanking the orebody on the south. These quartz-massive pyrite veins containing minor amounts of molybdenite and/or magnetite form a stockwork in weakly kaolinized quartz monzonite that extends southward beyond the limits of economic molybdenite mineralization. Pyrite in corresponding Stage 2 veins within the orebody is subordinate in abundance to molybdenite and magnetite, and may be associated with minor amounts of chalcopyrite. Major laminated quartz-molybdenite veins commonly contain minor amounts of pyrite either as parallel laminae synchronous with molybdenite deposition, or as subparallel ribbons and lenses following late fractures within the veins. Small stockwork veins also contain pyrite in association with molybdenite, magnetite and chalcopyrite.

Quartz veins containing pyrite alone and lacking alteration envelopes constitute Stage 4 of vein development, the final period of sulphide deposition at the mine. These small veins that occur within the orebody and the pyrite zone are distinguished on the basis of their cross-cutting relations with earlier pyrite-bearing veins, the lack of vein minerals other than pyrite, and the rare presence of bleached halos rather than alteration envelopes surrounding the veins. Within the bleached halos only leaching of magnesium and iron from kaolinized quartz monzonite has occurred, whereas alteration envelopes developed elsewhere are indicative of significant mineralogical and textural changes in wallrock.

In the three stages of molybdenite-bearing veins pyrite, like molybdenite, exhibits textures indicative of several periods of deposition. Early-formed pyrite has been shattered by small movements contemporaneous with mineralization and is invaded along the network of fractures by molybdenite. Matching walls of these veinlets show negligible replacement of pyrite by molybdenite (Plate 5-8). Later pyrite veinlets commonly enclose flakes of molybdenite and grains of magnetite (Plate 5-9), and may, in turn, be cut by small, late-stage molybdenite veins. Pyrite-chalcopyrite associations that generally develop late in the depositional sequence may also be transected by small molybdenite-bearing veins.

(d) Chalcopyrite and Bornite

Minor amounts of chalcopyrite with trace quantities of associated bornite occur with massive pyrite in Stage 3, and less commonly, Stage 2 veins in the orebody. Chalcopyrite is associated with pyrite as
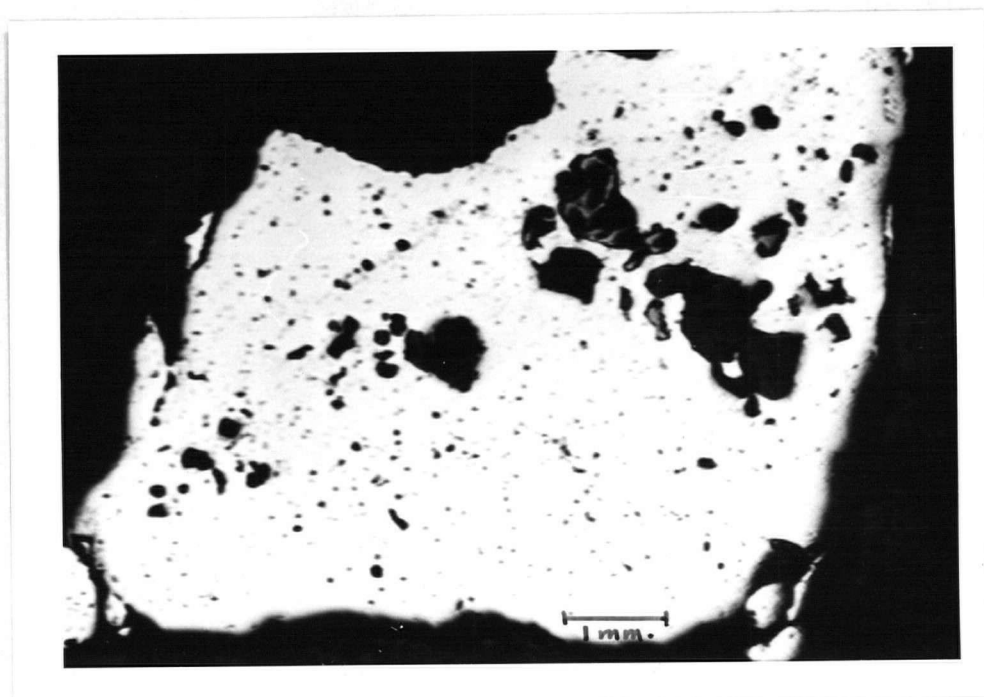
Plate 5-9

Stage 3 quartz-molybdenite-pyrite vein where relatively late pyrite (light grey) encloses molybdenite (black) and quartz (dark grey). Magnification 17X.
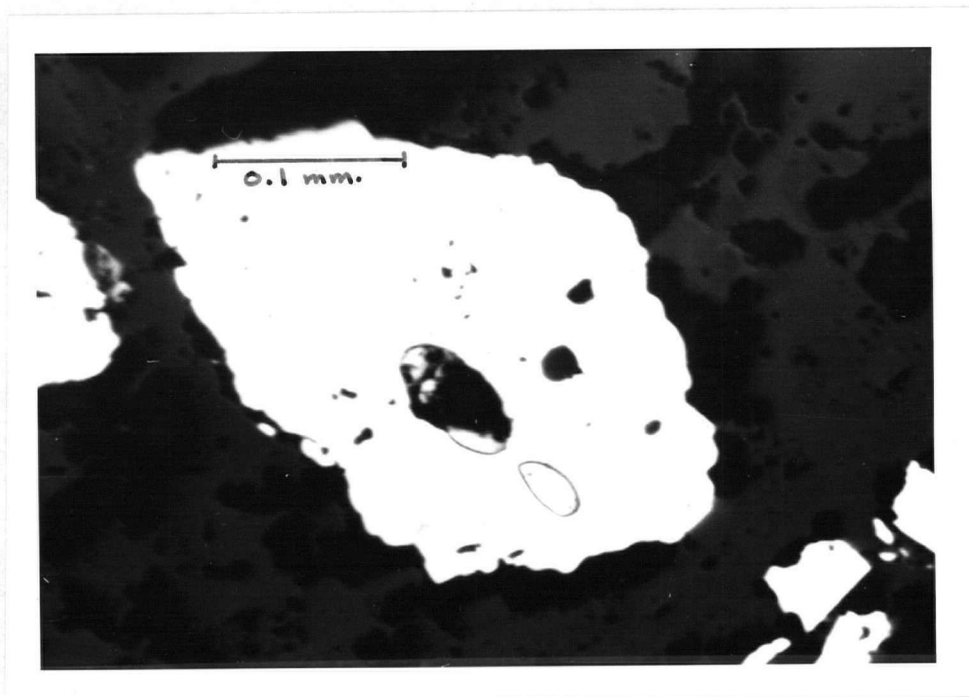
Plate 5-10

Round inclusions of chalcopyrite (grey) in pyrite (white). Magnification 320X.

small inclusions, intergranular masses and partial rims, and ramifying

veinlets that penetrate laterally from fractures, replacing the host.

Pyrite grains with and without associated intergranular chalcopyrite,

in places contain small round bodies of chalcopyrite in a texture

resembling exsolution (Plate 5-10).

Since very limited isomorphous solid solution exists between the

non-isostructural minerals pyrite and chalcopyrite (Mitchell, 1968),

and the size of the chalcopyrite unit cell precludes an omission solid

solution accommodation in pyrite lattice defects, the origin of chalco-

pyrite inclusions and intergranular masses as unmixing products of a

solid solution with subsequent migration to grain boundaries of the

host is unlikely. Chalcopyrite, like gold, may be present as admixed

solid inclusions in pyrite due to contemporaneous deposition (Hawley,

1952, p. 267). However, chalcopyrite inclusions with no visible

accompanying fractures in the pyrite host may simply represent replace-

ment along concealed ducts.

The bulk of chalcopyrite is clearly later than the pyrite it

penetrates and replaces. Replacement textures range from irregular

chalcopyrite veinlets cutting pyrite to relict grains of extensively-

replaced pyrite enclosed by massive chalcopyrite (Plate 5-11). Small

veinlets of massive chalcopyrite containing inclusions of molybdenite,

pyrite and magnetite occupy fractures that transect the earlier vein

minerals.

Two specimens from western part of orebody containing massive

chalcopyrite veinlets showed minute amounts of a mineral resembling

bornite within the veinlets and along adjacent hairline fractures.
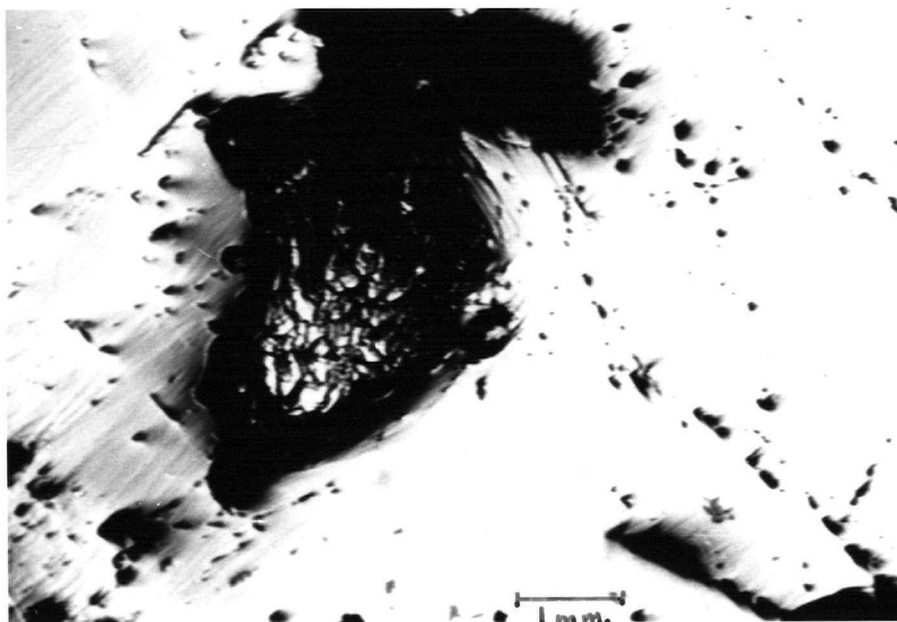
Plate 5-11

Relict grain of pyrite (grey, high relief) enclosed by chalcopyrite.
Magnification 17X.
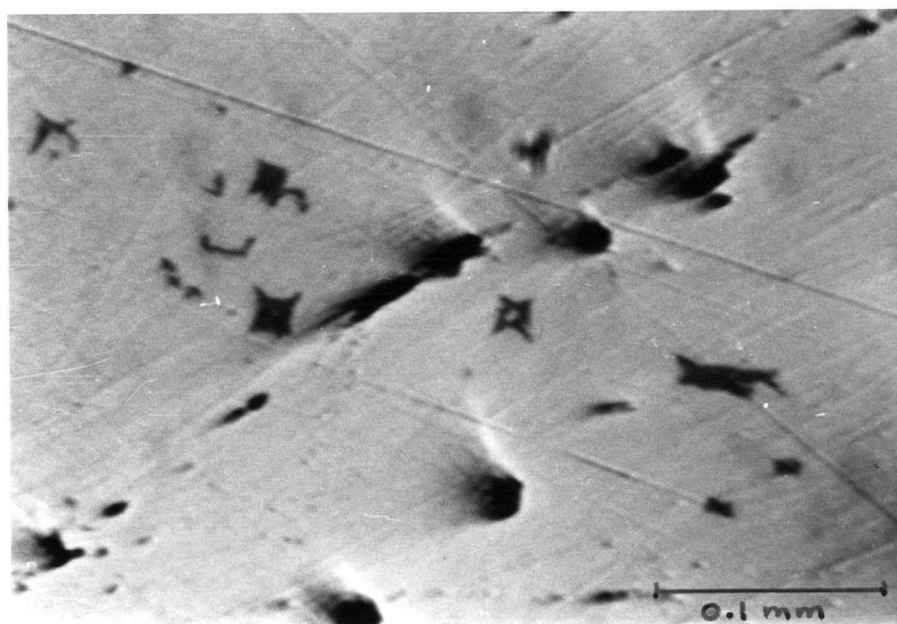
Plate 5-12

Star-shaped exsolution intergrowths of sphalerite (dark grey) in chalcopy-
rite (light grey). Polishing pits are black. Magnification 400X.

The amount of mineral available was insufficient for positive identification. Limited textural evidence indicates the mineral was deposited contemporaneously with chalcopyrite.

(e) Sphalerite

The majority of specimens of chalcopyrite examined under the reflecting microscope contained exsolution intergrowths of sphalerite in the form of small, star-shaped skeletal crystals (Plate 5-12). Edwards (1954, p. 100) notes that chalcopyrite-sphalerite exsolution intergrowths commonly take this form, with sphalerite "stars" elongated in the (111) planes of chalcopyrite. The orientation of the intergrowth is controlled by the orientation of mutual sulphur planes in the structures of the two crystals (Gruner, 1929, pp. 231-232). Although tetragonal, the crystal structure of chalcopyrite is closely related to that of sphalerite. The chalcopyrite unit cell (a = 5.24A; c = 10.30A) resembles two unit cells of sphalerite (a = 5.42A) stacked one on top of the other, so that the c axis is nearly twice as great as the a axis. Chalcopyrite is soluble to the extent of about 10% in sphalerite at temperatures above 350°C, and sphalerite to a somewhat less extent in chalcopyrite at higher temperatures (Edwards, 1954, p. 100).

In heating experiments Borchert (1934, pp. 156-157) synthesized a solid solution of sphalerite in chalcopyrite from which sphalerite "stars" unmixed below 550°C. The usefulness of this temperature as a geothermometer is questionable since equilibria between sulphur and metals were not studied. Recent work on the ternary sulphide systems Cu-Fe-S and Fe-Zn-S is summarized by Barton and Skinner (1967,

pp. 295-302), but experimental data are not available on the quaternary system Cu-Fe-Zn-S. From examination of the ternary systems, it is apparent that the partial pressure of sulphur would affect the position of the chalcopyrite-sphalerite solvus. Borchert's temperature of 550°C may be taken tentatively as a maximum for sphalerite-chalcopyrite exsolution.

(f) Beryl $Be_3Al_2Si_6O_{18}$

Discovery of an isolated occurrence of beryl at Endako mine was made by staff geologists in 1968. The pale bluish-green mineral occurs in radiating groups of slim hexagonal prisms 15 to 20 mm long and 1 to 2 mm in diameter. Beryl is intergrown with coarsely-crystalline, clear quartz, massive pink K-feldspar and molybdenite in a 1/2-inch to 1-inch-wide quartz-molybdenite-pyrite bismuthinite vein (Plate 5-13). Interstices between euhedral crystals of quartz and beryl are filled with hexagonal plates of molybdenite and massive white quartz. The vein transects weakly to moderately kaolinized quartz monzonite and is enveloped by K-feldspar. The specimen was not found in situ hence its precise location within the orebody is not known.

Beryl is taken as an indicator of relatively high pressure-temperature conditions from its typical occurrence in granite pegmatites and greisens, accompanied by other minerals of pegmatitic affiliation. Fluid inclusion studies on beryl from Connecticut pegmatites by Cameron, Rowe and Weis (1953, p. 233) yielded filling temperatures (uncorrected for pressure) up to 400°C. Hydrothermal synthesis of beryl has established approximate stability limits between 400°C under 400 bars water pressure (Wyart and Scavincar, 1957, p. 395) and 800°C

Plate 5-13

Radiating green prisms of beryl intergrown with quartz, K-feldspar and molybdenite. Pyrite and bismuthinite occur in the same vein. Ruler gives scale.

Plate 5-14

Intensely kaolinized Endako Quartz Monzonite that contains remnants of primary pink K-feldspar. Six-inch ruler gives scale.

under 2 kilobars water pressure (Van Valkenberg and Weir, 1957, p.

1808). At higher temperature and pressure beryl decomposes to phena-

kite (Be_2SiO_4), chrysoberyl ($BeAl_2O_4$) and glass in the presence of

water. The occurrence of beryl in K-feldspar-enveloped quartz-

molybdenite veins at Endako indicates high crystallization tempera-

tures prevailed in these Stage 1 veins.

(g) Bismuthinite Bi_2S_3

An isolated occurrence of bismuthinite at Endako mine was noted

from the same vein that contains beryl, as described previously.

Within the quartz-K-feldspar-molybdenite-pyrite vein are several flat

or elongated prisms of bismuthinite up to 10 mm long, 2 mm wide and 1

mm thick, possessing two well-developed directions of cleavage, pro-

bably (010) and (100), and longitudinal striae. Bismuthinite prisms

are interstitial to clear, euhedral quartz crystals, and are enclosed

by lenses of pyrite. Bismuthinite, pyrite and K-feldspar are rimmed

by euhedral hexagonal plates of molybdenite. Massive white quartz

accompanied the deposition of molybdenite, and filled interstices

between earlier clear, euhedral quartz crystals.

Bismuthinite is found typically in hydrothermal veins formed at

relatively high temperatures, and in granite pegmatites (Palache,

Berman and Frondel, 1944, p. 277). The mineral assemblage of the

Endako bismuthinite-bearing vein is similar to pegmatitic mineral

associations in Connecticut (Ibid.). Coarsely crystalline textures

of quartz and molybdenite from the vein are uncommon at Endako, and

reminiscent of pegmatitic molybdenite associations elsewhere. The

beryl-bismuthinite vein apparently represents the earliest phase of

Stage 1 mineral deposition, under pressure-temperature conditions
transitional between pegmatitic and hydrothermal.

(2) Post-Ore Minerals

Small calcite, chalcedony and quartz-specularite veins define post-
ore fracture trends in the orebody, and also occupy fractures re-opened
along earlier veins by post-ore movements. Stage 5 veins are characterized
by absence of sulphide minerals and wallrock alteration.

(a) Calcite

Pale brown to white calcite, the most abundant post-ore mineral,
commonly occurs as encrustations of coarse crystals along gaping frac-
tures in large quartz-molybdenite veins. Calcite, with minor amounts
of chalcedony, forms a matrix for vein breccia. Small veins of fine-
grained calcite occur throughout the quartz monzonite host rock and
transect all earlier veins. Microscopic stringers and blebs of
carbonate in altered plagioclase may represent a late-stage fixation
of residual lime in argillized feldspar under an increased partial
pressure of carbon dioxide.

(b) Chalcedony

Massive bluish- to greenish-grey chalcedony veins up to 1 inch
wide are sparsely distributed throughout the orebody. Banded and
vuggy grey chalcedony is subordinate to calcite in the matrix of vein
breccia. The presence of chalcedony with calcite indicates epithermal
conditions prevailed during the deposition of post-ore veins (Lindgren,
1937, pp. 356-376).

(c) Specularite

Specularite, the least abundant post-ore mineral, occurs with quartz in veinlets up to one-quarter-inch wide. Fine crystalline specularite with metallic lustre is distinct texturally from earthy hematite secondary after magnetite. Few cross-cutting relations with earlier veins were observed, but the continuity of quartz-specularite veins across sheared and mineralized zones in kaolinized quartz monzonite indicates their relative youth.

Post-ore veins may range in age from immediately post-mineralization (Late Jurassic or Early Cretaceous) to Eocene. The veins may be either a terminal stage of deposition from ore-bearing fluids, or younger epithermal deposits related to Tertiary volcanism. Structural relations and mineralogy of the veins offer tentative support for the earlier age. Post-ore veins are followed by the development of Stage 6 unmineralized fractures, the orientation of which indicates a relation to stresses generated by the emplacement of Stellako Quartz Monzonite in Early Cretaceous time (see "Structural Analysis of Orebody"). The mineralogy of post-ore veins may reflect the composition of a residual or terminal-stage ore fluid. With passage of time and continued cooling and fracturing of the deposit, low pressure-temperature epithermal conditions may have prevailed. Lack of sulphides in these veins may be due to a depletion of residual fluids in sulphur by earlier precipitation of sulphides. The late appearance of oxide and carbonate minerals may represent a concomitant increase in partial pressures of oxygen and carbon dioxide. Iron and lime leached from wallrock during hydrothermal alteration could be fixed in hematite and calcite under these conditions. Alternatively, the marked change in

mineralogy from that of earlier veins, the lack of associated wallrock

alteration, and the characteristically epithermal occurrence of calcite and

chalcedony fracture-fillings indicate the post-ore veins may be related

genetically to Tertiary volcanism. Presence of calcite veinlets in plagio-

clase porphyry and basalt mine dykes of probable Eocene age, and occurrence

of chalcedonic quartz in adjacent Endako Group lavas support this view.

Evidence for both hypotheses is not conclusive, and the two ages of post-

ore veins both may be present.

(3) Secondary Minerals

Within Endako orebody, development of the secondary minerals limonite,

hematite, ferrimolybdite, powellite, pyrolusite and malachite is not

extensive. The depth of oxidation varies from 1 to 5 feet in general,

although limonite penetrates more deeply along fractures and shear zones.

Rocks on south-facing slopes and within highly-fractured dyke zones show

the greatest depth of weathering. Thickest gossans are developed over

high-grade veins and pyritiferous zones, whereas much of the surface of the

orebody contains only limonite and manganese oxide "paint" along fractures.

The orebody probably was weathered to greater depths in pre-Pleistocene

time, but this gossan has been largely stripped off during glaciation. The

prevailing cool climate at Endako is not conducive to deep weathering, and

a relatively impermeable blanket of boulder clay has retarded oxidation of

the deposit in post-glacial time.

(a) Limonite

Oxidation of pyrite at or near surface by air-water processes has

produced ocherous pulverulent crusts and penetrative masses.

The material was not studied by X-Ray diffraction so specific mineral phases such as goethite, lepidocrocite or hematite could not be positively identified. No crystalline goethite was observed and the characteristic browns and reds of goethite and lepidocrocite were not seen. The material is believed to be predominantly amorphous hydrated ferric oxide, or limonite, possibly intermixed with some earthy varities of the above minerals.

Within the zone of oxidation, which seldom exceeds five feet in thickness, pyrite is replaced completely by massive limonite. No pseudomorphs of limonite after pyrite occur. Molybdenite and silicate minerals are coated by limonite, but not replaced. Thin crusts and films of ferrimolybdite and powellite occur directly over molybdenite in oxidized veins. Since molybdenite is only weakly oxidized and chalcopyrite is present in very minor amounts, no corresponding zone of supergene enrichment underlies the zone of oxidation. Limonite exists along fractures to depths of fifty feet below the present surface, and penetrates laterally from these fractures one to two inches into wallrock.

Two chemical processes are involved in the development of limonite after pyrite. Oxidation of pyrite by air-water yields ferric sulphate and sulphuric acid:

$$4FeS_2 + 15O_2 + 2H_2O = 2Fe_2(SO_4)_3 + 2H_2SO_4 \text{ (Blanchard, 1968, p. 46)}.$$
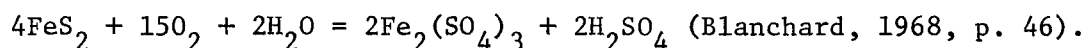
Under acid conditions iron will be transported as ferric sulphate resulting in leaching of pyrite and no precipitation of limonite. Calcium carbonate, chiefly in the form of bicarbonate, along with

weaker neutralizing agents such as calcic feldspar will precipitate

ferric oxide hydrate (limonite) from ferric sulphate solution:

$$Fe_2(SO_4)_3 + 3CaH_2(CO_3)_2 = 3CaSO_4 + Fe_2O_3 + 3H_2O + 6CO_2 \text{ (Ibid., p. 66)}.$$
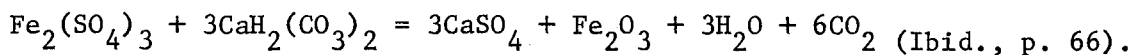
The shallow depth of oxidation and lack of extensive development

of limonite at Endako mine may be attributed to several factors. Py-

rite is only abundant locally, hence groundwater solutions will be

weakly acid in general. The moderate neutralizing effect of quartz

monzonite gangue containing carbonate veinlets is apparently sufficient

to precipitate the majority of limonite in place. Although rainfall

is light, evaporation and oxidation of groundwater has been retarded

by a boulder-clay blanket over most of the deposit, resulting in a

high water-table level. The resultant dilution of descending acid

solutions of ferric sulphate reduces the already low concentration of

ferric iron, inhibiting preciptation of limonite below the water-table.

Where large fractures permit the rapid descent of iron-bearing ground-

water solutions with less dilution and neutralization, limonite is

precipitated at depth.

(b) Hematite

The secondary occurrence of earthy hematite after magnetite was

described previously (see "Magnetite"). Normally magnetite does not

oxidize readily in quartz-feldspar gangue unless sulphides are present

(Blanchard, 1968, p. 164). At Endako, oxidation of pyrite has produced

acidic ferric sulphate solutions from which limonite is precipitated

above the water-table. Secondary hematite in the oxidized zone is

replaces subsequently by limonite, but limonite does not persist to

depth. The presence of hematite secondary after magnetite at depths of 150 feet below the present surface in an environment devoid of limonite indicates that deeply-circulating acidic groundwater, although dilute and low in oxygen, possessed the capability to oxidize magnetite. Ferrous iron is dissolved from magnetite and oxidized to insoluble ferric oxide, or hematite. A reaction of the following type may occur:

$$2Fe^{++} + 1/2O_2 + 2H_2O = Fe_2O_3 + 4H^+ \quad \text{(Drummond, 1967, p. 24)}.$$
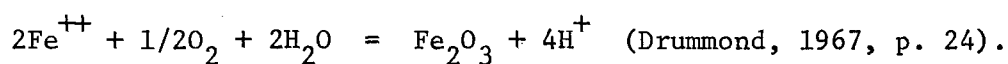
The irregular development of fine grains of hematite along hairline fractures and intergranular boundaries in magnetite (Plate 5-7) is a texture typical of martitization, or oxidation of magnetite to hematite (Edwards, 1954, pp. 78-79 and Pl. 75). The progressive decrease in abundance of hematite with depth indicates oxidation of magnetite is a supergene process.

(c) **Ferrimolybdite** $Fe_2(MoO_4)_3 \cdot 8H_2O$

At Endako mine, ferrimolybdite occurs as canary-yellow earthy coatings and fibrous crusts upon oxidized molybdenite veins. Approximately ten percent or less of molybdenite in the oxidized zone is oxidized, and then only to depths of one or two feet. No zone of supergene molybdenum enrichment underlies the oxidized zone. Molybdenite is not markedly affected by sulphuric acid or ferric sulphate, therefore is oxidized with difficulty under natural conditions and not easily taken into solution to form supergene zones of enrichment (Blanchard, 1968, p. 60). An exception is the large molybdenite deposit at Climax, Colorado where optimum conditions for oxidation and enrichment prevail, and economic concentrations of supergene molybdenum minerals occur. In the oxidized zone at Climax, molybdenite (MoO_3),

an unstable oxidation product of molybdenite, usually turns to ferri-
molybdite (Ibid.). Molybdite apparently is an intermediate product in
the breakdown of molybdenite, being generated by sulphuric acid attack
on molybdenite and subsequently oxidized to ferrimolybdite by reaction
with ferric sulphate.

(d) Powellite Ca(Mo, W)O$_4$

Powellite accompanies ferrimolybdite and limonite as thin, powdery
coatings on oxidized molybdenite veins. The pale brown to dirty white
mineral is not easily recognized in hand specimen, but is readily
identified by its golden yellow fluorescence in ultraviolet light.
Powellite, like ferrimolybdite, is restricted in its occurrence to the
upper part of the oxidized zone. Palache, Berman and Frondel (1951,
p. 1081) note that powellite, a secondary mineral formed by the alter-
ation of molybdenite, is found frequently as pseudomorphs after
molybdenite, and alters to ferrimolybdite. No powellite pseudomorph-
ous after molybdenite has been found at Endako mine.

(e) Pyrolusite MnO$_2$

Pyrolusite is a common secondary mineral throughout the Endako
area. In outcroppings of most plutonic rocks, biotite is broken down
by weathering, and manganese that substituted for ferrous iron in its
structure is oxidized and precipitated along fractures. Within the
orebody pyrolusite is more abundant than elsewhere, probably due to
liberation of manganese that substituted for ferrous iron in hypogene
magnetite and pyrite. Like limonite, pyrolusite does not penetrate
deeply into weathered rocks, but is abundant as thin black films
along near-surface fractures.

(f) <u>Malachite</u> $Cu_2CO_3(OH)_2$

Malachite is a rare secondary mineral at Endako mine due to low abundance of chalcopyrite from which it is derived. Thin coatings of the green mineral occur in oxidized chalcopyrite-bearing veins.

D. ALTERATION MINERALOGY

A study of hydrothermal alteration at Endako mine was undertaken by A.D. Drummond (1966b, 1966d, 1967, 1969), with assistance by E.T. Kimura and the author. Object of the study was to define and explain the relationship of mineralization to the various phases of alteration, and to establish practical exploration guides based on alteration features. Detailed results of the studies of alteration silicates in hand specimen, thin-section and with the X-Ray diffractometer appear in the above reports (Ibid.), and a summary of the findings is given below.

Identification of fine-grained alteration clay minerals by X-Ray analysis without the use of D.T.A. (Differential Thermal Analysis) or heat treatment facilities, is only approximate. The terms "sericite", "kaolinite" and "montmorillonite" refer respectively to the presence of a 10Å mica group mineral, a 7Å kaolinite group mineral, and a 14Å montmorillonite-type mineral. Where present, montmorillonite was glycolated and verified by a shift in the 14Å peak.

Three characteristic hydrothermal alteration phases at Endako mine include development of two types of alteration envelopes, i.e. zones of introduced silicates enclosing a central vein or fracture, and pervasive alteration of the host rock. K-feldspar-bearing envelopes and sericite-

bearing envelopes are developed around veins of Stages 1 and 2 respectively, and quartz monzonite on the outward sides of the envelopes has undergone varying degrees of pervasive kaolinization.

(1) K-feldspar-Bearing Envelopes

Hydrothermally-introduced K-feldspar has partially or wholly replaced original minerals in quartz monzonite adjacent to Stage 1 veins (Plate 5-6). K-feldspar envelopes occur in three forms: (a) envelopes containing essentially K-feldspar alone, with only traces of quartz; (b) envelopes containing abundant K-feldspar, with minor amounts of biotite (up to 10%) and quartz (up to 5%); and (c) envelopes containing predominant K-feldspar (60% or more), quartz and biotite in similar amounts as in non-feldspathized rock, and minor amounts of plagioclase. The latter type of envelope repre- sents a relative increase in K-feldspar at the expense of plagioclase, i.e. an increase in K-feldspar/total feldspar ratio over that in adjacent quartz monzonite. Although quite distinct, these three megascopic envelope forms are intergradational, and probably do not represent separate stages of K-feldspar addition. For example, an envelope containing 100% K-feldspar adjacent to the vein may become diffuse towards its outward edge and include partially-replaced primary silicates.

Introduced K-feldspar may be reliably distinguished from primary K-feldspar only on field or textural evidence. Hydrothermal K-feldspar is commonly salmon-pink whereas primary K-feldspar is predominantly paler flesh-pink. However, colour is not a reliable guide since both colour variations may occur in each type of feldspar. Under high magnification, salmon-pink K-feldspars are seen to contain minute grains of a red mineral, probably hematite. Meyer & Hemley (1967, p. 178) suggest red colouration

in hydrothermal K-feldspar is due to exsolution, as hematite, of Fe^{+3} initially present in aluminum sites. X-Ray patterns of the two colour types eliminated the possibility of more than one K-feldspar modification.

No consistent optical difference is evident between primary and introduced K-feldspar of both salmon-pink and flesh-pink variety. Both primary and introduced K-feldspar commonly are microperthitic. In general, primary K-feldspar tends toward slightly coarser perthitic textures, whereas introduced K-feldspar tends to be microperthitic or homogeneous. Difference in degree of lattice ordering in primary and secondary K-feldspar, resulting from differences in origin and cooling history, was considered as a possible cause of variation in perthite development. A comparison of degrees of triclinicity in primary and secondary K-feldspar, using an X-Ray diffractometer, showed only the disordered monoclinic modification, orthoclase, in both types. Presence of the coarser "patch" and "braid" types of perthite lamellae may indicate that a gradation between unmixed and replacement types of perthite exists in primary orthoclase (Gates, 1953, pp. 55-69), whereas finer "film" or "string" perthite in secondary orthoclase may be of unmixing origin alone.

In summary, megascopic differences between primary K-feldspar in quartz monzonite and hydrothermal K-feldspar in well-defined envelopes about Stage 1 veins, provide the only reliable basis for distinguishing the two types.

(2) Sericite-Bearing Envelopes

Envelopes composed essentially of a fine-grained mixture of quartz, sericite and pyrite are developed around Stage 2 quartz-molybdenite, quartz-magnetite, quartz-magnetite-molybdenite and quartz-pyrite veins. Quartz-

sericite-pyrite envelopes are narrower (up to 2 inches wide) and less abundant than K-feldspar envelopes, but have more sharply-defined boundaries (Plates 5-5, 5-6). Average composition of this type of envelope is quartz: 60-65%, sericite: 30-35%, and pyrite: 1-5%. No kaolinite or montmorillonite are present. Quartz occurs both as unreplaced primary grains and also as fine-grained mosaics intergrown with sericite, generated by breakdown of primary silicates. Original feldspars and biotite have been replaced by sericite and quartz. Iron from the breakdown of biotite has been sulphidized to form finely-disseminated pyrite. Rarely development of the envelope is incomplete, and relict feldspars and biotite are included. At intersections of sericite-enveloped veins and Stage 1 veins, hydrothermal K-feldspar is replaced by quartz-sericite, usually accompanied by a necking-down in width of the sericite envelope across the K-feldspar zone. Quartz and metallic minerals of the earlier vein are not replaced (Fig. 5-1 and Plate 5-6).

(3) Pervasive Kaolinization

Kaolinization of quartz monzonite has developed outward from K-feldspar and sericite envelopes, and outward from Stage 3 veins without such envelopes. Plagioclase, the most sensitive indicator of pervasive alteration, undergoes a progressive change from a hard, grey mineral to a greenish, pulverulent mixture of kaolinite and sericite. Distinct mineralogical changes permit the classification of three degrees of kaolinization; weak, moderate and intense.

(a) Weak Kaolinization

Salient mineralogical features of weakly kaolinized quartz monzonite are (1) preferentially-altered, greenish cores of plagioclase

grains, and (2) either fresh or chloritized biotite. There is little
change in the mineralogy of weakly kaolinized quartz monzonite from
that of fresh rock, other than partial replacement of plagioclase by
kaolinite and sericite, and biotite by chlorite. The calculated
average mode of 25 specimens of fresh Endako Quartz Monzonite is: pink
perthitic orthoclase: 44.5%, grey zoned oligoclase (An_{19}): 26.3%,
quartz: 22.6%, brown biotite: 4.6%, hornblende: 0.6%, accessory
minerals (magnetite, sphene, apatite, pyrite, zircon): 2.0% (Table
3-5). Plagioclase grains generally show a hard, unaltered rim and a
soft, greenish core. X-Ray analysis of the core indicates the major
alteration product is kaolinite, with subordinate sericite. Minor
amounts of a montmorillonite-type clay mineral occur locally as small
white grains in the core which swell noticeably upon exposure to the
air. In thin-section, small amounts of carbonate and a weakly pleo-
chroic green mineral, probably chlorite, are observed in altered
plagioclase. Orthoclase is not attacked at this stage of kaolinization.

(b) Moderate Kaolinization

Classification of moderately kaolinized quartz monzonite is based
upon the complete breakdown of plagioclase and the presence of
unattacked orthoclase. Essential and accessory mineral content is the
same as in weakly kaolinized rock. Biotite may be either chloritized
or secondary, the latter occurring in clusters and radiating groups of
fine plates. X-Ray analysis shows plagioclase is completely replaced
by a pulverulent green or white mass of kaolinite and sericite. No
montmorillonite is present in moderately or intensely altered quartz
monzonite. Minor amounts of carbonate and chlorite (?) are visible in
thin-section.

(c) Intense Kaolinization

The significant feature of intensely kaolinized quartz monzonite
is the noticeable replacement of K-feldspar by kaolinite and sericite.
Orthoclase may occur as bleached relict grains enclosed by white rims
of kaolinite and subordinate sericite, or as white masses composed
entirely of these secondary minerals. Original plagioclase is repre-
sented by pale green or white masses of kaolinite and sericite. Both
colour variations of altered plagioclase yield identical X-Ray patterns,
but in thin-section a greater development of very fine-grained second-
ary biotite is noted in white altered plagioclase relative to the green
type. Apparently ferrous iron that imparts a green colouration to
kaolinite in one case has been fixed in biotite in the other case, and
consequently coexisting kaolinite is white. Plate 5-14 depicts
intensely kaolinized Endako Quartz Monzonite that contains remnants
of pink K-feldspar.

E. ENVIRONMENT OF HYDROTHERMAL ALTERATION
AND ORE DEPOSITION

Hydrothermal alteration involves chemical reactions between circulat-
ing aqueous solutions and the host rocks of ore bodies. Provided that wall
rock alteration was simultaneous with ore deposition, the environment of
deposition is, to a degree, interpretable from assemblages of alteration
minerals. Wall rock alteration and ore deposition are controlled by changes
in dominant chemical equilibria in the ore-bearing fluid in response to
changes in temperature, pressure and wallrock reaction (Meyer and Hemley,
1967, p. 226). Equilibrium probably exists only between the solution and
the mineral phase being formed, not with all phases present in the rock.

The problem of interpreting equilibrium or non-equilibrium between hydro-
thermal solution and altering rock is simplified by consideration of the
specific chemical and geological conditions represented by successive stages
of characteristic alteration mineral assemblages.

Complex alteration mineral associations common to most orebodies
generally are composed of several superimposed stages, the recognition of
which necessitates careful interpretation of geometric criteria. The best
evidence for relative ages of alteration types is derived from intersecting
patterns of zonally-distributed assemblages, particularly symmetrically-
arranged alteration envelopes adjacent to ore-bearing veins. The scale of
mineral zonation ranges from regional or district patterns down to micro-
scopic relations. In order to estimate the chemical environment of ore
deposition in light of recent experimental work on stability relations of
alteration minerals, one must first recognize the distinct types of alter-
ation assemblages formed during ore deposition, and interpret the geomet-
rical criteria pertaining to their sequence of development.

(1) Types of Alteration

General classifications designate alteration mineral assemblages by
either dominant mineral phases; e.g. silicification, sericitization,
chloritization; or common associations such as greisen, skarn and propylite.
Descriptive classifications of this type are useful but offer little in-
formation on alteration chemistry.

Creasey (1966, pp. 55-61) and Burnham (1962, pp. 768-784) classify
types of alteration in granodioritic rocks on the basis of coexisting
mineral pairs plotted on ACF-AKF bulk composition diagrams for specific

pressure-temperature ranges. Various equilibrium assemblages may be used to define different "facies" of hydrothermal alteration under a broader grouping of "potassic", "argillic" and "propylitic" principal alteration types. Although this facies concept of hydrothermal alteration does not necessarily imply that phases form simultaneously in equilibrium with one another, it does involve the assumption that the represented phases reflect adjustment of the whole rock to stable equilibrium during the part of the process in question. The use of composition or petrographic diagrams does not account for persistence of metastable phases or complex features such as zonal distribution of alteration minerals and cross-cutting alteration envelopes of different ages.

Meyer and Hemley (1967, pp. 170-180) recognized the mineralogical uncertainty and structural complexity of altered rock, and concluded that the most significant classification of alteration types is one that stresses the nature of the chemical interchange between wall rocks and solution. From detailed geological studies of alteration and mineralization at Butte, Montana and related experimental studies of stability relations between various alteration minerals, Meyer and Hemley (Ibid.) concluded that the most important chemical changes taking place in the hydrothermal solutions relate to the H^+/OH^- balance, hence a useful classification would be one that arranges mineralogical types of alteration roughly in order of decreasing hydrogen metasomatism (Table 5-2).

<u>Table 5-2</u>

Types of Hydrothermal Alteration
(after Meyer and Hemley, 1967)

Alteration Type	Principal Minerals	Associated Minerals
(1) advanced argillic	dickite, kaolinite, pyrophyllite, sericite, quartz	alunite, pyrite, tourmaline, topaz, zunyite, amorphous clays
(2) sericitic	sericite, quartz, pyrite	K-feldspar, biotite, topaz, zunyite
(3) intermediate argillic	kaolinite-group and montmorillonite-group minerals, amorphous clays	K-feldspar, biotite, sericite
(4) propylitic	epidote and chlorite group minerals, albite, carbonates, sericite, pyrite, iron oxides, zeolites, montmorillonite	Phases include albitization, chloritic alteration, zeolitic alteration, carbonitization
(5) potassium silicate	K-feldspar, biotite, sericite, iron oxides, anhydrite	siderite, ankerite, calcite, chlorite
(6) silicification	quartz, opaline silica	Includes skarn. Grades to most other types, over a wide range of environment

The three principal types of alteration at Endako mine correspond to three distinct alteration types as designated by Meyer and Hemley (Ibid.). K-feldspar-bearing envelopes with biotite and quartz represent potassium silicate alteration. Quartz-sericite-pyrite envelopes are typical of sericitic alteration. Pervasive kaolinization with sericite and minor amounts of montmorillonite represents intermediate argillic alteration.

(2) Geometrical Aspects of Alteration

   (a) Interpretation of Age Relations of Zonally-
        Distributed Alteration Assemblages

      Mineralogical zoning of wall rock alteration is illustrated dia-

   grammatically in Fig. 5-2. The vertical line near the centre of the

   chart symbolizes a vein wall with alteration zones extending outward

   to the left. Relative widths of K-feldspar and sericite envelopes are

   depicted schematically along with relative zonal widths of the three

   intensities of kaolinization.

      Interpretation of relative ages of K-silicate and sericitic

   alteration at Endako mine is straightforward. At intersections of

   veins enveloped by the two assemblages, introduced K-feldspar is

   replaced by younger quartz-sericite-pyrite (Fig. 5-1 and Plate 5-6).

   A change of time is evident between K-feldspar and sericite stages,

   as well as a change in the chemistry of altering fluids.

      Age of the argillic assemblage relative to K-silicate and serici-

   tic alteration is not as obvious. Both K-feldspar and quartz-sericite-

   pyrite envelopes encroach upon fresh quartz monzonite as well as

   pervasively kaolinized rock. Intensity of kaolinization adjacent to

   K-feldspar envelopes rarely exceeds the "weak" stage, whereas weak to

   moderate kaolinization prevails adjacent to sericitic envelopes. A

   concentric zonal array of argillic alteration around veins and

   envelopes of Stages 1 and 2 is defined too insufficiently to be related

   anywhere to one vein or group of veins. The majority of argillic

   alteration shows no apparent relation to enveloped veins, but occupies

   broad diffuse zones surrounding the stockwork of Stage 3 veins. These

veins, like earlier ones, occasionally occur within fresh quartz monzonite. Zones of intense kaolinization are more restricted in extent than zones of moderate or weak kaolinization, and apparently are localized by areas of closely-spaced Stage 3 fractures.

The ambiguous relationship of argillic alteration to enveloped veins gives rise to three possible interpretations:

(1) Argillic alteration may have formed first, with K-feldspar and sericitic envelopes superimposed later. Kaolinized wall rock is replaced at outer edges of envelopes.

(2) Argillic alteration may have formed contemporaneously with both K-feldspar and sericite envelopes. While pervasive argillic alteration penetrated outward into unaltered rock, it simultaneously receded at its veinward edge as K-feldspar or quartz-sericite-pyrite encroached upon the kaolinized wall rock.

(3) K-feldspar and sericite envelopes may have formed before argillic alteration. Kaolinizing fluids followed Stage 3 fractures as well as earlier enveloped veins reopened at a later time, diffusing through the envelopes without affecting the earlier K-feldspar and sericite. Kaolinite in this case could be hypogene or supergene.

The early argillic alteration hypothesis (1) is tenuously supported by ample evidence of replacement of kaolinized plagioclase by both sericite and K-feldspar at outer edges of envelopes, and (2) by the encroachment of some K-feldspar and sericite envelopes and molybdenum-bearing veins upon fresh rock, indicating that channelways guiding this

WALL ROCK ZONES			VEIN MINERALS		STAGE
Fresh quartz monzonite	K-silicate assemblage: Kspar, biot, qtz		qtz mo		STAGE 1: Potassium Silicate Alteration
Fresh q.m. | Wk.perv. kaolin'n	K-silicate assemblage: Kspar, biot, qtz (up to 8" wide)		mt py (ber) (bis)		
Fresh quartz monzonite	Sericitic assemb. qtz, ser, py (up to 2" wide)		qtz mt mo py (cpy)	OREBODY	STAGE 2: Sericitic Alteration
Fresh q.m. | Weak to mod. perv.kaolin.					
Fresh quartz monzonite	Sericitic assemblage: qtz, ser, py (up to 1/2")		qtz py (mo) (mt)	PY. ZN.	
Fresh q.m. | Weak perv. kaolin'n					
Fresh quartz monzonite			qtz mo mt py (cpy) (sph)		STAGE 3: Intermed. Argillic Alteration
Fresh q.m.	| Intense perv. | kaolinization				
Fresh q.m.	| Moderate perv. | kaolinization				
Fresh q.m.	| Weak perv. | kaolinization				
No wall rock alteration			qtz py cal chal spec		STAGES 4 TO 6

FIGURE 5 - 2

MINERALOGICAL ZONING OF WALL ROCK ALTERATION AT ENDAKO MINE

Abbreviations:

ber = beryl; biot = biotite; bis = bismuthinite; cal = calcite; chal = chalcedony; cpy = chalco-pyrite; Kspar = K-feldspar; mo = molybdenite; mt = magnetite; perv = pervasive; py = pyrite; q.m. = quartz monzonite; qtz = quartz; ser = ser-icite; spec = specularite; sph = sphalerite; ( ) signifies minor or trace.

alteration and mineralization followed fractures younger than those guiding argillizing fluids. However, evidence for replacement of one set of minerals by another is irrelevant to the choice between interpretations (1) and (2) as to the growth history of the zones. K-feldspar may be replacing kaolinite at the outer edge of the envelope, but that does not mean that the entire zone of K-feldspar is later than the entire zone of kaolinite, or that K-feldspathization is later than kaolinization for the mineral deposit as a whole (Meyer and Hemley, 1967, pp. 181-182.)

Encroachment of enveloped veins upon fresh rock is only permissive evidence for their youth relative to pervasive argillization. Although wall rock adjacent to most Stage 1 and 2 envelopes apparently is argillized contemporaneously to some degree, hydrogen metasomatism of wall rock could be restricted by thermodynamic and kinetic factors. As Meyer and Hemley suggest for Butte (Ibid., p. 203, p. 228), the early K-silicate assemblage at Endako presumably was closer to the magmatic stage than were later alteration assemblages. Igneous rocks sustaining early K-feldspar alteration probably still contained substantial residual heat, and the same solutions that generated K-silicate alteration may have been prevented from accomplishing weak argillic alteration outward from K-feldspar envelopes by rock temperatures above the stability limits of kaolinite (Hemley, 1959, pp. 244-246). Only weak argillic or propylitic alteration could be effected by these fluids under optimum conditions of cooler, reactive country rocks due to the low base-leaching capacity, i.e. the weak capacity for hydrogen metasomatism, of solutions effecting K-silicate alteration (Meyer and Hemley, 1967, p. 209). Wall rocks adjacent to K-feldspar-enveloped

veins along the north side of Endako orebody show a marked lack of
argillic alteration relative to similar wall rocks located centrally
in the orebody, indicating a hotter and possibly deeper-seated environ-
ment of K-silicate alteration in the north.

Wall rock temperatures above the stability limit of kaolinite also
may have retarded argillization adjacent to some quartz-sericite-pyrite
envelopes. However, sericitization of feldspars and biotite involves
strong hydrogen metasomatism (Hemley and Jones, 1964, p. 543), and wall
rocks outside sericite envelopes are more likely to be argillized
contemporaneously than those adjacent to K-feldspar envelopes. Field
observations confirm the scarcity of fresh wall rock and the prevalence
of weak to moderate kaolinization adjacent to quartz-sericite-pyrite
envelopes.

Reaction curves for the system $K_2O-Al_2O_3-SiO_2-H_2O$ after Hemley
and Jones (Ibid.) are given in Fig. 5-3.

Chemical insulation of the channelway by newly-formed minerals in
the envelope could restrict reaction between wall rock minerals and
hydrothermal solution, although the resulting disequilibrium between
solution and altering rock would increase the reactive potential of
the rising solution (Hemley, 1959, p. 267; Hemley and Jones, 1964, p.
565). The impermeability to hydrothermal solutions of a dense envel-
ope of secondary minerals relative to unaltered rock also may be a
factor in restricting argillization outward of enveloped veins.

Geometric criteria favour formation of at least part of the
argillic alteration simultaneously with K-silicate and sericitic
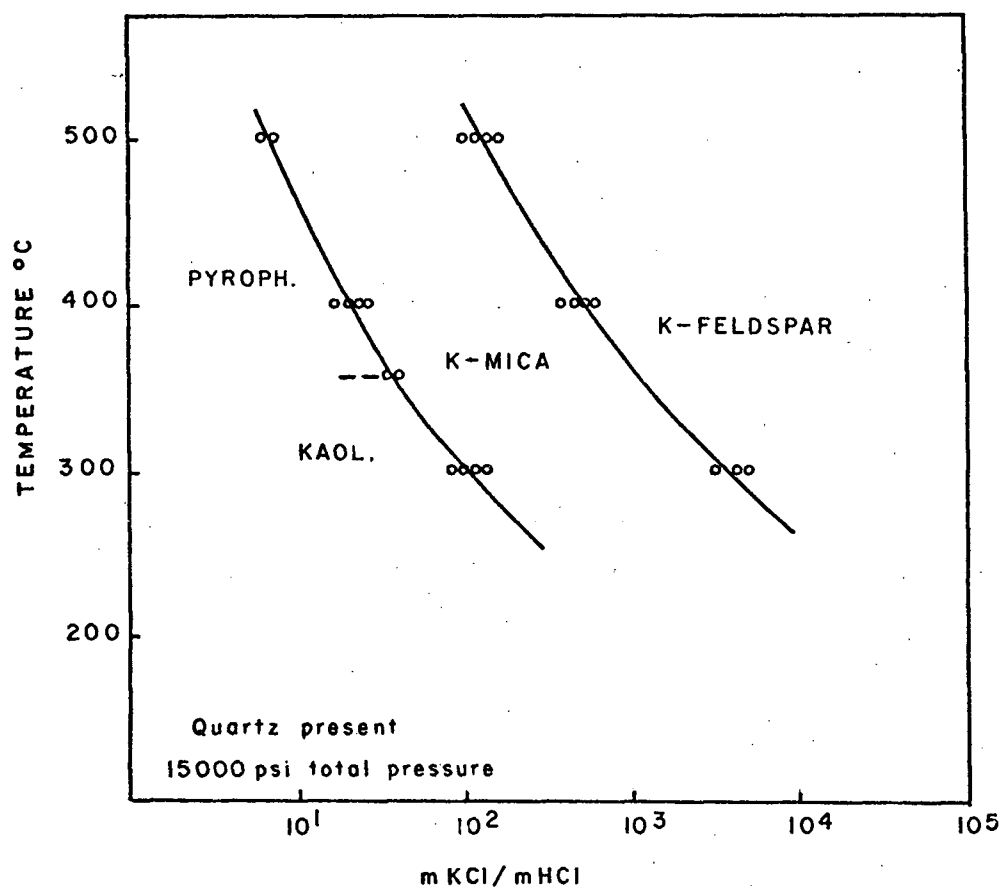
FIGURE 5-3

Reaction curves for the system $K_2O-Al_2O_3-SiO_2-H_2O$

From Hemley and Jones, 1964, Fig. 1

alteration. Although argillic zones are diffuse and lack ubiquitous
concentricity with sericite and K-feldspar envelopes, there exists a
definite, if minor, spatial relationship between enveloped veins and
pervasive alteration. Replacement of kaolinized wall rock at the outer
edges of envelopes indirectly favours contemporaneous over early
argillization since the possibility of early argillic alteration is
diminished by abundant geometric evidence for late argillization. The
simultaneous formation of inner sericitic and outer argillic alteration
envelopes at Butte has been described by Meyer, et al (1968), and at
San Manuel by Creasey (1965).

The most compelling evidence for late argillic alteration, aside
from chemical considerations, is its distribution relative to Stage 3
veins. In the western part of the orebody, large quartz-molybdenite
veins are surrounded by a restricted stockwork of smaller molybdenite-
bearing veins. In every case, both the large vein and its contiguous
stockwork are enveloped by a wide zone of argillic alteration with
diffuse margins. Where large veins are closely spaced, zones of kao-
linization coalesce into broad areas of pervasive alteration. The
more homogeneous pattern of Stage 3 fracturing and mineralization in
the eastern orebody is accompanied by a correspondingly uniform dis-
tribution of argillic alteration.

Intensity of argillic alteration is related to the density of Stage
3 fracturing. Closely-spaced fractures adjoining major faults and
veins in the central and western parts of the orebody probably facili-
tated development of intense pervasive kaolinization by channeling
larger amounts of hydrothermal solutions than penetrated equivalent

volumes of rock elsewhere. By comparison, the generally smaller and more widely-spaced veins throughout the rest of the orebody are accompanied by kaolinization of weak to moderate intensity. Fracturing, mineralization and weak argillic alteration all terminate abruptly along the northern periphery of the orebody. On the southern side, fracturing and mineralization diminish gradually outward to the limit of the pyrite zone, and attendant kaolinization also diminishes in intensity from moderate to weak.

Although the distribution and intensity of argillic alteration correlates strongly with Stage 3 fractures, such alteration is not likely to be exclusively late. In order to effect kaolinization outward from enveloped veins, late solutions would have to follow re-opened conduits along the veins. Enveloped veins that encroach upon unaltered rock would then represent closure of these channels to late argillizing fluids while other adjacent veins were re-opened. Both situations are unlikely to have occurred.

Whereas widespread channeling of late argillizing fluids by re-opened veins is geometrically improbable, the process is chemically feasible. Late solutions could have diffused through K-feldspar envelopes to kaolinize plagioclase in the wall rock without attacking K-feldspar. Hemley (1959, pp. 244-246) showed experimentally that, where quartz controls the activity of silica in solution, kaolinite and K-feldspar should react to form sericite. In recent experimental studies Fournier (1967b, pp. 218-226) has shown K-feldspar and kaolinite can coexist at 15,000 psi and less than 250°C, provided that a high activity of aqueous silica, compatible with gelatinous silica, is

maintained. At Endako, veins enveloped by K-feldspar are cut locally by parallel or subparallel quartz-molybdenite veinlets, indicating late re-opening and mineral deposition occurred to some extent along these channels. Although these Stage 3 veinlets probably conducted kaolinizing fluids, adjacent K-feldspar is not attacked.

Geometric criteria favouring late argillization could also be enlisted in support of a supergene origin for kaolinite. Intense kaolinization is associated with dense Stage 3 fracturing but does not show a corresponding statistical correlation to grade of molybdenite mineralization (Drummond and Kimura, 1969). The inference is that young supergene fluids descended along re-opened molybdenite-bearing veins as well as post-ore fractures, and altered wall rock feldspars to kaolinite. However, a hydrothermal origin for kaolinite is favoured for several reasons. Acidic supergene solutions would be expected to attack iron-bearing minerals such as biotite, magnetite and pyrite as well as feldspars, but these minerals commonly are quite fresh where coexisting or even intergrown with kaolinite. K-feldspar is unlikely to coexist metastably with kaolinite under the supergene conditions of low pressure, temperature and low aqueous silica activity. At Ely, Nevada Fournier (1967a, p. 69) notes that hypogene kaolinite has not attacked K-feldspar, in contrast to supergene zones nearby. In the foregoing discussion of secondary minerals at Endako, it was noted that the deposit lacked a supergene weathering profile. Kaolinite shows no evidence of dying out in deep diamond-drill holes 800 feet below the present surface.

In summary, the geometrical relations of zoned alteration assemblages indicate some argillic alteration formed contemporaneously with potassic and sericitic alteration, the first and second stages, respectively, of hydrothermal alteration. The majority of argillic alteration was guided by the widespread stockwork of younger Stage 3 fractures. Minerals unstable in a supergene environment are abundantly associated with kaolinite, hence a hypogene origin of argillic alteration is favoured.

(3) Regional Distribution of Alteration Features

Geological mapping in the open pit and logging of drill core permits identification of general trends in areal distribution of specific alteration features. Pit mapping is less useful in this respect than detailed core logging due to the inability of the pit geologist to examine closely alteration features on the unstable face. Sparse outcrop in the mine vicinity necessitates projecting drill hole data to surface. Statistical treatment of alteration features observed in diamond-drill core by Drummond (1967) and Dummett (1967) is useful in defining general trends in distribution of dominant alteration features within and adjacent to the orebody.

Geological sections along which diamond-drill core was re-logged for alteration studies were used also as control sections along which pyrite specimens for minor element analysis were taken from drill core. This sampling facilitated correlation between distribution of alteration minerals and minor element abundance in pyrite.

Within the Endako stockwork, three elongate overlapping zones of alteration and mineralization, the K-feldspar zone, the orebody proper, and

the pyrite zone follow parallel west-northwest trends from north to south,
respectively. Zones of dominant alteration are defined both by the relative
intensity of a particular assemblage and the relative lack of other assem-
blages. All three principal alteration mineral assemblages occur with
varying abundance throughout the stockwork, from the South Boundary fault
north to the limits of stockwork fracturing. Areal distribution of alter-
ation assemblages apparently is influenced by the trend of major quartz-
molybdenite veins that strike west to west-northwest and dip southward, and
by the density of stockwork fracturing as a whole. The orebody is located
roughly in the centre of an altered stockwork three to four times the area
of economic mineralization. Fig. 5-4 is a plan view of the distribution
of dominant alteration phases in the Endako mine area. A generalized cross-
section A-A (Fig. 5-5) shows the probable distribution of molybdenite and
alteration zones across the orebody and adjacent stockwork.

Veins enveloped by K-feldspar are abundant over the northern half of
the orebody (Fig. 5-4). As one progresses northward, molybdenite-bearing
veins diminish rapidly in size and density causing a concomitant decrease
in grade of MoS_2 as the 0.08% MoS_2 isopleth, marking the ore-waste cut-off,
is reached. Small, K-feldspar-enveloped barren quartz, quartz-molybdenite
and quartz-magnetite veins persist within weakly kaolinized to fresh quartz
monzonite, defining a "K-feldspar zone" about 800 feet wide that trends
parallel to the orebody and flanks it on the north. Veins enveloped by
K-feldspar are probably slightly less abundant within the K-feldspar zone
than throughout the orebody, but metallic vein minerals and quartz-sericite-
pyrite-enveloped veins are markedly less abundant, and degree of pervasive
argillic alteration is weaker than in the orebody to the south.

In plan, limits of the orebody are arbitrarily defined by the 0.08% MoS_2 isopleth, the economic cut-off between ore and waste. The boundary of the orebody, except the western extension under development at present, lies a short distance inside the boundary of the ultimate open pit, as shown in Fig. 5-4. Average thickness of the orebody, as shown in cross-section in Fig. 5-5, is about 1000 feet over its 6000-foot length. The western extension is a narrow zone of ore about 5000 feet long and averaging less than 500 feet wide. It follows a zone of large veins extending in a N 60 W trend from the western limit of the ultimate pit (Fig. 5-4). The transition from K-feldspar zone to orebody is marked by a sharp increase in abundance of metallic vein minerals, molybdenite in particular. Quartz-sericite-pyrite alteration envelopes increase in abundance, notably in the western end of the orebody and along the southern edge, but are numerically subordinate to K-feldspar-enveloped veins in the orebody. Quartz monzonite in the orebody may range from fresh to intensely kaolinized, with the average degree of argillic alteration being weak to moderate. Moderately to intensely kaolinized rock occupies an elongate, diffuse zone through the southern part of the orebody that marks the transition from dominant K-feldspar alteration in the north to sericite-pyrite in the south.

Intensity of fracturing and grade of MoS_2 diminish gradually southward away from the orebody, towards the "pyrite zone". This zone of relatively abundant pyrite flanks the orebody on the south and follows along parallel to the western extension, extending an indefinite distance to the west. The pyrite zone is contained within an area of dominantly weak argillic alteration about 1500 feet wide, roughly twice the width of the pyrite zone itself. The pyrite-sericite zone dies out at the South Boundary fault and has not been observed on the north side of the orebody, just as the zone of
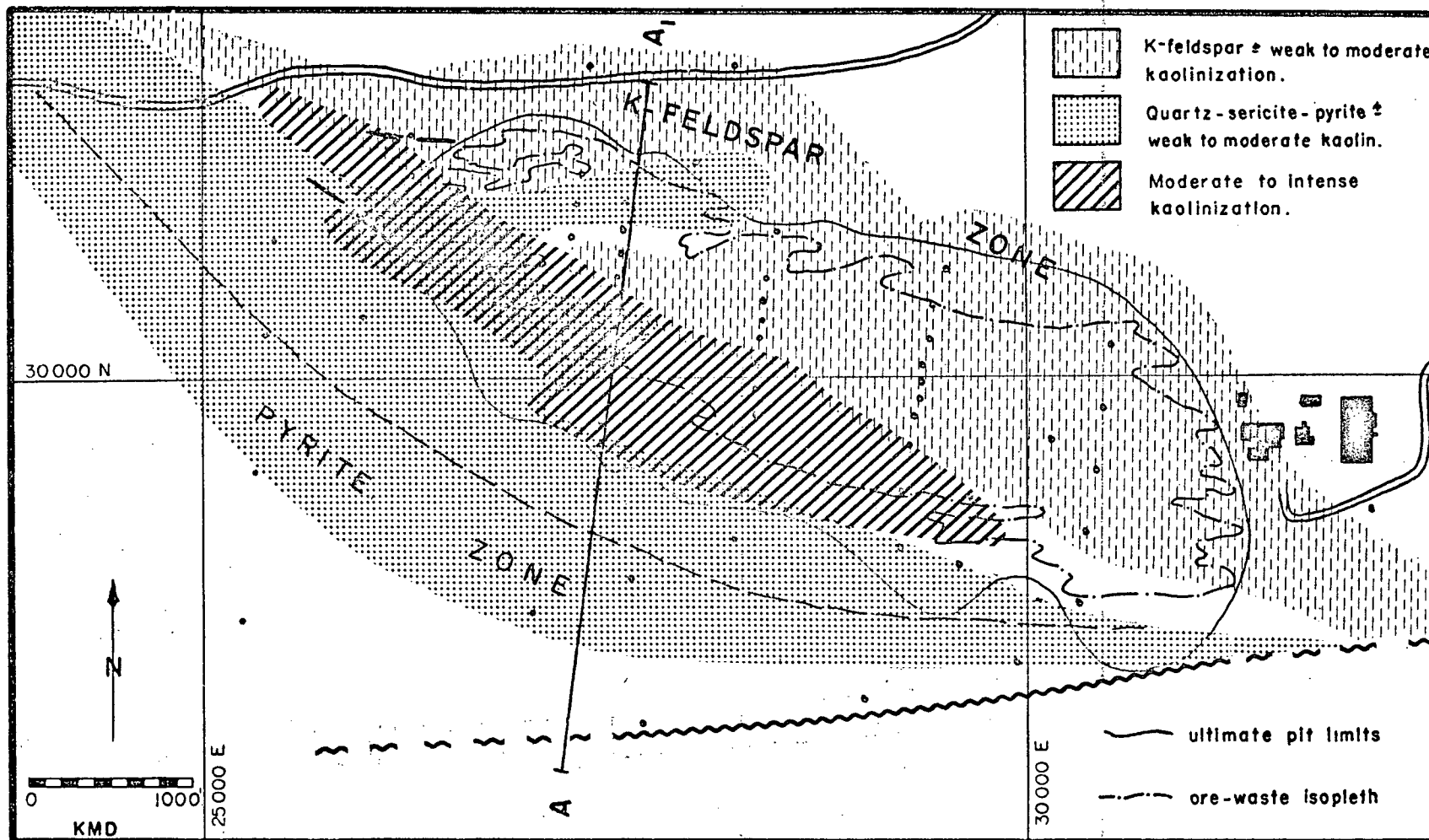
FIGURE 5-4

DISTRIBUTION OF ALTERATION FEATURES
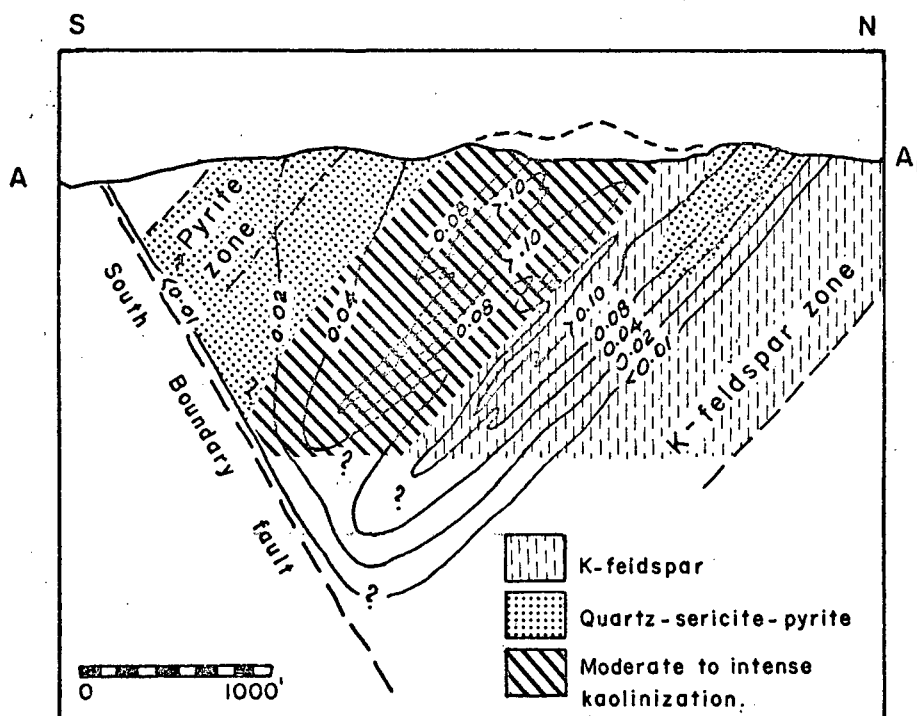
FIGURE 5-5

Generalized cross-section A-A₁ showing probable distribution of molybdenite (contours in % MoS₂) and alteration outside of pit area. After Drummond (1967).

abundant K-feldspar-enveloped veins is not seen on the south side of the orebody. Within the pyrite zone the abundance of pyrite is not significantly greater than within the orebody, except for local concentrations. Pyrite is dominant due to the relatively low abundance of molybdenite and magnetite. Similarly quartz-sericite-pyrite envelopes are only relatively abundant, their dominance being enhanced by the scarcity of K-feldspar-enveloped veins. Quartz-pyrite veins enveloped by quartz-sericite-pyrite are relatively abundant within the pyrite zone, whereas sericitic envelopes commonly enclose quartz-magnetite veins in the orebody. Younger pyrite-bearing veins of Stages 3 and 4 are present but not numerically significant. Pervasive argillic alteration grades from generally weak to moderate kaolinization over the southern edge of the orebody, to predominantly weak kaolinization over the pyrite zone and then to essentially unaltered rock south of the South Boundary fault.

Table 5-3 summarizes the geological events related to the formation of the Endako orebody.

TABLE 5-3

SUMMARY OF GEOLOGICAL EVENTS AT ENDAKO MINE

IGNEOUS EVENT AND AGE	STRUCTURAL EVENT	MINERALIZATION									ALTERATION
		QTZ.	MAG.	MO	PY	CPY	SPEC.	CAL.	CHAL		
Tertiary volcanism; emplacement of plagioclase porphyry and basalt dykes (50 ± 5 m.y.).	Minor movements parallel to dykes.			▮				▮	▮		Deuteric chlorite-calcite-epidote propylitization.
Emplacement of Stellako pluton (136 ± 5 m.y.).	Movement on EW and NE faults.										
Emplacement of younger Stage II plutons: Glenannan, Casey, Francois (140-137 ± 5 m.y.).	Post ore fracturing and faulting (Stage 6)	‖?						?			
Termination of cooling of Endako pluton.											
	Stage 5 veins						◆	◆	◆		None
	Stage 4 veins	⬥			◆						Minor bleaching
Hydrothermal alteration and mineralization (140 ± 5 m.y.)	Stage 3 veins		⬥	⬥		◆					Weak to intense pervasive kaolinization.
	Stage 2 veins										Quartz-sericite-pyrite envelopes.
	Stage 1 veins										Kspar,Kspar-biot.,qtz-Kspar-biot.envelopes.
Emplacement of acidic mine dykes (140 ± 5 m.y.)	Doming, antithetic stockwork fracturing										
Onset of cooling and crystallization of pluton	NNE compression, NNE and EW secondary shearing	Quartz	Magnetite	Molybdenite	Pyrite	Chalcopyrite	Specularite	Calcite	Chalcedony		
Emplacement of Endako quartz monzonite (141 ± 5 m.y.).	NE,NW and EW regional fracturing.										

CHAPTER VI

FLUID INCLUSION GEOTHERMOMETRY

A. INTRODUCTION

Many porphyry Cu-Mo deposits, including Endako, show mineral zoning on both a local and a regional scale. Such zonation commonly is attributed to thermal gradients extending outward from a "centre" of mineralization during mineral deposition.

Temperature is a major factor affecting the geometry of alteration and ore deposition through its influence on stabilities of mineral phases in the hydrothermal system. Other, possibly equally important controls are the compositions of hydrothermal fluid and altered host rock. Pressure affects mineral equilibria, but to a lesser degree than temperature and composition.

An important physical control of mineral zonation is structural setting, involving changes in fracture density, rock type and permeability over the orebody. Structural controls are evident in mapping. Chemical controls can be postulated from knowledge of relationships between observed mineral assemblages. Thermal controls, on the other hand, must be inferred from such indirect evidence as mineral stability data unless paleotemperature can be measured directly be some available geothermometer.

Vein quartz at Endako mine is amenable to fluid inclusion thermometry. Suitable quartz forms veins in the three main stages of mineral deposition. The presence of small primary fluid inclusions in a wide range of vein quartz allows measurement of formation temperatures of the three alteration

zones at Endako mine.

An independent method of paleotemperature determination will, within the limitations of the method used, establish both the thermal environment of mineral zonation and will give some indication or limits to temperature of deposition of those minerals associated with the specific minerals used. In the preceding chapter the nature, geometry and distribution of alteration assemblages at Endako were described. Drummond and Kimura (1969) compared experimentally established criteria in the system $K_2O-Al_2O_3-SiO_2-H_2O$ with our observed alteration phenomena, but only approximate temperature ranges of the three alteration assemblages can be derived from the broad stability fields depicted by Hemley (1959) (see Fig. 5-3).

Filling temperatures of quartz associated with the three alteration assemblages might support hypotheses on alteration genesis based upon mineralogical and geometrical criteria. Ideally, the formation temperatures of the alteration assemblages should fall within Hemley's experimentally extablished stability fields. The predominance of an alteration assemblage within an alteration "zone" permits extrapolation from the specific temperature for that assemblage to a general temperature for its related zone.

B. FLUID INCLUSIONS

Primary fluid inclusions are small portions of the fluid medium in which the host crystal grew. Inclusions are trapped by growth irregularities of many sorts in the growing crystal. Water vapour bubbles in the inclusions serve as geologic thermometers. The bubbles form as a result of the originally homogeneous fluid contracting more than the mineral host on cooling. As pressure in the inclusion drops below the total vapour

pressure of the multicomponent fluid at that temperature and at equilibrium, a bubble will appear and will increase in size as the temperature drops.

Sorby (1858) was the first to suggest that this process could be reversed; that is, simple heating of an inclusion will cause the bubble to gradually decrease in size, eventually disappearing at what is known as the "filling temperature". Any reversible phase change that occurs on cooling an originally homogenous fluid, such as appearance of a gas phase, precipitation of minerals from the fluid and splitting into immiscible fluids, may serve as a geologic thermometer.

The temperature at which a bubble in an inclusion vanishes may be taken as the trapping temperature only if the liquid was at its boiling point when trapped. The slightest shrinkage would then produce water vapour. If the liquid was under more than sufficient pressure to prevent its boiling, it would have to cool enough to relieve the excess pressure before it could begin to shrink and form vapour. Accordingly, the "filling temperature" derived from warming the inclusion would be lower than the trapping temperature (Roedder, 1962a). If pressure on the fluid can be estimated from geological field data on the depth of cover, the measure homogenization temperature can be corrected for pressure to yield the trapping or formation temperature.

In order to correct for pressure one must have some knowledge of the composition of the fluid, since a change in salinity significantly changes the boiling curve (Roedder, 1967). The composition of fluids in inclusions has been analyzed by Roedder (1958) using microchemical techniques. Most fluids in nature were found to be brines. Highly saline fluids do not behave like pure water at elevated temperature and pressure. Compared to

pure water, brines have a higher temperature two-phase field, a lower

vapour pressure, and a variable compressibility that necessitates either a

greater or a lesser pressure correction than for pure water. Roedder's

studies demonstrate that NaCl is the major salt in inclusion fluids, with

lesser amounts of Ca, K., Mg, SO_4^{-2}, CO_3^{-2} and HCO_3^{-}. Only traces of other

elements are found.

In order to determine accurately the salinity of an inclusion fluid,

the depression of the freezing point of the fluid may be observed on a

freezing stage. Roedder (1963) has noted the appearance of crystalline

phases other than ice ($NaCl.2H_2O$; $8CO_2.46H_2O$, etc.) on freezing, that assist

in the identification of different fluids and gases in the inclusions.

Another method of estimating the salt concentration is possible if NaCl

daughter crystals occur in the fluid inclusion. Halite, the commonest

daughter crystal mineral, is recognized by its cubic form, isotropism and

increase in solubility with temperature. An estimate of salinity may be made

from volume estimates of fluid, bubble and daughter crystal, and also from

the temperature of solution of the halite crystal. Presence of halite

daughter crystals indicates the inclusion fluid is saturated (Creasey, 1966,

p. 54).

C. METHOD OF STUDYING FLUID INCLUSIONS

(1) Suitable specimens for study must first be found. The clearest quartz

should be selected to facilitate observation of inclusions. Crushed grains

can be examined under a high-power binocular microscope to aid in selection

of specimens with the largest and most abundant fluid inclusions. Several

thin, doubly-polished plates were prepared from each selected specimen.

Endako quartz specimens selected for study were almost entirely of the milky variety due to the general absence of clear crystals. Doubly-polished plates were cut to a small size (10 mm square) to fit the heating stage, and ground to about 0.5 mm thickness for the sake of optical clarity.

(2) Fluid inclusions were examined carefully to determine their origin, if possible. Conclusive evidence on primary vs. secondary origin is rare. Secondary inclusions originate by the trapping of late fluids in rehealed cracks in the crystal at some time later than initial growth. Pseudosecondary inclusions are trapped, by subsequent zonal crystal growth, in cracks that penetrate a growing crystal.

Roedder (1967) cites the following criteria of origin:

(a) primary origin is supported but not proven by relatively large inclusion size, negative crystal shape, relation to crystal growth zones and similar filling ratios;

(b) secondary inclusions commonly are oriented along planes that cut across crystal growth zones, and often show different filling ratios;

(c) pseudosecondary inclusions also are located along planes that cut crystal growth zones, but these planes terminate at a face.

In the study of fluid inclusions, determining their origin is the greatest source of ambiguity. Recognition of the two main types is essential to fluid inclusion thermometry. Roedder (1971) has described a new technique for determining origin involving a hot wire probe. The bubble in a primary inclusion moves away from the probe, i.e. down a thermal gradient,

whereas the opposite effect is seen in secondary inclusions.

(3) The following observations, essential in the estimation of salinity and pressure corrections, are recorded prior to heating the specimen:

(a) the size and shape of inclusions,

(b) estimate of degree of filling of selected inclusion and those adjacent to it,

(c) note all phases present and estimate the volume % of each, and

(d) identify optically the daughter crystals and solid inclusions.

Endako fluid inclusions are very small, as is commonly the case in hydrothermal vein quartz. Fluid inclusion diameter averages 5 microns. The shapes of the 12 fluid inclusions selected for heating runs include 7 negative crystal cavities, 4 oval to spherical shapes and 1 irregular shape. Average degree of filling is 75 ± 10%. Seven of twelve inclusions are three-phase, i.e. saline water-water vapour-NaCl daughter crystal. No other phases were detected. Daughter crystals occupy 8 to 10 volume % of the inclusions.

These observed properties of Endako fluid inclusions are listed in Table 6-1. Photomicrographs of quartz specimens K-2, 103-425, 63 and 72 are given in Plates 6-1 to 6-4 respectively.

(4) In heating the quartz plates, temperature must be raised slowly and with frequent pauses to prevent over-runs and to allow the heating element and specimen to equilibrate.
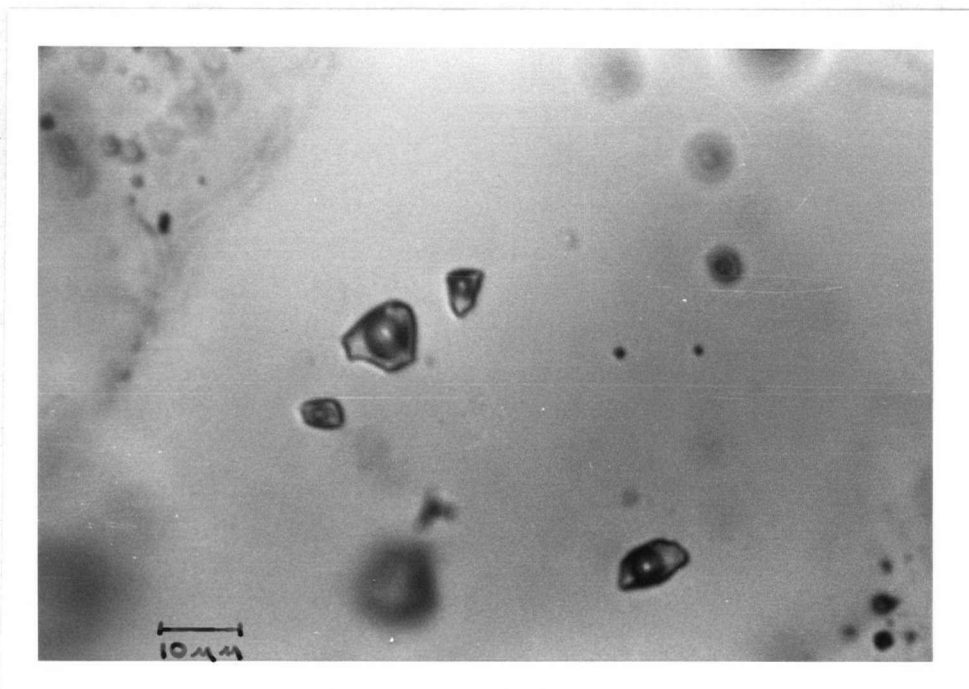
Plate 6-1

Quartz specimen K-2: a K-feldspar-enveloped quartz vein. The fluid inclusions are primary and have negative crystal shapes. Magnification 625X.
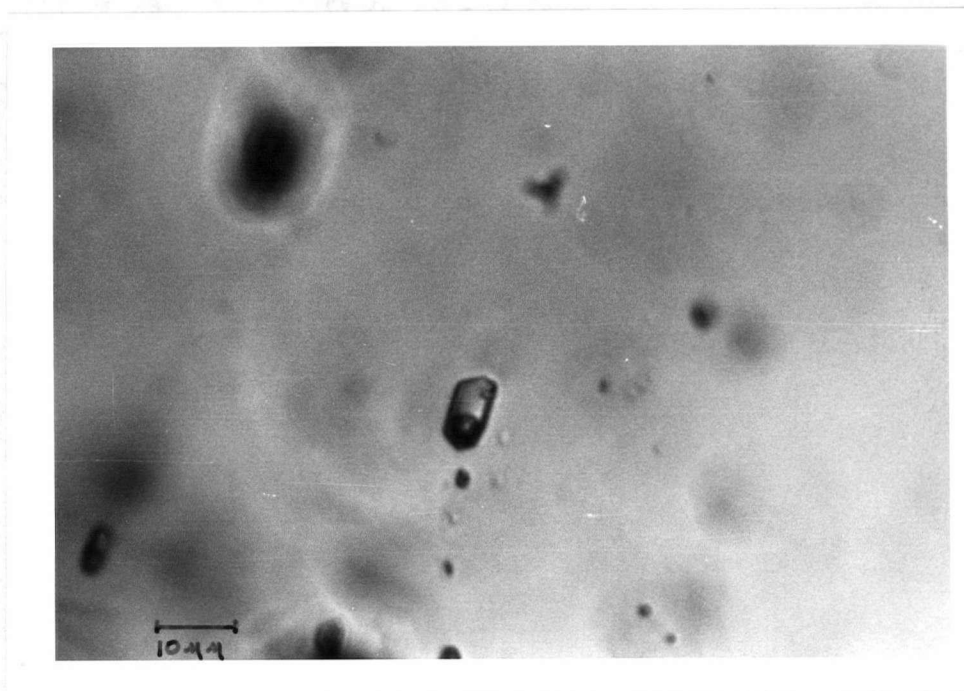
Plate 6-2

Quartz specimen 103-425: a sericite-enveloped quartz vein. The fluid inclusion is primary, has a negative crystal shape and contains a halite daughter crystal. Magnification 625X.
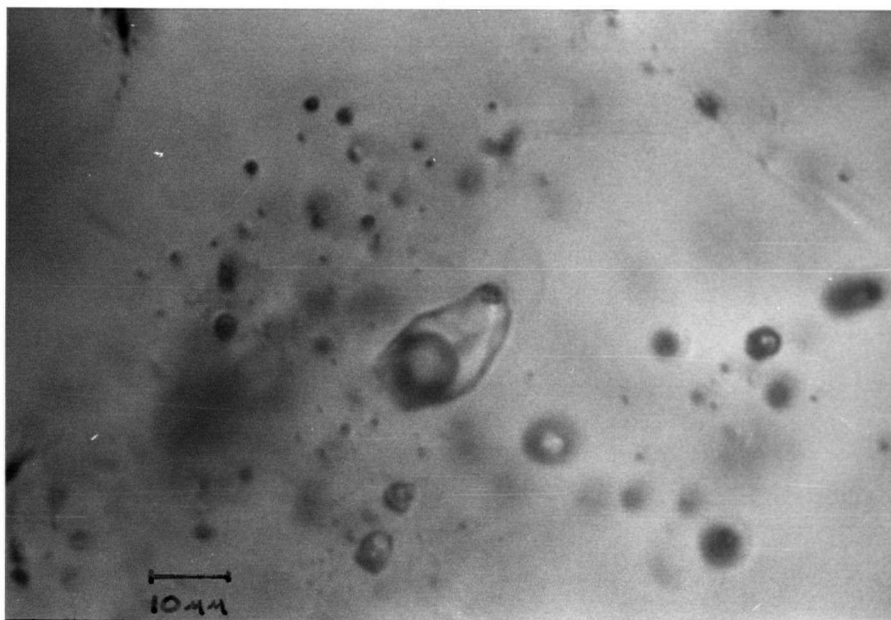
Plate 6-3

Quartz specimen 63: a quartz vein from pervasively kaolinized quartz mon-
zonite. The inclusion shape is partly faceted, partly oval. The inclusion
contains a small halite daughter crystal. Magnification 625X.
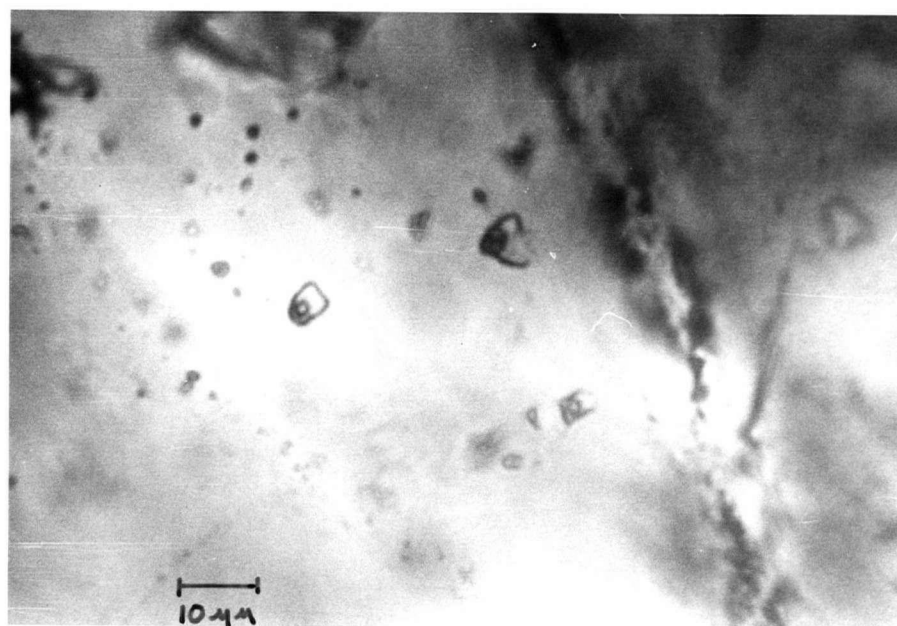
Plate 6-4

Quartz specimen 72: a quartz vein from pervasively kaolinized quartz mon-
zonite. Inclusion shapes vary from negative crystals to irregular.
Magnification 625X.

If the bubble disappears while others remain, if the entire fluid inclusion disappears, and/or the inclusion homogenizes at an anomalously low temperature, the fluid inclusion is secondary. Release of secondary fluid inclusions is accompanied by small decrepitations and movements of the specimen.

The phases in the inclusion were observed closely for changes during heating. If the bubble occupies less than 50% of the space, it will progressively shrink and ultimately disappear at the homogenization temperature. Halite daughter crystals may dissolve at a temperature lower than the homogenization point. The index of refraction of the inclusion fluid changes upon heating, often becoming semi-opaque.

When homogenization had been observed, the inclusion was cooled slowly and the temperature of reappearance of the bubble is noted. The run was repeated at least twice to minimize error.

Endako specimens were heated on a Unitron M500 heating stage mounted on a Leitz polarizing microscope with long focal length objective. Current to the heating element was controlled by a rheostat, and temperature was recorded by a thermocouple linked to a chart recorder. The unit was calibrated with temperature-sensitive marking crayons. The maximum temperature obtainable with the heating element is 500°C, and maximum instrumental error at that temperature is estimated to be ± 25°C. About one-half of the Endako fluid inclusions homogenized in the temperature range 450° - 500°+, necessitating some estimation and extrapolation in the 500-degree range.

The depression of the fluid freezing point is a function of the concentration of salt. Roedder (1963) freezes the inclusion solid on a

Table 6-1

Properties of Endako Fluid Inclusions

No. Plate	Alteration	Type	Phase 1 Vol. %	Phase 2 Vol. %	Phase 3 Vol. %
62	Ksp.	oval	fluid 70	gas 30	--
58	Ksp.	neg. xl.	fluid 60	gas 30	halite 10
K-2 Plate 6-1	Ksp.	oval	fluid 72	gas 20	halite 8
9	Ksp.	neg. xl.	fluid 60	gas 30	halite 10
43-297	Ser.	neg. xl.	fluid 80	gas 20	--
103-425 Plate 6-2	Ser.	neg. xl.	fluid 70	gas 30	--
63 Plate 6-3	Kaol.	oval	fluid 70	gas 20	halite 10
83	Kaol.	oval	fluid 62	gas 30	halite 8
72 plate 6-4	Kaol.	irreg.	fluid 72	gas 20	halite 8
24	Kaol.	neg. xl.	fluid 62	gas 30	halite 8

special stage then observes the appearance of a liquid phase on gradual warming. The temperature at which the last ice crystal melts is the freezing temperature. Attempts were made to freeze Endako specimens by enclosing a microscope within a refrigerated tank, leaving only the eyepiece and remote focusing controls exposed. This makeshift apparatus proved unsuccessful mainly due to sticking of microscope gears at low temperatures, and frosting of the eyepiece. Consequently, salinity of fluid inclusions was estimated from observed percentages of phases.

Calculation of the approximate apparent weight percent NaCl in fluid inclusions is straightforward. The fluid is assumed to be a saturated NaCl solution, due to the presence of halite daughter crystals in 7 of 12 inclusions tested. At room temperature saturated water contains 26.3 wt. % NaCl. Halite has a specific gravity of 2.16. Total salinity is given by:

[(Vol. % fluid) x 0.263] + [(Vol. % halite) x 2.16] = total wt. % Nacl.

The temperature at which the NaCl crystal dissolves in the saturated saline solution is a function of the pressure on the H_2O-NaCl system and the degree of filling of the inclusion. Therefore, by observing degree of filling and NaCl solution temperature, one should be able to obtain the pressure of formation from the experimental data of Lemmlein and Klevtsov (1961), Keevil (1942) and Sourirajan and Kennedy (1962). However, considerable error is possible because both wt. % NaCl and degree of filling are derived from the estimated volume % of phases. The H_2O-NaCl homogenization temperature is sensitive to small changes in degree of filling.

At the relatively high salinities calculated for Endako fluid inclusions, the homogenization temperatures of the corresponding H_2O-NaCl system

approach and even exceed the recorded inclusion homogenization temperatures. The disappearance of the crystal phase on heating was observed in only one specimen, K-2, and its precise temperature was difficult to ascertain. The index of refraction of the saturated solution and the halite crystal are similar, and the fluid in the inclusion becomes semi-opaque at elevated temperature. The H_2O-NaCl system in specimen K-2 homogenized between 400 and 450°C, and the vapour phase disappeared at 477°C.

Pressure Corrections

The homogenization temperature of a fluid inclusion, even if its composition is known, cannot give both the temperature and pressure of formation. However, if either is known, the other may be obtained. Usually pressure is estimated from field evidence plus an assumption that formation pressure equals either lithostatic or hydrostatic load. The estimated pressure is then used to calculate a pressure correction for the homogenization temperature.

Deposits that yield homogenization temperatures in the range of 500°C such as pegmatitic deposits, contact metamorphic deposits and some hydrothermal vein deposits indicate not only a high temperature and hence high pressure of formation, but also indicate a very high concentration of salts in the inclusions to permit the existence of a two-phase (liquid + gas) system far above the critical temperature for pure water (Roedder, 1967, p. 564).

The composition of the fluid, as pointed out by Roedder (Ibid.), can give direct information on the formation pressure. The vapour pressure of the H_2O-NaCl system involved, at the homogenization temperature, establishes a minimum formation pressure. The Endako data on composition and

Fig. 13. Isotherms, 400°C-600°C, showing compositions of coexisting gases and liquids.
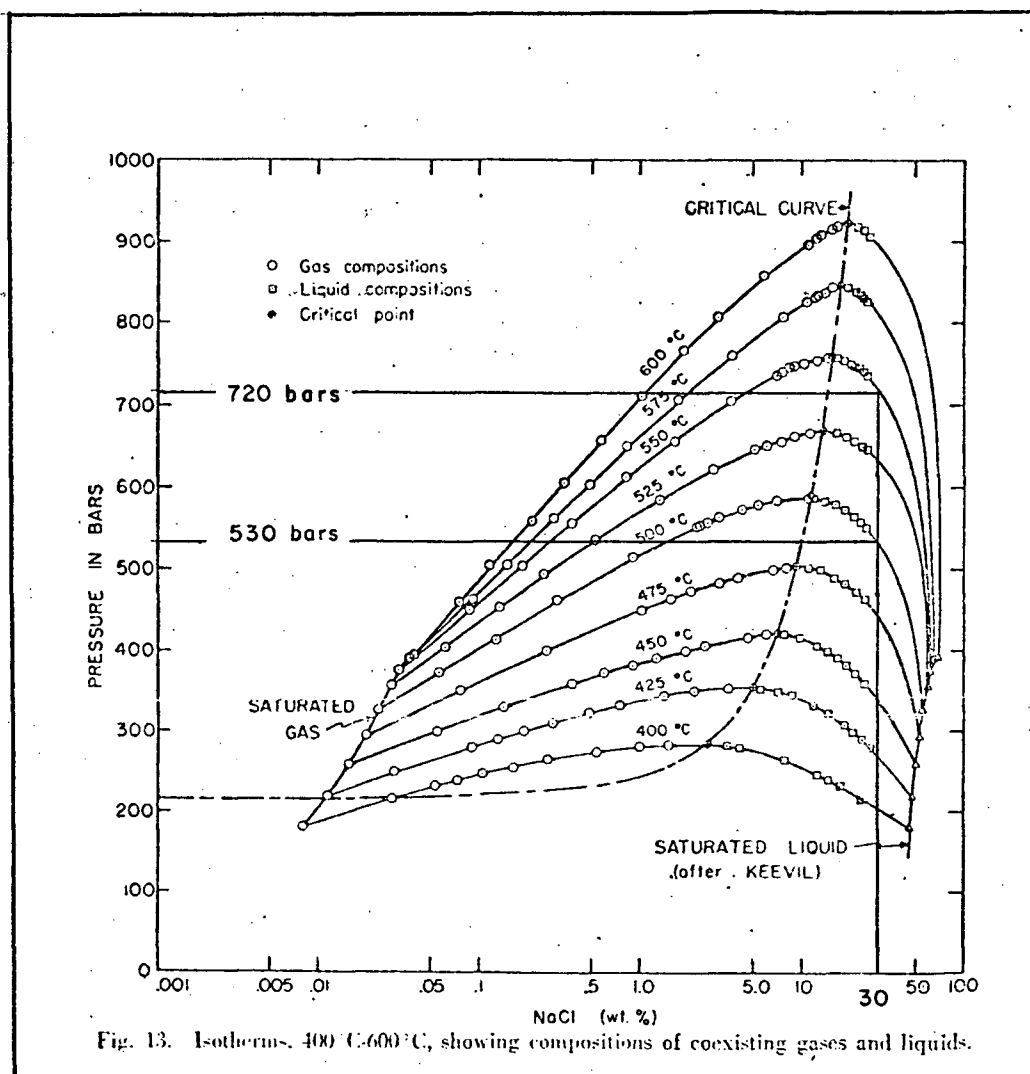
FIGURE 6-1

Vapour pressure of the H_2O – NaCl system at

homogenization temperatures of 500°C and 550°C.

From Sourirajan and Kennedy, 1962, Fig.13

homogenization temperatures may be used in conjunction with the P-X data of Sourirajan and Kennedy (1962, Fig. 13) on the H_2O-NaCl system to establish minimum formation pressure. As depicted in Fig. 6-1, the vapour pressure of a 30 wt. % NaCl solution, corresponding to the average Endako fluid composition, at 500°C is 530 bars, and at 550°C is 720 bars. These minimum formation pressures are equivalent to depths of 1.5 to 2 km.

Although Endako alteration and vein mineral assemblages indicate relatively high formation temperature, the deposit also shows characteristics of relatively shallow depth of emplacement. Pronounced mineral zoning over a relatively short distance across the deposit supports the existence of steep thermal gradients. The termination of sulphide deposition at the pyrite zone, in conjunction with localized sericitic alteration, supports the view that ore fluids were cooled and diluted by groundwater at the pyrite zone. Younger plutons bordering Endako Quartz Monzonite on the north and south show chilled, porphyritic margins and miarolytic cavities indicative of high level emplacement. Consideration of these geological features in conjunction with the minimum formation pressures calculated above supports a depth of emplacement in the order of 3 km and a corresponding formation pressure of 1000 bars.

The experimental data of Lemmlein and Klevtsov (1961, Fig. 4) are used to calculate pressure corrections for Endako homogenization temperatures. As shown in Fig. 6-2, their data offers pressure corrections only to 400°C and 30 wt. % NaCl. However, the isotherms were extrapolated and pressure corrections at 20 and 30 wt. % NaCl and 500, 1000 and 1500 bars were derived. The pressure range includes the minimum formation pressure, a realistic median pressure, and a maximum figure. The corrected filling temperatures are given in Table 6-2.
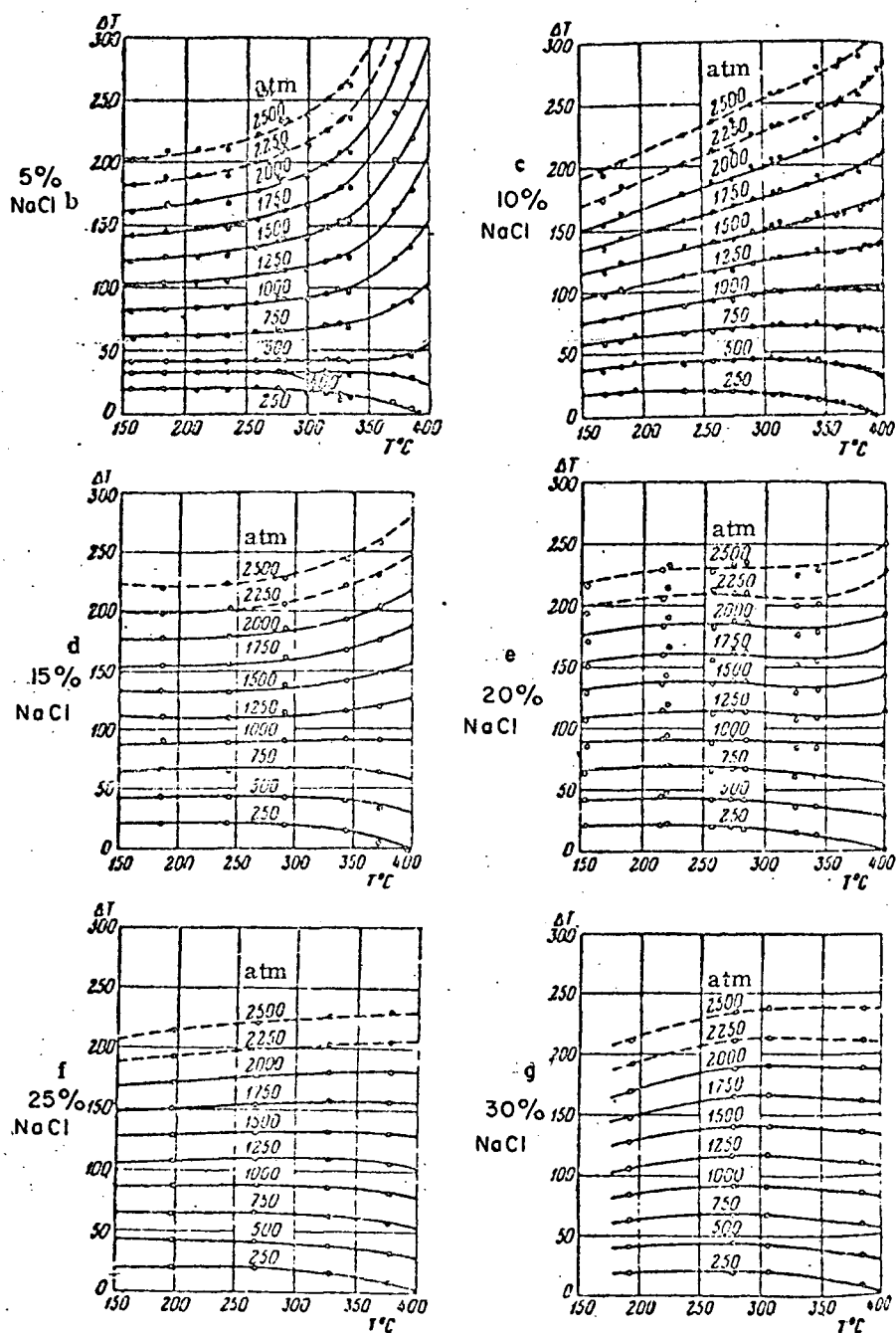
Fig. 4. Pressure corrections for homogenization temperatures:

a — for pure water; b — for 5% solution of NaCl; c — for 10% solution; d — for 15% solution; e — for 20% solution; f — for 25% solution; g — for 30% solution of NaCl.

FIGURE 6-2

Pressure   corrections   for   homogenization   temperatures.

From   Lemmlein   and   Klevtsov,   1961,   Fig. 4.

TABLE 6 - 2

Homogenization Temperatures and Pressure Corrections
for Endako Fluid Inclusions

No. Alt'n	Homo. T °C	Composition			Pressure Correction			Corr. fill. temp. (1000 b.)
		Wt.% NaCl (xl.)	Wt.% NaCl (liq.)	Total Wt.% NaCl	ΔT 500 b. (NaCl)	ΔT 1000 b. (NaCl)	ΔT 1500 b. (NaCl)	
62 Ksp.	400+	--	18	18	+25 (20)	+80 (20)	+140 (20)	480°C
58 Ksp.	460+	21	16	37	+15 (30)	+70 (30)	+125 (30)	530°C
K-2 Ksp.	477+	17	19	36	+20 (30)	+75 (30)	+130 (30)	552°C
9 Ksp.	525 (est.)	21	16	37	+10 (30)	+68 (30)	+120 (30)	593°C
43-297 Ser.	490	--	21	21	+20 (20)	+80 (20)	+170 (20)	570°C
103-425 Ser.	470 495 500	--	18	18	+25 +20 +18 (20)	+78 +80 +82 (20)	+165 +170 +173 (20)	548°C 575°C 582°C
63 Kaol.	342	22	18	40	40 (30)	90 (30)	135 (30)	432°C
83 Kaol.	380	17	16	33	+35 (30)	+80 (30)	+135 (30)	460°C
72 Kaol.	333 325	17	19	36	+39 +38 (30)	+90 +90 (30)	+138 +139 (30)	423°C 415°C
24 Kaol.	298	17	16	33	+45 (30)	+88 (30)	+136 (30)	386°C

Summary

The locations of specimens used in thermometry and their relation to the alteration zones is given in Fig. 6-3. The distribution of specimens was not designed to yield an optimum statistical representation of orebody paleotemperatures. Instead, specimens were selected on the basis of alteration association and optical quality of quartz. However, when compared to alteration zones the paleotemperatures coincide in a general way with thermal gradients inferred from alteration zonation.

The four corrected temperatures from K-feldspar-enveloped quartz veins show a range of 480-593°C and an average of 540°C. The homogenization temperatures of specimens 62, 58 and K-2 are minimum homogenization temperatures. In the case of No. 62, the precise homogenization point could not be determined due to a change in the index of refraction of the fluid. Specimen 62 and K-2 were not quite homogenized when the runs were terminated at 460° and 477°C, respectively due to limitations of the heating element. Similarly, the homogenization temperature of sample 9 was estimated to be 525°C although the run was stopped at 500°C. The average corrected temperature for the K-feldspar-enveloped veins may be as high as 600°C.

The corrected temperatures from sericite-enveloped veins show a range of 548° to 582°C, but three of the four temperatures were determined from plates prepared from one specimen. Consequently the average corrected temperature is taken as 570°C.

The five quartz veins taken from pervasively kaolinized wall rock show a range of corrected filling temperatures from 386° to 460°C, and an average of 423°C.
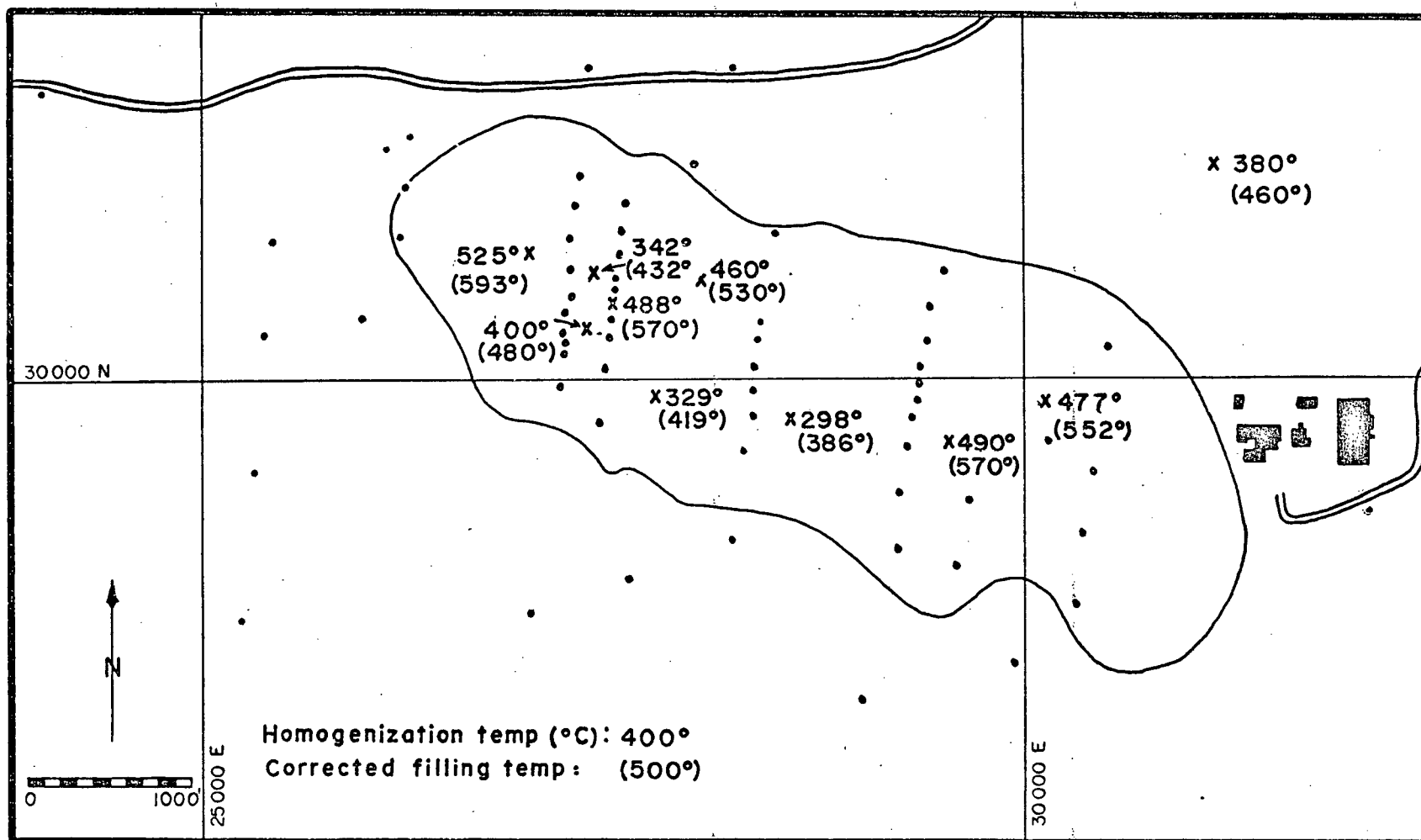
FIGURE 6-3

Location of geothermometry specimens and related paleotemperatures.

On the assumption that the paleotemperature of the dominant assemblage
in a mineral zone defines, in a general sense, the thermal environment of
that zone, the corrected filling temperatures listed above may be applied
to the three alteration zones at Endako mine. The "temperature" of the
K-feldspar zone is in the range of 540°-600°C. The orebody proper contains
all three alteration assemblages, but is assumed to have a "temperature"
range representative of the predominant kaolinite and sericite assemblages,
i.e. 423° to 570°C. The "temperature" of the pyrite zone is taken as the
kaolinite average of 423°, although sericite is abundant locally.

CHAPTER VII

MINOR ELEMENTS IN PYRITE

A. INTRODUCTION

Pyrite is ubiquitous at Endako mine, being second in abundance to molybdenite among metallic minerals. The molybdenite-to-pyrite ratio is about 10:1, therefore the pyrite content of the orebody is in the order of 0.02%. Pyrite was co-depositional with molybdenite during the three main stages of mineralization; hence, conclusions on the genesis of pyrite mineralization based upon distribution of contained minor elements also apply to molybdenite.

A quantitative spectrochemical study of the minor element content of pyrite from the orebody area was undertaken to ascertain if zonation of minor elements exists, and if so, what relationships occur between minor element zonation and the structural and mineralogical geometry of the ore deposit. Significant correlations may exist between minor element distribution and the thermal zonation of the orebody inferred from geothermometry of fluid inclusions and zonation of alteration mineral assemblages. Pyrite specimens were collected in a grid bracketing the orebody, separated and analyzed, and the assay data treated with several statistical techniques in order to bring out significant trends.

B. COLLECTION AND TREATMENT OF SPECIMENS

Ninety pyrite specimens were collected from diamond-drill core and surface at Endako mine and surrounding areas, but only the specimens

located within the limits of alteration and mineralization were used in this study. Sixty-seven specimens were selected mainly along six north-south drill sections, bracketing the orebody in a fairly even distribution of sample sites. Location of orebody pyrite specimens is given in Fig. 7-1.

In selecting pyrite for minor element analysis first consideration was given to its mode of occurrence. Only pyrite from Stage 1, 2 and 3 veins was selected, because of the pyrite-molybdenite association in these stages of sulphide deposition. Veins containing both pyrite and molybdenite were chosen where possible, but close intergrowths of the two minerals were rejected due to difficulties in separation. Minor amounts of pyrite occur as a primary accessory mineral in Endako Quartz Monzonite, and also as post-ore Stage 4 pyrite veins. These occurrences were readily recognized and excluded from the suite of analyzed specimens. Commonly pyrite is associated with molybdenite and magnetite, and less commonly with hematite and chalcopyrite, in quartz veins. Vein mineralogy and associated alteration mineralogy of each specimen were noted.

A second, but equally important consideration in selecting pyrite for spectrochemical analysis is its purity and lack of oxidation. Clean, massive pyrite with a minimum of associated minerals was preferred. Pyrite showing any traces of surface oxidation was rejected. Every effort was made to select specimens with a minimum of impurities.

Steps followed in the separation and purification of pyrite are given in Appendix 2. Briefly, much gangue was disposed of by cutting away with a diamond saw, after which the specimen was crushed, sieved and inspected under a binocular microscope. A pure specimen can, in some cases, be obtained at this stage; if not, heavy minerals were separated with

FIGURE 7-1
Location of Orebody
Pyrite Specimens

(sequence no.), (specimen no.)
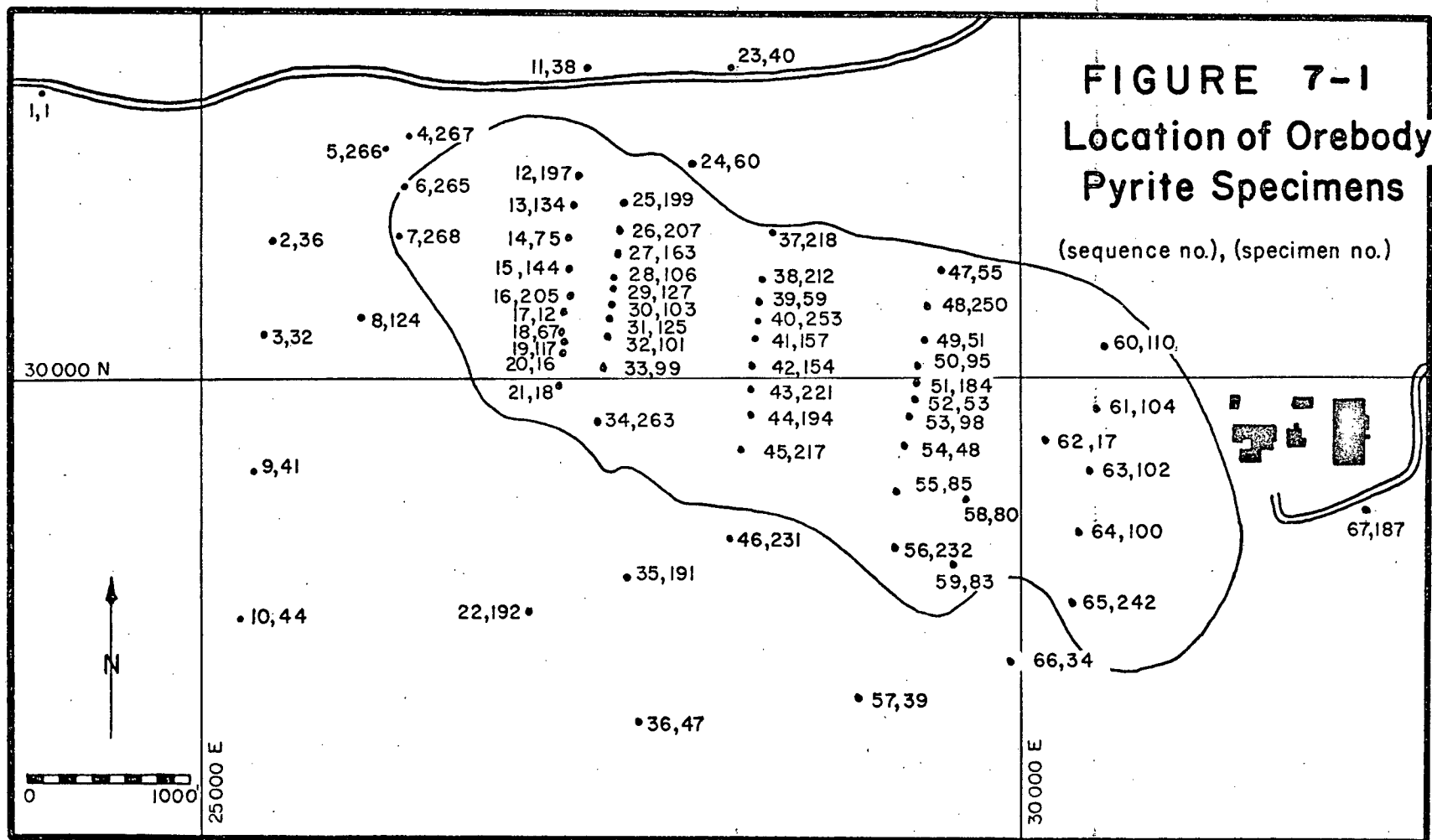
bromoform and magnetic minerals were then removed using a Franz isodynamic separator. These operations were repeated as required. The remaining heavy impurities were either hand-picked or removed with a superpanner. Excessive quartz was leached from the specimen with hydrofluoric acid. The average weight of a cleaned pyrite specimen was less than 1 gram.

C. PURITY OF SEPARATED PYRITE

The quality of each pyrite specimen was checked under a binocular microscope several times during preparation. Polished mounts of about one-third of the specimens analyzed were studied under a reflecting microscope. The purity of several specimens was checked with an X-Ray diffractometer. On the basis of these checks, all pyrite concentrates are believed to be at least 99% pure.

The possibility exists that some impurities in pyrite concentrates may have escaped detection. Titanium analyses are significantly higher than known concentrations in pyrite. Magnetite inclusions are noted in polished sections and magnetic separates of pyrite, but Ti content of magnetite is relatively low (see "Titanium" below). Sphene and leucoxene occasionally are detected in pyrite concentrates, but in much lower and probably less regular amounts than the 1% - 2% required to cause the uniformly high Ti analyses. The accuracy of titanium analyses is considered dubious, and consequently these results are not used in this study.

The concentration of copper in pyrite may be affected by chalcopyrite replacement of pyrite (see "Orebody-Pyrite"). Small chalcopyrite inclusions were detected in two polished sections of pyrite. The polymodal frequency distribution of copper in pyrite (Fig. 7-2) and the generally high and

erratic copper assays indicate that most copper in pyrite is derived from admixed chalcopyrite.

The concentration of zinc in pyrite is very erratic. Sphalerite exsolution bodies were noted in chalcopyrite, but were not identified in pyrite. Chalcopyrite inclusions in pyrite were analyzed by electron probe, and the Zn content found to be 5200 ppm compared to 230 ppm Zn in enclosing pyrite and 85 ppm Zn in a separate pyrite grain. Cu and Zn show strong correlation in statistical studies, supporting the view that the majority of Zn in pyrite is derived from exsolved sphalerite in chalcopyrite inclusions.

Most pyrite concentrates contained a few flakes of molybdenite that escaped the superpanner and could not be easily hand-picked. Most Mo in analyses probably is derived from this source. Semiquantitative spectrographic analyses of two pure molybdenite specimens revealed uniformly low minor element contents. Contamination of pyrite from this source, other than for Mo, was judged to be minimal.

D. MINERAL ANALYSIS

All quantitative analyses were performed at Queen's University with a Jarrell-Ash emission spectrograph and an A.R.L. densitometer. The spectrographer, Mr. L.C. Mes, carried out the analyses, assisted by the writer.

Pyrite specimens were prepared for burning in the arc by homogenizing a mixture of 75 mg sample, 75 mg base (SiO_2 + Al_2O_3 + Na_2CO_3) and 150 mg graphite containing 0.01% Pd as an internal standard.

Spectral lines were photographed upon a three-meter strip of 35 mm film. Intensity of the lines was measured with the densitometer, and quantitative results were calculated using existing pyrite calibration curves from Queen's files.

A duplicate spectrochemical analysis was run on every fifth pyrite sample. The duplicated results, in both arithmetic and logarithmic formats, were keypunched and run through an analytical precision program based on Garrett's method (1969, p. 568). The results are given in Table 7-1. Spectrochemical analyses of pyrites from the orebody area are given in Appendix 4, and analyses of regional pyrites are given in Appendix 5.

Precision is given in % at 95% confidence level. Arithmetic values of Pb, Zn, Cu and Ag have the lowest precision. In the logarithmic format Ag shows very low precision due to the predominance of near-zero analytical values, compared to a few relatively high values. Logarithmic Pb precisions are low for the same reason.

In general, the reproducibility of analyses was judged to be within acceptable limits for the method. Precision of analyses is limited mainly by the sensitivity of the particular element's spectral lines at the concentration measured. Inhomogeneity of specimens, mainly due to inclusions, also decreases precision.

Preliminary analysis of orebody pyrites (Appendix 3) determined that 19 elements are present in pyrite in detectable amounts. The eleven elements given in Table 7-1 below were looked for in all subsequent analyses. An additional eight elements were rejected as unsuitable for quantitative study for the reasons stated below.

Table 7-1

Analytical Precision of Spectrochemical Assays

Variable	Analytical Variance	Analytical Std. Dev.	Analytical Precision
LOGARITHMIC VALUES			
Ag	0.05	0.22	1089.57
Ba	0.00	0.04	7.20
Bi	0.03	0.17	56.96
Co	0.00	0.04	3.16
Cu	0.01	0.07	6.48
Mn	0.00	0.05	6.35
Ni	0.00	0.06	6.57
Pb	0.01	0.09	63.41
Sn	0.00	0.06	7.45
Sr	0.00	0.03	5.25
Zn	0.01	0.08	10.76
ARITHMETIC VALUES			
Ag	0.27	0.52	60.22
Ba	2.15	1.47	18.43
Bi	29.86	5.46	31.51
Co	609.23	24.68	24.14
Cu	12125.07	110.11	76.56
Mn	35.85	5.99	16.71
Ni	73.69	8.58	22.78
Pb	8.65	2.94	119.24
Sn	31.27	5.59	29.26
Sr	0.58	0.76	12.37
Zn	13864.38	117.75	79.15

1. <u>Boron</u> is present in all 9 preliminary analyses in small concentrations estimated to be 5 to 10 ppm. No calibration curves for boron were available.

2. <u>Calcium</u> is present in all preliminary analyses in uniformly low concentration. No calibration curves were available for quantitative determination. Calcium probably is derived from small quantities of admixed calcic feldspar and sphene.

3. <u>Chromium</u> is present in 4 of 22 preliminary and regional analyses in concentrations of 6, 16, 31 and 80 ppm. The chromium content of pyrite was judged to be too low and erratic to be useful in establishing trends.

4. <u>Magnesium</u> is present in all preliminary analyses in concentrations of .02% to .4%. Magnesium probably is derived from small amounts of admixed biotite.

5. <u>Molybdenum</u> is present in all preliminary analyses in rather high concentrations of 300 to 1000+ ppm. Some Mo probably is incorporated in pyrite but the majority obviously is derived from admixed molybdenite.

6. <u>Vanadium</u> is detected in nine preliminary analyses in concentrations estimated at less than 30 ppm. Hawley (1952) noted no significant variation in V content of pyrite related to depth, grain size or wall rock in four Canadian mines. Consequently no V determinations were attempted.

7. <u>Zirconium</u> is present in all preliminary analyses, but no quantitative determinations were made. Minor amounts of admixed zircon probably

account for all the Zr in pyrite.

8. _Titanium_ is present in pyrite in amounts ranging from 0.01% to 1.1%.
    The average Ti concentration is 0.35%. Titanium is not known to be
    accommodated in pyrite in these anomalously high concentrations. The
    only phase present in pyrite that is likely to be titaniferous is
    magnetite. No ilmenite inclusions or intergrowths in magnetite were
    seen. The electron probe was used to determine the Ti content of two
    pyrites containing magnetite inclusions, and one magnetite specimen.
    Pyrite S-18 contains an average of 125 ppm Ti, and pyrite S-117 con-
    tains an average of 207 ppm Ti. Magnetite inclusions in both specimens
    were slightly enriched in Ti relative to pyrite, but contained about
    the same Ti as the magnetite specimen, i.e. 290 ppm. This concentra-
    tion of Ti in magnetite cannot account for the anomalously high spec-
    trochemical analyses.

    Titaniferous minerals from veins and wall rock may have contaminated
    some pyrite concentrates. Sphene is a common accessory mineral in
    quartz monzonite, and leucoxene is recognized as an alteration product
    of biotite. A white mineral tentatively identified in polished section
    as leucoxene was analyzed on the electron probe and found to contain
    49% Ti. Thorough inspection of pyrite concentrates precludes the
    possibility of 1% - 2% admixed sphene or leucoxene in most specimens.
    Titanium assays derived from impurities would be more erratic and the
    standard deviation would be higher.

    If pyrite does not contain the high Ti concentrations indicated, nor
    are significant amounts of Ti contributed by magnetite or other titani-
    ferous minerals, then the Ti analyses must be in error. Preliminary

spectrochemical analyses (Appendix 3) were significantly lower in Ti

than analyses performed on the 67 orebody pyrites. Preliminary Ti

analyses were read from a pyrite calibration curve that was found to

be unsatisfactory. The majority of Ti analyses were read from a

silicate rock calibration curve, yielding "corrected" values 2X to 5X

the sulphide curve values for the same specimen. The two pyrite

specimens analyzed on the electron probe yielded 125 and 207 ppm Ti

vs. spectrographic analyses of 5350 and 4300 ppm Ti, respectively.

The highest Ti concentration in this study is 1.16% compared to the

recorded maximum Ti content of pyrite of 600 ppm (Fleischer, 1955,

p. 1003). Due to the uncertain reliability of the Ti calibration curve

used, the Ti analyses are disregarded in this study.

E. TREATMENT OF DATA

(1) Hand-Contoured Plans

Initially the eleven variables were plotted on 1" = 1000' orebody plans

and contoured. This technique was not successful in establishing trends due

to the high background "noise" of closely-spaced data points, and the bias-

ing of contours by numerous isolated highs and lows. Hand-contoured plans

for several elements are shown in Figs. 7-4, 7-5 and 7-6.

(2) Sections

Several north-south sections of each of the variables were plotted

with a similar lack of success in establishing trends. Sections plotted on

semi-log paper were smoother than raw data plots, and defined better the

more obvious minor element variations across the orebody. However, this

treatment of data also was judged unsatisfactory due to high background
"noise" and variance inherent in the geochemical data, with resultant
irregular "saw-toothed" profiles.

(3) Frequency Distribution Histograms

Early in the study, bimodal and polymodal populations were recognized
in some sets of data. Cu, Pb, Zn and Bi showed significant populations 3
to 10 orders of magnitude higher than the remainder. A decision was made
to apply trend surface analysis to the data, therefore it became important
to know the form of the density distribution of each variable.

Percent frequency histograms were prepared of the raw spectrochemical
data, and of base 10 logarithmic transforms of the same sets of data using
a Fortran IV computer program. Histograms of the eleven variables are
given in Figs. 7-2 and 7-3. The population (n) of each data set may be
less than the maximum of 67 if anomalously high and/or low values have been
deleted. Mean ($\bar{x}$) and standard deviation (s) are given for each histogram.
The bar interval in every case is one-quarter of the standard deviation.
To illustrate the variance of the frequency distributions, the abscissa is
calibrated in standard deviations above and below the mean.

All data sets are approximately lognormally distributed, i.e. log
frequency histograms are less positively skewed than raw data histograms.
Trend surfaces of raw and logged data sets for most of the elements show
a corresponding improvement in fit of surface to logged data versus raw
data.

FIGURE 7-2

PERCENT FREQUENCY

HISTOGRAMS OF

Co, Cu, Zn and Pb in

ENDAKO PYRITES.

COBALT
n = 66
x̄ = 227.5
s = 212.3
bar int. = s/4

COBALT log10
n = 66
x̄ = 2.20
s = 0.41
bar int. = s/4

COPPER
n = 67
x̄ = 233.2
s = 189.0
bar int. = s/4

COPPER log10
n = 67
x̄ = 2.21
s = 0.39
bar int. = s/4

ZINC
n = 66
x̄ = 109.3
s = 497.8
bar int. = s/4

ZINC log10
n = 66
x̄ = 1.32
s = 0.56
bar int. = s/4

LEAD
n = 66
x̄ = 11.0
s = 23.5
bar int. = s/4

LEAD log10
n = 67
x̄ = 0.18
s = 0.86
bar int. = s/4

251.

FIGURE 7-3

PERCENT FREQUENCY HISTOGRAMS OF Ni, Sn, Mn, Sr, Ba, Ag, and Bi in ENDAKO PYRITES.

(4) Trend Surface Analysis

(a) Method

Trend surface analysis is a method of fitting mathematically computed surfaces to spatially distributed data using a method known as least squares analysis. The surface represents systematic regional trends inherent in the data, whereas the residuals, obtained by subtracting the trend value from the original value, represent local fluctuations or anomalies (e.g. Sinclair, 1969).

The procedure commonly involves fitting a polynomial surface; linear, quadratic, cubic and so on, to a set of geographically distributed data, assuming some relationship exists among the coordinates and the variable being analyzed. Trend surfaces are fitted by least squares; that is, the total sum of squares of the deviations of the data points from the corresponding points on the surface are minimized. The least squares procedure is a standard statistical technique described in most introductory texts (e.g. Krumbein and Graybill, 1965, p. 333).

The equation of a first-degree (planar) surface is:

$$z = A + Bx + Cy$$

where x, y and z are variables and A, B and C are constants. Commonly x and y are coordinates and z is the observation at (x, y). A is a constant related to the average elevation of the surface, and B and C are slopes of the surface in the x and y directions, respectively. The degree of the surface is the maximum power of x and y found in a

term of the equation. A second-degree equation, representing a quad-

ratic surface, is:

$$z = A + Bx + Cy + Dx^2 + Exy + Fy^2$$

As the order of the equation increases, the surface more com-

pletely describes the data. Higher-order polynomials allow more

curvature in trends and provide smooth unbiased approximations of

hand-contoured data. Low-order surfaces, on the other hand, more

closely approximate regional gradients in data.

How well a calculated surface corresponds to the original data,

that is, the "fit" of the surface, is assessed by taking the ratio of

the variance accounted for by the surface to the total variance. The

ratio may be expressed as a decimal "coefficient of determination"

(Howarth, 1967) or as a percent (Krumbein and Graybill, 1965).

In selecting or rejecting a surface on the basis of its fit to

the original data, one may use the critical values for the coefficient

of determination established by Howarth (op. cit.). Sixty experimen-

tal tests of fitting trend surfaces to randomly-distributed data

indicate that if the percentage of the variance explained by the sur-

face falls below 6.0%, 12.0% and 16.2% for planar, quadratic and cubic

surfaces respectively, the distribution of data points is not signifi-

cantly different from random at the 95% confidence level.

Spectrochemical analyses of Endako pyrites were amenable to trend

analysis by virtue of the relatively uniform data point distribution

over the area of interest. Sampled drill holes were accurately

located ($\pm$ 0.1 ft.) on the surveyed mine grid. Most specimens were

taken at depths between 100 and 200 feet from the collar, yielding an essentially planar distribution of data points.

A computer program similar to that of Sampson and Davis (1966) for the IBM 7040 computer was used to calculate first to fourth-order trend surfaces for each of the eleven minor elements contained in Endako pyrites. Table 7-2 lists the coefficients of determination and standard deviations for surfaces computed from both raw and logarithmically transformed data.

(b) Results

Variables used in trend analysis were concentrations of each element in ppm plus the Co:Ni ratios. The first run used raw data and the second trial used logarithms to base 10 of the same data.

In every case except those of Ba and Co:Ni, the $\log_{10}$ quadratic surface has a higher coefficient of determination than the corresponding raw data surface. The improvement of fit with logarithmically transforming the data was anticipated by the shift to normal form in the $\log_{10}$ frequency histograms of these same data.

Quadratic surfaces were selected as the best representation of minor element trends for the following reasons:

1. The quadratic surfaces, as a group, were as good or a better fit to data than the linear, cubic or quartic surfaces.

2. Planar surfaces cannot adequately define the curved or concentric patterns common to classical examples of orebody zoning, whereas a quadratic surface is the lowest order giving curvature.

TABLE 7-2

Trend Surface Standard Deviations and Coefficients of Determinations

Variable	No.of Samples	Linear Surface Std.Dev.	Coef.det.	Quadratic Surface Std.Dev.	Coef.det.	Cubic Surface Std.Dev.	Coef.det.	Quartic Surface Std.Dev.	Coef.det.
Ag in py, ppm	67	2.8 ppm	.03	2.6 ppm	.10	2.7 ppm	.06	2.6 ppm	.11
Ag in py, $\log_{10}$	67	.52	.08	.50	.15	.50	.15	.50	.15
Ba in py, ppm	67	18.8 ppm	.11	17.0 ppm	.27	17.4 ppm	.23	17.1 ppm	.26
Ba in py, $\log_{10}$	67	.37	.07	.34	.21	.35	.19	.35	.20
Bi in py, ppm	67	61.4 ppm	.03	58.4 ppm	.12	58.0 ppm	.13	58.2 ppm	.13
Bi in py, $\log_{10}$	67	1.33	.06	1.28	.13	1.29	.11	1.30	.09
Co in py, ppm	67	209 ppm	.01	205 ppm	.04	211 ppm	-.01	205 ppm	.04
Co in py, $\log_{10}$	67	.36	.02	.35	.06	.38	-.08	.36	.03
Cu in py, ppm	67	185 ppm	.03	183 ppm	.05	198 ppm	-.11	188 ppm	-.00
Mn in py, ppm	67	43.4 ppm	.21	43.1 ppm	.22	42.9 ppm	.23	42.9 ppm	.22
Mn in py, $\log_{10}$	67	.56	.41	.55	.42	.54	.43	.55	.42
Ni in py, ppm	67	39.4 ppm	.13	37.6 ppm	.21	41.7 ppm	.03	37.7 ppm	.21
Ni in py, $\log_{10}$	67	.61	.35	.56	.45	.55	.48	.55	.48
Pb in py, ppm	67	23.4 ppm	.00	23.1 ppm	.03	23.4 ppm	.01	23.1 ppm	.03
Sn in py, ppm	67	25.7 ppm	.21	25.3 ppm	.23	26.1 ppm	.18	25.6 ppm	.21
Sn in py, $\log_{10}$	67	.64	.28	.63	.31	.64	.29	.63	.31
Sr in py, ppm	67	10.3 ppm	.02	10.1 ppm	.05	10.1 ppm	.05	10.1 ppm	.05
Zn in py, ppm	67	481 ppm	.05	470 ppm	.09	497 ppm	-.01	486 ppm	.03
Co/Ni ratio (0 trace transformed)	67	94.7	.22	93.0	.25	92.2	.26	93.0	.25
Co/Ni (0 Ni deleted)	57	3.34	.05	3.32	.07	3.32	.06	3.26	.10
Co/Ni (0 Ni deleted)$\log_{10}$	57	.33	.05	.33	.09	.33	.08	.32	.14

3.   The inherent erratic nature of minor element analyses does not

      justify surfaces more complex than second order.

Three of the $\log_{10}$ quadratic surfaces, Mn, Ni and Sn, showed

better fits to data than the rest. Their coefficients of determina-

tion improved markedly from those of raw data surfaces, i.e. Ni: 0.45

(0.21); Mn: 0.42 (0.22); and Sn: 0.31 (0.23). The two quadratic sur-

faces, the $\log_{10}$ quadratic residuals and the raw data for these three

variables are hand-contoured in separate orebody plans in Figs. 7-4,

7-5 and 7-6.

Manganese, nickel and tin quadratic surfaces are similar in con-

figuration and orientation. The three variables yield essentially

coplanar surfaces striking parallel to the west-northwest elongation

of the orebody, and dipping gently to moderately southwestward.

The barium raw data surface is a slightly better fit to data than

the corresponding logarithmic surface. The Ba surfaces are of differ-

ent configuration than the similar Mn-Ni-Sn surfaces, and show a

general change in trend between raw and logged data. Barium distribu-

tion trends may well be non-significant if the barium content of

pyrite is due largely to inclusions of host rock and/or potassic host

rock minerals. Hawley (op. cit.) found that the barium content of

pyrites from Canadian gold mines varied markedly with changes in wall

rock, and probably was due to wall rock inclusions. Endako Quartz

Monzonite, with an average Ba content of 300 ppm (Wertz, personal

communication, 1970), provides a readily available source of Ba

contamination.

FIGURE 7-4

TREND SURFACES OF Ni IN PYRITE

FIGURE 7-5

TREND SURFACES OF Mn IN PYRITE

FIGURE 7-6

TREND SURFACES OF SN IN PYRITE.
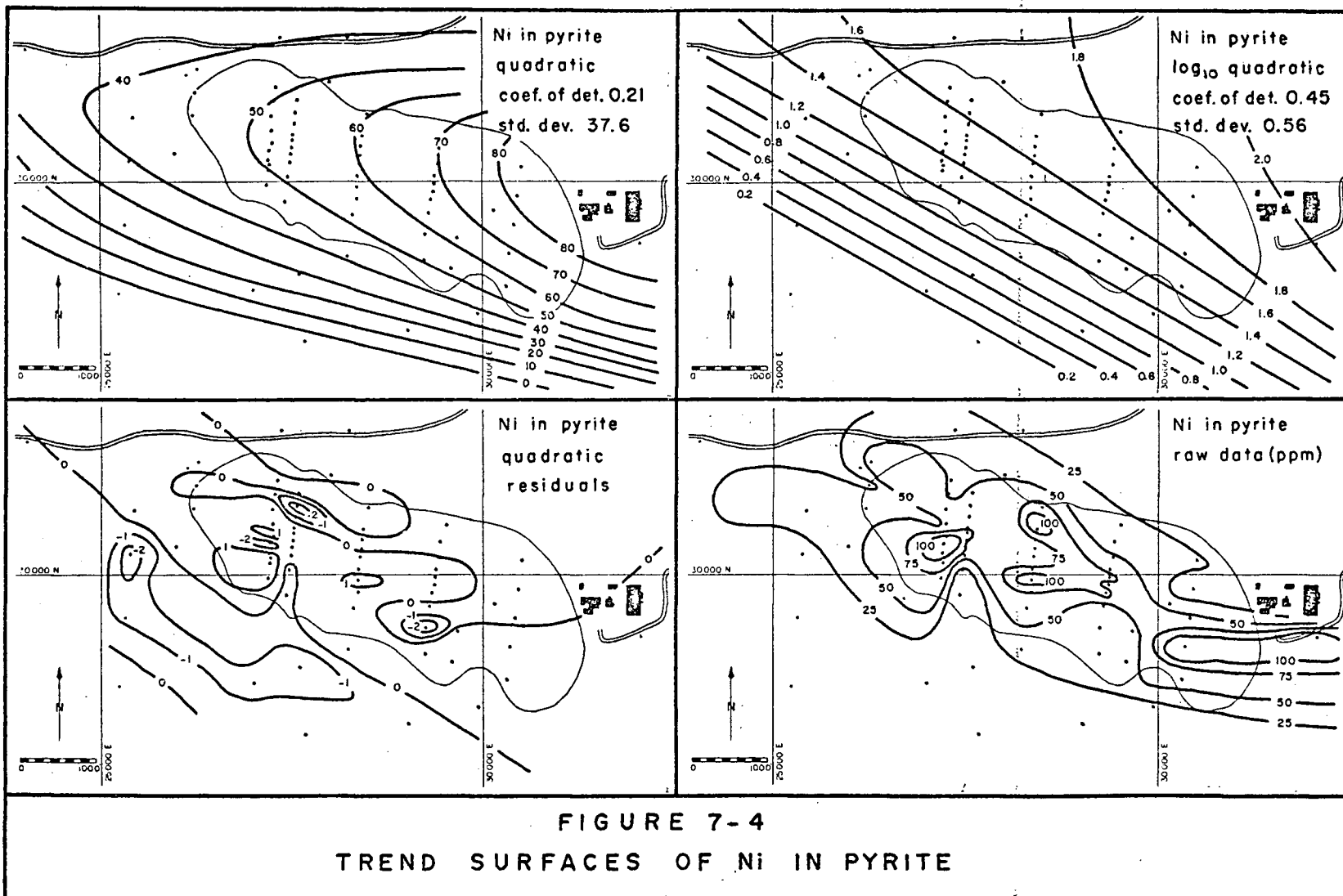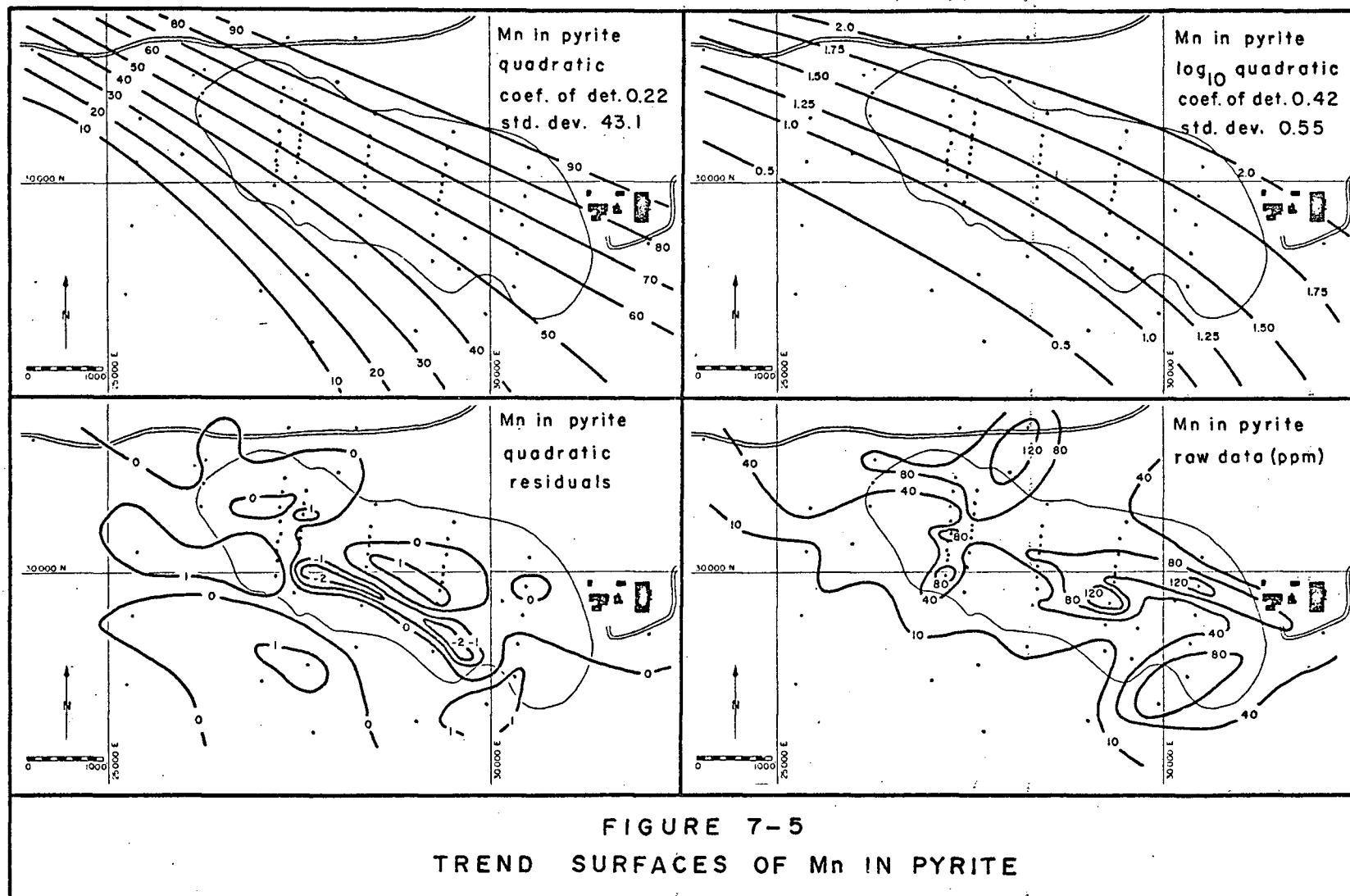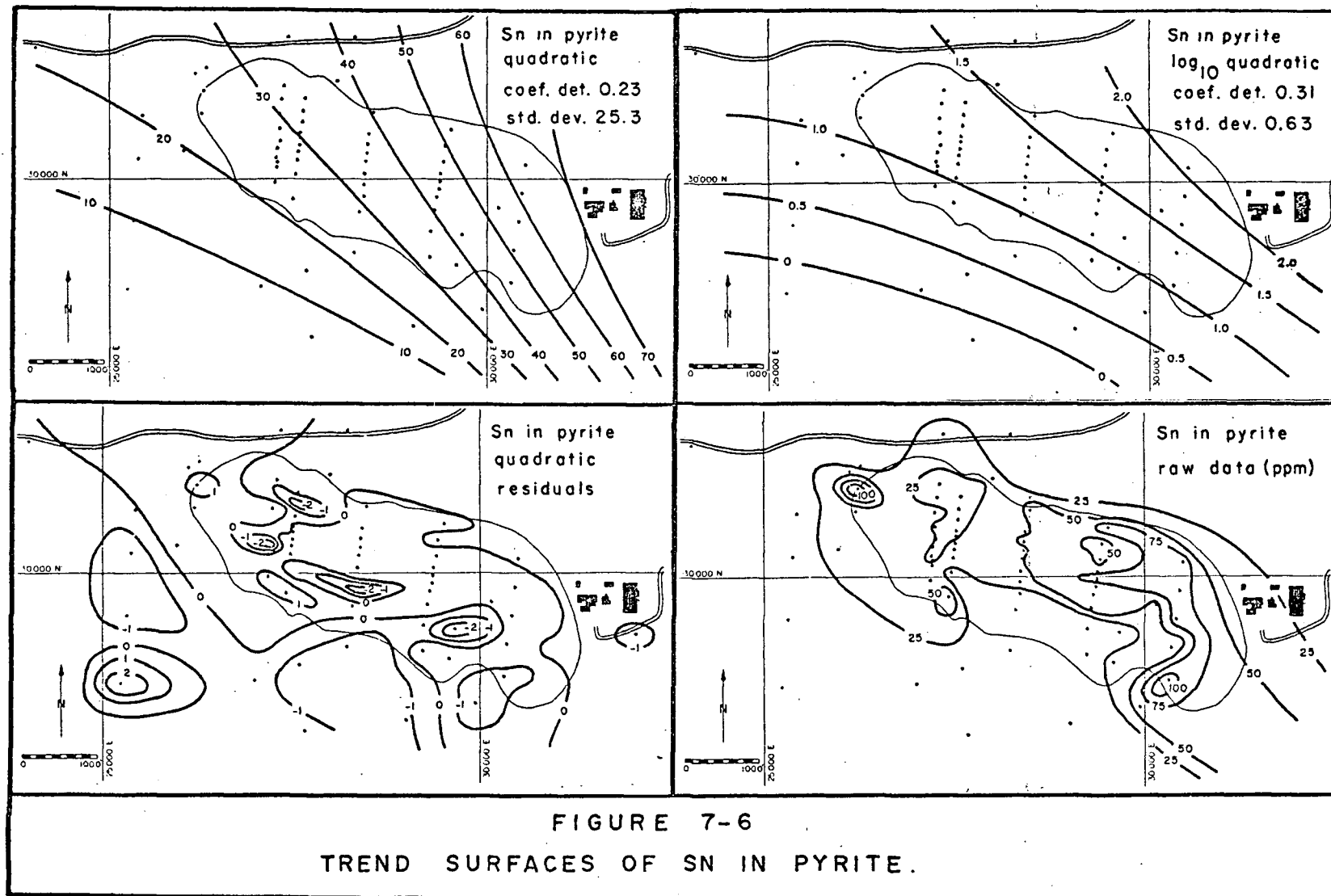
In computing the Co:Ni ratios, the low Ni spectrochemical assays were transformed by substituting 1/3 and 1/10 of the minimum detectable assay (4 ppm) for "trace" and "zero", respectively. The $\log_{10}$ quadratic surface of Co:Ni ratios is a poorer fit to data than the raw data surface, at 0.09 vs. 0.25. The Co:Ni quadratic surfaces strike north-westward along the axis of the orebody like the Mn, Ni and Sn surfaces. However, the Co:Ni surface dips in the opposite direction, from a high southwest of the open pit to a low northeast of the mine. The trend is due mainly to a sharp decrease in Ni content of pyrites outside the orebody, with the corresponding Co contents remaining relatively unchanged. The average Co:Ni ratio of 12 pyrites outside the southern limits of the orebody is 296 compared to an average ratio within the orebody of 9.2.

Nickel is concentrated predominantly in pyrites in the central orebody where Co has only an erratic distribution of localized highs. Cobalt shows two concentrations over the pyrite zone south and west of the orebody, a trend that is reflected in the Co quadratic surfaces. Both surfaces, however, are very poor fits to data and the trends are considered to be non-significant.

Silver and bismuth $\log_{10}$ quadratic surfaces are a slightly better fit to data than the corresponding raw data surfaces, at coefficients of determination 0.15 and 0.13 vs. 0.10 and 0.12, respectively. The fits to data, however, are still quite poor and of dubious validity. The surfaces depict similar increasing trends northwards and southwards from a long axis along the southern margin of the orebody.

Silver, with a mean of 2.5 ppm, is lowest in abundance of all elements in pyrite and is detectable only due to its high spectrographic sensitivity. Silver is concentrated in pyrites along the northern orebody periphery and south of the pyrite zone. A localized silver high that coincides with a major northeast fault in the western orebody area may reflect a relatively late stage of pyrite deposition.

Bismuth, with a mean of 35 ppm, also is in relatively low concentration in Endako pyrite. An anomalous linear zone of Bi values ranging between 100 and 300 ppm runs along the northern half of the orebody and is flanked by a large zone of zero Bi values overlying the southern periperhy of the orebody and the pyrite zone. The coincidence of the Bi high with the K-feldspar alteration zone may be related to a bismuthinite-K-feldspar association noted in early pegmatitic quartz-molybdenite-beryl veins.

Quadratic surfaces of the remaining four elements show poor fits to data: Zn: 0.09, Cu: 0.05, Sr: 0.05, and Pb: 0.03. The coefficients of determination of the three other orders of surface are even lower than the quadratic values. Frequency distribution histograms of these four variables are either strongly skewed or polymodal, or both.

In summary, trend surface analysis has revealed three definite trends in the distribution of minor elements in Endako pyrites. The principal, and probably most geologically significant, trend is the concentration of Ni, Sn and Mn over the orebody. Quadratic trend surfaces of the three elements are essentially identical, indicating that their concentrations in pyrite have been controlled by a single geological process related to the formation of the orebody. The

second trend is the concentration of Co (plus several other elements) over the pyrite zone south of the orebody, which, taken in conjunction with sharply diminished Ni assays in that area, results in high corresponding Co:Ni ratios. This trend may be related to mineralizing processes that gave rise to the mineralogically distinct pyrite zone. The third trend is defined mainly by the distribution of Bi and Ag, but also applies to Pb, Zn and Cu. trend surfaces, reflecting the erratic distribution of these elements, fit the data poorly yet show similar trends of a general low over the orebody and highs to the north and south. This trend may arise from several causes including thermal zonation, late-stage mineralization and wall rock contamination.

(5) <u>Correlation of Zonation in Minor Elements and Alteration Features</u>

(a) <u>Zonal Trends</u>

Trend surface analysis defines several apparently significant trends in zonation of minor elements. Nickel, manganese and tin concentrate over the orebody in coincident elongate zones parallel to the long axis of the orebody. The mutual highs of the three elements overlay the northern half of the orebody, and diminish regularly southward to a low south of the pyrite zone. Obviously this trend corresponds to molybdenite concentration in general, i.e. the orebody. More precisely, Ni, Mn and Sn correlate with a part of the orebody and adjacent host rock in which K-feldspar is the predominant alteration mineral. Like Mn, Ni and Sn in pyrite, K-feldspar alteration is relatively abundant along the north-central orebody axis but diminishes southward toward the pyrite zone where K-feldspar is essentially absent.

The pyrite zone is defined by the abundance of pyrite and seri-
citic alteration relative to molybdenite and to other alteration
assemblages. The arcuate zone that averages over 500 feet wide crosses
the southeastern end of the orebody, flanks it along the south side,
then diverges from the western end of the open pit and rejoins the
south side of the western extension. No single minor element is
concentrated exclusively in pyrites in this zone; however, two large
Co highs lie within the pyrite zone and highs in Cu, Zn, Ba and Sr
correlate with it to a lesser degree. Concentration of these elements
in sericite-associated pyrites in a zone peripheral to molybdenite
deposition indicates that genetic relationships may exist between the
zonal arrays of sulphides, alteration silicates and minor elements.

The third alteration zone is intermediate to the K-feldspar and
pyrite zones, covering the southern half of the orebody. The elongate
zone is defined by moderate to intense pervasive kaolinitic alteration,
contrasted with weak to moderate intensity elsewhere. Unlike the
other two alteration zones, no concentration of minor elements coincide
with this zone.

(b) Correlation of Raw and Trend Surface Data to Geology

The type of alteration associated with pyrite was recorded for
each specimen, permitting a correlation to be made between the speci-
fic alteration mineralogy of individual samples and the alteration
zones of the entire deposit. The relationship of spectrochemical assay
to alteration assemblage was compared for two elements, Sn and Bi,
that have different distributions that may reflect differing geological
controls.

The raw assay data for both Sn and Bi were grouped and plotted as three separate plans, depending on whether K-feldspar, sericite or kaolinite is the dominant alteration mineral associated with the pyrite specimen. The hand-contoured plans were compared to overall raw data plots and trend surfaces of the same variables.

Tin-kaolinite and tin-sericite distributions yield hand-contoured plans that show no correlation to any known geological control. The tin-K-feldspar association, on the other hand, yields a distribution of highs that coincide quite well with the K-feldspar zone. Bismuth values, when subdivided into alteration groups, yield a concentration of Bi-K-feldspar highs within the K-feldspar zone closely resembling the overall Bi high in that area. The Bi-sericite association appears to be non-significant, but the Bi-kaolinite plot shows an interesting concentration southwest of the pyrite zone. From these results the writer concludes that the Bi concentration in pyrite may result from at least two distinct geological causes whereas Sn correlates with only one geological factor. However, few concrete conclusions can be reached by such a qualitative comparison of trends in data.

Another approach to correlating minor element trends with geology was taken using $\log_{10}$ quadratic residuals (Figs. 7-4, 7-5, 7-6). The residuals from a significant trend surface represent anomalous depart-ures from the trend, and in the case of Endako may reflect structural controls. Tin, manganese, nickel and bismuth $\log_{10}$ quadratic residuals were plotted on orebody plans showing principal veins, faults and dykes. Residuals were contoured in units of standard deviations above and below the mean, and the highs and lows compared to structure.

Structural and spectrochemical data are somewhat concentrated in
Sections 1 and 4 in the western pit area due to relatively closely-
spaced data points and numerous large intersecting faults in that
area. Consequently, residuals of both variables correlate to these
northeast-striking faults to a degree. In general, however, the
residuals bear little relationship to known structures. The distri-
butions of minor elements may be affected less by local structures
than by the overall structural environment.

There may be a fundamental structural difference between the
eastern and western parts of the orebody, as postulated previously in
Chapter IV. Between the two areas, differences are observed in frac-
ture density, standard deviation of Mo assays, and proportion of large
veins to stockwork veinlets. A structural hypothesis is proposed that
involves intense domal fracturing in the east, giving way gradationally
to shear fracturing in the west. Alternative explanations for observed
structural differences are the structural level model of Kimura and
Drummond (1969), or possibly some multi-stage model of fracturing and
mineralization. If substantial structural disruption occurred between
the eastern and western parts of the orebody, or if mineralization was
multi-stage, then trend surfaces of minor elements in the two sub-areas
should reflect the difference. Conversely, if minor element trends
are similar, a single stage hypothesis is indicated.

Separate $\log_{10}$ quadratic surfaces were computed for Sn values east
and west of a major northeast fault crossing the west-central orebody.
The trend of the larger eastern surface is identical to that of the
overall Sn $\log_{10}$ quadratic surface, and the fit to data is better

(0.44 vs. 0.31). The trend of the smaller western surface is non-significant, at coefficient of determination 0.08. The only conclusion reached from this trial is that the overall Sn surface is the aggregate of the eastern and western trends which, taken alone, probably lack geologic significance. The test was not repeated for other variables, because it is apparent that the components of a general trend cannot be related to structural components of the whole orebody.

(c) Discriminant Analysis

Discriminant analysis assigns samples to previously defined populations on the basis of a number of variables considered simultaneously. The variables in this case are the minor element analyses of each sample. If control samples can be assigned to different populations on the basis of prior knowledge, they can then be used to establish mathematical criteria for the classification of additional samples. In addition, the validity of the original classification can be tested. The method establishes a discriminant function that represents a line or surface constructed in such a way to minimize the projected overlap of (i.e. discriminate between) the frequency distribution clusters of the variables.

Discriminant analysis was developed originally by R.A. Fisher (1936) for use in biological taxonomy. An illustrated description of the method, as applied to a geological classification problem, is given by Klovan and Billings (1967). The program used in this study was developed by the U.C.L.A. Health Sciences Computing Facility, for the Univac 1108 computer.

Discriminant analysis was used initially to test the grouping of pyrite specimens according to individual alteration associations. Pyrites were assigned to one of the following three groups: 32 specimens from K-feldspar - enveloped veins; 16 specimens from sericite-enveloped veins; and 19 specimens showing no alteration envelopes, but enclosed by pervasively kaolinized wall rock. The assigned groups coincide in a general way with the alteration zones defined in Chapter V. Discriminant analysis evaluated the assigned groupings as shown in Table 7-3:

Table 7-3

Discriminant Analysis of Pyrite-Alteration Groups

Assigned Group	Test Groups			Total Assigned
	1. K-Feldspar	2. Sericite	3. Kaolinite	
1. K-feldspar	21 (66%)	6 (18%)	5 (16%)	32
2. Sericite	1 (6%)	13 (81%)	2 (13%)	16
3. Kaolinite	3 (16%)	8 (42%)	8 (42%)	19

Some general conclusions may be drawn from these results. Only 42 of the 67 samples, or 63%, correspond statistically to their assigned groups, consequently one may conclude that these alteration associations cannot reliably discriminate between pyrites. Sericite-associated pyrites show the greatest tendency (81%) to group as assigned. By contrast, only 42% of the samples assigned to the kaolinite group are retained. Relatively few samples are relegated to the K-feldspar test group from assigned sericite or kaolinite groups. It is apparent that pyrites from enveloped veins, either K-feldspar or sericite, tend to group together to a greater degree than pyrites lacking alteration

envelopes. Both K-feldspar and sericite represent relatively high-temperature depositional environments, consequently these pyrites might have concentrated minor elements that tend to be excluded from the pyrite lattice at lower temperature. In this manner, characteristic "suites" of minor elements may be preferentially acquired by higher temperature pyrites.

The second discriminant analysis trial is designed to test the validity of pyrite groupings on the basis of three broadly-defined zones of <u>dominant</u> alteration throughout the mine area. Boundaries of the alteration zones are superimposed on a sample plan, separating pyrite specimens into 3 groups (Fig. 7-7). The test groups include 29 pyrites from the K-feldspar zone, 26 pyrites from the kaolinite zone, and 12 pyrites from the sericite-pyrite zone. Results of discriminant analysis of these assigned groupings are given in Table 7-4:

<u>Table 7-4</u>

Discriminant Analysis of Alteration Zones: 1

Assigned Zone	Test Groupings			Assigned Total
	1. K-feldspar	2. Kaolinite	Sericite 3. + py.	
1. K-feldspar	22 (76%)	6 (21%)	1 (3%)	29
2. Kaolinite	2 (8%)	19 (73%)	5 (19%)	26
3. Sericite-Pyrite	2 (17%)	1 (8%)	9 (75%)	12

The results show that 50 of the 67 samples, or 75%, correspond to their assigned group. All three assigned zones have essentially the same degree of correlation (75%) to the test groupings. These results
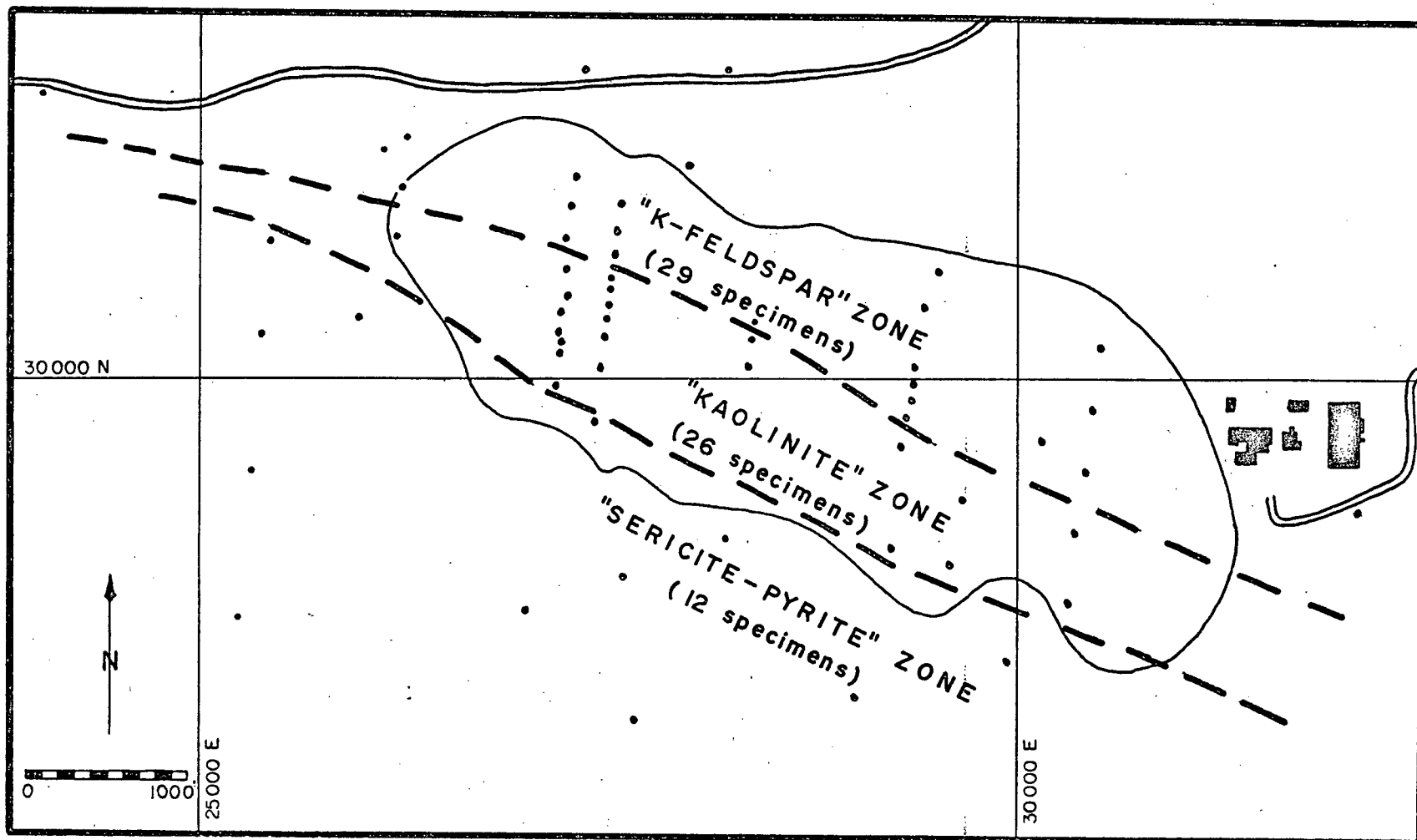
FIGURE 7-7

Allocation of test groups for discriminant analysis.

are markedly different from the first trial of pyrite - alteration envelope assemblage groups, indicating that the Endako pyrites are more validly grouped by alteration zones than by individual alteration associations.

The K-feldspar test zone in this instance, like the K-feldspar test assemblage in the first trial, is relegated fewest samples from other groups. K-feldspar appears to be the most significant alteration assemblage from the standpoint of concentration of minor elements in associated pyrite.

In 9 of 17 cases, samples that are rejected from the assigned alteration zone have individual alteration associations corresponding to that of their newly-assigned group. If the individual alteration associations did not influence the test groupings, a correlation closer to 1/3 would be expected.

The validity of the test groups in the second trial is tested by re-grouping the data as directed by discriminant analysis, and running it through the computer again. For example, samples rejected from the K-feldspar zone and relegated to the sericite-pyrite zone are grouped with the latter. The results of the third trial are given in Table 7-5.

Table 7-5

Discriminant Analysis of Alteration Zones: II

Assigned Zone	Test Groupings			Assigned Total
	1. K-feldspar	2. Kaolinite	3. Sericite + Py.	
1. K-feldspar	24 (96%)	1 (4%)	0	25
2. Kaolinite	0	24 (92%)	2 (8%)	26
3. Sericite-Pyrite	1 (6%)	0	15 (94%)	16

As expected, the assigned groups correlate very well (94%) with the test groups. All four samples rejected from the Trial 3 test groups had the lowest probabilities of membership in their previous respective test groups. Rejection of these samples in this trial is due to redefinition of the discriminant functions by the newly assigned groups. Consequently, samples having the lowest probability of belonging to the assigned group are reassigned.

The groups defined in this discriminant analysis trial represent a statistically sound classification, based on spectrochemical analyses of samples. In this respect, the close correspondence between the configurations of these groups and alteration zones bears comment. The tripartite division of alteration zones into elongate groups parallel to a significant minor element trend permits a natural classification of the zones based upon an inherent gradient in minor elements. The concordance of the Sn quadratic surface, representing a significant minor element trend, with alteration zones defined both geologically and by discriminant analysis (Fig. 7-8) shows the marked parallelism of zonation in minor elements and alteration.

Although discriminant classification of alteration associations does not correlate to assigned groups to the same degree as does a classification of alteration zones, the relationship of minor elements in pyrite to alteration environment is not fortuitous. The interrelationship is evident in the concordance of "high-temperature" minor elements and "high-temperature" alteration assemblages. Both the accommodation of minor elements by pyrite and the development of alteration minerals have zonal expressions of regional extent that reflect similar hydrothermal histories.
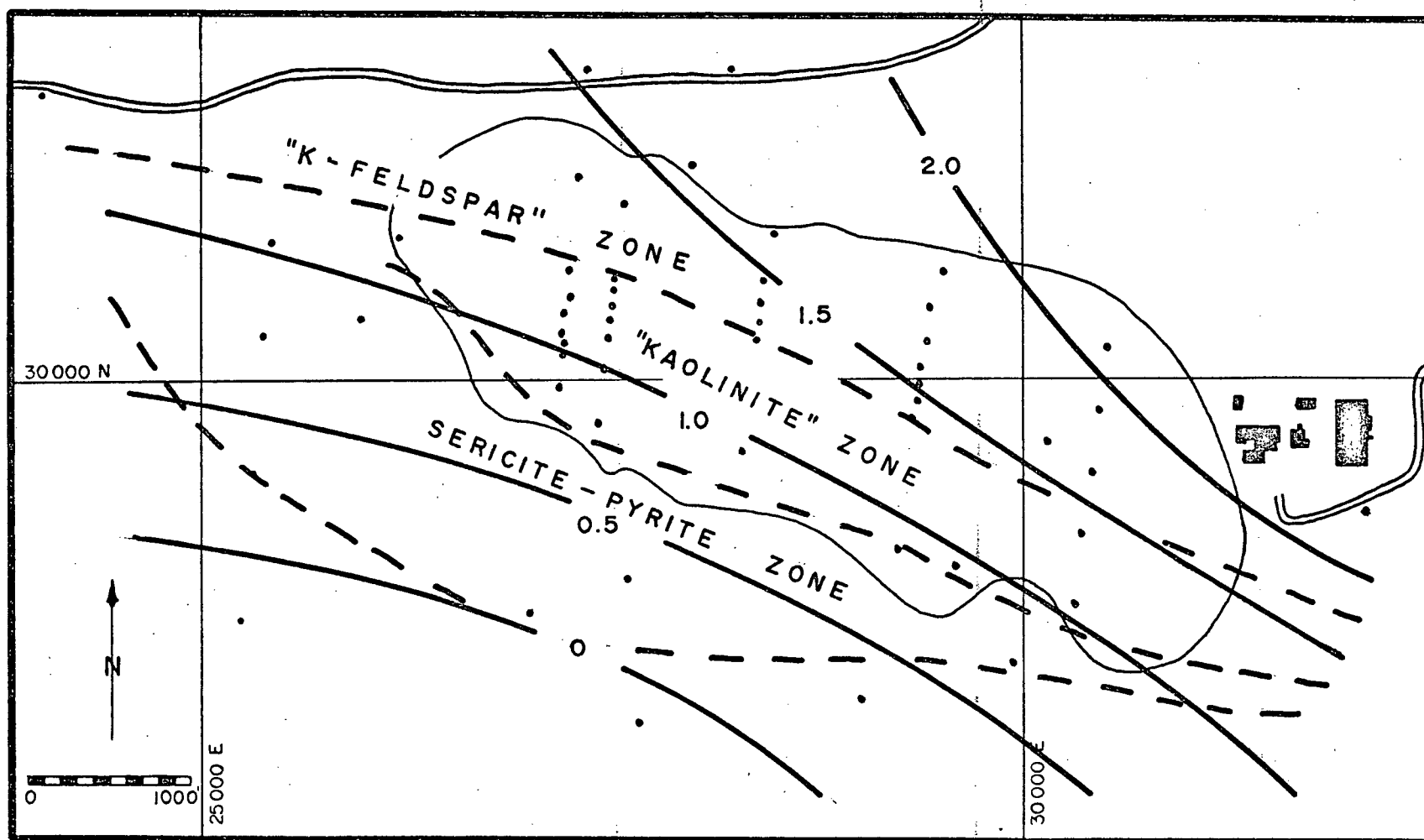
FIGURE 7-8

Concordance of Sn quadratic surface and alteration zones.

(6) Factor Analysis

The foregoing statistical treatments of pyrite spectrochemical data are attempts to reveal inherent geochemical trends. These trends may be directly relatable to geological causative factors, thus providing information on the hydrothermal system. Trend analysis has defined several significant minor element trends. However, trend analysis deals with only one variable at a time, and surfaces must be superimposed or otherwise physically compared to illustrate interaction of variables. Discriminant analysis is a multivariate technique in that all variables are used to establish discriminant functions. Discriminant analysis defined a group but not its characteristics. That is, the method does not specify the principal variables in any group. Consequently, the geological significance of groups classified by discriminant analysis may be unclear.

Factor analysis is a multivariate analytical technique that combines variables into new fundamental quantities (factors) fewer in number than the measured variables, and also specifies the relative weighting of each original variable in the new variable. It is possible to express the overall variability in data in terms of these factors, thus providing a method of relating minor element variations to possible geological causes.

Visual interpretation of complex multielement data may serve to recognize only the obvious features, leaving subtle though significant aspects undetected. Interpretation of these pyrite spectrochemical data requires consideration of several possible geological controls, including the physico-chemical environment of deposition (P, T, K^+/H^+, composition of host rock, etc.); the permeability of the orebody (size, density and distribution of fractures, source of hydrothermal fluids and net direction of flow); and

the assemblage of coexisting minerals among which minor elements could be partitioned. The end result of the interaction of these possible causes of minor element distribution is measurable, but the roles of the various controls remains obscure. Factor analysis can separate the minor element variations related to different geological causes (factors) and hence permit a more thorough interpretation.

(a) Method

Two methods of factor analyses were used in this study. R-mode factor analysis studies the intercorrelations between the variables determined on each sample. Q-mode analysis establishes the intercorrelations of the samples themselves. The important distinction between the methods is evident in their application: if a comparison of samples is desired, with the objective of proposing new sample sites, then Q-mode analyses should be carried out; R-mode analyses would in this case draw attention to variability in the measured properties and would be of use in a new area where the significance of variations is not clearly understood.

The method of R-mode factor analysis may be best explained with a simple example. Consider that Co and Ni have been determined in rocks ranging in composition from acidic to basic. Cobalt minerals are associated with granite and nickel minerals with gabbro. We may wish to identify areas where the Co and Ni patterns are related to mineralization in an area where the rock background values vary considerably. If maps of the two elements are plotted, each will contain only 50% of the information and there will be redundancy in data relating to the various rock units. A Co:Ni ratio plot contains 100% of the information,

but the expected range of Co:Ni ratios has to be determined for each rock type before interpretation can proceed.

A Co:Ni covariance plot (Fig. 7-9) expresses the degree to which the two variables tend to be linearly related. The covariance may be expressed in terms of two new axes whose mutual origin is the Co and Ni mean. The major axis F_1 is the best line of fit to data as computed by the method of least squares. The second axis F_2 is placed at right angles to F_1 through the origin. F_1 may contain 85% of the total data variance and F_2 the remaining 15%. Values along F_1 will describe any sample within the compositional field of granite to gabbro, and values along F_2 will describe any variations from this shifting background scale. F_1 and F_2 now describe the data in terms of the geological environment, i.e. F_1 is a changing background related to different rock units and F_2 is the presence of mineralization in those units.

This graphical process is actually an R-mode factor analysis where new linear combinations of data define axes that relate to geological processes dominant in the environment.

The essential steps in the factor analysis procedure as carried out by the computer, are as follows:

(i)   The data are read into the computer as a data matrix in either Q- or R-mode. If data are lognormally distributed, logarithmically transforming the raw data will yield more meaningful statistical results by shifting the distribution to a more normal or Gaussian form.
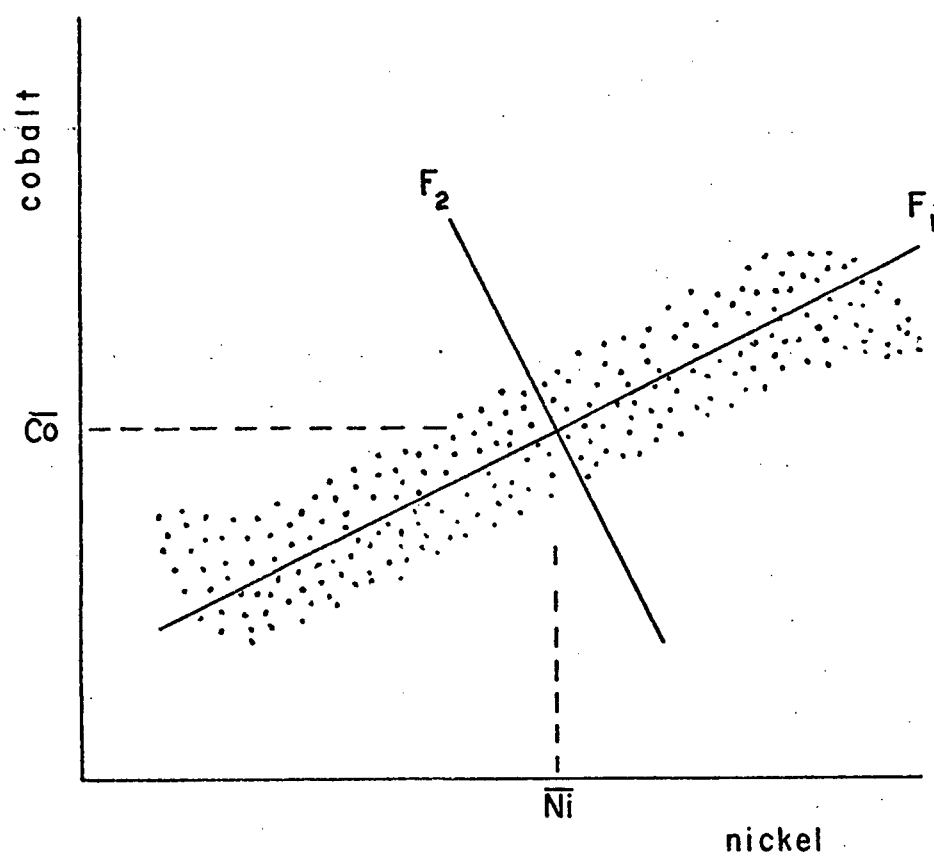
FIGURE 7-9

Co — Ni Covariance Plot

(ii)   Means and standard deviations of the variables are calculated.
Data for factor analysis must be normalized to allow for equal
weighting of variables with ranges of different magnitudes. Data
are normalized by subtracting the mean and dividing by the stan-
dard deviation.

(iii) Correlation coefficients are computed for each pair of variables
for the 67 Endako samples. A perfect sympathetic correlation
yields a coefficient of +1.0, a perfect antipathetic correlation
a coefficient of -1.0, and a random relationship a value of zero.
A matrix of coefficients in R-mode, between pairs of Endako vari-
ables, is dimensionally 11 x 11. A comparable similarity matrix,
the cos theta matrix for Q-mode analysis, is 67 x 67. The cor-
relation matrix contains all the information on the relationships
between samples and/or variables, but does not show these rela-
tionships in easily interpretable form. Factor analysis determines
the minimum number of independent dimensions needed to account for
most of the information in a correlation matrix.

(iv)   Data variability is explained by erecting a number of mutually
orthogonal axes in the multidimensional data space. The sample
points form a hyper-ellipsoid in n-dimensional space, the axes of
which are called factors. In R-mode, the Endako data space is 11-
dimensional, thus up to 11 axes may be placed mutually at right
angles in the space. Since the aim of factor analyses is to
simplify the data, less than 11 axes will be chosen. The major
and minor axes can be located by computing the eigenvalues and
eigenvectors of the correlation matrix, which are the roots of a

series of partial differential equations. By noting the number
of axes required to explain most of the information, the minimum
number of dimensions in which to portray the sample vectors is
determined. The proportion of the overall data variability con-
tained in each factor is expressed by the magnitude of the eigen-
values. The percentage of total variance accounted for by each
vector and the cumulative percentage of variance explained by
successive vectors is calculated, allowing assessment of the
statistical significance of successive vectors, and selection of
the optimum number of factors.

(v)   Factor axes are located in such a way as to maximize the variance
along each axis. The loadings of each variable on each factor,
i.e. the "composition" of the factors in terms of the original
variables, is determined from the eigenvectors in the preceding
step. The Principal Factor axes obtained can be difficult to
interpret; thus a further stage of modification is carried out.
The principal factor axes are orthogonally rotated (remaining 90°
apart) about the origin. The axes are rotated by the Varimax
Criterion which has the effect of bringing the position of the
principal axes as close as possible to that of the original axes.
Varimax rotation clarifies the factors by giving only a few high
loadings and a remainder of low loadings, thus aiding interpreta-
tion.

(vi) The score for each sample on each of the factors is computed in
Q-mode analysis. The rotated factor score matrix gives the
amounts of the "new" variables (factors) at each sample locality.

The Varimax factor matrix, together with the original transformed data, are used to generate the factor scores which are expressed in units of standard deviations above and below the zero mean of the score. The distribution of factor scores can be plotted, contoured and visually compared to other spatially-distributed geologic data.

A detailed explanation of factor analysis is given by Imbrie and Van Andel (1964), and a similar but more intuitive explanation is given by Klovan (1968). Many examples of the geological applications of factor analysis now appear in the literature. The reader is referred to a sedimentology example offered by Klovan (1966), and a geochemical application given by Garrett and Nichol (1969).

(b)   Results of R-mode Analysis

R-mode factor analysis was carried out by a computer program developed by the U.C.L.A. Health Sciences Computing Facility.

The initial steps in the program are computation of means, standard deviations and correlation coefficients. A matrix of the coefficients is given in Table 7-6.

Table 7-6

R-mode Correlation Coefficient Matrix

	Ag	Ba	Bi	Co	Cu	Mn	Ni	Pb	Sn	Sr	Zn
Zn	.447	.202	.183	.028	.338	.177	.035	.137	.135	.213	1.0
Sr	.269	.513	.145	.086	.382	.494	.241	.128	.379	1.0	
Sn	.245	-.067	.141	-.102	.185	.562	.679	.035	1.0		
Pb	.400	.265	.421	.010	.346	.024	-.107	1.0			
Ni	.088	-.191	.071	.210	.136	.654	1.0				
Mn	.404	-.047	.298	-.029	.212	1.0					
Cu	.390	.323	.056	.286	1.0						
Co	-.067	.152	-.217	1.0							
Bi	.294	.101	1.0								
Ba	.101	1.0									
Ag	1.0										

From the coefficients it is evident that Ni-Mn-Sn, Pb-Ag-Zn and Ba-Sr intercorrelate sympathetically, and that Co varies antipathetically with Sn, Mn and Bi.

Eigenvalues are derived from the correlation matrix. The proportion of the total variance contained in each factor is expressed by the magnitude of the eigenvalues. Eigenvalues and percentages of variance explained by each are given in Table 7-7.

Table 7-7

R-mode Eigenvalues

No.	Eigenvalue	Percentage of Variance	Cumulative % Of Variance
1	3.207	29.1	29.1
2	2.003	18.3	47.4
3	1.453	13.2	60.6
4	1.092	9.9	70.5
5	.946	8.6	79.1
6	.649	5.9	85.0
7	.529	4.8	89.8
8	.434	4.0	93.8
9	.307	2.8	96.6
10	.213	1.9	98.5
11	.165	1.5	100.0

The choice of the number of factors to be used is somewhat sub-
jective. There is a distinct break in the pattern of decreasing
eigenvalues at No. 5, indicating that only those factors above the
break be used. Furthermore, the eigenvalues above No. 5 are greater
than unity, indicating they should be used if there are unities in
the diagonal of the correlation matrix (Harman, 1967). At this stage
it appears desirable to use as many factors as are necessary to explain
the intercorrelations in data, since the number of causative geological
processes is not yet known. A five-factor model was chosen for the
above reasons.

The loadings of each variable on to the five factors are computed then rotated by the Varimax criterion. Table 7-8 gives the normalized Varimax factor loadings.

Table 7-8

R-mode Normalized Varimax Factor Loadings

Variable	Factor I	Factor II	Factor III	Factor IV	Factor V
Ag	.215	.004	.396	.022	.723*
Ba	-.198	.149	.134	.876*	.066
Bi	.182	-.273	.787*	.031	.065
Co	.014	.921*	-.092	-.001	-.074
Cu	.140	.527*	.180	.370	.482
Mn	.839*	-.062	.137	.112	.192
Ni	.898*	.227	-.061	-.102	-.050
Pb	-.105	.191	.843*	.148	.160
Sn	.832*	-.069	.036	.073	.106
Sr	.429	-.107	.031	.811*	.152
Zn	.028	-.043	-.023	.118	.875*

*major component of factor

The first factor, accounting for 29% of the data variability, is predominantly a Mn-Ni-Sn association. It was noted previously that these three elements yield essentially identical trend surfaces that indicate concentration over the orebody. Consequently Factor I is presumed to be an "orebody" factor, related to molybdenite deposition.

The second factor is essentially a Co and Cu association that accounts for a further 18% of the total variance. The concentration

of Co and Cu highs over the pyrite zone indicates that Factor II is related to a mineralizing process distinct from that which occurred within the orebody.

Factor III is a Pb-Bi-minor Ag association that accounts for some 13% of the total variance. Bismuthinite is associated with K-feldspar alteration, and Pb values in pyrite are highest south of the pyrite zone. The factor may reflect mineralizing processes that gave rise to peripheral concentrations of Bi, Pb and possibly Ag, in pyrite.

The fourth factor, accounting for some 10% of the data variance, is a Ba-Sr association. The two elements intercorrelate significantly but do not vary systematically over the deposit. Few quantitative data are available on Ba and Sr in pyrite (Fleischer, 1955). Hawley (1952) found marked variation of the Ba and Sr contents of pyrites from different host rocks, and related most Ba and Sr in pyrite to inclusions. The replacement of alkali ions in feldspars by Ba and Sr probably accounts for most of the 300 ppm Ba and 220 ppm Sr in Endako Quartz Monzonite (Wertz, pers. comm., 1970), and the subsequent contamination of pyrite by admixed or included feldspar grains. Factor IV is best related to contamination rather than to any chemical or geological process.

Factor V is principally Ag and Zn, but also consists of minor contributions from Cu, Mn, Pb, Sn and Sr. This factor may represent one or a combination of several effects: (1) minor elements released from country rock during alteration and metalization, and incorporated in pyrites; (2) contamination by included and admixed country rock; and (3) peripheral concentrations of these elements, and/or late-stage

low-temperature mineralization.   Somewhat similar effects would be obtained by all the above processes.

The erratic distributions of the principal components of Factors III, IV and V are consistent with a wall rock contamination hypothesis rather than a more systematic geological control.   The significance of the various factors is further clarified by the following Q-mode factor analysis treatment.

(c)   Results of Q-mode Analysis

Q-mode factor analysis was carried out initially by a computer program developed by the U.C.L.A. Health Sciences Computing Facility. An improved Q-mode program, developed by Sinclair and Wilson of the Department of Geology at the University of British Columbia, was used for all subsequent runs.

Initially, a comparison was made between raw and logarithmically transformed data by computing Q-mode factors from both data sets. Generally similar factors were obtained, with the order and composition of the factors differing slightly.   The difference in results is due mainly to the greater variance shown by untransformed variables.   A Chi-square test points up this distinction between the two data formats, and also shows that the variables Pb, Zn and Bi are the least likely to vary systematically in either format.   In these trials, as in previous statistical analyses, the logarithmically transformed data yields superior results, due mainly to the log-normal distribution of most geochemical variables.

The correlation coefficient matrix in Q-mode is derived by rank-
ing the variables from each sample successively against their counter-
parts in a 67 x 67 array. To save computer time, neither this lengthy
matrix nor the derived eigenvector matrix is printed out. The program
prints out the following matrices for the first set of seven factors,
accounting for 99.1% of the total variance: factor matrix; factor
scores matrix; Varimax factor matrix; and Varimax factor scores matrix.

The Varimax factor matrix gives communality values greater than
.96 for all 67 samples with the first group of 7 factors. The commu-
nality expresses the percentage of the variance on that sample
explained by all 7 factors. Samples whose variance is not adequately
explained by the factors would show anomalously low communalities.
The amount of each factor is given, in standard deviation form, for
every sample site. With this matrix, the distribution of the factors
can be mapped.

Varimax factor scores give the standarized scores (either + or -)
of each variable on every factor. Rotated factors generally have only
a few high loadings, which allows one to readily identify the principal
components of the factors. A factor can thus be interpreted according
to the geological significance of those variables.

The program successively drops off the last factor and recalculates
the loadings of the remaining factors. In this manner the seventh
factor, accounting for only 0.89% of the total variance, is dropped and
a new 6-factor Varimax factor matrix and Varimax factor score matrix
are printed out.

The sixth factor is then dropped and the process is repeated again. After computation of 5 factors, the computer prints out factor score maps for each factor. Hand-contouring of these factor score values shows the areal distribution of the factors.

The process is repeated successively until factor scores have been derived and plotted for only 2 factors. The successive Varimax factor components, with corresponding variance percentages, are given for the seven-factor model through to the two-factor model in Table 7-9.

(d) Interpretation

(1) Choice of Factors:

The choice of a 3-factor model was influenced by the following observations:

(i) In the first five successive computations, from seven factors down to a three-factor model, the first three factors are retained essentially unchanged (Table 7-9).

(ii) The components of the three Q-mode factors are identical with those of the first three R-mode factors, showing that the samples intercorrelate in the same way as the variables. The composition of the 3 Q-mode factors is given in the Q-mode Varimax factor scores: Table 7-10.

Table 7-9

Successive Q-mode Varimax Factor Components

Factor	Components	% of var.	Factor	Components	% of var.
F_1	Mn, Ni, Sn	48.44	F_1	Ni, Mn, Sn	47.08
F_2	-Co, -Cu (-Ba)	20.66	F_2	-Co,-Cu,-Ba,(-Sr)	21.27
F_3	-Bi, -Pb	24.43	F_3	-Bi, -Pb	25.51
F_4	-Ag	1.98	F_4	-Ag	1.99
F_5	Bi, -Pb	1.87	F_5	-Pb-Sn, Bi	1.79
F_6	-Sn,-Zn,(Co,Mn)	.83			97.64 Cum.
F_7	Mn,-Ni,-Sn	.89			
		99.10 Cum.		****	
			F_1	Ni, Sn, Mn	46.42
	****		F_2	-Co,-Cu,-Ba,(-Sr)	20.83
			F_3	-Bi, -Pb	27.23
F_1	Ni, Mn, Sn	47.39	F_4	-Ag, +Bi	1.95
F_2	-Co,-Cu (-Ba, -Zn)	20.91			96.44 Cum.
F_3	-Bi, -Pb	24.96		****	
F_4	-Ag	1.99	F_1	Ni, Mn, Sn	50.43
F_5	-Pb, +Bi	2.24	F_2	-Co,-Cu -Ba	21.63
F_6	Mn, -Sn	.96	F_3	-Bi, -Pb	22.62
		98.45 Cum.			94.68 Cum.
				****	
			F_1	Mn,Bi,Sn,Ni	56.59
			F_2	-Co,-Cu-Ba, (-Zn-Sr)	34.98
					91.57

<u>Table 7-10</u>

Q-mode Varimax Factor Scores

Variable	Factor I	Factor II	Factor III
Ag	0.148	-0.035	-0.873
Ba	0.242	-1.243	-0.489
Bi	0.001	1.003	-2.317*
Co	0.665	-1.818*	-0.267
Cu	0.630	-1.537*	-0.589
Mn	1.671*	0.904	-0.374
Ni	1.878*	0.466	0.285
Pb	-0.694	0.150	-1.887*
Sn	1.658*	0.617	0.025
Sr	0.527	-0.776	-0.331
Zn	0.503	-0.854	-0.571
Variance %	50.43	21.63	22.62
Cum.Var. %	50.43	72.05	94.67

*principal component of factor

(iii)   Three Q-mode factors explain a high proportion (94.67%) of
total variance. The addition of a fourth factor accounts
for only an additional 1.76% of the variability. The curve
of cumulative variance vs. number of factors (Fig. 7-10)
shows a marked change in slope at 3 factors indicating that
this is the minimum number of axes required to adequately
explain the data variability.

The normalized Varimax factor component plots for Q-mode factors I, II and III are hand-contoured in Figs. 7-11, 7-13 and 7-14. The factor components for all 67 samples are given in Appendix 6. The maps show a marked separation of factors I and II over the ore zone and pyrite zone, respectively.

(2) Factor I:

Scores on factor I (Mn, Ni, Sn) are distributed in a well-defined high inside the 0.7 isopleth that coincides closely with the periphery of the open pit (Fig. 7-11). Within the 0.7 isopleth several 0.8 + highs occur oriented along the central axis of the orebody. High factor I scores extend westward along vein zones in the western extension and Denak zone, and southeastward over low grade ore outside the present pit limits. Factor I scores diminish gradationally outwards to the south.

As indicated with trend surfaces and R-mode analysis, the factor I Mn-Ni-Sn association is uniquely related to the molybdenite deposit. The concentration of high factor I scores along the axis of the orebody, and their progressive diminishment south-westward away from the centre of molybdenite deposition shows that a relationship exists between abundance of molybdenite and abundance of the minor elements Mn, Ni and Sn in pyrite.

The zonation of the factor I elements Mn, Ni and Sn is believed to be due mainly to thermal gradients. All three elements are, to a degree, temperature sensitive in the extent of their substitution in the pyrite lattice (see Fleischer, 1955).
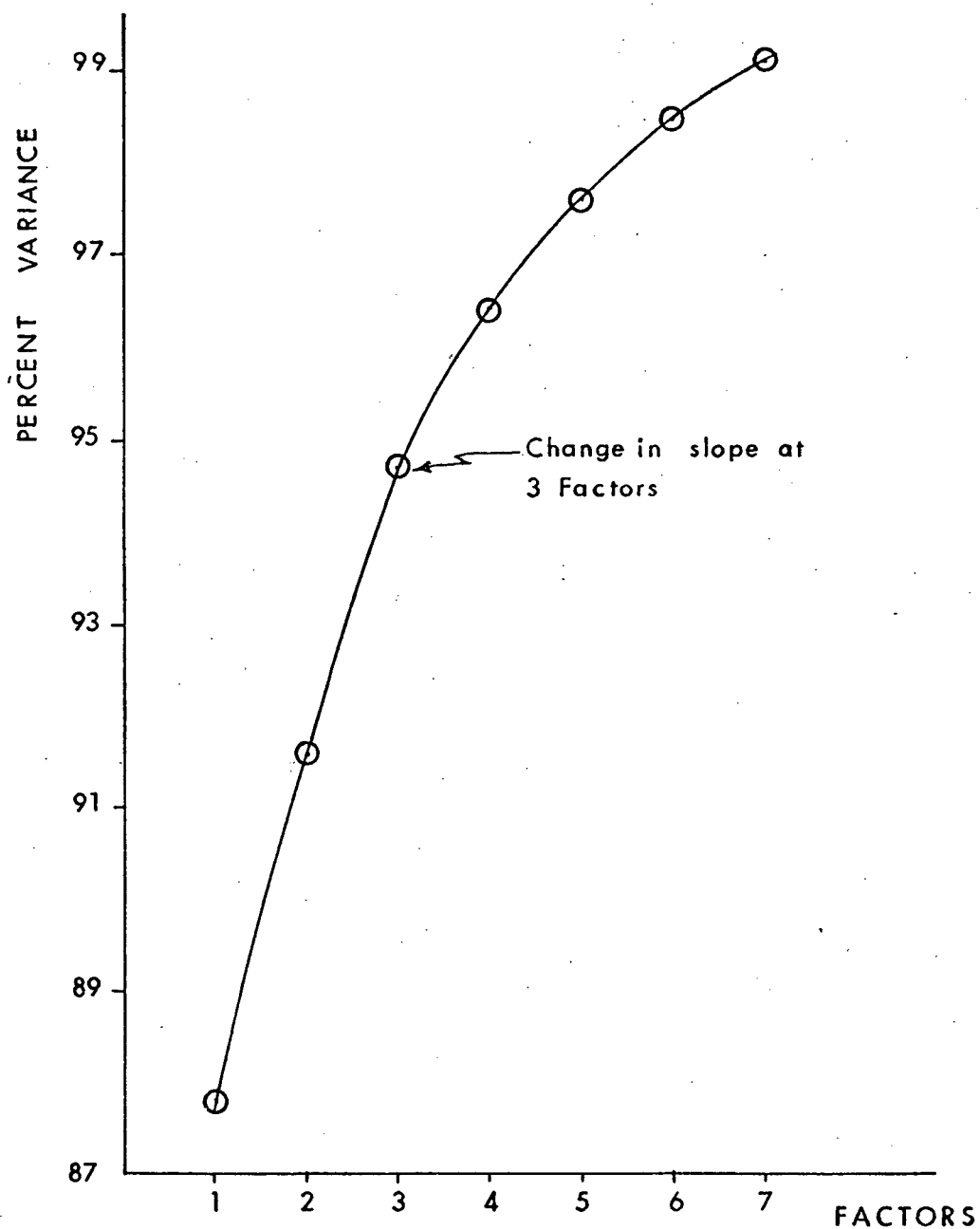
FIGURE 7-10

PERCENT VARIANCE EXPLAINED
BY SUCCESSIVE Q-MODE FACTORS.

KMD/71
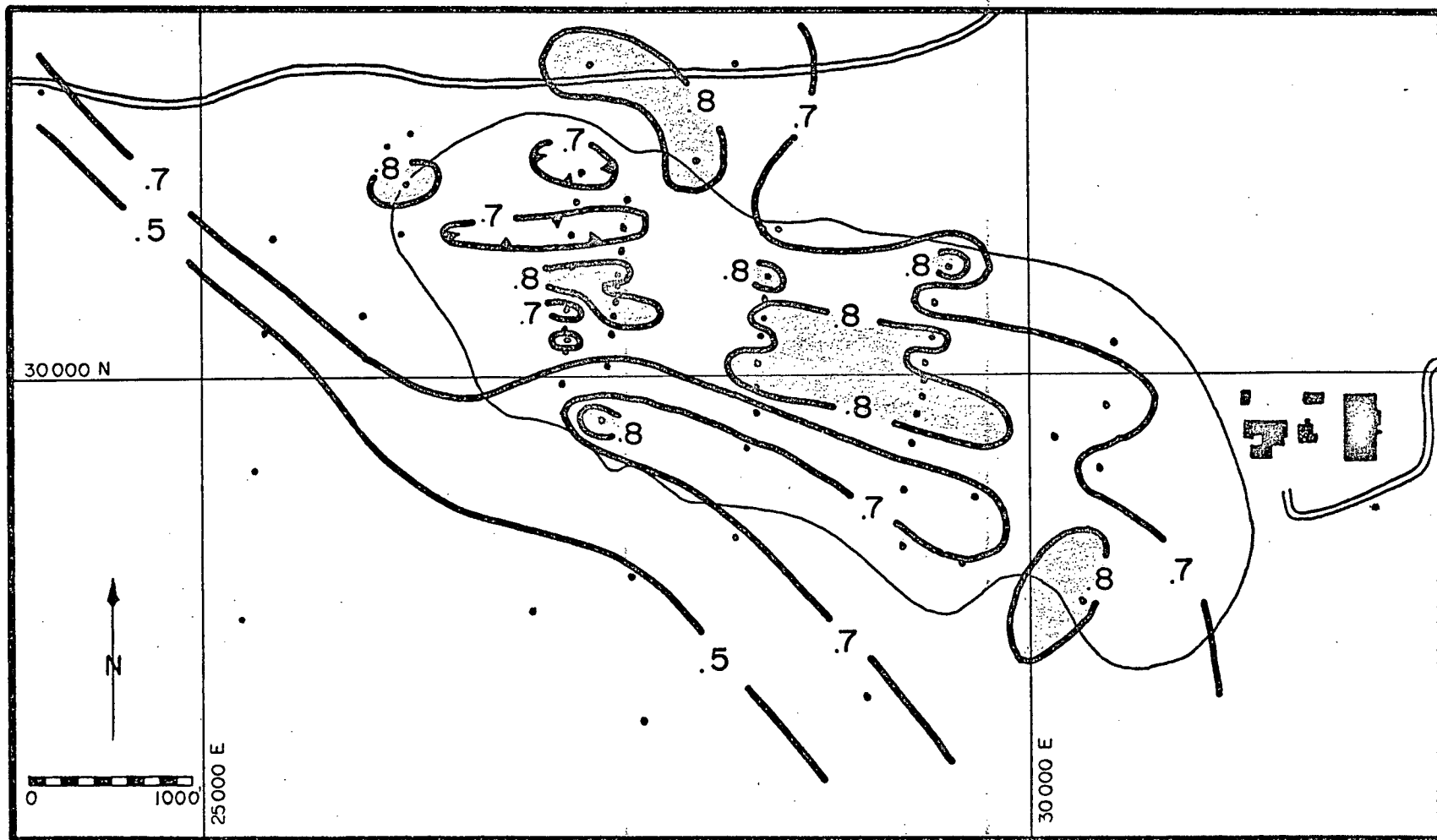
FIGURE 7–11

FACTOR I (Mn, Ni, Sn) SCORES .

FIGURE 7-12

Co : Ni ratios from Endako pyrites
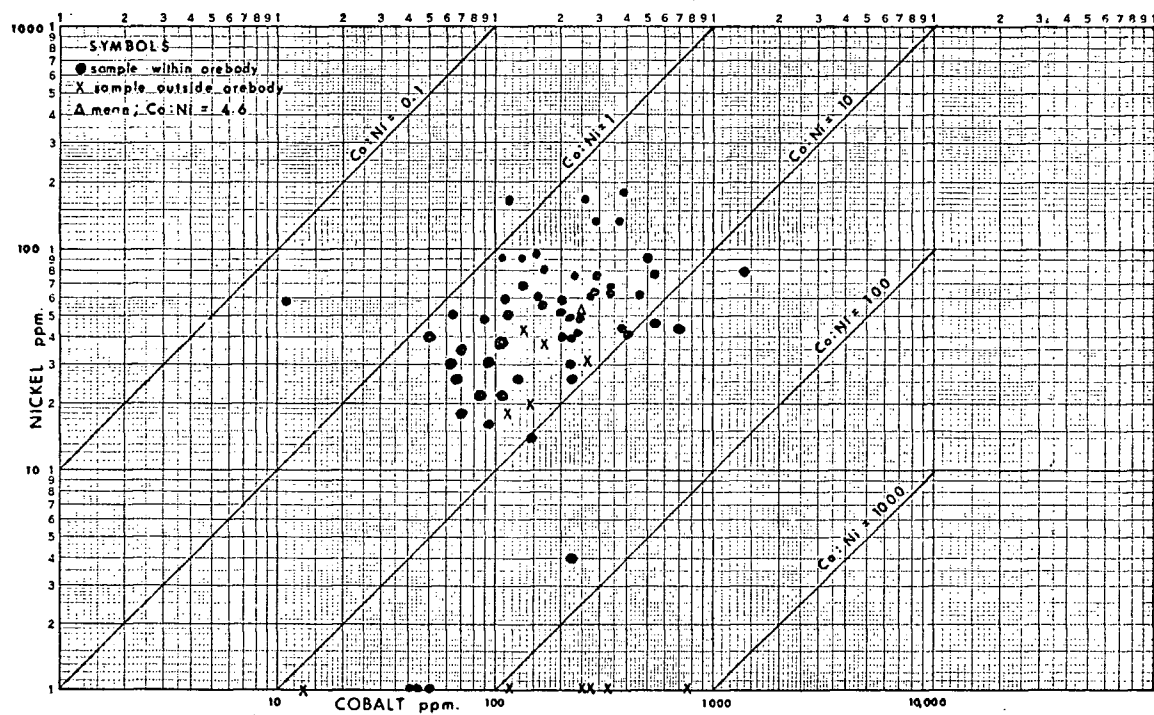
(i) Nickel:

An isomorphous solid-solution series between pyrite and its isostructural Ni-analogue vaesite contains a hiatus at 60%-90% NiS_2 that gives way to continuous solid solution above 700°C (Klemm, 1965). The temperature dependence of a major component solid-solution series may not be directly applicable to Endako pyrites with a low Ni content, averaging 50 ppm. However, Klemm's experimental data show that the pyrite lattice more readily accepts Ni at elevated temperatures, indicating that even minor amounts of available Ni would be preferentially concentrated in highest temperature pyrite.

Hawley (1952) found that the Ni content was slighly higher in high temperature pyrites, whereas Gavelin and Gabrielson (1947) found little or no effect of temperature of formation. Auger (1941) and Hawley (op. cit.) found no systematic trend in variation of Ni content of pyrite with depth in seven Canadian gold mines. Hegemann (1943) shows that in "high temperature" hydrothermal pyrite Co predominates over Ni, and Co:Ni ratios average 10 to 30 as compared to around 1 for "low temperature" hydrothermal pyrite. Hegemann's temperature ranges apparently are based on mineral assemblages. The Endako average Co:Ni ratio is 4.6 (Fig. 7-12).

Numerous examples in the literature show that Ni in hydrothermal pyrite frequently is more abundant and always more variable than in pyrite from other types of deposits. Few quantitative data are available on Ni contents of pyrite

from porphyry-type deposits. Price (1971), in a current
University of British Columbia M.Sc. thesis study of minor
elements in pyrite, has compared statistically data from
Endako and four other western Canadian porphyry Cu-Mo
deposits including Berg, Casino, Molymine and Tchentlo Lake.
Price has found that the Ni and Co contents of all types of
hydrothermal pyrite studied including the five porphyries,
can be related qualitatively to major metals in the deposit.
A common temperature of formation is the most probable geo-
logical control relating mineral assemblages and Co-Ni
contents of pyrite from different types of deposits.

(ii) Manganese:

The mineral hauerite (MnS_2) is isostructural with pyrite. In
hauerite, the Mn d-electrons are in the "high-spin" state,
leading to ionic bonding compared to predominantly covalent
bonding in pyrite (Nickel, 1970). Consequently only limited
isomorphous substitution of Mn^{+2} for Fe^{+2} occurs in the
pyrite lattice (Mitchell, 1968). The limits of isomorphous
substitution probably are less than the 1% maximum Mn content
of pyrite reported by Fleischer (op. cit.) but within the
range of Endako pyrites, i.e. mean 54 ppm, maximum 240 ppm.

Interstitial solid solution of the relatively large Mn^{+2} ion,
whose octahedral covalent radius is 1.55 $\overset{\circ}{A}$ compared to 1.23
$\overset{\circ}{A}$ for Fe^{+2}, may be encouraged by pyrite lattice expansion at
high temperature. Temperature of formation, however, was
found to produce no significant trends in the variation of

the Mn content of pyrites studied by Auger (1941), Hawley
(1952) and Gavelin and Gabrielson (1947).

In the causes of mineral zoning, temperature is believed
secondary to relative stabilities of ionic complexes by
Barnes (1962). Mn forms the least stable complexes of the
common ore minerals, in order of decreasing stability:

    Hg-Cd-Pb-Cu-Zn-Sn-Ni-Fe-Co-Mn
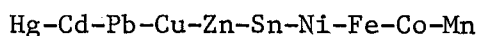
which corresponds well to most mineral zoning sequences.
Barnes notes that alabandite (MnS), a mineral not often seen
in nature, would represent the innermost zone of Mn, but the
distribution of Mn also may be complicated by co-existing
soluble salts, such as the "outer zone" carbonate rhodo-
chrosite.

A further complication in the interpretation of Mn zoning
is the possibility of Mn concentrating in pyrite by adsorp-
tion on growing crystals, physical admixture of Mn-rich
wall rock or mineral inclusions, and presence of tarnishes
on pyrite. The last factor can be minimized by careful
inspection, and adsorption and inclusion may be, to a limited
degree, influenced by formation temperature.

(iii) <u>Tin</u>:

Mitchell (op. cit.) allows that a limited amount of Sn can
substitute isomorphously for Fe in pyrite. The extensive
substitution of Sn for Fe, Cu and Zn in such tetrahedrally

coordinated minerals as sphalerite and chalcopyrite is due to the isostructural nature of stannite. Extensive substitution of Sn for Fe in pyrite is unlikely due to dissimilar ionic charges and covalent radii.

Microscopic inclusions of cassiterite and stannite are a possible cause of relatively high Sn in pyrites from massive sulphide and stratiform volcanic-exhalative deposits. Hawley (op. cit.) related local "high temperature" affinities for Sn mainly to wall rock and mineral contamination, and found most Sn variations in pyrite to be non-systematic. Sn contamination is unlikely to have occurred at Endako where no Sn minerals have been recognized, and the host rock contains an average of 2 ppm. Sn (Wertz, op. cit.).

The concentration of Sn in hydrothermal pyrite may result from the sulpherization of mineral phases such as magnetite, ilmenite and rutile that potentially may concentrate available Sn. At Endako, magnetite is deposited mainly in early, Stage 1 K-feldspar-enveloped veins. The correspondence of magnetite distribution with K-feldspar zonation supports the possible concentration of Sn in sulpherization pyrite. In this case the Sn content of pyrite may be either a direct or an indirect result of thermal gradients.

(3) Factor II:

High scores on factor II (Co and Cu) are distributed in a definite zone inside the 0.8 and 0.7 isopleths that overlies the

pyrite zone almost exclusively (Fig. 7-13). Factor II scores

diminish to the north and the south of this high. Factor II is

closely related to the peripherally-located pyrite zone or,

conversely, antipathetically related to the orebody. Some

relationship probably exists between the abundance of the minor

elements Co and Cu, and either the thermal history, chemical

complexity or physical nature of the pyrite zone.

(i)   Cobalt:

Like Ni, Co can be a major element in pyrite. Cattierite

(CoS_2) is isostructural with pyrite, but intermediate members

of the isomorphous solid solution series are not abundant in

nature. A CoS_2-FeS_2 solid solution series was synthesized

by Klemm (1965), demonstrating that complete solid solution

was possible at formation temperatures in the order of 400°C.

Pyrite from epigenetic sulphide ore deposits generally con-

tains considerable amounts of Co, and has Co $>$ Ni, but many

exceptions exist. Co abundance in pyrites from a single

deposit can vary widely, as it does at Endako, but the Co

content and the Co:Ni ratio appear to be characteristic of

the individual deposit (Hawley, 1952; Gavelin and Gabrielson,

1947). Price (1971) has shown statistically that the Co-

contents of the porphyry Cu-Mo deposits Endako, Berg and

Casino do not differ significantly from one another.

With an increase in silica during magmatic differentiation,

the absolute Co and Ni contents of a rock decrease, but the
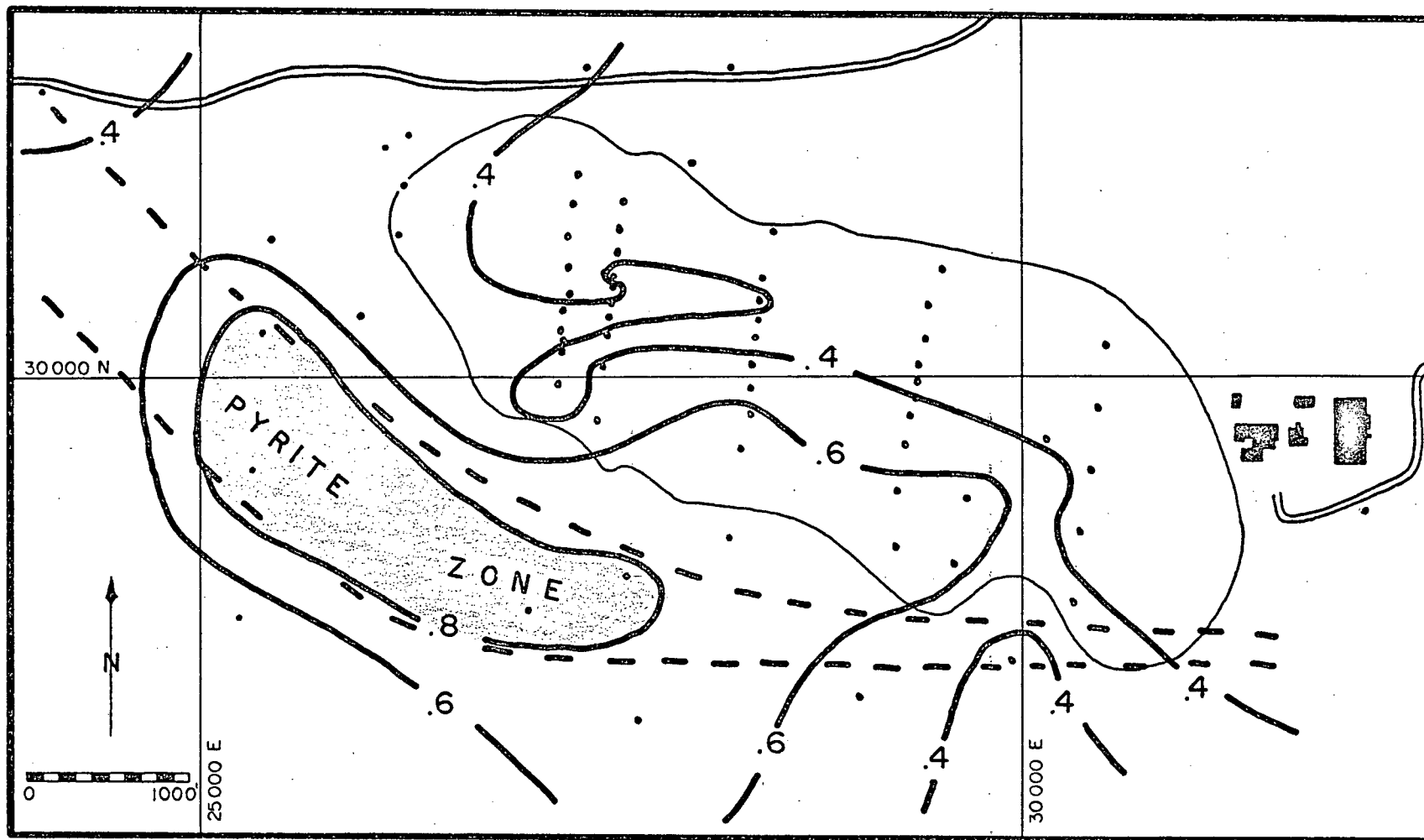
FIGURE 7-13

FACTOR II (Co, Cu) SCORES

Co:Ni ratio increases, indicating that Co is enriched rela-
tive to Ni in the residual melt, i.e. nickel is accommodated
in early ferromagnesian minerals at a greater rate than Co.
Endako Quartz Monzonite is higher in Co, at 7 ppm average,
than the world geochemical average of 1 ppm for low-calcium
granites (Goldschmidt, 1954). Endako pyrite is high in Co
relative to other elements, with a mean of 227 ppm and a
maximum of 995 ppm.

Sulphurization of Co-rich ferromagnesian minerals at Endako
is not believed responsible for high peripheral Co concen-
trations because the same argument supports a high Ni content,
which has been shown to drop off sharply over the pyrite zone.
Furthermore, the host quartz monzonite, although relatively
Co-rich for that rock type, is too low in absolute Co content
to contain a Co-rich mafic phase. However, reactions may
occur in the vicinity of the pyrite zone that would affect
the relatively low stability of a Co-transporting ionic
complex (Barnes, 1962). Groundwater dilution of hydrothermal
fluids at the outer limit of stockwork fracturing may cause
deposition of Co and concomitant intensification of hydro-
lytic decomposition of wall rock to quartz-sericite-pyrite
and kaolinite assemblages (Hemley and Jones, 1964). The
result would be a peripheral zone relatively enriched in
pyrite, sericite and Co compared to the molybdenite deposit
on one side and unmineralized rock on the other side. The
pyrite zone is viewed as an ore zone - host rock interface
generated principally by the cooling and dilution of hydro-
thermal fluids.

(ii) Copper:

Copper is a common minor element in hydrothermal pyrite.
Carstens (1941) notes that pyrite of hydrothermal deposits
generally contains more Cu than pyrite of sedimentary depo-
sits. Mitchell (op. cit.) has recorded more extensive
isomorphous substitution of Cu than previously believed
possible. The Cu and Fe electronic configurations, electro-
negativities and effective ionic radii are rather dissimilar,
tending to inhibit isomorphous substitution. The difficulty
in detecting true isomorphous substitution, in contrast to
chalcopyrite inclusion or admixture, limits the usefulness
of Cu in pyrite research.

The majority of Cu probably is present in pyrite either as
interstitial substitution or as discreet mineral inclusions.
Interstitial solid solution of Cu would be encouraged by
expansion of the pyrite lattice at elevated temperature.
However, the incompatibility of excessive Cu in the pyrite
structure would result in exsolution as chalcopyrite on
cooling, as occurs commonly in Endako pyrites.

Copper is distributed erratically in Endako pyrites. The
Cu-in-pyrite distribution can best be related to the occur-
rence of vein chalcopyrite, rather than to a more systematic
geological control. In many cases, chalcopyrite contaminates
pyrite as small ramifying veinlets and inclusions. Chalco-
pyrite occurs relatively late in the Endako vein mineral
sequence, mainly veining and replacing minerals in Stage 3

quartz-molybdenite veins. The appearance of Cu as a relatively late and possibly low temperature phase within the orebody supports the view that concentration of Cu with Co in the pyrite zone is a feature related mainly to fortuitous Stage 3 fracturing, and indirectly to thermal gradients. Solid solution Cu, exsolution and inclusion chalcopyrite in Endako pyrite all may result from a relatively late pulse of Cu mineralization.

(iii) Barium-Strontium-Zinc:

Ba and Sr are minor components of factor II. The role of these two elements was discussed previously under R-mode factor analysis, where Ba and Sr comprise R-mode factor 4. As stated previously, Ba and Sr are not known to concentrate to any degree in pyrite, and probably are present almost entirely as contaminants from wall rock.

Zn is a third minor component of factor II. Zn is very erratically distributed over the orebody, and probably is a non-significant component of the factor. Hegemann (1941) regards Zn reported in analyses of pyrite as a measure of the amount of admixed sphalerite present, and probably very little Zn is present in isomorphous substitution. Mitchell (1968) suggests that Zn fills defect sites in the pyrite lattice.

Microscopic studies and electron microprobe analyses of chalcopyrite inclusions in pyrite reveal numerous minute

star-shaped exsolution bodies of sphalerite (Plate 5-12).

Zn and Cu intercorrelate in statistical analyses, indicating

the two elements may coexist extensively in Endako pyrite.

Thus the reasons cited above for the appearance of Cu in

factor II would apply also to Zn.

(4) Factor III:

Values for factor III (Bi, Pb, etc.) are less coherently

distributed than the scores of factors I and II. High scores on

factor III fringe the orebody on the northeast, flank the pyrite

zone on the south, and occur as isolated highs in the western ore-

body (Fig. 7-14). Factor III scores are low over the orebody and

pyrite zone with the lowest values distributed linearly along the

central axis of the orebody.

Factor III is principally Bi and Pb, but also consists of

minor contributions from Ag, Ba, Cu, Mn, Sr and Zn. This factor

may represent one or a combination of three effects: (1) minor

elements released from country rocks during metallization and

incorporated in pyrites; (2) contamination of pyrite samples by

admixed country rock and/or other contaminants; and (3) concen-

tration of Bi along the north side of the K-feldspar zone and

concentration of Pb south of the pyrite zone. The apparent erra-

tic distribution of factor III values over the area sampled is

consistent with a wall rock contamination process, but does not

offer proof.
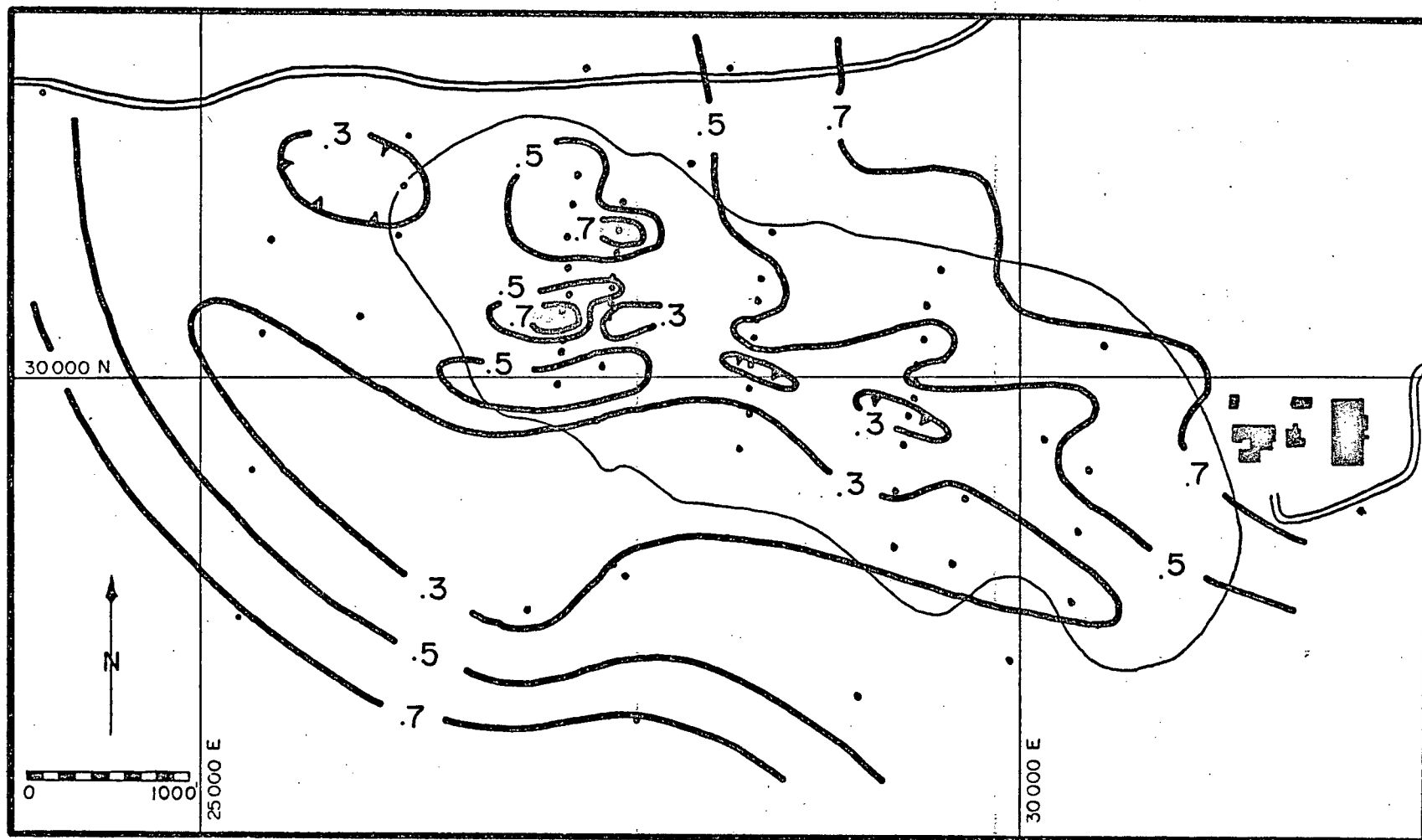
FIGURE 7-14

FACTOR III (Bi, Pb) SCORES

High factor III scores and relatively high Bi values coincide in a general way with the K-feldspar zone, indicating that Bi may be concentrated in K-feldspar-enveloped veins. One example of a bismuthinite-beryl-K-feldspar association was found. Similarly high factor III scores and high Pb and Ag values flank the south side of the sampled area, in a distribution that suggests lateral zonation of Pb and Ag. The non-systematic distributions of Bi and Pb data appear to preclude any significant zonal trends, and these apparently systematic distributions of factor III components probably lack significance.

(e) Summary

The obvious correlation of factors I and II to ore and pyrite zone respectively, strongly implies that the factors are related to mineralizing processes that gave rise to the two mineralogically distinct zones.

The contribution of minor elements to pyrites from host rock is not a significant feature in interpreting factors I and II. The main basis for this conclusion is the uniform nature of the quartz monzonite host rock throughout both ore and pyrite zones. The main differences between the two zones are found in different proportions of the dominant minerals pyrite and molybdenite, and the nature and intensity of wall rock alteration.

Alteration zoning, from dominant K-feldspar along the north side of the orebody, through moderate intensity of kaolinization and sericitization, to weak argillic alteration in the pyrite zone, suggests

decreasing temperatures of formation from the ore zone towards the south. Contemporaneity of alteration and mineralization implies similar temperature variations for sulphide deposition.

Fluid inclusion studies support the proposed thermal gradient trend. The minimum temperatures of filling for fluid inclusions in quartz range from above 500°C down to 380°C, corresponding to formation temperatures of the dominant potassic, sericitic and argillic alteration assemblages in the K-feldspar zone, orebody proper and pyrite zone, respectively.

In view of the coincident mineral and thermal zoning, it seems reasonable to interpret factors I and II as representing the two extremes of physical conditions under which pyrite and molybdenite were deposited. Factor I depositional processes are best related to a paramagmatic environment of dominant potassic alteration and relatively high-temperature mineral assemblages. Highest factor I scores correspond to the K-feldspar zone, indicating that the hydrothermal "source" existed in this area.

Factor I scores diminish southward towards the high of factor II over the pyrite zone, which represents the outer limit of sulphide deposition from hydrothermal fluids originating within the orebody. The principal processes involved include (1) cooling of fluids mainly by groundwater dilution, but also by endothermic reactions, conduction and possibly boiling and/or throttling; and (2) increased hydrolysis of ore fluids by initial dilution causing localized sericitic alteration. Kinetics of hydrothermal reactions are impeded by the reduction

in temperature, consequently alteration and sulphide deposition terminate at this ore fluid-groundwater interface.

Alternative interpretations were considered for the factors. Different categories of pyrite may be involved in factors I and II, such as vein or massive pyrite in the orebody compared to pyrite disseminated in wall rock in the pyrite zone. Sampling techniques largely eliminated any such discrepancies, and no obvious pattern in pyrite data exists. Different ages of pyrite undoubtedly occur, but only pyrite associated with molybdenite was sampled thus limiting the span to the ore deposition period. Correlations were attempted between pyrites and their respective alteration associations, but the trends detected related to the overall zonal pattern of minor elements. These and other interpretations of the factors provide no systematic controls but present many inconsistencies, and were consequently rejected.

CHAPTER VIII

SUMMARY AND CONCLUSIONS

A. PETROGENESIS

The long axis of the belt of Topley Intrusions is oriented some 15° to

20° more westward than most of the northwest structures in this part of the

Cordillera. The batholith flanks and intrudes the southwestern margin of a

flexure in the Stuart Lake High, an elongate, fault-bounded belt of Cache

Creek metamorphic rocks in central British Columbia. This belt of Carboni-

ferous-Permian rocks was uplifted in late Triassic time along steeply-dipping

peripheral faults that subsequently may have provided conduits for rising

Topley magma. To the south and west of Stuart Lake High, Topley rocks

intrude volcanic and sedimentary rocks of the Takla-Hazelton Assemblage

that were laid down intermittently in Late Triassic to Middle Jurassic time.

The oldest Topley unit, the Middle Jurassic Simon Bay Diorite Complex,

includes rocks variously classified as quartz diorite, diorite or gabbro.

A northwesterly-trending chain of outcrops show primary foliation oriented

predominantly northwestward concordant with the batholithic trend. Although

the outcroppings give little idea of its form, the Simon Bay Diorite Complex

may be a single mesozonal pluton whose primary foliation reflects pre-

existing structural controls upon its emplacement.

The most abundant Topley rock type is medium to coarse-grained, potash-

rich pink granite and quartz monzonite. These Stage Two Topley plutons

tend to be equidimensional, and in a few exposures are seen to intrude

diorite. The rocks generally exhibit no alteration or internal deformation,

but possess textural and petrological characteristics of discordant epizonal plutons. The Stage Two Topley rocks are closely grouped in radiometric age (137 - 141 m.y.) and represent a relatively short period of differentiation of the parental Topley magma, with enrichment in silica and alkalies in the youngest phases.

Endako and Nithi Quartz Monzonites have the most basic composition of this group, and structural relations indicate they may be the oldest Stage Two phases. The early phases are succeeded by a family of coarse-grained pink quartz monzonites including the Glenannan pluton in the map-area and the Tatin and Titan units to the north. The youngest Stage Two units, Casey Alaskite and Francois Granite, have pronounced epizonal characteristics in common, as well as relatively acidic compositions. Both granite and alaskite probably were derived from a common residual magma enriched in silica and alkalies. The plutons probably were emplaced almost simultaneously as elongate dyke-like bodies flanking Endako Quartz Monzonite.

The youngest intrusive rocks, defining Stage Three of Topley plutonism, include Stellako Quartz Monzonite and Granodiorite, and Fraser Quartz Monzonite. These rocks are more calcic than their predecessors, and tend to transect the "grain" of older units. Mainly because of a similarly high content of mafic xenoliths, White (1970) provisionally correlates Carr's Triangle Quartz Monzonite with this group of young intrusions.

Topley Intrusions are overlain by extensive andesitic and basaltic Endako Group flows of Eocene age. Related andesitic dykes traverse the map-area, commonly following northwesterly-trending faults that are post-mineral structures in Endako mine.

Potassium-argon dating by White, et al (Ibid.) shows that the Stage

Two rocks present a remarkable uniformity in isotopic age, with 18 samples

tightly grouped about the mean of 138 m.y. Dating of hydrothermal biotite

at Endako mine (White, et al, 1968) shows the orebody to be essentially the

same age as the host Endako Quartz Monzonite. Dioritic rocks in the same

area are at least 17 m.y. older than the family of pink quartz monzonites,

and Fraser Quartz Monzonite is 27 m.y. younger. The radiometric dates may

imply either one protracted and intermittent magmatic event, or three

separate and unrelated events (Ibid.).

B. STRUCTURE

The structural setting of the Endako area is one of plutonic elonga-

tion under regional stress. Axes of open folds in the oldest rock unit,

the Takla-Hazelton Assemblage south of Fraser Lake, trend uniformly north-

westward whereas folds in younger overlying flows do not show this trend.

Oldest Topley diorites are foliated parallel to the regional northwest

trend of the unit, and younger Topley quartz monzonite bodies show a general

west-northwest elongation in the Endako area. South of Francois Lake,

large, steeply-dipping conjugate shears trending north and northeast indi-

cate that these relatively old rocks underwent regional N 22° E compression.

The concordance of northwest structural trends within Topley Batholith, the

parallelism of this trend with that of fold axes in older Takla-Hazleton

rocks to the south, and conjugate fault evidence of a north-northeast com-

pressional axis support the view that the Topley Intrusions were emplaced

as elongate bodies normal to a regional NNE compression.

Several faults of regional extent have been mapped in the vicinity of

Endako mine. The largest, the Casey Lake fault, is a major structure about 15 miles long that extends from Shovel Creek on the north to Nithi River on the south. A large wedge of Endako Quartz Monzonite and Casey Alaskite has been displaced over 2 miles northward along the Casey Lake fault and the subparallel Tailings Creek fault to the west. The South Boundary fault is a five-mile-long, east-west structure that dips between 45° and 60° north. Predominantly normal movement on the fault in the mine vicinity influenced development of major veins and stockwork.

Endako orebody is an elongated elliptically-shaped zone of stockwork that occurs wholly within Endako Quartz Monzonite. The orebody may be considered as a series of major east-west veins oriented en echelon to form a zone elongated in a northwesterly direction. The orebody, including the western extension (Denak Zone), is 11,000 feet long by 1,200 feet wide. The average dip of mineralized stockwork is a fairly consistent 50° south over the orebody length, but the depth of economic mineralization varies from a minimum of 100 feet at the east end to over 1000 feet at the west end.

The development of Endako orebody was influenced by three related igneous events: emplacement and crystallization of Endako Quartz Monzonite, intrusion of residual granitic magma as pre-mineral dykes, and ascent of hydrothermal fluids through the localized zone of intense fracturing.

Early compressional stresses, active during emplacement and cooling of Endako pluton, apparently generated localized doming and fracturing in the vicinity of the mine; an area occupying the intersection of regional east-west, northwest and northeast fracture systems. Intrusion of pre-mineral dykes accompanied the principal structural adjustment of the pluton; wrench

faulting along principal orebody faults and secondary shears, doming of the orebody area, and antithetic faulting along conjugate southward and north-westward-dipping fractures. Many large veins and smaller stockwork veinlets follow the predominant EW/50°S and NE/5-30°NW fracture directions.

C. ORE CONTROLS

Three interrelated geological controls: structural, chemical and thermal effects, combine to control the nature and distribution of vein and alteration minerals at Endako mine.

(1) Structurally, Endako orebody is an elongated, elliptically-shaped zone of stockwork that occurs wholly within Endako Quartz Monzonite. Configuration of stockwork is the principal ore-localization factor. From east to west along the length of the orebody, relatively homogeneous stockwork generated by intense domal movement gives way to poorly developed stockwork adjacent to large shear veins. Homogeneity of ore values varies accordingly. Stockwork fracturing and ore values terminate abruptly along the north side of the orebody, but diminish gradually southward towards the pyrite zone that marks the southern limit of sulphide deposition.

(2) Chemical control of hydrothermal mineralization and alteration is evident from the spatial and temporal relationships between alteration assemblages of Stages 1, 2 and 3. K-feldspar envelopes are cut by sericitic envelopes, and the wall rock enclosing these envelopes is pervasively kaolinized. The mechanism relating potassic, sericitic and argillic alteration is a progressive ion leaching or migration of Ca^{++}, Na^+, Mg^{++}, Fe^{++} and Fe^{+++} toward the vein, with simultaneous outward migration of K^+ and H^+.

The K^+/H^+ activity ratio controls outward diffusion of K^+ and H^+ and varies outward from the vein mainly in response to variations in temperature, K^+ and H^+ concentration gradients, rate of removal of leached constituents, and pressure. Reaction curves for the system K_2O - Al_2O_3 - SiO_2 - H_2O developed by Hemley (1959) show that temperature and K^+/H^+ activity ratio are the most significant variables in determining stability of phases in the system. Drummond (1969) notes that the relative age sequence of K-feldspar-sericite-kaolinite is in agreement with a chemical control based on the activity ratio of K^+/H^+ in a nearly isothermal environment.

(3) Thermal controls are evident in zonation of alteration assemblages from north to south across the orebody. A relative abundance of K-feldspar-bearing envelopes defines a "K-feldspar zone" about 800 feet wide parallel to the orebody and flanking it on the north. The transition to the orebody proper is marked by a sharp increase in the abundance of molybdenite, sericitic envelopes and intensity of pervasive kaolinization. The transition to the "pyrite zone" is marked by a sharp decrease in the abundance of K-feldspar alteration, a gradual diminishment in intensities of molybdenite mineralization, kaolinization and sericitic alteration, and an increase in the relative abundance of pyrite.

Alteration zonation suggests decreasing temperatures from the ore zone towards the south, implying similar variations for sulphide deposition. Fluid inclusion studies support this trend. Minimum filling temperatures for fluid inclusions in quartz from K-feldspar-enveloped veins are slightly higher than 500°C; those for inclusions in quartz from sericite-enveloped veins centre around 480°C; whereas those for quartz veins without envelopes but within pervasively argillized rock range from 380°C to 460°C. These

temperatures are in agreement with Hemley's (1959) experimental data for stability fields of the alteration phases.

Minor element content of pyrite shows a similar temperature-dependent trend across the area sampled. Q-mode factor analysis of 11-element spectro-chemical data from 67 orebody area pyrites defines two principal factors which correlate exclusively to orebody and pyrite zone. Factor I (Mn, Ni, Sn) is interpreted as a relatively high temperature, paramagmatic depositional environment centred over a hydrothermal "source" corresponding to the K-feldspar zone. Factor I effects diminish progressively southward towards the factor II high, over the pyrite zone. Factor II (Co, Cu) is interpreted as the low temperature environment at the outer limit of sulphide deposition. Ore fluids that originated within the orebody became cooled and diluted as they migrated southward away from their source.

Within a single vein or vein system, thermal gradients may have been less significant than chemical controls in affecting the stability of an alteration or sulphide phase, but on a megascopic scale temperature gradients have controlled the relative abundance of mineral assemblages in the orebody area.

D. SUMMARY

The Endako stockwork has localized within an early quartz monzonitic phase of Topley Batholith by wrench faulting and doming generated by cooling of the batholith and intrusion of pre-ore dykes. Hydrothermal fluids effecting alteration and mineralization of the stockwork were generated contemporaneously with the cooling of the Endako pluton. Abundant early potassic alteration and relatively high fluid inclusion temperatures attest to the

paramagmatic affiliation of vein and alteration mineral assemblages. Cross-cutting relations indicate a relative age sequence among the alteration stages which is in agreement with a chemical control based primarily on the activity ratio of K^+/H^+. Concurrent north-south zonation of stockwork mineralization, principal alteration assemblages, fluid inclusion temperatures, and minor element content of pyrite indicates thermal gradients diminished southward across the orebody from a "high" centred over the K-feldspar zone.

E. NEW FIELDS OF STUDY INDICATED

To the best of the writer's knowledge this study is the first systematic application of the stress indicatrix technique of structural analysis to a porphyry-type stockwork ore deposit. It was gratifying to note that the apparently random array of stockwork structures responded well to structural analysis. If sufficient structural data is available, similar studies should be made of other porphyry Cu-Mo deposits with a view to expanding and/or clarifying knowledge of their origins. A comparison of the structural histories of British Columbia porphyry Cu-Mo deposits may establish structural criteria valuable in mineral exploration.

From a practical point of view, the Endako study suggests that pyrite geochemistry may provide a means of outlining targets for detailed exploration, especially if the following conditions are fulfilled:

(1) a reasonable geographic distribution of samples exists,

(2) pure pyrite separates are obtained,

(3) multi-element analyses are obtained, and

(4)   the data are treated using a multivariate statistical analysis
technique.

Several similar geostatistical studies of pyrite from porphyry Cu-Mo
deposits are underway at the University of British Columbia at time of
writing.   Comparison of Endako data with these and other studies may well
provide valuable geochemical guides to exploration.

Respectfully submitted,

Kenneth M. Dawson
Date

BIBLIOGRAPHY

Ambrose, J.W. (1967) Personal communication.

Anderson, E.M. (1942) The Dynamics of Faulting; 1st ed., Oliver and Boyd.

Armstrong, J.E. (1937) West Half of Fort Fraser Map-area, B.C.: Geol. Surv., Canada, Paper 37-13.

——————— (1938) Northwest Quarter of the Fort Fraser Map-area, B.C.: Geol. Surv., Canada, Paper 38-10.

——————— (1944a) Smithers, British Columbia: Geol. Surv., Canada, Paper 44-23.

——————— (1944b) Hazelton, British Columbia: Geol. Surv., Canada, Paper 44-24.

——————— (1949) Fort St. James Map-area, Cassiar and Coast Districts, British Columbia: Geol. Surv., Canada, Mem. 252.

——————— , and Gray, J.G. (1941) Fort Fraser (East Half), British Columbia: Geol. Surv., Canada, Map 630A.

——————— , and Tipper, H.W. (1948) Glaciation in North Central B.C.: Amer. Jour. Sci., 246.

——————— , and Hoadley, J.W. (1947) Carp Lake, British Columbia: Geol. Surv., Canada, Paper 47-13.

Auger, P.E. (1941) Zoning and district variations of the minor elements in pyrite of Canadian gold deposits: Econ. Geol., V. 36, pp. 401-423.

Baadsgaard, H., Folinsbee, R.E., and Lipson, J. (1961) Potassium-argon dates of biotites from Cordilleron granites: Bull. Geol. Soc. Amer., 72, pp. 689-702.

Ball, C.W. (1963a) Petrology and Minerography of Country rock and Molybdenite Ore from Diamond-Drill Core: unpubl. rept. from files of Endako Mines Ltd.

——————— (1963b) Preliminary Geological report on molybdenite showings at Nithi Mountain: unpubl. rept. from files of Endako Mines Ltd.

——————— (1963c) Report and Regional Geological Map of Endako Molybdenum Comp: unpubl. rept. from files of Endako Mines Ltd.

Bapty, H. (1963) Endako Mines Ltd.: Ann. Rept. Minister Mines, Brit. Col., pp. 30-38.

Barnes, H.L. (1962) Mechanisms of mineral zoning: Econ. Geol., 57, pp. 30-37.

Barton, P.B. and Skinner, B.J. (1967) Sulphide Mineral Stabilities: in Geochemistry of Hydrothermal Ore Deposits; H.L. Barnes, ed., New York, Holt Rinehart and Winston, 670 p.

Beaudoin, P.G. (1968) Geology of the Takla Volcanics, Endako Mine Area, British Columbia: unpubl. B.A.Sc. thesis, Univ. of Brit. Col.

Blanchard, R. (1968) Interpretation of Leached Outcrops: Nevada Bur. Mines Bull. 66.

Borchert, H. (1934) Uber Entsmischungen im System Cu-Fe-S: Chemie der Erde, 9, pp. 145-172.

Bostock, H.S. (1948) Physiography of the Canadian Cordillera, with special reference to the area north of the fifty-fifth parallel: Geol. Surv., Canada, Mem. 247.

Bright, E.G. (1967) Geology of the Topley Intrusives in the Endako Area, British Columbia: unpubl. M.Sc. thesis, Univ. of Brit. Col.

Buddington, A.F. (1959) Granite emplacement with special reference to North America: Bull. Geol. Soc. Amer., 70, pp. 671-747.

Burnham, C.W. (1962) Facies and types of hydrothermal alteration: Econ. Geol., V. 57, pp. 768-784.

Cameron, E.N., Rowe, R.B. and Weis, P.L. (1953) Fluid inclusions in beryl and quartz from pegmatites of the Middleton District, Connecticut: Amer. Min., V. 38, pp. 218-262.

Camsell, C. (1916) Exploration in the Northern Interior of British Columbia: Geol. Surv., Canada, Sum. Rept. 1915, pp. 70-75.

Carr, J.M. (1964) Endako Mines Ltd.: Ann. Rept. Minister Mines, Brit. Col., pp. 58-64.

———————— (1966) The Geology of the Endako Area: in Lode Metals in Brit. Col., 1965, pp. 114-135.

Carstens, C.W. (1941) Om geokjemiske undersokelser av malmer: Norsk. Geol. Tidssker, V. 21, p. 213-221.

Carter, N.C. (1968) Personal communication.

de Cizancourt, H. (1947) Some Geometrical Features of Structural Problems: Revue de l'Institut Francois du Petrole et Ananales des Combustibles Liquides, V. 11, Nos. 1-5.

Coulomb, C.A. (1773) Essai sur une application des règles des maximis et minimis à quelques problèmes de statique relatifs à l'architecture: Acad. Sci. Paris Mém., pres. Divers Savants, 7.

Creasey, S.C. (1965) Geology of San Manuel Area, Pinole County, Arizona: U.S. Geol. Surv. Prof. Paper, 471.

———————— (1966) Hydrothermal Alteration: in Geology of the Porphyry Copper Deposits of Southwestern North America, Titley and Hicks, eds., Univ. of Arizona Press, 287 p.

Dawson, G.M. (1876) Report on Explorations in British Columbia, chiefly in the basins of the Blackwater, Salmon and Nechacco Rivers, and on Francois Lake: Geol. Surv., Canada, Rept. of Progress 1876-77, Pt. III, pp. 17-94.

Dawson, K.M. (1965a) Survey of available pebbles suitable for regrind mills: unpubl. rept. from files of Endako Mines Ltd.

———————— (1965b) Geological Report on the Bingo Nos. 1-10, 31-40 Mineral Claims: Brit. Col. Dept. Mines. Assessment Rept.

———————— (1967) Analysis of structural features of Endako orebody: unpubl. research project at Dept. of Geol., Queen's Univ., Kingston, Ont.

Drummond, A.D. (1966a) Preliminary report on rock descriptions of the Endako Mine area: unpubl. rept. from files of Endako Mines Ltd.

———————— (1966b) Results of X-Ray diffractometer analyses on Endako alteration phases: unpubl. rept. from files of Endako Mines Ltd.

———————— (1966c) Structural features of the Endako orebody: unpubl. rept. from files of Endako Mines Ltd.

———————— (1966d) Nomenclature for hydrothermal alteration study: unpubl. rept. from files of Endako Mines Ltd.

———————— (1966e) Report on geology of Nithi Mountain: unpubl. rept. from files of Endako Mines Ltd.

———————— (1967) Hydrothermal alteration study for Endako Mines Ltd. (N.P.L.): unpubl. rept. from files of Endako Mines Ltd.

———————— and Kimura, E.T. (1969) Hydrothermal alteration at Endako - a comparison to experimental studies: Can. Inst. Min. Met. Bull., V. 62, No. 687, pp. 709-714.

Duffell, S. (1959) Whitesail Lake Map-area: Geol. Surv., Canada, Mem. 299.

———————— and McTaggart, K.C. (1952) Ashcroft Map-area, British Columbia: Geol. Surv., Canada, Mem. 262.

———————— and Souther, J.G. (1956) Terrace Map-area: Geol. Surv., Canada Prelim. Map 11-1956.

———————— and ———————— (1964) Geology of Terrace Map-area, British Columbia: Geol. Surv., Canada, Mem. 329.

Dummett, H.T. (1967) Hydrothermal Wall Rock Alteration Study; Preliminary Zonation of the Western Part of the Endako Open Pit: unpubl. rept. from files of Endako Mines Ltd.

Edwards, A.B. (1954) Textures of the Ore Minerals: 2nd ed., Melbourne; Brown, Prior and Anderson.

Fisher, R.A. (1936) The use of multiple measurements in taxonomic problems: Annals of Eugenics, V. 7, pp. 179-188.

Fleischer, M. (1955) Minor elements in some sulphide minerals: Econ. Geol., 50th Ann. Vol., A. Bateman, ed., 1955.

Fournier, R.O. (1967a) The Porphyry Copper Deposit Exposed in the Liberty Open-Pit Mine near Ely, Nevada; Part I: Syngenetic Formation: Econ. Geol., V. 62, No. 1, pp. 57-81.

———————— (1967b) The Porphyry Copper Deposit Exposed in the Liberty Open-Pit Mine near Ely, Nevada; Part II: The Formation of Hydrothermal Alteration Zones: Econ. Geol., V. 62, No. 2, pp. 207-227.

Garrett, R.G. (1969), The determination of sampling and analytical errors in exploration geochemistry; Econ. Geol. V.64, pp. 568-569.

———————— and Nichol, I. (1969) Factor analysis as an aid in the interpretation of regional geochemical stream sediment data: Quarterly Colorado Sch. of Mines, V. 64, No. 1, pp. 245-264.

Gates, R.M. (1953) Petrogenic Significance of Perthite: Geol. Soc. Amer., Mem. 52, pp. 55-69.

Gavelin, S. and Gabrielson, O. (1947) Spectrochemical investigation of sulphide minerals from ores of the Skellefte district. The significance of minor constituents for certain practical and theoretical problems of economic geology: Sver. Geol. Undersokn., Ser. C, No. 491, Arsbok 41, No. 10, p. 1-45.

Goldschmidt, V.M. (1954) Geochemistry: Oxford Univ. Press, 730 p.

Gray, J.G. (1938) East Half, Fort Fraser Map-area, British Columbia: Geol. Surv., Canada, Paper 38-14.

Gruner, J.W. (1929) Structure of Sulphides and Sulphosalts: Amer. Min., 14, pp. 231-232.

Hanson, G. and Phemister, T.C. (1929) Topley Map-area, British Columbia: Geol. Surv., Canada, Sum. Rept. 1928, Pt. A, pp. 50-77.

Harman, H.H. (1967) Modern Factor Analysis: 2nd ed., Chicago Univ. Press, 474 p.

Hawley, J.E. (1952) Spectrographic studies of gold in some Eastern Canadian gold mines: Econ. Geol., V. 47, pp. 260-304.

Hegemann, F. (1941) Die isomorphen Beziehungen van Mn, Zn, Co, Ni und Cu zu Pyrit und Magnetkies: Zeitschr. Krist, V. 103, pp. 168-177.

——————— (1943) Die geochemische Bedeutung von Kobalt und Nickel in Pyrit: Zeitschr. angev. Mineral., V. 4, p. 122-239.

Hemley, J.J. (1959) Some Mineralogical Equilibria in the System $K_2O-Al_2O_3-SiO_2-H_2O$: Amer. Jour. Sci., V. 257, pp. 241-270.

——————— and Jones, W.R. (1964) Chemical aspects of hydrothermal alteration with emphasis on hydrogen metasomatism: Econ. Geol., V. 59, pp. 538-569.

Holland, S. (1962) Endako Mines Ltd.: Ann. Rept. Minister Mines, Brit. Col., pp. 17-19.

——————— (1964) Landforms of British Columbia. A Physiographic Outline: B.C. Dept. Mines and Petrol. Resources, Bull. 48.

Howarth, M.K. (1964) The Phanerozoic time-scale: Quart. Jour., V. 120.

Howarth, R.J. (1967) Trend Surface Fitting to Random Data - on Experimental Test: Amer. Jour. Sci., V. 265, pp. 619-625.

Hubbert, M.K. (1951) Mechanical Basis for Certain Familiar Geological Structures: Bull. Geol. Soc. Amer., V. 62, pp. 355-372.

Inbrie, J. and Van Andel, T.H. (1964) Vector analysis of heavy mineral data: Geol. Soc. Amer. Bull., V. 75, pp. 1131-1156.

Keevil, N.B. (1942) Vapour pressures of aqueous solutions at high temperatures: Amer. Chem. Soc. Jour., V. 64, pp. 841-850.

Kerr, F.A. (1936) Mineral Resources along the Canadian National Railway Between Prince Rupert and Prince George, British Columbia: Geol. Surv., Canada, Paper 36-20.

Kimura, E.T. and Drummond, A.D. (1966) Geology of the Endako molybdenum deposit: unpubl. paper presented at Can. Inst. Min. Met., B.C. Sect. Meeting, Victoria, B.C., October 1966.

——————— and ——————— (1967) Diamond Drill Program on CM Group of Mineral Claims: unpubl. rept. from files of Endako Mines Ltd.

——————— and ——————— (1969) Geology of the Endako molybdenum deposit: Can. Inst. Min. Met. Bull., V. 62, No. 687, pp. 699-709.

——————— and Thon, R. (1967) Personal communication.

Klemm, D.D. (1965) Synthesen und analysen in den Dreieicks diagrammer Fe As S - Co As S - Ni As S und $FeS_2 - CoS_2 - NiS_2$: Neves. Jahrb. Mineral Abhandl., V. 103, pp. 205-255.

Klovan, J.E. (1966) The use of factor analysis in determining depositional environments from grain size distributions: Jour. Sed. Petrol., V. 36, No. 1, pp. 115-125.

_____ (1968) Selection of Target Areas by Factor Analysis: Proc. of the Symp. on Decision-Making in Mineral Exploration I, Vancouver, B.C., Univ. of Brit. Col. Extension Dept., pp. 19-27.

_____ and Billings, G.K. (1967) The classification of geological samples by discriminant-function analysis: Bull. Canadian Petroleum Geol., V. 15, No. 3, pp. 313-330.

Koo, J.H. (1968) Geology and Mineralization of the Lorraine Property Area, Omineca Mining Division, British Columbia: unpubl. M.Sc. thesis, Univ. of Brit. Col.

Knopf, E.B. and Ingerson, E.I. (1938) Structural Petrology: Geol. Soc. Amer., Mem. 6, pp. 137-162.

Krumbein, W.C. and Graybill, F.A. (1965) An Introduction to Statistical Models in Geology: New York, McGraw-Hill, 475 p.

Lay, D. (1927-1934) Northern Mineral Survey District No. 2; Ann. Repts. Minister of Mines, B.C.: 1927, pp. C150-C153, C155-C160; 1928, pp. C177-C182; 1929, pp. C181-C182, C185-C187; 1934, p. C13.

Leech, G.B., Lawden, J.A., Stockwell, C.H. and Wanless, R.K. (1963) Age Determinations and Geologic Studies: Geol. Surv., Canada, Paper 63-17, p. 140.

Lemmlein, G.G. and Klevtsov, P.V. (1961) Relations in the system H_2O-NaCl: translated in Geochemistry No. 2, pp. 148-158.

Lindgren, W. (1937) Succession of Minerals and Temperatures of Formation in Ore Deposits of Magmatic Affiliation: Trans. Amer. Inst. Min. Met. Eng., V. 162, pp. 356-376.

Lodder, W. (1970) Personal communication.

Mathews, W.H. (1964) Potassium-argon age determinations of Cenozoic volcanic rocks from British Columbia: Bull. Geol. Soc. Amer., V. 75, pp. 465-468.

Meyer, C. and Hemley, J.J. (1967) Wall Rock Alteration; in Geochemistry of Hydrothermal Ore Deposits, H.L. Barnes, ed., New York, Holt Rinehart and Winston, 670 p.

_____ Shea, E.P., Goddard, C.C. and Anaconda Staff (1968) Ore Deposits at Butte, Montana; in Ore Deposits of the United States 1933/1967, V. II, J. Ridge ed., Graton-Sales Vol., A.I.M.E., New York, 1880 p.

Mitchell, R.H. (1968) A semiquantitative study of trace elements in pyrite by spark source mass spectrography: Norsk Geol. Tidssker, pp. 65-80.

Mohr, O. (1882) Über die Darstellung des Spannungzustandes eines Korpelementes, Zwil Ingenieure, 28, pp. 113-156.

Nickel, E.H. (1970) The application of ligand-field concepts to an understanding of the structural stabilities and solid solution limits of sulphides and related minerals: Chem. Geol., V. 5, pp. 233-241.

Palache, C., Berman, H. and Frondel, C. (1944) Dana's System of Mineralogy: V. I, New York, Wiley, 834 p.

_____ , _____ and _____(1951) Dana's System of Mineralogy: V. II, New York, Wiley, 1124 p.

Peterson, D.W. (1960) Descriptive modal classification of igneous rocks: Amer. Beol. Inst., Data Sheet 23, Geotimes, No. V, p. 30.

Price, B. (1971) M.Sc. thesis in progress, Univ. of Brit. Col., Dept. Geol.

Roedder, E. (1958) Technique for the extraction and partial chemical analysis of fluid-filled inclusions from minerals: Econ. Geol., V 53, pp. 235-269.

_____ (1962a) Ancient fluids in crystals: Scientific Am., V. 207, pp. 38-47.

_____ (1962b) Studies of fluid inclusions I: Low temperature application of a dual purpose freezing and heating stage: Econ. Geol., V. 57, p. 1045-1061.

_____ (1963) Studies of fluid inclusions II: Freezing data and their interpretation: Econ. Geol., V. 58, pp. 167-211.

_____ (1967) Fluid inclusions as samples of ore fluids: in Geochemistry of Hydrothermal Ore Deposits, H.L. Barnes, ed., New York, Holt Rinehart and Winston, 670 p.

_____ (1971) Fluid inclusion studies on the porphyry-type ore deposits at Bingham, Utah, Butte, Montana, and Climax, Colorado: Econ. Geol., V. 66, pp. 98-120.

Roots, E.F. (1954) Geology and Mineral Deposits of Aitken Lake Map-area, British Columbia: Geol. Surv., Canada, Mem. 274.

Sampson, R.J. and Davis, J.C. (1966) Fortran II Trend Surface Program with Unrestricted Input for the IBM 1620 Computer: Kansas State Geol. Surv. Spec. Publ. 26.

Sander, B. (1930) Gefugekunde der Gesteine: Vienna, Jules Springer.

Selwyn, A.R.C. (1877) Report on Exploration in British Columbia: Geol. Surv., Canada, Rept. of Progress, 1875-76, pp. 29-87.

Sinclair, A.J. (1969) An Introduction to Trend Surface Analysis in Mineral Exploration: Proc. of Symp. on Decision-Making in Mineral Exploration II, Vancouver, B.C., Univ. of Brit. Col. Extension Dept., pp. 163-176.

_____ and Libby, W.G. (1969) Distribution of major minerals in a stock of Nelson plutonic rock, south-central British Columbia; Geol. Assoc. Canada Proc., Vol. 20, pp. 41-46.

Sorby, H.C. (1858) On the microscopic nature of crystals, indicating the origin of minerals and rocks: Geol. Soc. London Quart. Jour., 14, Part I, pp. 453-500.

Sourirajan, S. and Kennedy G.C. (1962) The system $H_2O-NaCl$ at elevated temperatures and pressures: Amer. Jour. Sci. V. 260, pp. 115-141.

Souther, J.G. and Armstrong, J.E. (1966) North Central Belt of the Cordillera of British Columbia: Can. Inst. Min. Met., Spec. Vol. 8, pp. 171-184.

Stephens, F.H. (1965) Endako Mines: Western Miner, V. 38, No. 5.

Stevenson, J.S. (1940) Molybdenum Deposits of British Columbia: B.C. Dept. Mines, Bull. 9.

Tipper, H.W. (1957) Anahim Lake, Coast District, British Columbia: Geol. Surv., Canada, Map 10-1957.

_____ (1959) Revision of the Hazelton and Takla Groups of Central British Columbia: Geol. Surv., Canada, Bull. 47.

_____ (1962) Age Determinations and Geologic Studies: Geol. Surv., Canada, Paper 62-17, pp. 134-136.

_____ (1963) Nechako River Map-area: Geol. Surv., Canada, Mem. 324.

Thon, R. (1968) Personal communication.

Van Valkenberg, A. and Weir, C.E. (1957) Beryl studies, 3 BeO Al_2O_3 $6SiO_3$: Bull. Geol. Soc. Amer., V. 68, pp. 1808, Abstract.

Vokes, F.M. (1963) Molybdenum Deposits of Canada: Geol. Surv.,Canada, Economic Geol. Rept. No. 20.

Wertz, J. (1970) Personal communication.

Wheeler, J.O. (1966) Eastern Tectonic Belt of Western Cordillera in British Columbia: Can. Inst. Min. Met., Spec. Vol. 8, pp. 27-46.

White, W.H., Harakal, J.E. and Carter, N.C. (1968) Potassium-argon ages of some ore deposits in British Columbia: Can. Inst. Min. Met., Bull. 61, pp. 1326-1334.

_____ Sinclair, A.J., Harakal, J.E. and Dawson, K.M. (1970) Potassium-argon ages of Topley Intrusions near Endako, British Columbia: Can. Jour. Earth Sci., V. 7, No. 4, pp. 1172-1178.

Wisser, E. (1960) Relation of Ore Deposition to Doming: Geol. Soc. Amer. Mem. 77.

Wyart, J. and Scàvincar, S. (1957) Synthèse hydrothermale du beryl: Bull. Soc. Franc. Min. Crist., V. 80, p. 395.

Appendix 1

CALCULATION OF Or-Ab-SiO$_2$ RATIOS FOR TOPLEY ROCKS

Or-content of Orthoclase from Bright (1967)

Average mode (recal. to 100%)	Or-content of K-spar	Ab-content of plag	Or-Ab-SiO$_2$ calc. ratios		Recal. to 100%	
Simon Bay:						
Orth. 9.0	Or$_{100}$		Or(orth)	9.0	Or	14
			Ab(orth)	0		
Plag. 82.1		Ab$_{62}$	Ab(plag)	51.0	Ab	73
Qtz. 8.9			SiO$_2$	8.9	SiO$_2$	13
				68.9		
Endako:						
Orth. 47	Or$_{82}$		Or(orth)	38.6	Or	41
			Ab(orth)	8.4		
Plag. 29		Ab$_{81}$	Ab(plag)	23.5	Ab	34
Qtz. 24			SiO$_2$	24	SiO$_2$	25
				94.5		
Nithi:						
Orth. 36.0	Or$_{95}$		Or(orth)	34.2	Or	37
			Ab(orth)	1.8		
Plag. 33.5		Ab$_{75}$	Ab(plag)	25.2	Ab	30
Qtz. 30.5			SiO$_2$	30.5	SiO$_2$	33
				91.7		
Glenannan: Granite						
Orth. 55.4	Or$_{92}$		Or(orth)	51.0	Or	53
			Ab(orth)	4.4		
Plag. 21.9		Ab$_{78}$	Ab(plag)	17.1	Ab	23
Qtz. 22.7			SiO$_2$	22.7	SiO$_2$	24
				95.2		
Glenannan: Qtz. Monz.						
Orth. 45.0	Or$_{87}$		Or(orth)	39.2	Or	43
			Ab(orth)	5.8		
Plag. 33.6		Ab$_{71}$	Ab(plag)	23.9	Ab	33
Qtz. 21.4			SiO$_2$	21.4	SiO$_2$	24
				90.3		
Casey:						
Orth. 43.8	Or$_{82}$		Or(orth)	36.0	Or	38
			Ab(orth)	7.8		
Plag. 21.5		Ab$_{77}$	Ab(plag)	16.6	Ab	26
Qtz. 34.7			SiO$_2$	34.7	SiO$_2$	36
				95.1		

Appendix 1   (Continued)

Average mode (recal. to 100%)	Or-content of K-spar	Ab-content of plag	Or-Ab-SiO$_2$ calc. ratios		Recal. to 100%	
Francois:						
Orth. 50.0	Or$_{100}$		Or(orth)	50.0	Or	52
			Ab(orth)	0		
Plag. 19.0		Ab$_{76}$	Ab(plag)	14.4	Ab	15
Qtz. 31.0			SiO$_2$	31.0	SiO$_2$	33
				95.4		
Stellako:						
Qtz. Monz.						
Orth. 33.1	Or$_{90}$		Or(orth)	29.8	Or	33
			Ab(orth)	3.3		
Plag. 36.4		Ab$_{76}$	Ab(plag)	27.7	Ab	34
Qtz. 30.5			SiO$_2$	30.5	SiO$_2$	33
				91.3		
Stellako G.D.:						
Orth. 18.6	Or$_{90}$		Or(orth)	16.8	Or	21
			Ab(orth)	1.8		
Plag. 60.9		Ab$_{66}$	Ab(plag)	40.2	Ab	53
Qtz. 20.5			SiO$_2$	20.5	SiO$_2$	26
				79.3		
Fraser:						
Orth. 34.0	Or$_{90}$		Or(orth)	30.6	Or	33
			Ab(orth)	3.4		
Plag. 48.0		Ab$_{82}$	Ab(plag)	39.4	Ab	47
Qtz. 18.0			SiO$_2$	18.0	SiO$_2$	20
				91.4		

Appendix 2

PYRITE SEPARATION AND PURIFICATION

1.   Specimens of pyrite in diamond drill core are selected on the basis of mineral association, purity and lack of oxidation. Specimens showing molybdenite, hematite, magnetite, chalcopyrite, etc. in association with pyrite are rejected. Pyrite with visible surface oxidation is rejected.

2.   Extraneous quartz and wall rock are cut away with a diamond saw.

3.   Specimen is broken with a hammer and crushed in a piston and cylinder impact crusher. Sieving and crushing are repeated until whole specimen is - 0.5 mm diam.

4.   Heavy minerals are separated with bromoform, then washed in methyl hydrate. The specimen is then dried and disaggregated.

5.   Magnetic minerals are removed with a hand magnet.

6.   The specimen is sieved with 140 mesh screen and the fine fraction set aside. The majority of quartz grains which have become mixed with the heavy minerals are removed in the fine fraction. The fines tend to impede operation of the isodynamic separator, hence are removed. The fine fraction provides a duplicate specimen for future analysis.

7.   The +140 mesh fraction is run through a Franz isodynamic separator three times, at 0.4 amps, 0.75 amps and 1.4 amps respectively to remove iron oxides, biotite, hornblende and any other weakly magnetic minerals.

Appendix 2   (Continued)

8.   The specimen is examined under binocular microscope for the presence

of heavy minerals other than pyrite, particularly molybdenite.   If

impurities are present in small quantity, the specimen is hand-picked

clean with a fine brush.   If impurities are present in the order of

several percent, the specimen is cleaned in the Superpanner.

9.   Grinding with a mortar and pestle divides composite quartz-pyrite

grains.   Specimen is then placed in a separatory funnel with bromoform

a second time, and the heavy fraction separated and washed with methyl

hydrate.

10.   Dried, disaggregated specimen is examined under binocular microscope

for the presence of quartz, a few grains of which are almost always

present.   If excessive quartz is present, i.e. about 1% or more, the

specimen is leached in hydrofluoric acid for 24 hours, diluted,

filtered, dried and examined again.   Average weight of cleaned specimen

is about .6 gm.

Appendix 3

PRELIMINARY SPECTROCHEMICAL ANALYSES OF OREBODY PYRITES
(ppm)

	1	2	3	4	5	6	58	63	73
Ag	3	tr.	tr.	2	0	2	2	3	4
B	P	P	P	P	P	P	P	P	P
Ba	11	37	34	30	26	0	140	5	4
Bi	114	0	73	4	43	7	4	200	400
Ca	P	P	P	P	P	P	P	P	P
Co.	1640	121	70	430	1640	20	1910	20	103
Cu	300	250	600+	600+	600+	180	600+	600+	600+
Cr	80	6	31	16	0	0	0	0	0
Mg	2000	2000	2000	2000	700	200	1000	3000	4000
Mn	P	0	0	0	0	0	P	0	0
Mo	1000+	1000+	1000+	1000+	950	350	320	1000+	1000+
Ni	10	10	10	10	49	0	64	0	0
Pb	0	0	0	0	0	0	295	68	0
Sn	0	0	0	0	0	0	15	8	0
Sr	nc	nc	nc	nc	nc	nc	nc	nc	nc
Ti	19	43	113	88	20	20	1000	103	132
V	30-	30-	30-	30-	30-	30-	30-	30-	30-
Zr	P	P	P	P	P	P	P	P	P
Zn	0	0	0	0	62	0	14	6	0

Abbreviations: tr. = trace; P = present; nc = not checked.

Specimen Locations: 1 to 5: NW end of pit, 3399 bench, 31120 N, 27200 E.
6, 58, 63, 73: centre ridge, 3465 bench, Stella vein.

Appendix 4

SPECTROCHEMICAL ANALYSES OF OREBODY PYRITES (ppm)

Seq.	Spec.	Ag	Ba	Bi	Co	Cu	Mn	Ni	Pb	Sn	Sr	Zn
1	1	2	44	46	112	124	31	18	11	13	11	28
2	36	2	36	3	136	300	44	44	0	10	23	23
3	32	0	68	0	760	135	0	0	0	0	15	12
4a	267	8	28	18	160	680	88	56	0	20	14	4200
4b	267	6	26	14	156	1200	74	64	0	24	14	3600
5a	266	tr.	8	tr.	68	54	tr.	36	0	50	4	16
5b	266	tr.	8	tr.	72	56	tr.	34	0	46	4	18
6	265	2	4	0	70	104	44	18	0	122	24	26
7	268	5	10	0	380	500	26	44	21	32	4	18
8	124	2.4	14	8	162	184	34	38	0	32	12	18
9	41	0	44	0	16	200	0	0	0	0	10	16
10	44	4	88	120	117	500	0	0	25	24	14	610
11	38	3	11	0	220	132	70	30	0	40	18	38
12	197	4	7	50	64	84	82	50	78	17	9	1220
13a	134	3	23	48	240	300	50	40	tr.	8	11	21
13b	134	2	28	52	230	280	56	44	tr.	8	13	21
14	75	1	3	120	132	80	20	68	32	52	4	0
15	144	.6	8	34	90	34	38	48	0	14	8	8
16a	205	1	11	62	160	114	96	180	0	28	13	10
16b	205	.6	11	86	156	102	82	156	0	24	13	16
17	12	3	50	32	41	300	14	0	15	0	11	8
18	67	2	40	0	370	240	68	134	15	24	27	10
19	117	0	12	50	500	280	28	92	0	9	7	44

Appendix 4 (Continued)

Seq.	Spec.	Ag	Ba	Bi	Co	Cu	Mn	Ni	Pb	Sn	Sr	Zn
20	16	.8	3	32	154	300	74	96	0	34	10	36
21a	18	1.8	30	200	280	300	120	80	40	50	20	24
21b	18	1.8	34	200	300	300	114	74	30	36	20	20
22	192	0	11	0	270	49	0	0	0	0	5	0
23a	40	1	6	60	82	310	128	22	0	17	13	23
23b	40	2	5	70	88	280	128	22	0	14	10	40
24	60	7	3	15	240	140	124	50	0	26	10	21
25	199	10	22	0	280	156	90	62	0	18	12	62
26	207	20	16	184	50	188	84	0	134	0	10	152
27	163	3	6	36	66	340	240	26	0	14	26	14
28a	106	1.2	14	0	370	480	40	66	0	20	6	34
28b	106	1.8	14	0	300	430	34	58	0	20	6	24
29	127	2.6	58	280	1400	420	26	80	10	8	6	10
30	103	1.2	12	0	220	350	48	50	0	28	6	10
31	125	2	6	0	540	700	18	78	0	42	5	30
32	101	1.4	12	7.8	112	600	28	50	17	40	18	10
33	99	3	8	10	94	210	0	16	22	4	6	16
34a	263	1	6	0	128	152	14	10	0	70	4	14
34b	263	0	8	0	160	128	20	18	0	52	4	16
35	191	2	6	0	250	100	0	0	0	0	2	14
36	47	6	51	25	326	219	0	0	53	0	9	81
37	218	2.4	34	100	132	500	70	90	46	56	18	16
38a	212	1	10	6	116	46	52	156	0	28	10	14
38b	212	1	10	14	120	62	60	184	0	38	10	16

Appendix 4   (Continued)

Seq.	Spec.	Ag	Ba	Bi	Co	Cu	Mn	Ni	Pb	Sn	Sr	Zn
39a	159	1.0	8	tr.	440	120	36	44	14	66	8	18
39b	159	1.6	8	tr.	360	126	26	40	24	62	8	22
40	253	2.2	12	10	50	42	42	40	0	32	10	16
41	157	3.4	64	8	200	510	114	58	22	50	64	36
42	154	2	4	0	168	300	66	80	0	28	19	14
43	221	1.4	24	12	290	110	18	136	0	46	16	28
44	194	1	6	0	520	184	0	46	0	0	4	12
45	217	2.2	36	0	460	310	42	62	0	24	18	112
46	231	1.4	18	0	260	74	14	32	0	0	6	8
47a	55	3	6	10	94	54	44	32	0	90	8	7
47b	55	3	5	8	90	48	38	32	0	86	8	8
48	250	1.2	6	204	62	34	54	30	16	36	8	18
49	51	1	8	14	11	52	82	58	0	44	10	9
50	95	3	26	70	330	520	92	68	17	54	12	17
51	184	2	14	6	108	126	100	90	0	88	24	16
52	53	1	11	1	200	220	50	52	0	32	7	12
53a	98	1	16	tr.	220	190	206	78	0	48	23	16
53b	98	1.5	18	tr.	240	190	220	72	0	58	24	14
54	48	3	64	0	106	600	130	38	8	68	52	24
55	85	1	12	0	41	21	0	0	0	7	4	6
56	232	1.2	24	0	202	240	26	40	0	12	8	8
57	39	2	3	17	220	46	16	4	0	0	2	20
58	80	0	9	0	700	22	8	44	0	0	4	12
59	83	1	14	0	220	80	0	44	0	28	4	7

Appendix 4   (Continued)

Seq.	Spec.	Ag	Ba	Bi	Co	Cu	Mn	Ni	Pb	Sn	Sr	Zn
60	110	3.4	40	270	222	240	38	26	22	90	10	28
61	104	2.6	42	46	108	156	132	22	0	78	26	16
62	17	1	11	14	128	36	36	26	0	44	5	94
63	102	4	7	28	110	500	16	60	94	84	5	66
64	100	.6	74	38	260	50	68	168	0	34	24	9
65	242	2.6	10	0	164	188	96	56	0	122	10	32
66	34	5	48	3	142	96	118	20	0	66	14	30
67a	187	2	31	0	410	300	70	188	4	26	23	14
67b	187	2	30	.6	360	500	70	172	9	24	24	14

		Ag	Ba	Bi	Co	Cu	Mn	Ni	Pb	Sn	Sr	Zn
Mean		2.5	22	35	240	240	54	52	11	33	13	109
Std. Dev.		2.8	20	63	228	191	49	43	24	29	10	498

Appendix 5

SPECTROCHEMICAL ANALYSES OF REGIONAL PYRITES
(ppm)

	37	43	316	538	JI	U3	B9-125	CM-1	462	489
Ag	0.7	2	tr.	2.6	0	90	tr.	3	2	1
Ba	54	48	18	nc	18	8	nc	36	9	3
Bi	2	22	0	tr.	9	96	50	39	0	0
Ca	nc	nc	nc	P	nc	nc	P	nc	nc	nc
Co	38	26	45	114	120	156	260	600	1210	42
Cu	50	48	67	600+	14	250	600+	36	14	460
Cr	nc	nc	0	0	nc	nc	0	nc	0	0
Mn	32	26	tr.	0	350	300	0	84	tr.	tr.
Mo	nc	nc	nc	P	P	P	P	P	nc	nc
Ni	8	10	0	10-	0	0	10-	92	0	71
Pb	0	0	0	1480	22	780	0	46	0	0
Sn	14	38	tr.	nc	0	0	nc	0	0	0
Sr	21	11	3	3	62	5	4	26	2	1
Ti	1520	6600	3200	0	7800	3100	820	1400	8	315
Zn	19	9	4	480	8	0	4	20	4	29

Abbreviations: tr. = trace; P = present; nc = not checked.

Specimen Locations

```
    37: Pyrite zone, south end of Section 6.
    43: Pyrite zone, south end of Section 3.
   316: Western extension, 32900 N., 21800 E.
   538: 3366 bench, 30900 N., 27600 E.
   J-1: 2500' north of orebody, 33600 N., 28200 E.
   U-3: Utica claims, 7000' SW of mine, 23800N., 24000 E.
B9-125: Bell claims, about 2000' SE of orebody.
  CM-1: 3000' WSW of Macdonald Lake, 28300 N., 40850 E.
   462: Nithi Mtn., trench on main showing.
   489: Nithi Mtn., Tan claims on north slope.
```

Appendix 6

NORMALIZED VARIMAX FACTOR COMPONENTS

SAMPLE	COMM.	FACTOR I	FACTOR II	FACTOR III
1	0.9936	0.4375	0.1341	0.4285
2	0.9890	0.6104	0.2076	0.1820
3	0.9744	0.1219	0.7922	0.0859
4	0.9438	0.5758	0.1867	0.2375
5	0.8922	0.5861	0.3664	0.0475
6	0.9669	0.7311	0.1866	0.0823
7	0.9152	0.5443	0.2409	0.2147
8	0.9908	0.6356	0.1585	0.2059
9	0.9310	0.1236	0.7732	0.1033
10	0.9208	0.1502	0.2996	0.5503
11	0.9814	0.6867	0.2253	0.0881
12	0.9486	0.4407	0.0886	0.4707
13	0.9728	0.5719	0.1567	0.2714
14	0.8891	0.4999	0.0378	0.4623
15	0.9706	0.6563	0.0974	0.2463
16	0.9729	0.6686	0.0894	0.2420
17	0.9494	0.1463	0.2647	0.5890
18	0.9271	0.5903	0.2253	0.1844
19	0.9406	0.6030	0.1704	0.2266
20	0.9756	0.6704	0.1072	0.2224
21	0.9887	0.4700	0.0912	0.4388
22	0.8656	0.1151	0.8173	0.0675
23	0.9672	0.6105	0.1076	0.2819
24	0.9773	0.6631	0.1103	0.2266
25	0.9701	0.6676	0.2347	0.0977
26	0.9376	0.1386	0.1552	0.7062
27	0.9670	0.6316	0.1041	0.2643
28	0.9907	0.6570	0.2625	0.0805
29	0.9735	0.4213	0.1457	0.4330
30	0.9891	0.6895	0.2343	0.0762
31	0.9831	0.6604	0.2630	0.0767
32	0.9722	0.5146	0.1437	0.3417

Appendix 6   (Continued)

SAMPLE	COMM.	FACTOR I	FACTOR II	FACTOR III
33	0.9246	0.2774	0.2725	0.4501
34	0.9822	0.6852	0.2423	0.0725
35	0.9634	0.1263	0.7530	0.1207
36	0.9956	0.0542	0.4021	0.5436
37	0.9839	0.4736	0.0942	0.4321
38	0.9893	0.7110	0.1042	0.1848
39	0.9146	0.5911	0.2142	0.1947
40	0.9701	0.6996	0.0705	0.2299
41	0.9788	0.5115	0.1523	0.3362
42	0.9836	0.7183	0.2049	0.0768
43	0.9833	0.6482	0.1572	0.1945
45	0.9069	0.3372	0.5877	0.0751
46	0.9886	0.6321	0.2800	0.0878
47	0.9193	0.5034	0.4017	0.0949
48	0.9883	0.4770	0.0487	0.4743
49	0.9836	0.7257	0.0602	0.2141
50	0.9912	0.4977	0.1095	0.3928
51	0.9935	0.7091	0.1145	0.1764
52	0.9972	0.6872	0.1822	0.1306
53	0.9855	0.7347	0.1907	0.0746
54	0.9324	0.5949	0.2191	0.1860
55	0.9416	0.4318	0.3721	0.1961
56	0.9217	0.4552	0.3654	0.1794
57	0.9382	0.4090	0.3327	0.2583
58	0.9725	0.6221	0.2977	0.0802
59	0.9908	0.6138	0.3041	0.0821
60	0.9101	0.3455	0.1820	0.4725
61	0.9187	0.7430	0.1075	0.1495
62	0.9659	0.7179	0.1865	0.0956
63	0.9240	0.6725	0.1014	0.2261
64	0.9833	0.6924	0.1176	0.1900
65	0.9717	0.7022	0.1969	0.1009
66	0.9881	0.6641	0.1285	0.2074
67	0.9193	0.2808	0.1663	0.5529
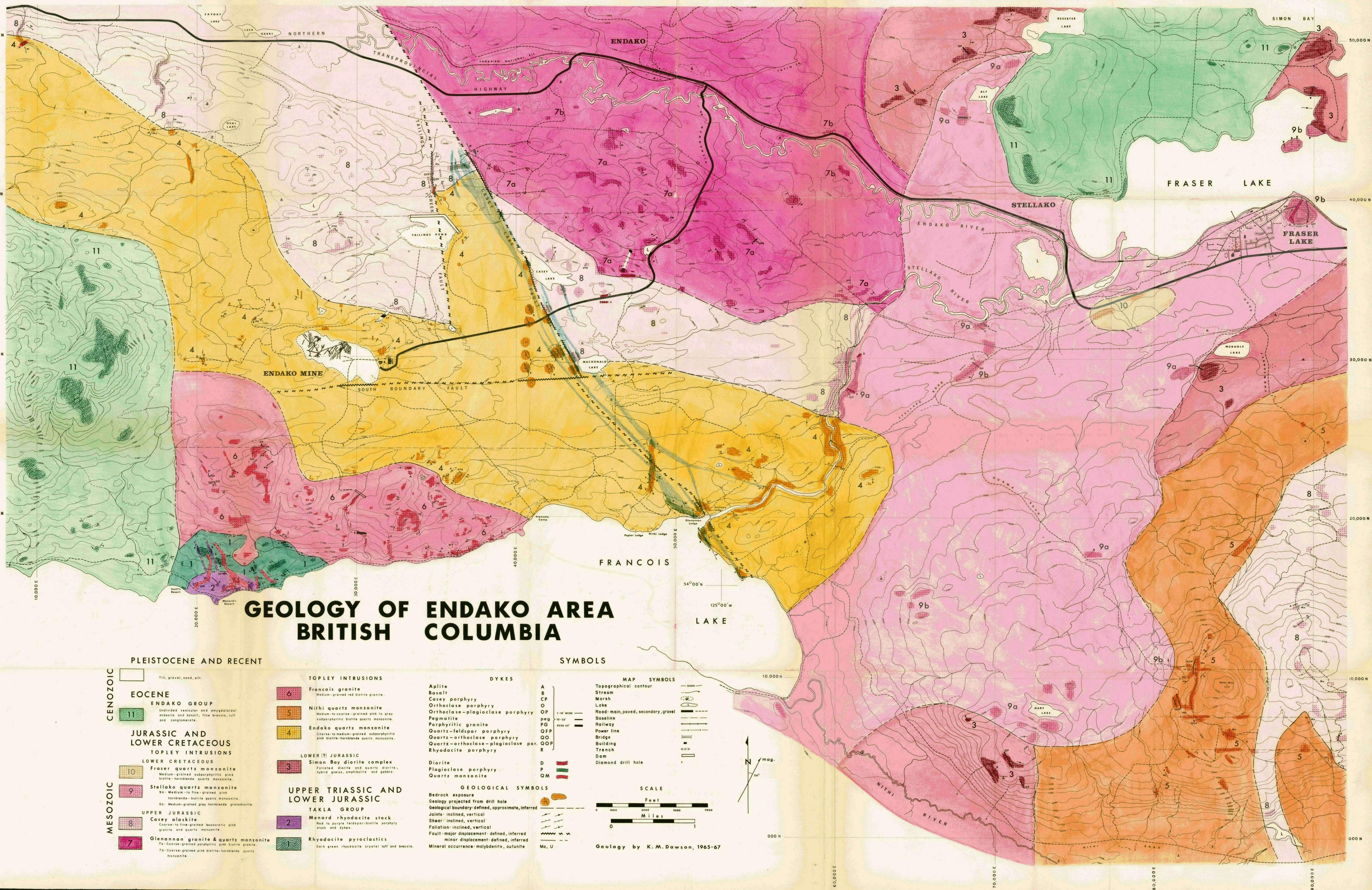
GEOLOGY OF ENDAKO AREA
BRITISH COLUMBIA

PLEISTOCENE AND RECENT

CENOZOIC

Till, gravel, sand, silt.

EOCENE

ENDAKO GROUP

11 — Undivided vesicular and amygdaloidal andesite and basalt, flow breccia, tuff and conglomerate.

JURASSIC AND LOWER CRETACEOUS

TOPLEY INTRUSIONS

MESOZOIC

LOWER CRETACEOUS

10 — Fraser quartz monzonite
Coarse- to medium-grained porphyritic pink granite and quartz monzonite.

9 — Stellako quartz monzonite
9a: Medium- to fine-grained pink hornblende - biotite quartz monzonite.
9b: Medium-grained grey hornblende granodiorite.

UPPER JURASSIC

8 — Casey alaskite
Coarse- to fine-grained leucocratic pink granite and quartz monzonite.

7 — Glenannan granite & quartz monzonite
7a: Coarse-grained porphyritic pink biotite granite.
7b: Coarse-grained pink biotite-hornblende quartz monzonite.

TOPLEY INTRUSIONS

6 — Francois granite
Medium-grained red biotite granite.

5 — Nithi quartz monzonite
Medium- to coarse-grained pink to grey subporphyritic biotite quartz monzonite.

4 — Endako quartz monzonite
Coarse- to medium-grained subporphyritic pink biotite-hornblende quartz monzonite.

LOWER (?) JURASSIC

3 — Simon Bay diorite complex
Foliated diorite and quartz diorite, hybrid gneiss, amphibolite and gabbro.

UPPER TRIASSIC AND LOWER JURASSIC

TAKLA GROUP

2 — Menard rhyodacite stock
Red to purple feldspar-biotite porphyry stock and dykes.

1 — Rhyodacite pyroclastics
Dark green rhyodacite crystal tuff and breccia.

SYMBOLS

DYKES	
Aplite	A
Basalt	B
Casey porphyry	CP
Orthoclase porphyry	OP
Orthoclase-plagioclase porphyry	OPP
Pegmatite	peg
Porphyritic granite	PG
Quartz-feldspar porphyry	QFP
Quartz-orthoclase porphyry	QO
Quartz-orthoclase-plagioclase por.	QOP
Rhyodacite porphyry	R
Diorite	D
Plagioclase porphyry	P
Quartz monzonite	QM

MAP SYMBOLS
Topographical contour
Stream
Marsh
Lake
Road: main, paved, secondary, gravel
Baseline
Railway
Power line
Bridge
Building
Trench
Dam
Diamond drill hole

GEOLOGICAL SYMBOLS
Bedrock exposure
Geology projected from drill hole
Geological boundary: defined, approximate, inferred
Joints: inclined, vertical
Shear: inclined, vertical
Foliation: inclined, vertical
Fault: major displacement - defined, inferred
minor displacement - defined, inferred
Mineral occurrence: molybdenite, autunite — Mo, U

SCALE
Feet
Miles

Geology by K. M. Dawson, 1965-67

ENDAKO

STELLAKO

FRASER LAKE

FRANCOIS LAKE

NITHI RIVER

ENDAKO MINE

SOUTH BOUNDARY FAULT

TRANSPROVINCIAL HIGHWAY

MODAL ANALYSIS SPECIMENS
ENDAKO AREA, B.C.

FRASER LAKE

DESERTER LAKE

ALF LAKE

OVAL LAKE

CASEY LAKE

MACDONALD LAKE

MUDHOLE LAKE

TAILINGS POND

ENDAKO MINE

FRANCOIS

LAKE

MARY LAKE

54°00'N
125°00'W

N mag.

PLEISTOCENE AND RECENT
☐ Glacial deposits

EOCENE
11 Endako Group

JURASSIC AND
LOWER CRETACEOUS
TOPLEY INTRUSIONS
LOWER CRETACEOUS
10 Fraser quartz monzonite
9 Stellako quartz monzonite

UPPER JURASSIC
8 Casey alaskite
7 Glenannan granite

TOPLEY INTRUSIONS
6 Francois granite
5 Nithi quartz monzonite
4 Endako quartz monzonite

LOWER (?) JURASSIC
3 Simon Bay diorite

UPPER TRIASSIC AND
LOWER JURASSIC
TAKLA GROUP
2 Menard rhyodacite stock
1 Rhyodacite pyroclastics

SYMBOLS
Modal analysis specimen   • 137
Geological boundary:
   Defined
   Approximate
   Inferred
Fault: defined, inferred
Lake
Road, paved

SCALE
Feet
0   7000
Miles
0

K.M. Dawson, 1968